Development of
in vitro and *in vivo* Bioreactors
for Bone Tissue Engineering

Martin A. Koch

Technical University of Catalonia

2010

Development of *in vitro* and *in vivo* Bioreactors for Bone Tissue Engineering

Martin Andreas Koch

Doctoral Thesis
Biomedical Engineering Doctoral Programme

Supervised by Dr. Damien Lacroix

Department of Materials Science and Metallurgy (CMEM)
Universitat Politècnica de Catalunya (UPC)

March 2010

For Natàlia

I'd take the awe of understanding over the awe of ignorance any day.
Douglas Adams
English humorist and science fiction novelist (1952 - 2001)

Acknowledgements

Contents

List of Figures

List of Tables

Abbreviations

2D	Two dimensions
3D	Three dimensions
ASCII	American Standard Code for Information Interchange
Ain	Analogue input
AISI	American Iron and Steel Institute
ANOVA	Analysis of Variance
AO	Acridine orange
ASTM	American Society for Testing and Materials
BASIC	Beginner's All-purpose Symbolic Instruction Code
BIBITE	Biomaterials, Biomechanics and Tissue Engineering
BIC	Bone-implant contact
BMSC	Bone marrow stromal cell
BMU	Basic Multicellular Unit
CAD	Computer Assisted Design
CAT	Computer Assisted Tomography
CATIA	Computer Assisted Three-Dimensional Interface Application
cDNA	complementary DNA
COM	serial port interface
CSD	Critical Size Defect
DMEM	Dulbecco's Modified Eagle Medium
DNA	Deoxyribonucleic acid
Dout	Digital output
DPX	Di-n-butylPhthalate in Xylene
EB	Ethidium bromide
ECM	Extracellular matrix
EEC	European Economic Community
ETSEIB	School of Industrial Engineering of Barcelona
FEP	Fluorinated ethylene propylene
HA	Hydroxyapatite
HBSMC	Human bladder smooth muscle cells
HSS	High Speed Steel

ID	Identification
i.D.	Inner diameter
LDH	Lactate Dehydrogenase
LFL	Long Flex Life
MSC	Mesenchymal Stem Cell
MAPK	Mitogen-activated Protein Kinasis
NBV	New bone volume
o.D.	Outer diameter
PBS	Phosphate Buffered Saline
PBT	Poly butylene terephthalate
PEOT	Poly ethylene oxide terephthalate
PES	Polyethersulfone
PLA	Poly lactic acid
PTFE	Polytetrafluoroethylene
RAEC	Rat aortic endothelial cells
RLT	RNA Lysis Buffer
rMSC	Rat mesenchymal stem cells
RNA	Ribonucleic acid
rpm	Revolutions per minute
RS-232	Recommended Standard 232
RTK	Receptor Tyrosine Kinasis
RT-PCR	Reverse transcription polymerase chain reaction
SBF	Simulated body fluid
SEM	Scanning Electron Microscopy
SD	Standard deviation
spp	Species
T/F	True or false
TCP	Tricalcium Phosphate
TESPA	3-Triethoxysilylpropylamine or 3-aminopropiltrietoxysilane
UPC	Technical University of Catalonia
USA	United States of America
USB	Universal Serial Bus
VAC	Alternating current voltage
VDC	Direct current voltage

Abstract

Large bone defects constitute a challenge for the clinical field, because they cannot be repaired by the body itself, but require the implantation of suitable bone grafts. To overcome the drawbacks of grafts from autologous or allogous sources, modern bone tissue engineering aims to replace lost tissue by cultivating cells *in vitro* on porous biomaterials. The cell culture on large porous scaffolds has shown to be difficult, requiring bioreactors, which are used for tissue culture and the study of cell behaviour in 3D scaffolds. Of special interest is the mechanical conditioning of the cultured tissue for bioreactor-based bone tissue engineering, which is able to enhance the osteogenic potential of the synthetic grafts.

In this work two bioreactor systems were developed to allow insight into bioactive properties of different scaffold materials and the mechanoregulation of cell or tissue behaviour. An *in vitro* perfusion bioreactor system was developed for the cell seeding and culture on porous biomaterial cylinders. Several studies for the determination of applicable cell seeding parameters were conducted, as well as experiments of cell culture under steady fluid flow with additional mechanical stimulation by alternating fluid flow. A bone chamber system was developed as an *in vivo* bioreactor. The system produced a large bone defect in dog tibia and allowed the repeated implantation of large porous scaffolds of different material compositions. The ingrowing tissue was observed to allow conclusions about osteoconductive or osteinductive properties of the scaffolds. Additionally a compression device was developed to apply cyclic loading on the scaffolds *in vivo* to study the effect of mechanical stimulation on tissue development.

The studies with the developed *in vitro* perfusion bioreactor system have shown that it is possible to seed cells throughout large porous scaffolds, which

is deemed crucial for the further cell culture. The long time cell culture showed the proliferation of mesenchymal stem cells up to two weeks. The stimulation pattern used in the study enhanced the expression of osteocalcin, indicating an enhanced cell activity, but the absence of RunX2 and collagen I expression rendered the determination of differentiation inconclusive.

The developed bone chamber system proved to be functional in the surgical environment during the *in vivo* experiments. Occurring complications during the experiments did not allow the application of the cyclic loading of implanted scaffolds. Delayed bone formation due to created bone defect and remaining scaffold material did not allow final conclusions about the scaffold material properties. Nevertheless the study provides input for further development of the device and clinical protocol.

The conducted studies constitute a novelty regarding the creation of bioreactors for the study of synthetic porous scaffolds of large dimensions *in vitro* and *in vivo*. The developed systems form the basis for further studies in mechanobiology of bone cells and tissue.

Scope

Advances in biomaterial sciences in the last decades have given new possibilities for tissue engineering. The successful combination of living cells with specially designed materials can form functional living tissue, a controlable source for implantable tissue substitutes. The demand for remedy of tissue failure in the clinical field as well as the need for scientific research towards a deeper understanding of tissue-material interaction, lead to the development of bioreactors as tissue engineering tools.

Regarding the role of mechanotransduction in the formation, maintenance and repair of bone, the objective of this thesis was the development of bioreactors for the study of mechanical stimuli application in the field of bone tissue engineering. The development included an *in vitro* perfusion bioreactor and a device for compressive loading of implanted scaffolds *in vivo* to give an insight into the interaction of cells and tissue to biomaterials. The emphasis in this studies lies in the use of porous scaffolds of large dimensions, a property which constitutes a major challenge in tissue culture.

The developed perfusion bioreactor system is used to seed and culture cells on large porous scaffolds. The scaffold has to be characterized by technical relevant properties, such as permeability and porosity which are crucial for the determination of the applicability of the specific scaffold type. Cell seeding is accomplished by perfusion of the scaffolds with cells suspended in medium and filtration of the cells into the scaffold. A high seeding efficiency and heterogeneous cell distribution is highly important for the further cell culture with the aim of obtaining a structure similar to premature bone. For cell culture, the cell-loaded scaffold is perfused with medium during long periods. The bioreactor system is used to establish conditions favourable for cell survival and proliferation. Different fluid flow shear stress patterns

stimulate undifferentiated mesenchymal to differentiate into the osteoblastic cell type. The objectives of the *in vitro* experiments consist in finding the optimal parameters to achieve a high cell seeding prior to culture and the most applicable fluid flow pattern during culture to produce bone-like tissue in the scaffold.

A bone chamber system is developed for the application of compressive loads on implanted scaffolds. This system is a reusable bone chamber, allowing the *in vivo* test of different materials consecutively in the same animal. The bone chamber is used to implant different scaffolds materials into dog tibia with and without application of cyclic loading. The objective is to investigate the role of material properties and mechanical stimulation for tissue ingrowth and the development of a procedure that allows to test materials in as few as possible animals and reduce the inter-animal variability. The technical objectives lie in the development of a repeatable implanting system, including tools for implantation and sample extraction which is usable in the surgical environment. An actuator has to be developed which features a sufficient resolution in linear displacement and force measurement to control and monitor the compression of the samples *in situ*.

One of the possible approaches for scientific investigation in the field of tissue engineering consists in the use of numerical models for simulation of tissue development. Even if not in the scope of the presented thesis it is important to mention that the obtained results from the conducted experiments can be used as feedback in the development of numerical models. This data input might serve as a further step towards the interconnection of experiment and simulation in tissue engineering.

Chapter 1

Introduction

When large amounts of bone are lost due to trauma, pathologies (such as osteosarcoma) or is needed for joint fusion, a suitable bone substitute must be provided for implantation into the defect. A common practice is the implantation of allografts or autografts, which consist of bone tissue taken respectively from another patient or from a harvesting site in the same patient. Every year about 450,000 bone grafts are needed by doctors in the USA alone [1]. To relieve patients from harvesting of suitable grafts, bone tissue engineering aims at generating grafts by combining synthetic materials and cells. The generation of *in vitro* cultured bone on such synthetic materials has shown to be difficult, because bone is a complex, living tissue with a need for the right signalling for adequate development.

1.1   Bone tissue

Bone is an essential tissue in the body, which serves as support, protection, leverage, storage of minerals and lipids and blood cell production [2]. About 65 % of bone is mineral matrix, which consists of small crystals of largely impure hydroxyapatite situated between collagen fibres. The mineral content gives bone the strength to support large loads. 35 % of bone consists of organic matrix, cells and water. The organic matrix itself contains 90 % collagen (mostly type I with traces of types III, V and X) and 10 % other proteins (mostly osteocalcin, osteopontin, osteonectin, bone sialoprotein) [3].

Initially bone is laid down as immature (or woven) bone. It consists of a matrix of interwoven coarse collagen fibres and randomly distributed osteo-
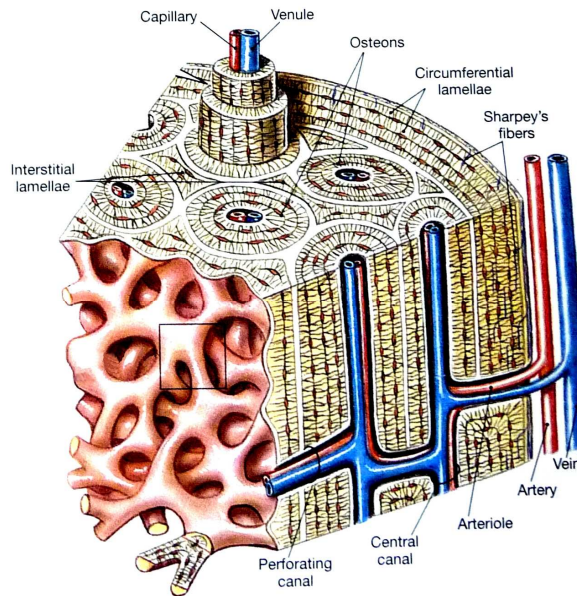
Figure 1.1: Structure of compact and cancellous bone. Modified from [2].

cytes. Woven bone can be found in the developing embryo, fracture healing or under pathological conditions (e.g. osteosarcoma or ectopic ossification). The immature woven bone is replaced by mature (or lamellar) bone which is built up from layers (lamellae) of 3 to 7 μm thickness. The lamellae occur in three major patterns: Circular rings as part of the osteons, circumferential lamellae which cover the whole bone shaft uninterrupted and interstitial lamellae which fill gaps in the haversian system [3].

All bones consist of spongy bone on the inside, covered by compact bone [2]. Compact (or cortical) bone constitutes 80 % of the total bone mass. Its main units are osteons (or Haversian systems) which are cylindrical structures composed of lamellae surrounding blood vessels (see Figure 1.1). The remaining 20 % of bone mass consists of cancellous (or spongy or trabecular) bone, which is made of struts (or trabeculae) of lamellar structure [2].

Bones are lined on the exterior (except in joints and tendon anchorage) with the periosteum, a membrane that isolates the bone, routes the the circulatory and nervous supply and participates in bone growth and repair. The interior surfaces of bones are lined with a flat layer of osteoprogenitor cells, the endosteum. This cell layer lines marrow cavities, trabeculae and the inner surfaces of the central channels and is active in bone growth, repair

and remodelling [2].

Four types of cells are active in the bone formation, resorption and maintenance, which are bone-lining cells, osteoblasts, osteocytes and osteoclasts. Bone-lining cells are flattened elongated cells which line the majority of adult bone surface. They are in-active osteoblasts and play a role in bone formation, stress/strain sensing and serve as an ion barrier. Osteoblasts are cuboidal cells (15 to 30 μm thick) with large nucleus, endoplasmatic reticulum, Golgi apparatus and collagen vesicles which produce the unmineralized bone matrix (osteoid). They are derived from osteoprogenitor cells from periosteum, endosteum and bone marrow. When embedding themselves in the osteoid, osteoblasts become osteocytes. In the human adult there are about 10 times more osteocyctes than osteoblasts. Osteocytes are embedded in the lacunar-canalicular system where they connect through small channels (canaliculi) the other osteocytes and bone-lining cells over gap junctions. The functions of osteocytes are strain sensing, information transduction to surface cells, bone mineral stabilization by maintenance of a ionic milieu and microdamage detection. The resorption of bone is effectuated by osteoclasts, which are multinucleated (1 to 50 nuclei) large cells (20 to 100 μm). Osteoclasts are located in cavities on the bone surface, the so called Howship's lacunae, where they produce an acidic environment (pH 3.5) to solubilise mineral and organic components of the bone matrix. The osteoclasts are derived from the mononuclear phagocygotic lineage of the hematopoeitic marrow [3].

Bone is remodelled over time by formation and absorption of the bone matrix. Osteoblasts and osteoclasts form the 'basic multicellular unit' or BMU's (or 'bone remodeling units') which remove microdamages, replace dead and hypermineralized bone to adapt to local stress. During bone regeneration only 19 of 20 parts of bone are replaced by the basic multicellular units, creating a negative bone balance, called the 'bone remodelling-dependent bone loss' [3, 4]. To achieve an adaption of bone mass to mechanical requirements, bone can translate mechanical signals into bone formation or resorption. This process is called mechanotransduction.

1.2 Mechanotransduction

The structure of load bearing bone is guided by biological regulatory processes, as is known since the 19th century [5, 6], where it was stated that bone structure and density is oriented to applied loads (see Figure 1.2).
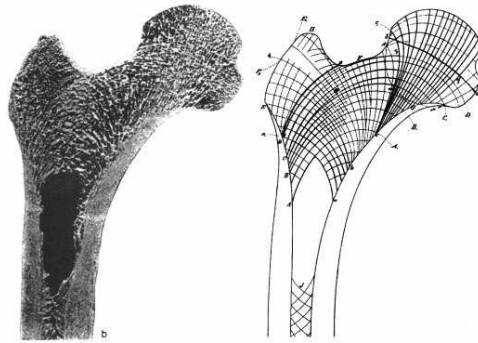
Figure 1.2: A cut through a proximal femur. The trabecular structure is oriented in the main lines of stress. Modified from [7].

It has been shown in humans that load bearing increases bone mass in relevant bones, as in weightlifters' femur [8], tennis players' radii [9], whereas the absence of loading, as in astronauts [10] or during prolonged bed rest [11] decreases the bone mass significantly. The correlation between bone mass and loading was described by Frost in the mechanostat model (see Figure 1.3). The model shows that during the absence of loading, an increased activity of the bone remodelling units (BMUs) causes an decrease in bone mass. When load is applied, BMUs remodel bone with a minimal bone loss. At a mild overload, the bone mass is increasing with the formation of mature bone. If bone is overloaded, mainly woven bone is deposited accompanied by microdamage, constituting a pathological situation.

Analogue to the control of the bone remodelling by loading, mechanical stimulation is important for fracture healing. When fixating bone fractures, it was observed that a stiff fixation can suppress the callus formation and delay the fracture healing process considerably. When a certain mechanical loading is permitted, especially in a low-magnitude high-frequency range, fracture healing can be enhanced. Too much strain however causes the formation of fibrous tissue, leading to an unsuccessful fracture healing [13–17]. The influence of mechanical loading on fracture healing can be explained
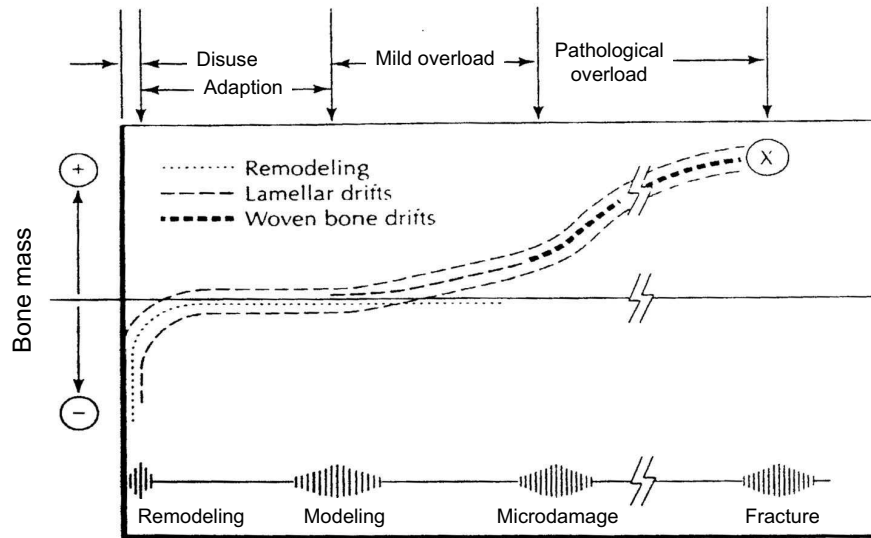
Figure 1.3: Frost's mechanostat theorem shows the dependency of bone mass on loading conditions in load bearing bones [12].

by the influence of mechanical signals on the differentiation of mesenchymal stem cells (MSCs), where a certain magnitude of strain is needed to generate bone, but excessive signals lead to fibrous tissue (see Figure 1.4). The theoretical model of fracture healing based on mechanical stimulation of tissue differentiation was implemented successfully into numerical models which were able to show the applicability of the theory [18]. The differentiation of MSCs, directed by mechanical stimulation, has been successfully conducted in *in vitro* experiments, which shows the applicability of numerical models [19–22].

The alteration in bone structure and bone mass by mechanical loading is governed on cellular level. The path from mechanical signal to changes in gene expression includes the signal, a correspondent sensor and a pathway to the DNA transcription in the cell nucleus. Even though it is not clear how this pathway works, certain details emerged by thorough studies (see Figure 1.5). It has been shown that the appropriate mechanical stimuli for bone cells are mechanical strain as well as fluid flow shear stress [25, 26]. During loading, bone cells are stretched due to the strain of the matrix and a fluid
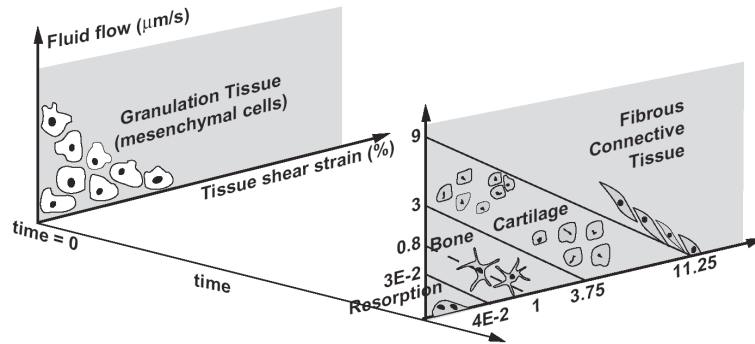
Figure 1.4: Tissue strain and fluid flow are influencing the mesenchymal stem cell differentiation over time as represented by this model [18].

flow is induced through the pericellular matrix in the lacunar-canalicular network, deforming the processes of the osteocytes [27, 28]. As second theory on the mechanosensation of bone the microdamage model has been proposed [29]. This theory states that the increase of bone mass in certain locations is guided by accumulating microcracks due to a overloading of bone. In experiment it has been shown that regions of accumulated microdamages also showed an increased BMU activity [30, 31] and the applicability of this theory has been implemented successfully in computational models [32, 33]. It is estimated that 30 % of bone remodelling is initiated by microdamage [34].

The mechanical stimulus is received by a sensor and passed over the cell membrane to the cell interior. Different cell components have been proposed to take part in this process of mechanosensation:

- Integrins, connecting the cytoskeleton with the extracellular matrix, transmitting extracellular signals to the interior [35, 36].

- G proteins, forming part of focal adhesion points, are activated by conformational changes by shear stress and stretching [37, 38].

- Membrane molecules taking part in the mechanosensations (receptor tyrosine kinasis (RTK) and mitogen-activated protein kinasis (MAPK)) [39, 40].

- Stretch-activated ion channels, whose permeability for specific ions (e.g. Na^+, K^+, Ca^{2+}) is influenced by mechanical strain [41].

- Tensegrity of the cytoskeleton, containing semi-flexible microfilaments
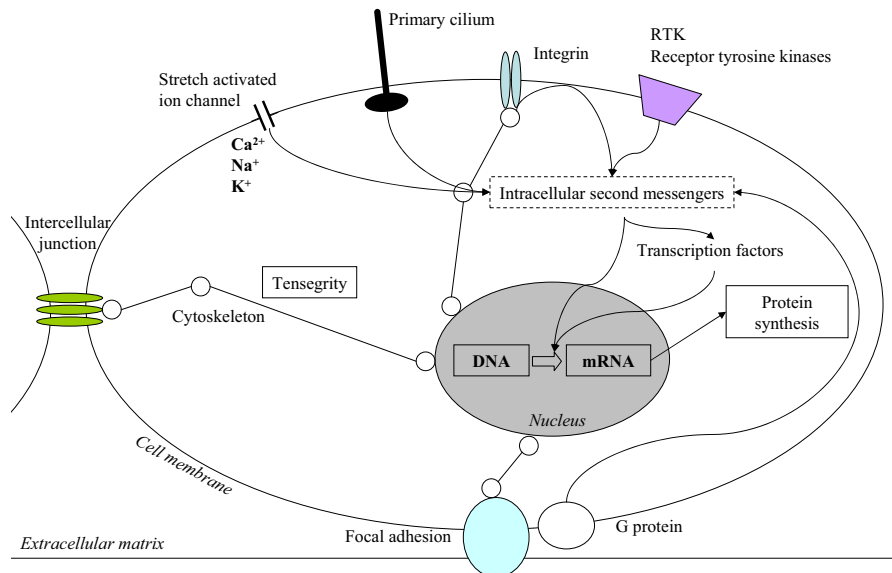
Figure 1.5: The sensation and transduction pathways of mechanical loading on cellular level. Modified from [23] and [24].

and rod-like microtubules, connects the cell membrane with the nucleus membrane and transmits movements [42].

Recently the primary cilia, microtubule-based antenna-like structures that emanates from the surface of cells [43], have been proposed as suitable mechanoreceptors [44]. Even though the pathways for mechanotransduction are not known entirely, it has been shown that mechanical strains influence those different cell components. The sensors transduce the signal to the cell interior via the cytoskeleton or intracellular signaling molecules (e.g. Rho, Raf, ERK1/2, JNK, p38), which alter the gene transcription in the cell nucleus either directly or via transcription factors (e.g. AP-1, Egr-1, NFκB) [24].

1.3 Bone tissue engineering

One of the most promising approaches of bone tissue engineering consists of the *in vitro* cultivation of cells on a biocompatible matrix or scaffold to achieve an implantable tissue (see Figure 1.6) [45, 46]. The most challeng-
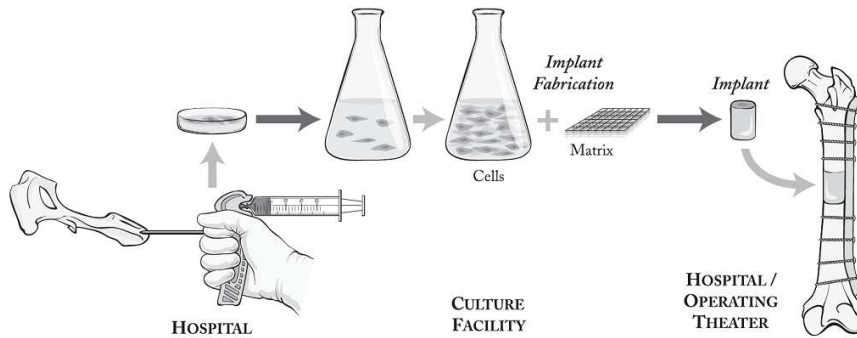
Figure 1.6: Schematic of a promising bone tissue engineering approach. Mesenchymal stem cells are harvested from the patient, expanded and cultured on biomaterials. The achieved engineered tissue is implanted into the bone defect. From [45].

ing step of this approach lies in the culture of expanded cells on scaffolds to obtain applicable differentiated tissue, which can sustain loads after implantation in defects, accelerates healing of large bone defects and can be integrated into the healthy tissue.

The scaffolds used for the tissue culture can either be synthetic porous materials or decellularized extracellular matrix (ECM) of bone grafts (see Figure 1.7). Other common methods include the stacking of cell-ECM sheets or inclusion of cells in hydrogels.

Synthetic scaffold materials provide control over composition and structure, which cannot be obtained with decellularised bone explant. With this approach it is possible to provide spatial alignment and chemical clues to cells, to achieve the adequate differentiation and bone cell activity. The most commonly used scaffold materials for bone tissue engineering are synthetic polymers, bioceramics, composites and metal alloys. The advantage of synthetic polymers lies in the control of physiochemical properties and delivery kinetics for specific molecules. They have the disadvantage of a possible induction of immune inflammatory response after implantation [48]. Bioceramics consisting of hydroxyapatite (HA), tricalcium phosphate (TCP) or a combination of both are widely studied and used for bone repair because of their osteoconductive and osteointegrative properties [48]. Porous scaffolds of bioceramics can have similar internal architectures as natural trabecular bone, which provides a large surface for tissue development and cell attachment [48]. The major benefit of porous metal alloys compared to other bone
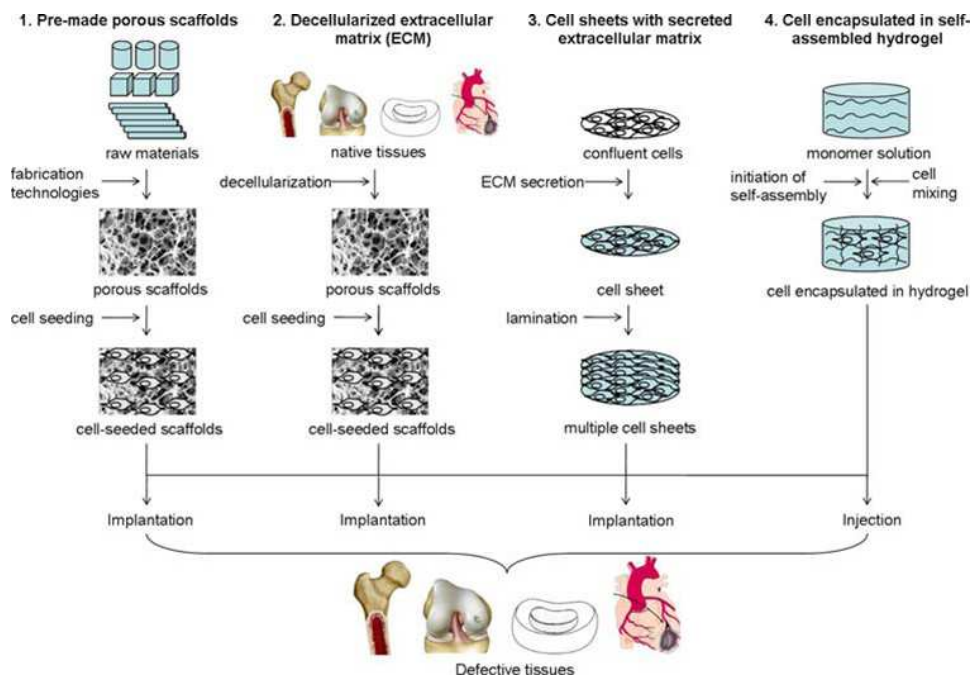
Figure 1.7: Different approaches of tissue engineering, using different scaffold-cell combinations. From [47].

graft substitutes consists in its mechanical strength for weight-bearing applications with an elastic modulus closer to that of bone than any other material [49, 50]. These unique properties combined with good biocompatibility, open-pore structure and shape memory characteristics make porous nickel-titanium a very promising candidate material for a bone graft substitute [51], even though a possible release of nickel is considered a major drawback, leading to the development of nickel-free shape memory titanium alloys [52]. Nevertheless the lack of biodegradability of metal alloys is highly unfavourable, because it is intended to leave as few foreign material in the patient's body to minimize the risk of adverse effects. Composites are materials that consist of a material that gives the composite its structural strength and a matrix material that binds the strong material and distributes load in the composite. Combining generally weak polymer materials with particles (e.g. calcium phosphate glass) can yield strong constructs, manufactured at low temperatures and incorporating organic molecules (e.g. growth factors) which are not neutralised by the manufacturing process [53].

The cultivation of cells on those scaffold types is challenging, because the
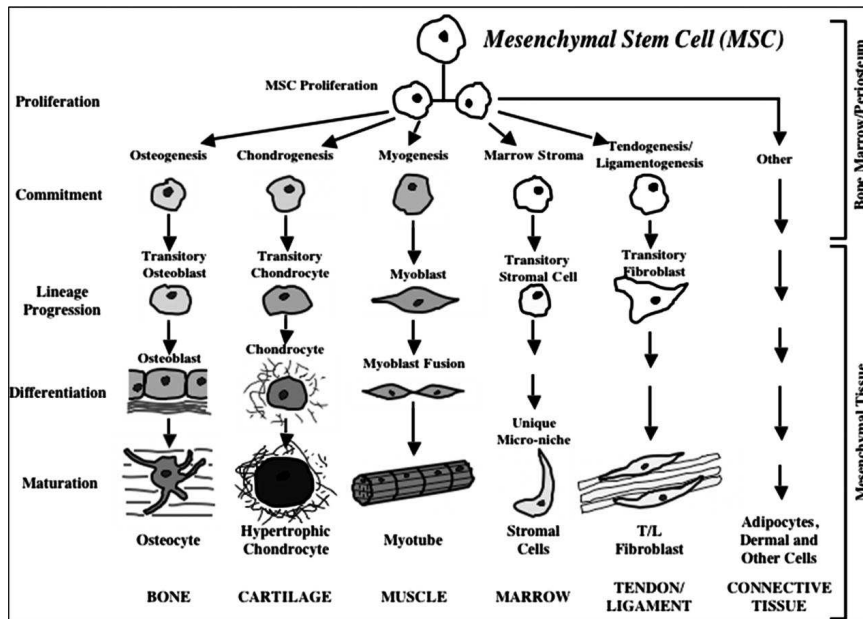
Figure 1.8: The pathways a multipotent mesenchymal stem cell can follow in its differentiation (from [55]). The stem cells differentiate depending on the external stimulus into different types of musculoskeletal cells.

cells have to be accessed by signalling molecules, growth factors and nutrients and metabolism products have to be removed from the cells in order to obtain a viable environment [54]. In bone tissue engineering a special interest exists in mesenchymal stem cells, because these multipotent cells have the ability to differentiate in the cell types of the muskoskeletal system (see Figure 1.8). To achieve the appropriate culture conditions, bioreactors are used, including culture under dynamic conditions [56], in perfusion bioreactors [57] and in bioreactors applying strains [58]. Bioreactors are not solely used to sustain a viable environment for cells, but also to apply stimuli which can enhance cell activity or guide cell differentiation [59, 60] or even as tissue model in cancer research [61]. Therefore the use of bioreactors is of high importance for bone tissue engineering, because it provides insights into tissue-material interaction and cell response on different culture environments.

Bibliography

[1] R. F. Service. Tissue engineers build new bone. *Science*, 289:1498–1500, Sep 2000.

[2] F. H. Martini, editor. *Fundamentals of Anatomy and Physiology*. Prentice Hall international, 4th edition, 1998.

[3] S. C. Cowin, editor. *Bone Mechanics Handbook*. CRC Press, 2nd edition, 2001.

[4] B. L. Langdahl, L. Mortensen, A. Vesterby, E. F. Eriksen, and P. Charles. Bone histomorphometry in hypoparathyroid patients treated with vitamin D. *Bone*, 18:103–108, Feb 1996.

[5] J. H. Wolf and J. Wolff. Julis Wolff and his "law of bone remodeling". *Orthopade*, 24:378–386, Sep 1995.

[6] W. Roux. *Der Kampf der Teile im Organismus*. Leipzig: Engelmann, 1881.

[7] R. Huiskes. If bone is the answer, then what is the question? *J Anat*, 197 (Pt 2):145–156, Aug 2000.

[8] B. E. Nilsson and N. E. Westlin. Bone density in athletes. *Clin Orthop Relat Res*, 77:179–182, 1971.

[9] A. L. Huddleston, D. Rockwell, D. N. Kulund, and R. B. Harrison. Bone mass in lifetime tennis athletes. *JAMA*, 244:1107–1109, Sep 1980.

[10] J. H. Keyak, A. K. Koyama, A. LeBlanc, Y. Lu, and T. F. Lang. Reduction in proximal femoral strength due to long-duration spaceflight. *Bone*, 44:449–453, Mar 2009.

[11] J. Rittweger, B. Simunic, G. Bilancio, N. G. De Santo, M. Cirillo, G. Biolo, R. Pisot, O. Eiken, I. B. Mekjavic, and M. Narici. Bone loss in the lower leg during 35 days of bed rest is predominantly from the cortical compartment. *Bone*, 44:612–618, Apr 2009.

[12] H. M. Frost. Bone's mechanostat: a 2003 update. *Anat Rec A Discov Mol Cell Evol Biol*, 275:1081–1101, Dec 2003.

[13] V. C. Mow and R. Huiskes. *Basic orthopaedic biomechanics and mechanobiology.* Lippincott Williams and Wilkins, 3rd edition.

[14] A. E. Goodship, T. J. Lawes, and C. T. Rubin. Low-magnitude high-frequency mechanical signals accelerate and augment endochondral bone repair: preliminary evidence of efficacy. *J Orthop Res*, 27(7):922–930, 2009.

[15] A. K. Ulstrup. Biomechanical concepts of fracture healing in weight-bearing long bones. *Acta Orthop Belg*, 74:291–302, 2008.

[16] L. Claes, K. Eckert-Hubner, and P. Augat. The effect of mechanical stability on local vascularization and tissue differentiation in callus healing. *J Orthop Res*, 20(5):109–1105, 2002.

[17] H. T. Aro and E. Y. Chao. Bone-healing patterns affected by loading, fracture fragment stability, fracture type, and fracture site compression. *Clin Orthop Relat Res*, 293:8–17, 1993.

[18] D. Lacroix and P.J. Prendergast. A mechano-regulation model for tissue differentiation during fracture healing: analysis of gap size and loading. *J Biomech*, 35:1163–1171, 2002.

[19] G. H. Altman, R. L. Horan, I. Martin, J. Farhadi, P. R. Stark, V. Volloch, J. C. Richmond, G. Vunjak-Novakovic, and D. L. Kaplan. Cell differentiation by mechanical stress. *FASEB J*, 16:270–272, Feb 2002.

[20] A. A. Tomei, F. Boschetti, F. Gervaso, and M. A. Swartz. 3D collagen cultures under well-defined dynamic strain: a novel strain device with a porous elastomeric support. *Biotechnol Bioeng*, 103:217–225, May 2009.

[21] D. Pelaez, C. Y. Huang, and H. S. Cheung. Cyclic Compression Maintains Viability and Induces Chondrogenesis of Human Mesenchymal Stem Cells in Fibrin Gel Scaffolds. *Stem Cells Dev*, Apr 2008.

[22] M. C. Qi, J. Hu, S. J. Zou, H. Q. Chen, H. X. Zhou, and L. C. Han. Mechanical strain induces osteogenic differentiation: Cbfa1 and Ets-1 expression in stretched rat mesenchymal stem cells. *Int J Oral Maxillofac Surg*, 37:453–458, May 2008.

[23] *Biomaterials Science An introduction to materials in medicine*, chapter Mechanical Forces on Cells, pages 288–289. Elsevier Academic Press, 2004.

[24] J. H. Wang and B. P. Thampatty. An introductory review of cell mechanobiology. *Biomech Model Mechanobiol*, 5:1–16, Mar 2006.

[25] P. J. Ehrlich and L. E. Lanyon. Mechanical strain and bone cell function: a review. *Osteoporos Int*, 13:688–700, Sep 2002.

[26] S. Stolberg and K. E. McCloskey. Can shear stress direct stem cell fate? *Biotechnol Prog*, 25:10–19, 2009.

[27] J. You, C. E. Yellowley, H. J. Donahue, Y. Zhang, Q. Chen, and C. R. Jacobs. Substrate deformation levels associated with routine physical activity are less stimulatory to bone cells relative to loading-induced oscillatory fluid flow. *J Biomech Eng*, 122:387–393, Aug 2000.

[28] Y. Han, S. C. Cowin, M. B. Schaffler, and S. Weinbaum. Mechanotransduction and strain amplification in osteocyte cell processes. *Proc Natl Acad Sci USA*, 101:16689–16694, Nov 2004.

[29] R. B. Martin and D. B. Burr. A hypothetical mechanism for the stimulation of osteonal remodelling by fatigue damage. *J Biomech*, 15:137–139, 1982.

[30] T. C. Lee, A. Staines, and D. Taylor. Bone adaptation to load: microdamage as a stimulus for bone remodelling. *J Anat*, 201:437–446, Dec 2002.

[31] T. C. Lee, F. J. O'Brien, T. Gunnlaugsson, R. Parkesh, and D. Taylor. Microdamage and bone mechanobiology. *Technol Health Care*, 14:359–365, 2006.

[32] D. Taylor and P. J. Prendergast. A model for fatigue crack propagation and remodelling in compact bone. *Proc Inst Mech Eng H*, 211:369–375, 1997.

[33] P. T. Scannell and P. J. Prendergast. Cortical and interfacial bone changes around a non-cemented hip implant: simulations using a com-

bined strain/damage remodelling algorithm. *Med Eng Phys*, 31:477–488, May 2009.

[34] D. B. Burr. *Proceedings of the 12th Conference of the European Society of Biomechanics*, chapter Damage detection and behavior in bone, pages 38–39. Dublin: Royal Academy of Medicine in Ireland, 2000.

[35] M. G. Coppolino and S. Dedhar. Bi-directional signal transduction by integrin receptors. *Int J Biochem Cell Biol*, 32:171–188, Feb 2000.

[36] A. Katsumi, A. W. Orr, E. Tzima, and M. A. Schwartz. Integrins in mechanotransduction. *J Biol Chem*, 279:12001–12004, Mar 2004.

[37] S. R. Gudi, C. B. Clark, and J. A. Frangos. Fluid flow rapidly activates G proteins in human endothelial cells. Involvement of G proteins in mechanochemical signal transduction. *Circ Res*, 79:834–839, Oct 1996.

[38] S. R. Gudi, A. A. Lee, C. B. Clark, and J. A. Frangos. Equibiaxial strain and strain rate stimulate early activation of G proteins in cardiac fibroblasts. *Am J Physiol*, 274:C1424–1428, May 1998.

[39] J. Liu, T. Liu, Y. Zheng, Z. Zhao, Y. Liu, H. Cheng, S. Luo, and Y. Chen. Early responses of osteoblast-like cells to different mechanical signals through various signaling pathways. *Biochem Biophys Res Commun*, 348:1167–1173, Sep 2006.

[40] C. Bougault, A. Paumier, E. Aubert-Foucher, and F. Mallein-Gerin. Molecular analysis of chondrocytes cultured in agarose in response to dynamic compression. *BMC Biotechnol*, 8:71, 2008.

[41] M. Tanno, K. I. Furukawa, K. Ueyama, S. Harata, and S. Motomura. Uniaxial cyclic stretch induces osteogenic differentiation and synthesis of bone morphogenetic proteins of spinal ligament cells derived from patients with ossification of the posterior longitudinal ligaments. *Bone*, 33:475–484, Oct 2003.

[42] D. E. Ingber. Cellular mechanotransduction: putting all the pieces together again. *FASEB J*, 20:811–827, May 2006.

[43] E. J. Michaud and B. K. Yoder. The primary cilium in cell signaling and cancer. *Cancer Res*, 66:6463–6467, Jul 2006.

[44] A. M. Malone, C. T. Anderson, P. Tummala, R. Y. Kwon, T. R. Johnston, T. Stearns, and C. R. Jacobs. Primary cilia mediate mechanosensing in bone cells by a calcium-independent mechanism. *Proc Natl Acad Sci USA*, 104:13325–13330, Aug 2007.

[45] K. H. Kraus and C. Kirker-Head. Mesenchymal stem cells and bone regeneration. *Vet Surg*, 35:232–242, Apr 2006.

[46] S. Sundelacruz and D. L. Kaplan. Stem cell- and scaffold-based tissue engineering approaches to osteochondral regenerative medicine. *Semin Cell Dev Biol*, 20:646–655, Aug 2009.

[47] B. P. Chan and K. W. Leong. Scaffolding in tissue engineering: general approaches and tissue-specific considerations. *Eur Spine J*, 17 Suppl 4:467–479, Dec 2008.

[48] R. Cancedda, B. Dozin, P. Giannoni, and R. Quarto. Tissue engineering and cell therapy of cartilage and bone. *Matrix Biol*, 22:81–91, Mar 2003.

[49] V. Itin, V. E. Gyunter, S. A. Shabalovskaya, and Sachdeva R.L.C. Mechanical properties and shape memory of porous nitinol. *Mater Charact*, 32:179–188, 1994.

[50] S. A. Shabalovskaya, V. I. Itin, and V. E. Gyunter. Porous ni-ti-a new material for implants and prostheses. *Proc Int Conf Shape Memory Superelastic Tech*, 1:7–12, 1994.

[51] S. Kujala, J. Ryhänen, A. Danilov, and J. Tuukkanen. Effect of porosity on the osteointegration and bone ingrowth of a weight-bearing nickel-titanium bone graft substitute. *Biomaterials*, 24:4691–4697, Nov 2003.

[52] M. González, J. Peña, J. M. Manero, M. Arciniegas, and F. J. Gil. Design and characterization of new ti-nb-hf alloys. *J Mater Eng Perform*, 18(5-6):490–495, 2009.

[53] M. Navarro, M.P. Ginebra, J.A. Planell, S. Zeppetelli, and L. Ambrosio. Development and cell response of a new biodegradable composite scaf-

fold for guided bone regeneration. *J Mater Sci Mater Med*, 15:419–422, Apr 2004.

[54] G. Vunjak-Novakovic. The fundamentals of tissue engineering: scaffolds and bioreactors. *Novartis Found Symp*, 249:34–46, 2003.

[55] A. I. Caplan. Adult mesenchymal stem cells for tissue engineering versus regenerative medicine. *J. Cell. Physiol.*, 213:341–347, Nov 2007.

[56] G. Vunjak-Novakovic, B. Obradovic, I. Martin, P. M. Bursac, R. Langer, and L. E. Freed. Dynamic cell seeding of polymer scaffolds for cartilage tissue engineering. *Biotechnol Prog*, 14:193–202, 1998.

[57] D. Wendt, S. Stroebel, M. Jakob, G.T. John, and I. Martin. Uniform tissues engineered by seeding and culturing cells in 3D scaffolds under perfusion at defined oxygen tensions. *Biorheology*, 43:481–488, 2006.

[58] M. van Griensven, S. Diederichs, S. Roeker, S. Boehm, A. Peterbauer, S. Wolbank, D. Riechers, F. Stahl, and C. Kasper. Mechanical Strain Using 2D and 3D Bioreactors Induces Osteogenesis: Implications for Bone Tissue Engineering. *Adv Biochem Eng Biotechnol*, 112:95–123, 2009.

[59] E. Leclerc, B. David, L. Griscom, B. Lepioufle, T. Fujii, P. Layrolle, and C. Legallaisa. Study of osteoblastic cells in a microfluidic environment. *Biomaterials*, 27:586–595, Feb 2006.

[60] H.L. Holtorf, T.L. Sheffield, C.G. Ambrose, J.A. Jansen, and A.G. Mikos. Flow perfusion culture of marrow stromal cells seeded on porous biphasic calcium phosphate ceramics. *Ann Biomed Eng*, 33(9):1238–1248, 2005.

[61] A. M. Mastro and E. A. Vogler. A three-dimensional osteogenic tissue model for the study of metastatic tumor cell interactions with bone. *Cancer Res*, 69:4097–4100, May 2009.

Chapter 2

Scaffold Characterisation for the Perfusion Bioreactor System

2.1 Introduction

The use of perfusion bioreactors is a promising approach to the culture of tissues on biomaterials for the purpose of tissue engineering. The success of bone cell culture under fluid flow is highly influenced by the scaffold properties, including porosity and permeability of the scaffold. The porosity of a scaffold is highly important, because it determines the surface area for cell attachment. Consequently high porosity can enhance cell proliferation in cell culture [1]. Permeability represents the accessibility of the pores in the scaffold. If the scaffold is highly porous, but the pores cannot be accessed, cells cannot be seeded throughout the scaffold homogeneously and the transport of nutrients and waste products is limited to the accessible areas. Pore interconnection (or permeability) is of high importance for the applied shear stress stimulus on the cells by perfusion, because it determines the number of flow pathways through the scaffolds and hence the fluid flow velocities occurring in those pathways (see Figure 2.1). One limitation is that a permeability value does not give any conclusion about its effects on individual cells. So the measured permeability mostly serves as a global parameter. It gives a rough idea, if the material geometry is in an applicable
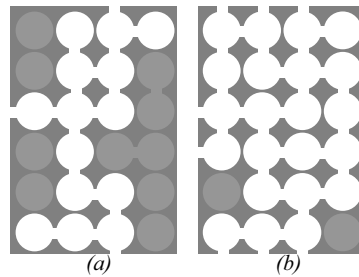
Figure 2.1: A schematic representation of porous and permeable materials. Dark grey represents the material walls, white the accessible pores and light grey the porosity isolated from the scaffold exterior. Even though both examples ((a)+(b)) have a similar porosity, the higher permeability of (b) provides more pathways through the sample and opens up a larger part of the porous area.

range and if the pressure build-up in the perfusion system is small enough to run the perfusion system.

In the present study the porosity and permeability of polymer/glass composite scaffolds, consisting of a poly lactic acid matrix and titanium stabilised calcium phosphate glass particles as reinforcement, were characterized for the use in a perfusion bioreactor. The material used was characterized for mechanical properties and biocompatibility by Navarro [2] and Charles-Harris [3] previously.

2.2   Objectives

The objectives of this Chapter were the fabrication of polymer/glass composite scaffolds for perfusion culture bioreactor and the determination of the applicability of the scaffolds for this type of bioreactor by measuring porosity and permeability.

2.3   Materials and methods

2.3.1   Scaffold fabrication

The following characterization was conducted on porous composite scaffolds consisting of poly lactic acid (poly(95L/5DL) lactic acid) and titanium stabilised calcium phosphate glass ($44.5P_2O_5$-$44.5CaO$-$6Na_2O$-$5TiO_2$ glass molar composition, particle size < 40 μm). The porosity was obtained by solvent casting and particle leaching method (NaCl particle size 80 μm - 210 μm). It was intended to fabricate scaffolds with dimensions of 6 mm in diameter and 12 mm in length (see Figure 2.2). The dimensions were the same as used in previous mechanical testing [2, 3]. By using the same fabrication technique and hence the same moulds and materials, it was assured to achieve scaffolds of the same structure as in previous studies.

Figure 2.2: PLA/glass scaffolds used for the material characterization and later cell culture.

The scaffolds were fabricated by dissolving poly lactic acid (PLA) in trichloromethane ($CHCl_3$ or chloroform) in 5 % weight/volume ratio over two days. Glass and salt particles (NaCl) were added to this solution, whereas the amount of glass was 50:50 in relation to the weight of PLA and the amount of salt was 94 % in relation to the total weight of solid components. The used quantities for production were 250 ml trichloromethane, 12.5 g PLA, 12.5 g glass particles and 391.67 g salt particles. The paste was then pressed into
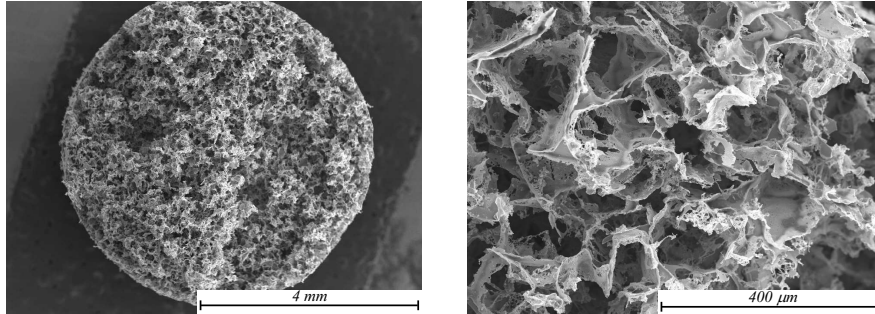
(a) 15 times magnification showing the whole diameter of the scaffold.

(b) 150 times magnification showing the highly interconnected cube-like pores left behind after NaCl extraction.
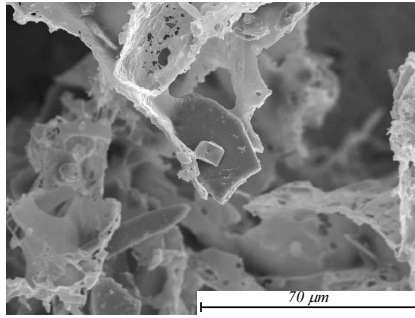
(c) 800 times magnification showing glass particles adhered to the polymer material.

Figure 2.3: Scanning electron microscopy images of the PLA/glass composite scaffolds.

Teflon moulds. During two days of rest the solvent vaporized and the samples were extracted from the moulds. The samples were washed in distilled water for two more days to extract the salt particles from the scaffolds and they were dried at 37 °C for storage and further processing. The dimensions of the produced scaffolds were measured with a slide calliper (TESA ShopCal, serial number 1K375806). Figure 2.3 shows scanning electron microscopy (SEM) images of the produced scaffolds. For the SEM images, scaffolds were frozen in liquid nitrogen and broken in two. The fragments were mounted on a copper plate and sputtered with gold. The cube-like pores can be clearly seen under 150 times magnification (see Figure 2.3b). In even higher magnification the glass particles can be seen (see Figure 2.3c). The glass is not totally embedded into the polymer, making its surface available for cell attachment.

2.3.2 Permeability measurement

The permeability measurement method used was based on Darcy's law which is stated in 2.1, where Q is the fluid flow in m^3/s, k is the intrinsic permeability coefficient in m^2, A the cross-sectional area of the sample in m^2, η the dynamic viscosity of water in Pa·s (0.001002 Pa·s [4]), P the pressure gradient in Pa and x is the length of the sample in m [5].

$$Q = k \times \frac{A \times \Delta P}{\eta \times \Delta x} \tag{2.1}$$

The pressure gradient to which the sample was subjected can be calculated by Pascal's law (Equation 2.2).

$$\Delta P = \rho \times g \times (\Delta h) \tag{2.2}$$

By inserting in Equation 2.2 the density of water ρ (1000 kg/m^3), the gravitational acceleration g (9.81 m/s^2) and the height of the water column given by the height of the water basin of the permeameter h (0.255 m) the pressure gradient of 2.5 kPa was calculated. This pressure was held constant during the experiments by adding water to the basin while the water was running through the sample.

The Darcy equation shows that the fluid flow through a porous sample depends on the dimensions of the sample (length and cross-section area), the viscosity of the used fluid and the applied pressure gradient (see Equation 2.1). Additionally the flow depends on the intrinsic factor k, the permeability factor. In this experiment it was intended to measure this material-specific factor for the PLA/glass scaffolds. The samples were wetted prior measurement to establish a defined condition. Prewetting was conducted by immersion of the scaffold in a 30 % vol. ethanol solution for 1 minute. Using higher concentrations of ethanol have shown to shrink the scaffolds in previous tests. This effect may be caused by damage of the PLA polymer chains by the ethanol. After the immersion in ethanol, scaffolds were washed three times in distilled water. The scaffolds were kept for at least 1 day in distilled water before measurement.

It was assumed that swelling of the scaffolds took place by immersion in water and might affect the permeability of the material. The scaffolds

used in these experiments were grouped into four groups of different prewetting periods (1, 3, 6 and 9 days). The effect of the prewetting period was evaluated by measuring the permeability for two hours. The permeability measurement itself was conducted with an in-house developed constant head permeameter (see Figure 2.4) [6].
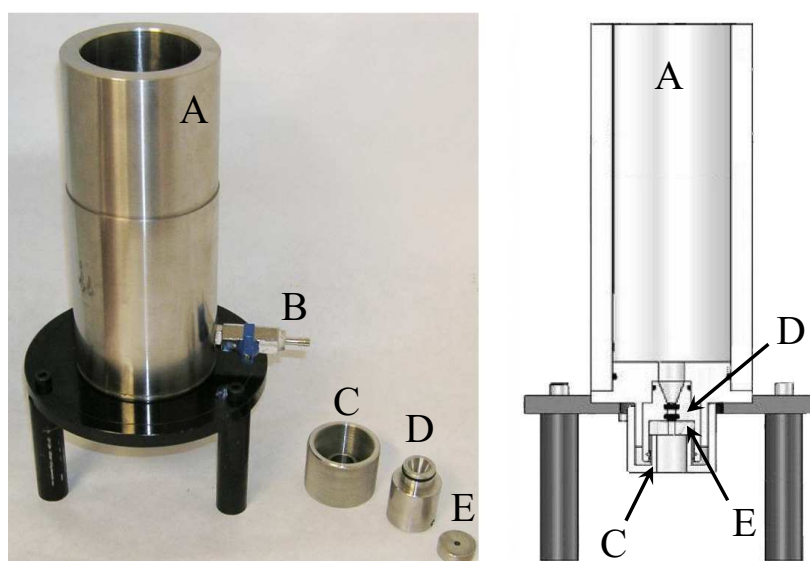
Figure 2.4: Constant head permeameter used for the material characterization. (A) water basin, (B) water outlet, (C) fixation, (D) sample holder, (E) disk securing sample from slipping out.

The scaffolds were taken out of the prewetting bath and measured (diameter and length) with a slide calliper. The scaffolds were then inserted in the sample holder as shown in Figure 2.5 by pushing them with an insertion bolt through a Teflon guide, which assured the perpendicular insertion into the sample holder's sealings.

After fixating the sample holder to the water basin, distilled water was poured into the basin, establishing a water column of 255 mm height over the sample. A timer was started and the water level was kept constant by pouring water into the basin. After a certain time (first two measurements after 1 and 3 minutes, from 5 to 120 min in 5 minutes steps) the out-flowing water was collected for 40 seconds and weighed. The measured water weight in combination with the fluid density and the measurement time were used
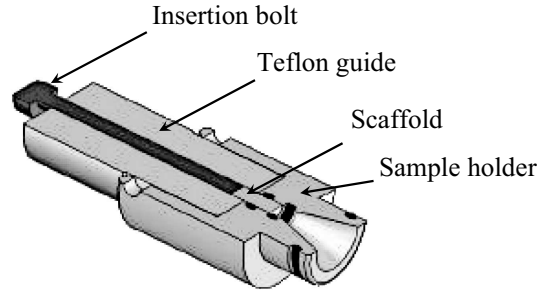
Figure 2.5: Scaffold insertion in the permeameter's sample holder. The scaffold is pushed through a Teflon guide into the sample holder, using a bolt.

to calculate the fluid flow Q. Using the Darcy equation the permeability constant k was calculated for every measured point of time.

2.3.3 Porosity measurement

Mercury immersion   The porosity of the scaffolds was measured by mercury immersion. Following the Archimedes principle, the buoyancy force occuring by immersing a body in a liquid equals the weight of the displaced liquid volume. Because the mercury does not penetrate the immersed scaffold's pores, the volume of the scaffold with its air containing compartment is replaced and reflected in the measured buoyancy force.

The measurement was conducted by positioning a container with mercury on a precision scale (Cobos Precision, M-150-SX, Serial No. B06291). A mechanical apparatus was used to hold the scaffold under the mercury level. The arm of this apparatus was put in the mercury to a defined depth and the scale was set to zero, so the buoyancy force of the arm did not influence the measurements. The scaffold was put on the scale and the weight was measured ($m_{scaffold}$). After this, the scaffold was immersed by use of the mechanical apparatus in the mercury down to the beforementioned defined depth. The weight indicated on the scale was registered (m_{Hg}).

With the weight of substituted mercury $m_{scaffold}$ the volume of the scaffold V was calculated considering the mercury density ($\rho_{Hg} = 13.546$ g/ml [7]):
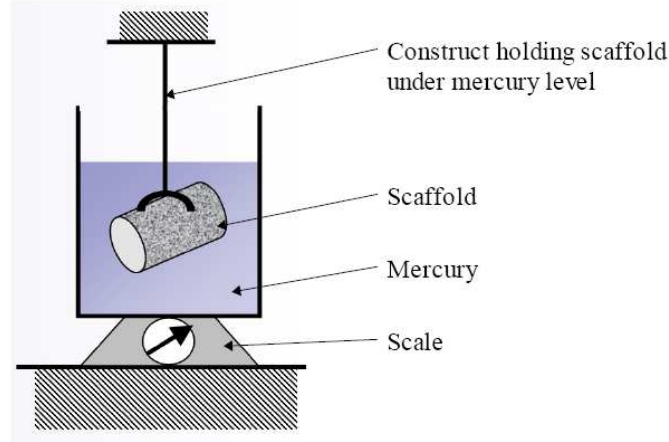
Figure 2.6: Experimental setup for porosity measurement by mercury immersion.

$$V = \frac{m_{Hg}}{\rho_{Hg}} \qquad (2.3)$$

Knowing the weight $m_{scaffold}$ and the volume of the scaffold V the apparent density $\rho_{scaffold}$ was calculated:

$$\rho_{scaffold} = \frac{m_{scaffold}}{V} \qquad (2.4)$$

With the apparent density $\rho_{scaffold}$ and the density of the material ($\rho_{PLA/glass}$ = 1.705 g/cm^3 [2]) it is possible to calculate the porosity P of the material [8]:

$$P[\%] = \left(1 - \frac{\rho_{scaffold}}{\rho_{PLA/glass}}\right) \times 100 \qquad (2.5)$$

For validation of the measured porosity the theoretical porosity of the scaffolds was calculated. This was done by calculating the volume ratio of ingredients that are extracted from the sample to the total amount of ingredients (see Equation 2.6).

$$P = \frac{V_{NaCl} + V_{CHCl_3}}{V_{NaCl} + V_{PLA/glass} + V_{CHCl_3}} = 96.7\% \qquad (2.6)$$

Mercury porosimeter   For the measurement of scaffold pore size distribution a mercury porosimeter type AutoPore IV 9500 (Micromeretics Instru-

ment Corp.) was used. The automated porosimetry is based on the intrusion of mercury into the porous structure. The pressure needed to press mercury into a pore corresponds to the pore size, assuming a cylindrical dimension of the pore. The relationship between applied pressure P and the pore diameter D is defined by Equation 2.7 with the mercury surface tension γ and the mercury contact angle Θ [9].

$$D = \frac{-4 \times \gamma \times cos\Theta}{P} \tag{2.7}$$

By inserting the surface tension constants used by the AutoPore porosimeter for surface tension γ (485 dynes/cm or 0.485 N/m) and the mercury contact angle Θ (130°) in Equation 2.7, the pore sizes measurable at the low and high pressure used by the AutoPore can be determined at 0.50 psi (3.4 kPa) with 360 μm and at 30,000 psi (206.8 MPa) with 6 nm. For the assessment of the pore size distribution three measurements were conducted. In every measurement three scaffolds were inserted into the sample holder to minimize the amount of mercury used in every measurement. The mean of the three pore size distribution curves and the total porosity was then calculated.

2.4 Results

2.4.1 Scaffold fabrication

By measuring the dimensions of the produced scaffolds before the permeability measurement it was observed that the mean length of 20 samples was 11.4 mm ± 0.1 mm and the mean diameter was 5.7 mm ± 0.1 mm. The results for the scaffold dimension showed that the scaffolds were 5 % in length and 5.3 % in diameter smaller than the mould dimensions of 12 mm length and 6 mm diameter.

2.4.2 Permeability measurement

The fluid flow Q was measured over two hours for 20 scaffolds and the permeability coefficient k was calculated. Preliminary test had shown that the permeability of the soft PLA/glass scaffold dropped during two hours of continuous perfusion to a stable value. Hence the measurement of fluid flow on the scaffold was conducted over two hours, measuring after 1, 3, 6 and 9 days prewetting, five samples for each group (Figure 2.7). The resulting perme-
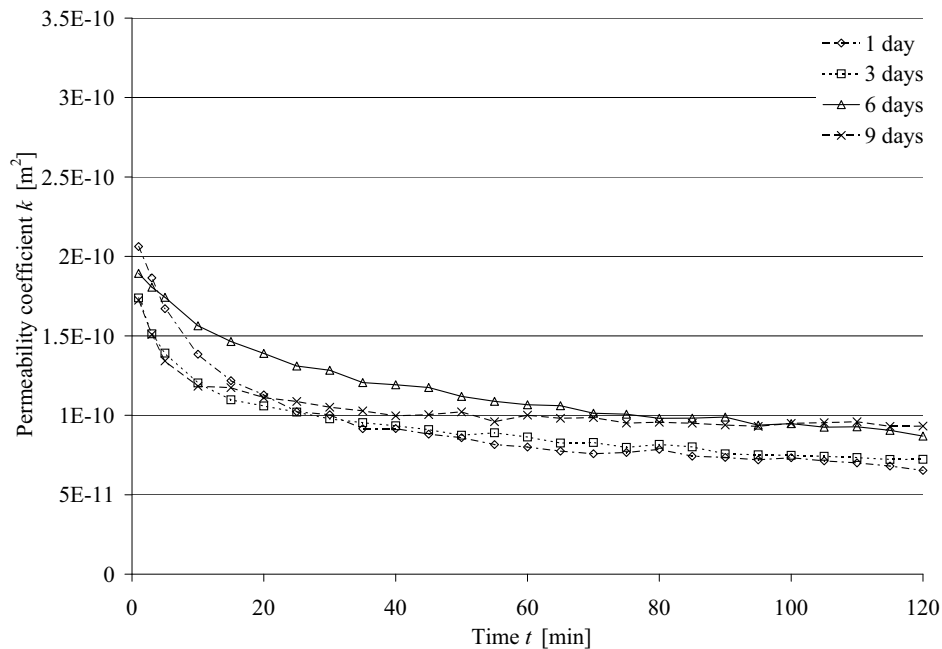
Figure 2.7: Permeability measured after different prewetting periods for PLA/glass scaffolds (n=5 per group).
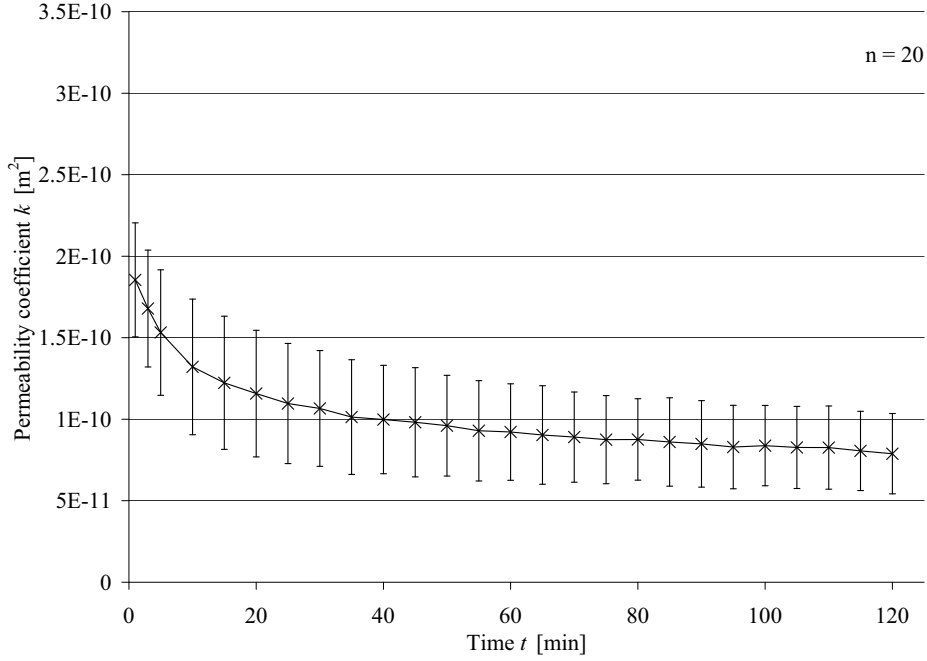
Figure 2.8: Average permeability graph measured over time for PLA/glass composite scaffolds.

abilities had high standard deviations with up to 36 % for 1 day prewetting, 48 % for 3 days, 35 % for 6 days and 34 % for 9 days. All scaffolds showed a drop of permeability over the two hours of measurement. The graphs for different prewetting times depicted similar trends and amplitudes, suggesting that the prewetting time had no effect on the permeability. By conducting an ANOVA analysis to compare each group at every recorded time point, no statistically significant differences were observed ($p < 0.05$) between the four prewetting groups.

After validation of the independence of the prewetting period on the permeability, the mean of all 20 scaffolds measured over time was calculated (see Figure 2.8). It was observed that the mean values dropped from 1.7×10^{-10} m^2 $\pm$ 3.6×10^{-11} m^2 more than 50 % over 2 hours showing a standard deviation of about 30 %. After the permeability decrease the coefficient was determined at the nearly stable state with 8.1×10^{-11} m^2 $\pm$ 2.4×10^{-11} m^2.

In the perfusion bioreactor system, which was developed as part of this thesis, fluid flow velocities v in ranges of 1 mm/s to 10 mm/s [8] were used. The found permeability coefficient signifies for this fluid flow velocities a

pressure build-up calculated by the converted Darcy equation (Equation 2.8).

$$\Delta P = \frac{Q \times \eta_{H_2O} \times \Delta x}{k \times A} = \frac{v \times \Delta x \times \eta_{H_2O}}{k} \tag{2.8}$$

By inserting values for scaffold length x (12 mm), dynamic viscosity of water η_{H_2O} (0.001002 Pa·s) and permeability coefficient k (8.1×10^{-11} m^2) into Equation 2.8, pressure gradients over the scaffold were calculated as 150 Pa for 1 mm/s and 1.5 kPa for 10 mm/s.

2.4.3 Porosity measurement

Mercury immersion   Scaffold porosity was measured for 5 samples by mercury immersion. For the calculation of porosity based on Equation 2.5 the constants for PLA/glass density ρ_{sample} (1.705 g/cm^3 [2]) and mercury density ρ_{Hg} (13.546 g/cm^3 [7]) were taken from the literature. The measured values for sample weight m_{sample} and displaced mercury weight m_{Hg} as well as the calculated volume V_{Hg} and porosity P are listed in Table 2.1. The calculated porosity resulted in a mean porosity of 95.7 % with a standard deviation of 0.3 % for the five samples.

m$_{sample}$ [g]	m$_{Hg}$ [g]	V$_{Hg}$ [cm^3]	$\rho_{apparent}$ [g/cm^3]	P [%]
0.014	2.364	0.17	0.080	95.3
0.013	2.443	0.18	0.072	95.8
0.017	3.091	0.23	0.075	95.6
0.020	3.980	0.29	0.068	96.0
0.021	4.101	0.30	0.069	95.9

Table 2.1: Porosity of PLA/glass samples assessed by mercury immersion.

Mercury porosimeter   The total porosity of the PLA/glass was determined with 95.4 % $\pm$ 0.2 % which differs only 0.3 % from the porosity measurement method used beforehand. The pore size distribution presented in Figure 2.9 shows a peak, where 90.7 μm $\pm$ 0.1 μm pore diameters occupy 25.5 % $\pm$ 1.1 % of the total pore space (see Figure 2.9).
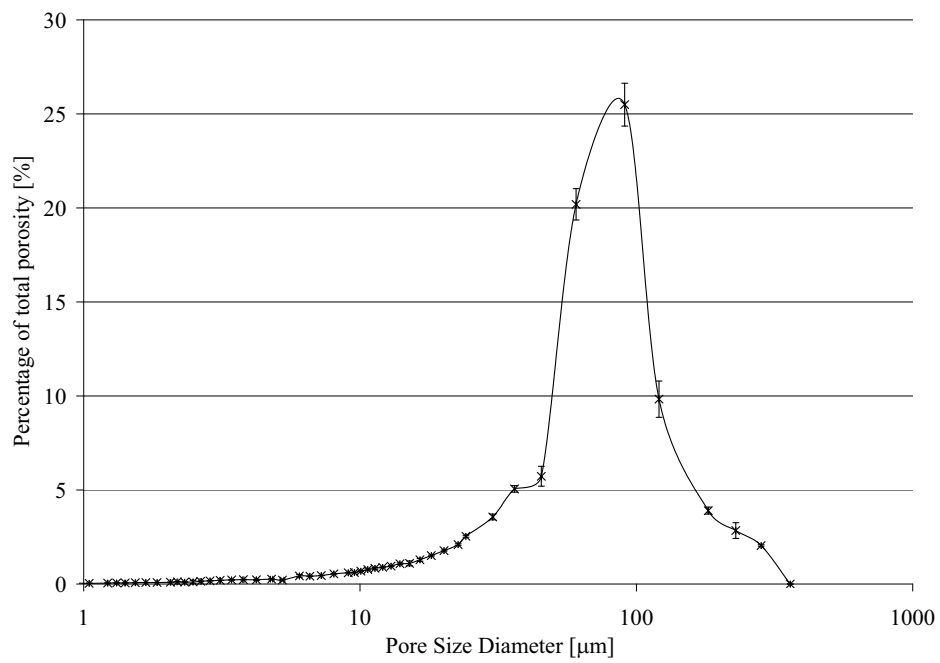
Figure 2.9: Pore size distribution of the PLA/ glass composite samples measured by the Autopore IV porosimeter (n=3).

2.5 Discussion

The measurement of the produced PLA/glass composite dimensions suggested that the scaffolds shrank after salt extraction 5 % in length and 5.3 % in diameter compared to the mould dimensions of 12 mm length and 6 mm diameter. This does not influence the permeability measurements theoretically, because the dimensions are considered in the used equation. However for the further use in a perfusion bioreactor it is recommended to make new moulds for scaffold production, which account for the shrink factor of 5 % (12.6 mm length and 6.3 mm diameter) to assure the scaffolds fit into the perfusion chambers of the bioreactor system.

By conducting the described measurements it was possible to obtain the porosity and permeability of the manufactured PLA/glass composite scaffolds. The presented values for permeability were obtained by measurement with a constant head permeameter. A time-dependency of the measurement was observed, an appropriate pre-treatment (wetting of the samples) was established and evaluated. The time-dependent drop in permeability is assumed to be based on the influence of internal fluid flow and pressure on the thin-walled soft composite material. The large standard deviations between different samples (about 30 %) are attributed to the measurement method and material heterogeneity. The long measurement time required to keep the water steady manually over two hours, which introduces sources of error. The used constant head permeameter has the advantage of subjecting the sample to constant conditions (i.e. constant pressure gradient), which minimizes changes in the sample during the measurement and facilitates the data acquisition. The disadvantage of this system is the possible deformation of the sample caused by the insertion method. Furthermore it is impossible to know the state of the sample inside the sample holder, because the sample is not visible during the experiment. Due to the scaffold extraction method after the experiment, it is not possible to distinguish deformations of the scaffold caused by insertion, water pressure or sample extraction.

The measured porosity of 95.7 % was 1 % smaller than the theoretical value of 96.7 % as calculated in Equation 2.6. The small standard deviation of 0.3 % shows the high reproducibility of the measurement which points to a consistent scaffold quality. The pore distribution assessed by mercury in-

trusion porosimetry showed that the pore diameters are distributed around about 100 μm which is similar to the salt particle size of 80 μm to 210 μm. An ideal pore size for materials used in tissue engineering is stated as 100 μm to 400 μm [10, 11] to allow enhanced bone ingrowth. Regarding this requirement the produced scaffolds are applicable for the use in bone tissue engineering.

Comparable studies showed permeability for polymer scaffolds (Polyvinyl alcohol, 150 μm pore size, porosity 60 %), lying in the same magnitude as the scaffolds measured here (2×10^{-10} m^2) [12]. Better permeability may be achieved by other scaffold production methods. Barry et al. [13] for example achieved methacrylate scaffolds with a permeability of 2×10^{-8} m^2 with about 90 % porosity by venting from polymer discs saturated with CO_2. Avoiding the random distribution of pores, Lee et al. [14] used rapid prototyping methods to make Poly(Propylene Fumarate) scaffolds. The result were scaffolds with 100 % open pores (size 300 μm) which reached even with a small porosity of 19 % a permeability of 2×10^{-11} m^2.

Even though it is not intended to culture a mature trabecular bone on the scaffolds, it is interesting to compare the scaffold characteristics with bone, to have an understanding of the structural similarity of both materials. The measured permeability coefficient of the porous PLA/glass composite corresponded to physiological values of trabecular bone in the magnitude of 10^{-8} to 10^{-14} m^2 [15–17]. The measured porosity was at the maximum of the physiological range found in trabecular bone with 30 % - 90 % [18].

2.6 Conclusions

- The produced cylindrical PLA/glass composite scaffolds resulted in dimensions 5% smaller than intended. This does not play a crucial role for the presented measurements, but it is recommended to use moulds, which take in account the shrink factor of 5% (12.6 mm length and 6.3 mm diameter) to produce scaffolds applicable for the bioreactor system.

- The high standard deviation observed for the permeability coefficient of the PLA/glass material may result from systemic error of the measurement method or heterogeneity of the scaffolds. It is suggested that the permeability measurement is much more sensitive to pore structure than the porosity measurement. Because the permeability measurement gives only a clue for the technical applicability of the material for the perfusion system, the high deviation of the permeability is regarded as tolerable.

- The porosity measurements conducted in this study showed high reproducibility and reasonable results compared to the theoretical porosity. Hence the used method of mercury immersion is deemed as appropriate for the characterization of the material. The porosity distribution assessed by mercury porosimetry showed that the scaffolds had pores big enough for intrusion by cells, which makes them applicable for bone tissue engineering.

- The similar porosity of PLA/glass composite and similar porous scaffold materials does not correlate with their differences in permeability, showing that porosity and pore interconnection depend on material and manufacturing method. It is recommended to include permeability as an essential property in scaffold characterization.

Bibliography

[1] M. E. Gomes, H. L. Holtorf, R. L. Reis, and A. G. Mikos. Influence of the porosity of starch-based fiber mesh scaffolds on the proliferation and osteogenic differentiation of bone marrow stromal cells cultured in a flow perfusion bioreactor. *Tissue Eng*, 12:801–809, 2006.

[2] M. Navarro Toro. *Desarrollo y caracterización de materiales biodegradables para regeneración ósea*. PhD thesis, Technical University of Catalonia, 2005.

[3] M. Charles-Harris Ferrer. *Development and Characterisation of Completely Degradable Composite Tissue Engineering Scaffolds*. PhD thesis, Technical University of Catalonia, 2007.

[4] I. F. Swindells, J. R. Coe, and T. B. Godfrey. Absolute viscosity of water at 20 °C. *J Res Natl Inst Stand Technol*, 48(1):2–31, 1952.

[5] F. J. O'Brien, E. Farrell, and M. A. Waller. *Topics in Bio-Mechanical Engineering*, chapter Scaffolds and cells preliminary biomechanical analysis and results for the use of a collagen GAG scaffold for bone tissue engineering. Trinity Centre for Bioengineering and National Centre for Biomedical Engineering Science, 2004.

[6] E. Puig. Disseny i fabricació duna màquina per mesurar el coeficient de permeabilitat a laigua dels biomaterials. Final Year Project Report at the Technical University of Catalonia, 2005.

[7] *Taschenbuch der Physik*. Verlag Harri Deutsch, 1998.

[8] Q.P. Hou, D.W. Grijpma, and J. Feijen. Porous polymeric structures for tissue engineering prepared by a coagulation, compression moulding and salt leaching technique. *Biomaterials*, 24(11):1937–1947, 2003.

[9] S. Lowell and J. E. Shields. *Powder Surface Area and Porosimetry*. Chapman and Hall, London, 2 edition, 1991.

[10] L. Galois and D. Mainard. Bone ingrowth into two porous ceramics with different pore sizes : An experimental study. *Acta Orthop Belg*, 70(6):598–603, 2004.

[11] E. Tsuruga, H. Takita, H. Itoh, Y. Wakisaka, and Y. Kuboki. Pore size of porous hydroxyapatite as the cell-substratum controls bmp-induced osteogenesis. *J Biomech*, 121:317–324, 1997.

[12] M. V. Chor and W. Li. A permeability measurement system for tissue engineering scaffolds. *Meas Sci Technol*, 2007.

[13] J. Barry, M. Silva, and S. Cartmell. Porous methacrylate tissue engineering using carbon dioxide to control porosity and interconnectivity. *J Mater Sci*, 41:4197–4204, 2006.

[14] T. C. Lee, F. J. O'Brien, T. Gunnlaugsson, R. Parkesh, and D. Taylor. Microdamage and bone mechanobiology. *Technol Health Care*, 14:359–365, 2006.

[15] E.A. Nauman, K.E. Fong, and T.M. Keaveny. Dependence of intertrabecular permeability on flow direction and anatomic site. *Ann Biomed Eng*, 27:517–524, 1999.

[16] M.J. Grimm and J.L. Williams. Measurements of permeability in human calcaneal trabecular bone. *J Biomech*, 30(7):743–745, 1997.

[17] P. W. Hui, P. C. Leung, and Andy Sher. Fluid conductance of cancellous bone graft as a predictor for graft-host interface healing. *J Biomech*, 29(1):123–132, 1996.

[18] Y.-X. Qin, W. Lin, Y. Xia, E. Mittra, C. Rubin, and R. Müller. *Advanced Bioimaging Technologies in Assessment of the Quality of Bone and Scaffold Materials*, chapter Non-invasive Bone Quality Assessment Using Quantitative Ultrasound Imaging and Acoustic Parameters, page 125. Springer, 2007.

Chapter 3

Development of a Perfusion Bioreactor System

3.1 Introduction

The goal of bone tissue engineering is the combination of cells and bioma-
terials to achieve *in vitro* cultured tissue substitutes used to bridge critical
tissue defects in patients. One of the main approaches consists in the culture
of cells on porous scaffolds, where the cells provide the active biological func-
tion for the integration, while the material provides support for the cells. It
has been shown that cell culture on scaffolds can be enhanced by the use of
bioreactor systems [1–3]. Bioreactor systems have to provide an uniform cell
seeding in 3D scaffolds, a control of nutrients and gases in culture medium,
an efficient mass transfer to the growing tissue and allow the application
of physiological stimuli to developing tissues [2]. One particular bioreactor
design which gained high interest in bone tissue engineering is the one of
perfusion bioreactor systems. By pushing fluid through porous scaffolds,
cells can be seeded on scaffolds and nutrients transported to the cells. It
has been shown that static culture leaves large porous scaffolds with regions
of insufficient nutrient concentration to sustain cell viability [3]. Perfusion
culture overcomes this shortcoming by enhancing cell viability and hence
improving the generated tissue structure [4, 5].

Different research groups have developed and used perfusion bioreactor
systems for tissue engineering research [4, 6–12, 12–15]. In general the de-

(a) Perfusion chamber design realised by Jaasma et al. [11].

(b) Perfusion chamber design used for longitudinal perfusion by Bancroft et al. [17].
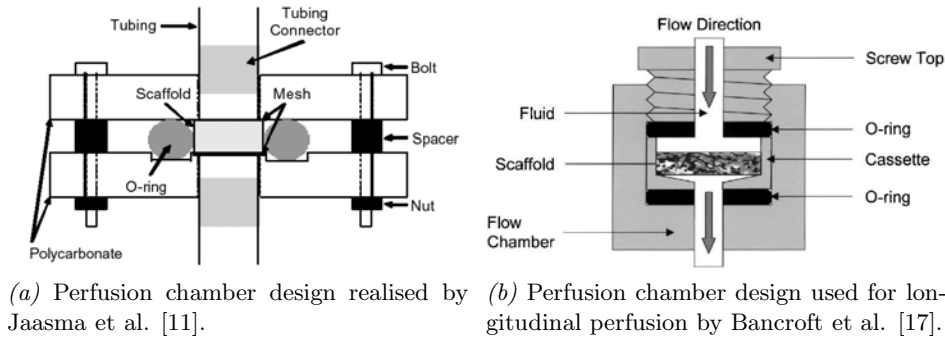
Figure 3.1: Perfusion chamber designs for perfusion bioreactor systems.

signs of the systems are quite similar, only distinguished by the different sample holder dimensions, the type of propulsion of the fluid through the scaffold and the level of complexity of the system. Perfusion bioreactor systems are used for different materials ranging from polymers [6] over calcium phosphate ceramics [7] to titanium meshes [8, 9]. Usually the scaffolds used are flat discs, with diameters larger than their heights [10–13], rather than diameters smaller than their heights [14]. The distance of perfusion through those scaffolds was usually in the range of a few millimetres (e.g. 6 mm as in [12]). Different propulsion systems were used for perfusion bioreactors. By moving a membrane to push fluid through scaffolds, small volumes of medium could be moved for the cell seeding and stimulation during cell culture [15], whereas peristaltic pumps were used to transport large amounts of fluids with the advantage of an easier control of fluid flow velocity [4, 16].

Some of the used perfusion bioreactor designs were modular systems, in which one perfusion chamber contains an individual scaffold (see Figure 3.1) [11, 12]. Other designs use blocks of sample holders for simultaneous perfusion of several scaffolds [6, 13]. Either way every scaffold is connected to its own channel of the perfusion system to allow control over the perfusion of the individual scaffolds. The modular perfusion chambers have the disadvantage of the large amount of system parts needed for larger sample numbers. But the individual design allows the replacement of damaged components and facilitates the reconfiguration of the system for different perfusion arrangements.

Furthermore the perfusion bioreactor systems used in research span a wide range of complexity. One of the more simple systems used was the

perfusion bioreactor developed by Olivier et al. [14], where a large scaffold was attached on a nozzle and immersed in cell suspension or medium. The medium was then pushed or pulled through the nozzle and hence through the scaffold. This design is very convenient, because it unified sample holder and medium reservoir, reducing the components of the system. More complex systems were developed for example by Wendt et al. [4] containing different tubing systems for cell seeding and cell culture and incorporating an oxygen sensor (see Fig. 3.2). Another sample for more complex systems was the modular perfusion bioreactor developed by Orr and Burg which not only served for perfusion cell culture, but also incorporated a mechanism for hydrostatic compression of the sample. Simple systems have the advan-
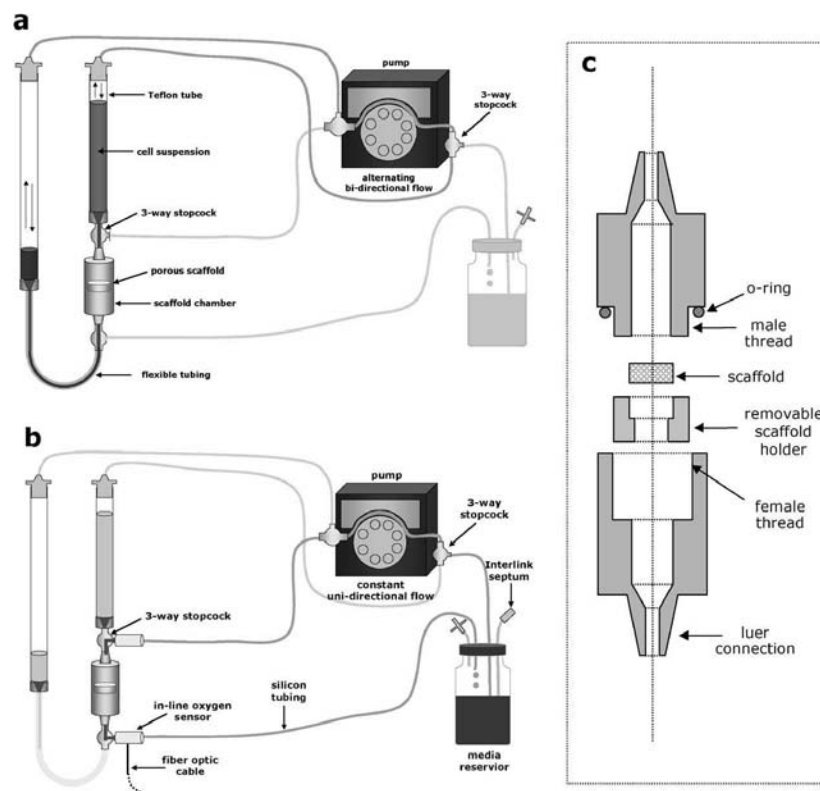
Figure 3.2: Complex perfusion bioreactor system developed by Wendt et al. [4] with configuration for cell seeding (a) and cell culture (b). The scaffolds were placed in perfusion chambers (c).

tage of consisting of as few as necessary components, keeping assembly and installation straightforward. The disadvantage consists in the limitation of control parameters, whereas more advanced systems have the possibilities of controlling perfusion parameters as well as culture parameters. Without any doubt increasing complexity brings in more factors for errors and contamination, which should be decreased as much as possible.

Based on those designs it was intended to develop a perfusion bioreactor system for cell seeding and cell culture by longitudinal perfusion of porous scaffolds. The system had to be applicable for large scaffold sizes, which up to day constitute a difficulty in bone tissue engineering. It should incorporate a direct fluid propulsion system to ensure perfusion of large medium volumes over long terms in cell culture. To allow the assembly in different experiment setups it had a modular structure and the system was held simple to reduce risks of contamination during assembly and mounting.

3.2   Objectives

The objective of the work presented in this chapter consisted in the development of a perfusion bioreactor system. The requirements for the development were:

- The perfusion bioreactor system should be adequate for cell seeding and cell culture over long periods with programmable perfusion fluid flow velocity profiles.

- Ideally the system incorporated mechanisms for cell seeding and cell culture in one assembly, to avoid the contamination risk of transferring seeded scaffolds to a culture system.

- A main component of the perfusion system was the perfusion chamber which held the scaffolds for perfusion. The perfusion chamber had to be applicable for scaffold dimensions of 6 mm diameter and 12 mm length and different material types, ranging from soft porous polymers to brittle glass ceramics.

3.3 Materials and methods

3.3.1 Scaffold material

The validation experiments for the perfusion bioreactor system were conducted with porous PLA/glass composite scaffolds fabricated as presented in Chapter 2.3.1. Scaffolds were fabricated by solvent casting particle leaching technique in polytetrafluoroethylene (PTFE) moulds. For this PTFE moulds with dimensions of 6.3 mm diameter and 13 mm depth were used to compensate the shrinking of the scaffold material previously observed in the scaffold characterisation (see Chapter 2). To confirm the sample dimensions, six fabricated scaffolds were measured with a calliper (TESA ShopCal, serial number 1K375806).

3.3.2 The perfusion bioreactor system

3.3.2.1 Perfusion bioreactor system assembly

System for cell seeding experiments The perfusion system for the cell seeding experiments presented in Chapter 4 consisted of system tubing and perfusion chambers, a peristaltic pump and a laptop computer (Acer Travelmate 372TCi) running custom software to control the pump. The pump dedicated for this perfusion bioreactor system was a commercially available pump peristaltic with 8 channels (type IPC, Ismatec, Art. No. ISM 931). The pump could support pressures of up to 1 bar (10^5 Pa) and its rotational speed could be adjusted in steps of 0.1 %. In this assembly, pump tubing of 2.79 mm inner diameter was used, which allowed fluid flow ranging from 0.35 ml/min to 35 ml/min. The pump had a RS-232 connection which allowed the control of the pump movements by commands sent from the connected laptop computer. The accuracy of the pump was stated by the manufacturer as $< \pm 1$ % per channel, where the accuracy between channels was stated with ± 5 %. The overall accuracy depended on different factors (e.g. type of the tube material, tube life time, temperatures and viscosity), so the deviation could amount up to 10 %. The main reason for inaccuracy is the tubing rather than the pump itself.

A USB-to-serial adapter (Prolific 2303) was used to connect the laptop to the peristaltic pump. For this, a RS-232 cross-linked cable was used as

an extension cable and modified to match the necessary connections for the peristaltic pump (see Table 3.1). For use of the connector with the laptop the USB-to-serial adapter was installed as COM port 2 using the driver version 2.0.2.8 provided by the adapter manufacturer.

Sub-D 9 (female)	Sub-D 9 (male)	Signal	Function
2	2	Tx	Transmit Data
3	3	Rx	Receive Data
5	5	GND	Electric ground

Table 3.1: Pin assignment on both Sub-D connectors for connection of pump to computer.

The tubing used for the perfusion system was chosen considering the application for cell culture and for pneumatically driving the cell suspension level for cell seeding. The tubing connected to the perfusion chambers was Tygon LFL (i.D. 6.4 mm, o.D. 9.6 mm) for the cell seeding experiments. Tygon LFL features a broad chemical resistance and non-ageing characteristics [18]. Tubing for the connection to the pump was stiff fluorinated ethylene propylene (FEP) tube (i.D. 3.2 mm, o.D. 4.8 mm) to prevent the buffering of the driving pneumatic force by the elasticity of the tube. FEP is characterized by its chemical inertness, toughness, flexibility, low coefficient of friction and non-stick characteristics [19]. All tubing materials were autoclavable or sterilisable by gamma-ray. The tubing was connected with polypropylene Luer-Lok connectors [20] which guaranteed the connectability to other commercially available standard components, like polycarbonate three way stopcocks, syringes and syringe filters.

The pump and the computer were located outside of the incubator (Thermo Forma Scientific Series II CO_2 Water Jacketed Incubator 3110) used to keep the perfusion chambers under continuous conditions, because they could not withstand the atmosphere in the incubator. Off-the-shelf pump tubing (Tygon LFL, 400 mm, i.D. 2.79 mm, o.D. 4.72 mm) was inserted into the pump cassette and connected via a three way stopcock to stiff FEP tubing (i.D. 3.2 mm, o.D. 4.8 mm, length 150 cm). The free connection on the valve was connected to syringe filters (0.22 μm, PES membrane), which allowed the escape of air during the injection of cell suspension into the system at the beginning of cell seeding. The stiff tubes were guided through a plastic disc with 5 mm diameter holes which was fixated with a threaded outlet

(i.D. 20 mm, o.D. 26 mm, length 85 mm). This outlet combined with the plastic disc ensured the sealing of the incubator interior, preventing leakage of the atmosphere to the outside. The stiff tubes were then connected inside the incubator to bigger diameter tubing (i.D. 6.4mm, o.D. 9.6 mm, length 15.5 cm, Tygon LFL), representing the tubing above the perfusion chambers. The perfusion chambers were connected to these tubes and held vertically in a custom-made rack. Between each other the perfusion chambers were connected with two pieces of tubing (length 8 cm each) and a three way stopcock representing the tubing under the perfusion chambers. All tubing was connected by attached Luer-Lok connectors (male or female) tightened with zip ties. Figure 3.3 and Figure 3.4 show the assembly of the seeding perfusion system.

The intended use of the cell seeding system began with the connection of the components with the scaffolds situated in the perfusion chambers. The valves on the top of the system (near the peristaltic pump) were opened to permit air to exit from the system. Then the cells were injected suspended in 10 ml of medium. This set the fluid on the start level on both sides of the system. All valves were closed and the alternating perfusion was conducted by initiating the control software. After the cell seeding, the top valves were opened again and the remaining medium was extracted (see Figure 3.5).
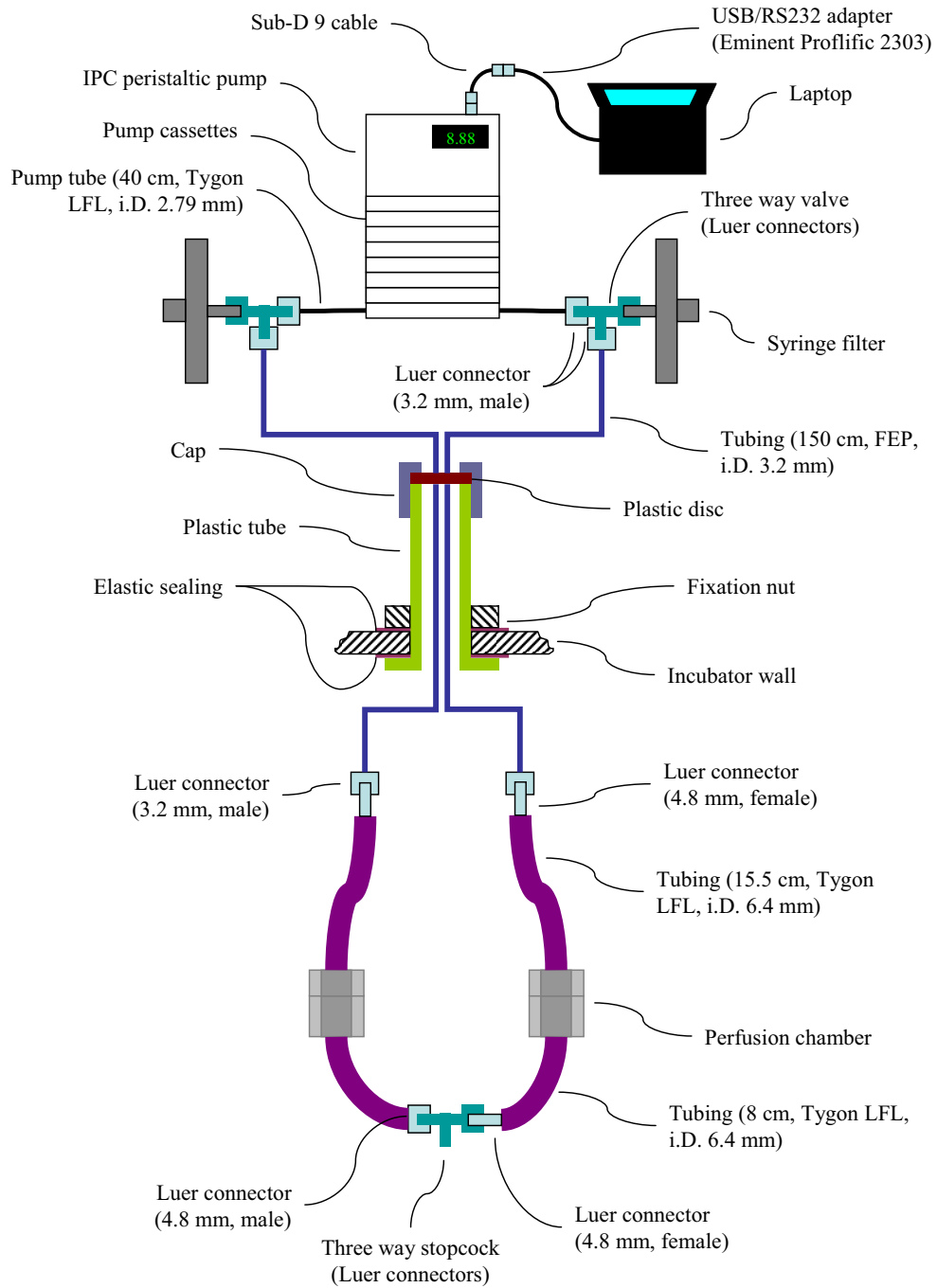
Figure 3.3: Graphic representation of the component assembly for the cell seeding experiments.

(a) Perfusion chambers mounted vertically in the incubator.

(b) FEP tubing exiting the incubator on the inside.
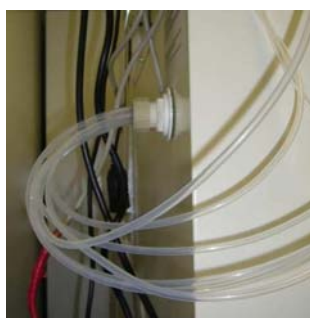
(c) FEP tubing exiting the incubator on the outside.

(d) Laptop and peristaltic pump situated on top of the incubator.

Figure 3.4: Setup of the perfusion system in the cell culture facilities.
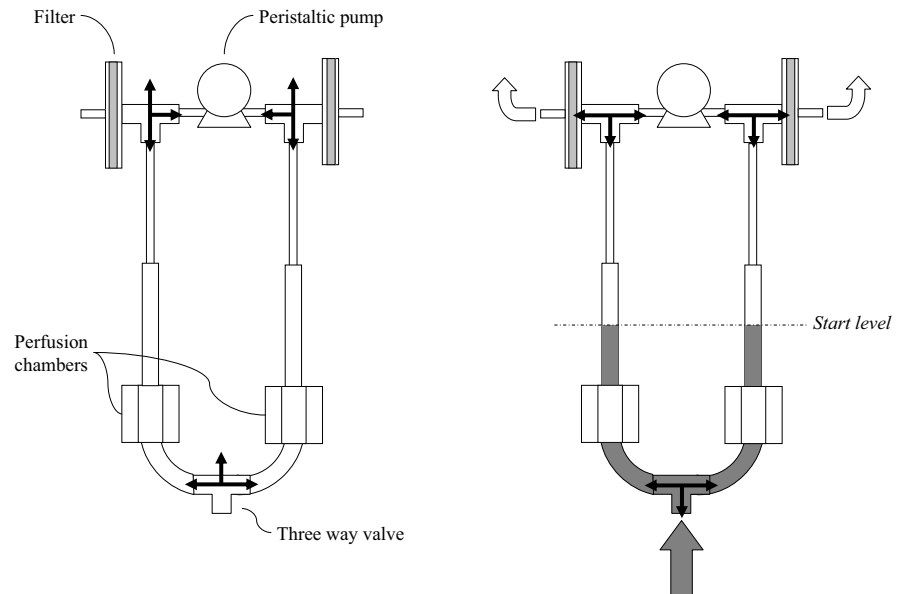
(a) The empty system before cell seeding. Perfusion chambers contain scaffolds.

(b) Cell suspension is inserted in bottom valve. Air escapes through filter on top valves.
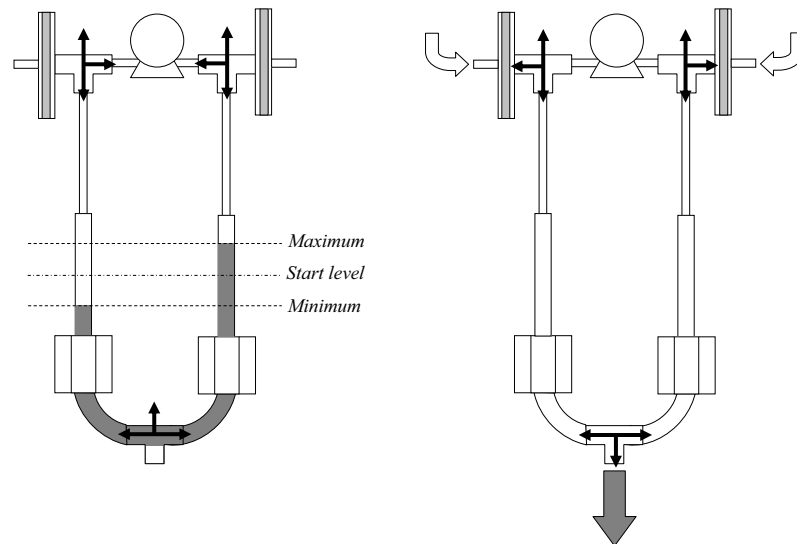
(c) Fluid levels in tubing oscillates between minimum and maximum level.

(d) After cell seeding the suspension is extracted through bottom valve. Air can enter through the top valves.

Figure 3.5: Use of the perfusion bioreactor system for cell seeding.

System for cell culture experiments   For the cell culture experiments (as described in Chapter 5) the seeding and culture were conducted in the same perfusion system. Compared to the system used in the seeding experiments presented before, some system components were changed. Two three way stopcocks were added above the perfusion chambers and the valve between the chambers eliminated (see Figure 3.6). The assembly of the system used in the cell seeding experiments was changed to allow the incorporation of a medium reservoir and the elimination of tubing to minimize the medium volume needed to fill the system. The tubing material was exchanged for silicone peroxide (Masterflex L/S 17, Cole-Parmer), because of the better properties regarding its use in cell culture and maintenance. Silicone peroxide is transparent, non-toxic, has broad resistance against chemicals and high temperatures [21]. Pump and controlling computer were left untouched from those changes.

As described in the system for cell seeding experiments a pump and computer were located outside of the incubator. The pump tube (Tygon LFL, 400 mm, i.D. 2.79 mm, o.D. 4.72 mm) was connected on both ends with three way stopcocks which connected to syringe filters on one end and to FEP tubing (i.D. 3.2 mm, o.D. 4.8 mm, length 150 cm) at the other end. The FEP tubing was led into the incubator through the door and clamped into place by the elastic door sealing. The FEP tubing was connected to silicone peroxide tubing (15.5 cm, i.D. 6.4 mm, o.D. 9.6 mm). Those large diameter tubes were connected over three way stopcocks to the perfusion chambers, which were joined by silicone peroxide tubing (10 cm, i.D. 6.4 mm, o.D. 9.6 mm) on the bottom (see Figure 3.6).

After the cell seeding the system was converted for the cell culture (see Figure 3.7). A 250 ml bottle (opening diameter 30 mm) was used as a reservoir. Three FEP tubes (i.D. 3.2 mm, o.D. 4.8 mm) were inserted into the reservoir through a rubber stopper which was used to close the reservoir. One tube connected the reservoir interior with the exterior to allow gas exchange through a filter. The two other tubes reached into the medium for the fluid transport through the system. Both tubes were connected to three way stopcocks, one connecting directly to the FEP tubing leading to the outside of the incubator, the other connected over a silicone peroxide tube (40 cm length, i.D. 2.79 mm) to the three way stopcock over one chamber.

The second FEP tube coming from the pump was connected to the other three way stopcock ion top of the second perfusion chamber, closing the circulatory system. The assembly for cell seeding and culture in an incubator is depicted in Figure 3.8.
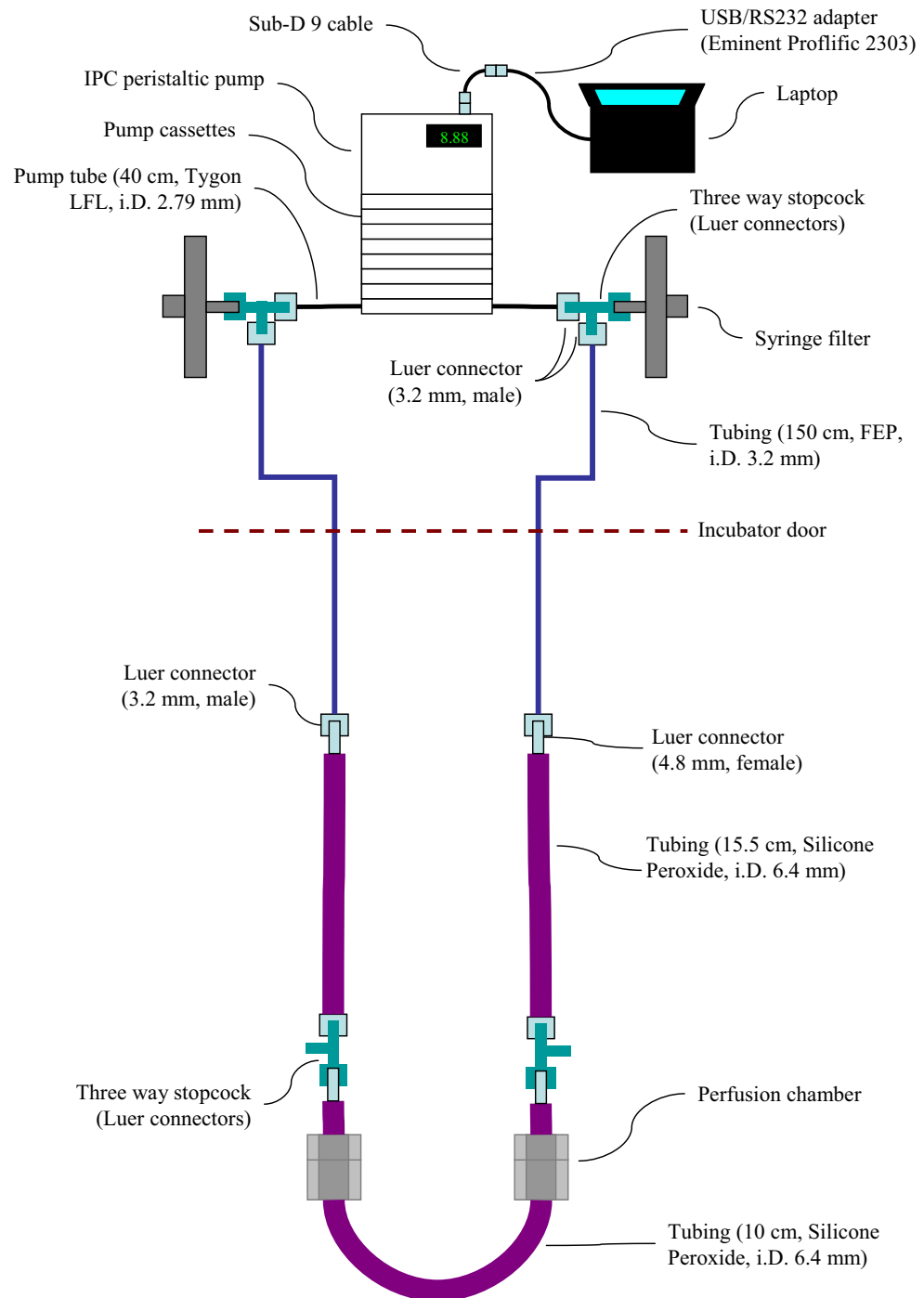
Figure 3.6: Schematic of the tubing connection for the cell culture experiments in the seeding phase.
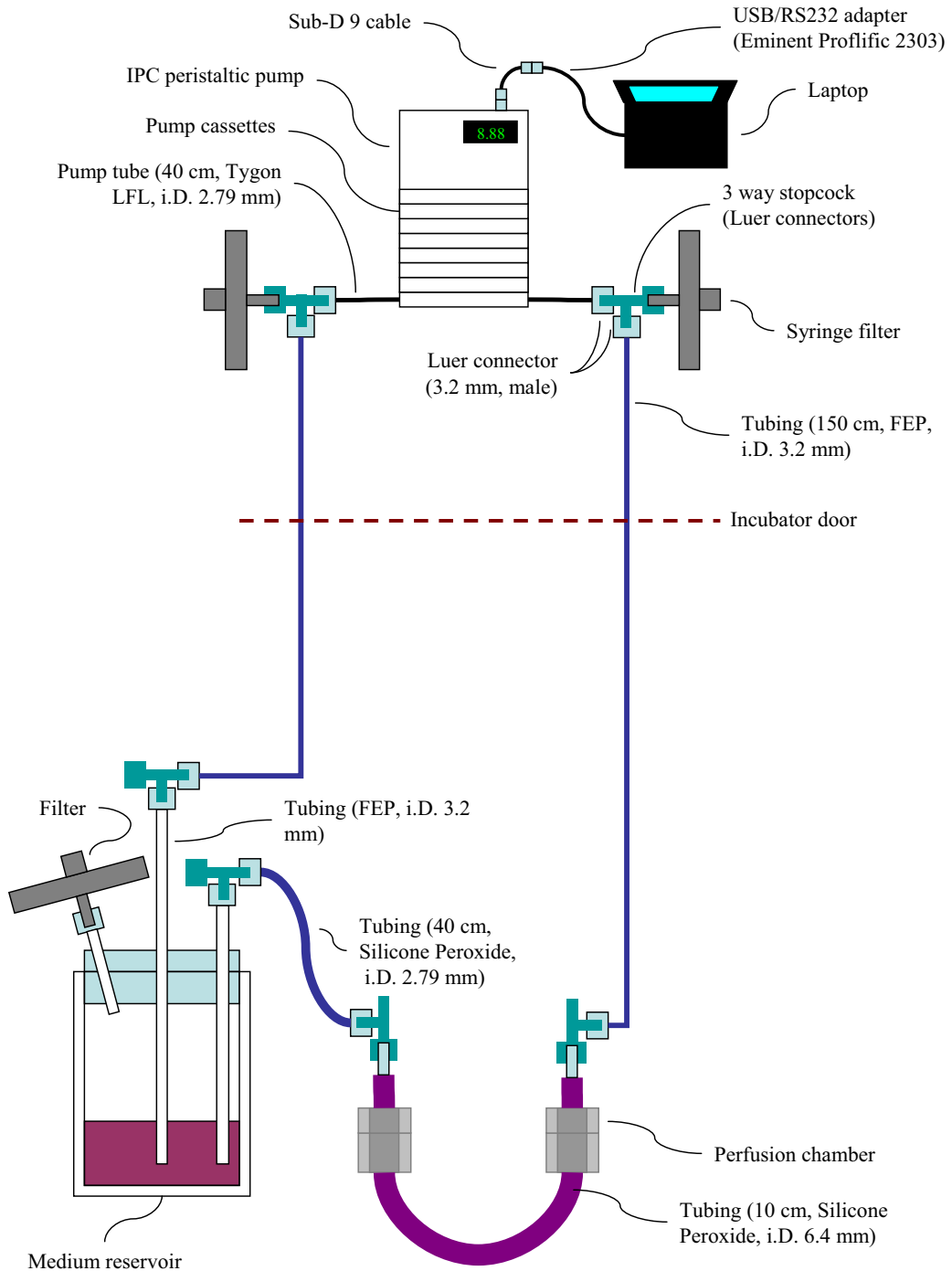
Figure 3.7: Schematic of the tubing connection for the cell culture experiments in the culture phase.

(a) Cell seeding phase including tubing for cell suspension level oscillation.

(b) Cell culture phase including the medium reservoir.

Figure 3.8: Mounting of tubing for the cell culture experiments in an incubator.

To use the system, the empty tubing was connected with the perfusion chambers which contained the scaffolds. For cell seeding the cell suspension was injected into the system through one of the three way stopcocks located on top of the perfusion chambers. Air was permitted to escape during the suspension injection through the filters situated near the pump. When the suspension was filled in and the suspension had the same level on both sides of the system, the pump was used to oscillate the levels, pushing the suspension through the scaffolds repeatedly. After cell seeding, the cell suspension was extracted through the valve above the perfusion chambers. To prevent a vacuum formation, the air inlets near the pump were opened to let air into the system. For cell culture, the two large diameter tubes above the perfusion chambers were taken off and the medium reservoir was connected to the system. By running the pump in either direction at low fluid flow rate the system was filled with medium. The pump was the used to apply the programmed perfusion pattern over a long period. After cell culture, the system was drained by letting air through the filter connected at the reservoir. See Figures 3.9 and 3.10 for a schematic of the perfusion bioreactor system use.
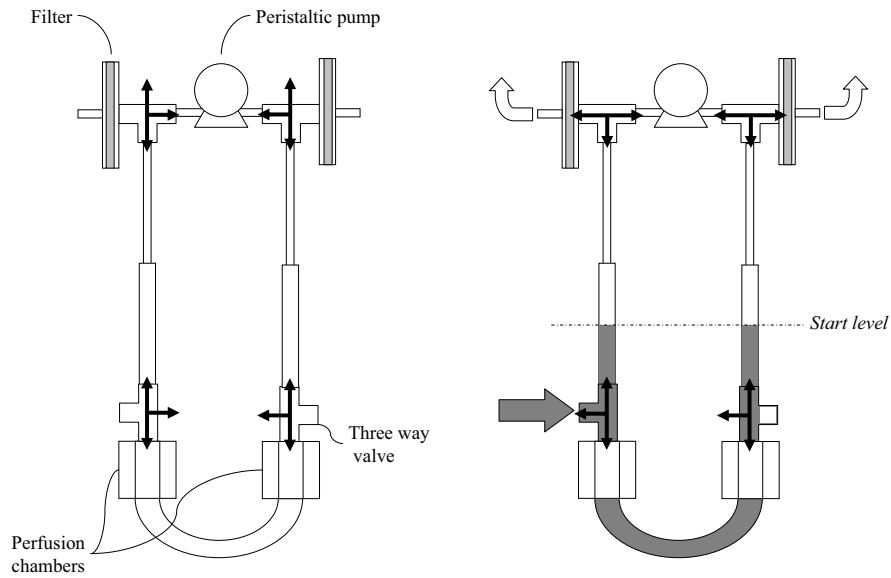
(a) The empty system before cell seeding. Perfusion chambers contain scaffolds.

(b) Cell suspension is inserted in side valve. Air escapes through filter on top valves.
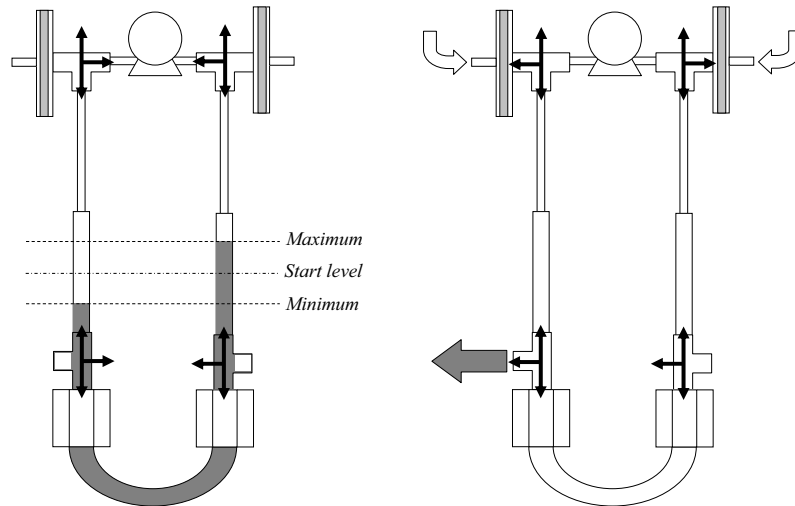
(c) Fluid levels in tubing oscillates between minimum and maximum level.

(d) After cell seeding the suspension is extracted through side valve. Air can enter through the top valves.

Figure 3.9: Use of the perfusion bioreactor system for cell culture (1 of 2).
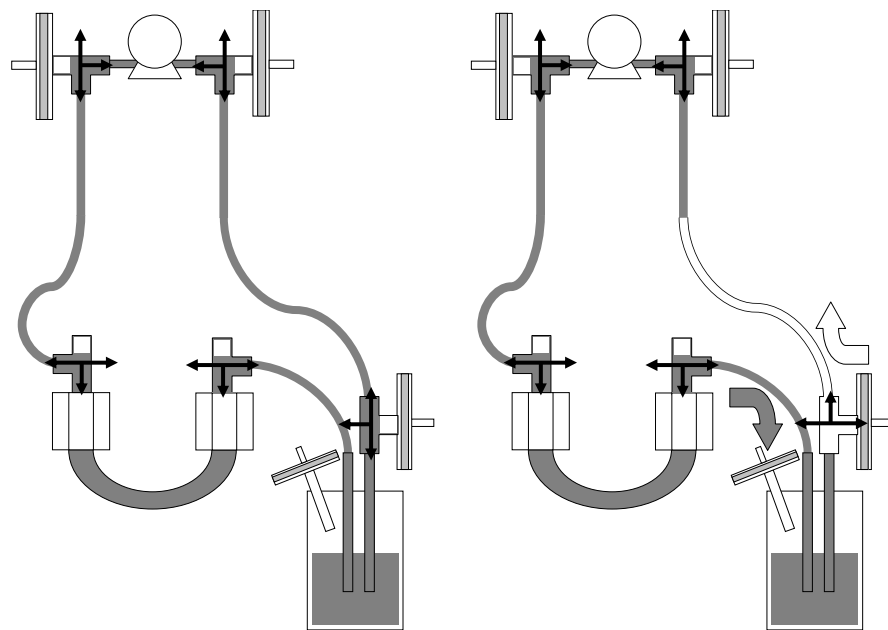
(a) Tubing pump is connected directly to the chambers and the medium reservoir. The entire tubing is perfused constantly with medium during culture.

(b) At the end of culture the tubing are emptied by letting air into the system at the reservoir.

Figure 3.10: Use of the perfusion bioreactor system for cell culture (2 of 2).

3.3.2.2 The perfusion chamber

The perfusion chamber for the bioreactor system was designed using CA-TIA Version 5 (Dassault Systemes) as 3D computer assisted design (CAD) program and fabricated in the workshop of the School of Industrial Engineering of Barcelona (ETSEIB). The design process for the perfusion chamber started from scratch, no previous model had been taken as a basis for the design. The presented design was the final product after three development iterations as presented in Figure 3.11. The idea for the first version was to inject the scaffold material directly into the polytetrafluoroethylene (PTFE) sample holder before polymerization to guarantee the sealing of the scaffold against the sample holder wall and prevent a compression of the scaffold. This had to be discarded, because the material adhered to the walls during fabrication and the scaffolds could not be extracted without destroying them in the process. Additionally the first version featured a bonding of the tubing to the chamber by silicone adhesive, which proofed not to be a good measure to attach the tubing (see Figures 3.11a and 3.11b). The sec-

(a) Version 1 assembled.

(b) Version 1 parts.

(c) Version 2 assembled.

(d) Version 2 parts.

(e) Version 3 assembled.

(f) Version 3 parts.
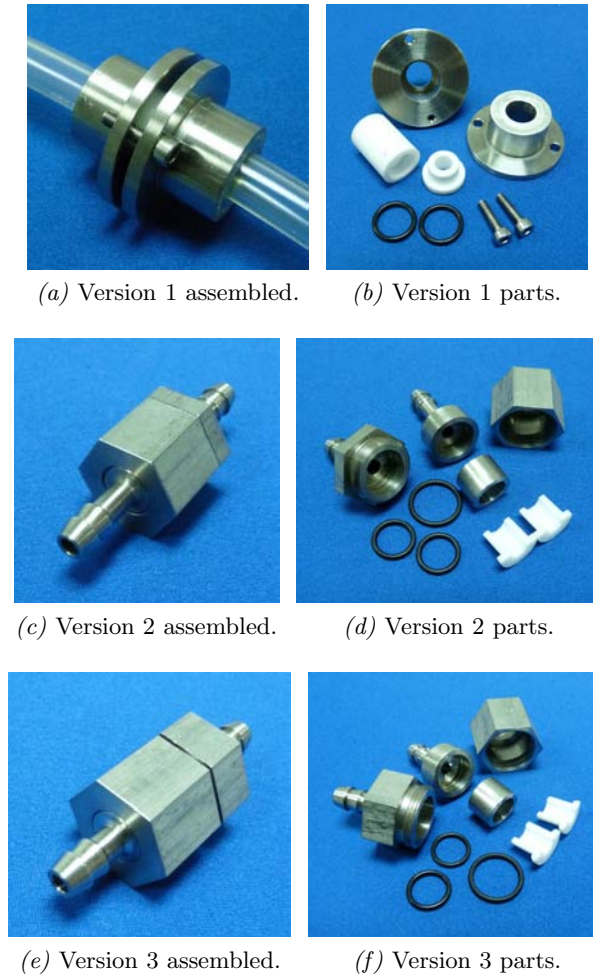
Figure 3.11: The three development stages of the perfusion chamber.

ond version of the perfusion chamber added the half-shell sample holder and tube connections (see Figures 3.11c and 3.11d). This version was identical in the inner dimensions to the final version, only the exterior dimensions were changed to make assembly easier.

The final version of the perfusion chamber was designed to hold scaffolds of 6 mm diameter and 12 mm length and allow a longitudinal perfusion of the scaffolds. PTFE was chosen for the half-shells of the sample holder to prevent the adhesion of the tissue developing in the scaffold to the chamber walls and to facilitate the scaffold extraction after the experiments. Stainless steel (ASTM A176 [22]) was selected as material for sample holder shell and housing, because of its long service life, which allows a prolonged use, especially of the threading. Furthermore stainless steel withstands the high

temperatures of the autoclaving process. In this design, a scaffold was situated between two PTFE half-shells which were then pushed into a stainless steel shell. The PTFE half-shells and the stainless steel shell constituted the sample holder. The sample holder was sealed against two lids with nitrile sealings (O-ring, i.D. 10.1 mm, o.D. 13.3 mm). Those sealings ensured that the fluid perfused the scaffold and did not escape along the outside of the sample holder. To prevent fluid from leaking out of the chamber, a nitrile sealing (O-ring, i.D. 14.1 mm, o.D. 17.3 mm) was placed between the two lids, sealing of the space containing the holder. The sealings had a diameter of 1.6 mm and lay in 1 mm deep grooves. The design was made to compress the sealings about 0.6 mm for sealing of the chamber. The two lids positioned over the holder were equipped with hose connectors which connected to elastic tubing with an inner diameter of 6.4 mm. One of the lids was threaded (Lid A), while the other had a smooth cylindrical exterior (Lid B). This allowed a nut to be slid over lid B and threaded onto lid A. This design prevented torsion of the O-rings when assembling the chamber, because the two lids were not forced to turn in respect to each other around the longitudinal axis. In Figure 3.12 a cross-sectional view of the chamber design is presented. A full set of the technical drawings of the perfusion chamber is provided in Appendix A.
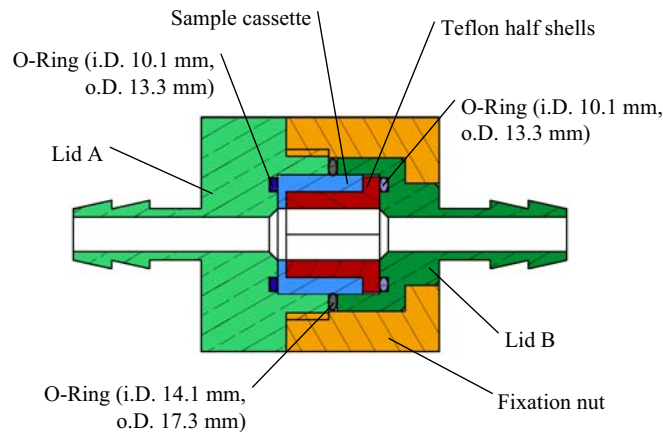
Figure 3.12: Cross-section of the perfusion chamber design.

Perfusion chambers were assembled as depicted in Figure 3.13. One scaffold was placed between the PTFE half-shells and the half-shells were inserted into the stainless steel shell (see Figures 3.13a and 3.13b). One O-ring was inserted in the groove at the bottom of lid A (see Figure 3.13c) and the sample holder was inserted into lid A (see Figure 3.13d). Another O-ring was slipped over the sample holder (see Figure 3.13e). The last O-ring was inserted into lid B (see Figure 3.13f) and the lid was slid over the sample holder (see Figure 3.13g). The fixation nut was then put over lid B and tightened with lid A (see Figure 3.13h).

(a) Sample holder parts and scaffold.

(b) Scaffold inserted in sample holder.

(c) O-ring placed in Lid A.

(d) Sample holder inserted in Lid A.

(e) O-ring slid over the sample holder.

(f) O-ring placed in Lid B.

(g) Lid B mounted on sample holder.

(h) Fixation nut threaded on Lid A.

Figure 3.13: Assembly of the final perfusion chamber design.

3.3.3 Software development

The software for the perfusion bioreactor system was written in `BASIC` and developed using iterative validation by testing small functional routines before incorporation into the main program. The software was written and compiled in Microsoft Visual Basic (Version 1.00) to obtain an executable file which was copied to the laptop used in the experiments. The syntax used to control the pump was provided by the manufacturer of the peristaltic pump. Table 3.2 lists the ASCII commands used in the developed software.

Command	Function
1J	Set pump clockwise
1K	Set pump counter-clockwise
1H	Start pump
1I	Stop pump
1S00999	Set pump to 99.9 % of max. Flow

Table 3.2: ASCII commands used to control the peristaltic pump and their corresponding functions.

3.3.3.1 Cell seeding software

The cell seeding software was developed to control the peristaltic pump to generate an oscillating movement of cell suspension through the scaffolds. During the preparation of the system for the cell seeding, cell suspension was injected at the bottom of the system. During each oscillation cycle, the entire volume of the bottom part of the system (4.5 ml) was to be moved through the scaffolds in both directions. It was defined that half of the bottom volume had to be moved in every half cycle through the scaffold to minimize the length of ascending tubes on top of the perfusion chambers. The bottom volume combined with the selected fluid flow velocity determined the time needed to move the volume in one cycle and hence the frequency of the oscillation. Equation 3.1 shows the relation between the frequency f, the constants cross-sectional area A at the scaffold entry and volume V and the variable velocity v.

$$f = \frac{1}{t} = \frac{Q}{V} = \frac{A \times v}{V} \tag{3.1}$$

Table 3.3 shows the four fluid flow velocities for the cell seeding experiments and their corresponding frequencies. Hence high perfusion velocities lead to high perfusion frequencies.

v [mm/s]	f [Hz]
1	0.006
5	0.03
10	0.06
15	0.09

Table 3.3: Fluid flow velocities used in the cell seeding experiments and their corresponding theoretical frequencies.

The oscillating velocity profile was chosen as a square wave form which signified that the software had to invert the direction of the fluid flow after every half-cycle. It is important to notice that lower perfusion velocities decrease the perfusion frequency and hence increase the total seeding time for a constant perfusion cycle number.

Function of the cell seeding software   The parameters determined by the user were the velocity of the fluid flow v and the number of cycles n_{cycles}. The fluid flow velocity was converted by the software to volume velocity Q based on the convention that the entrance area A of the scaffold was 28.27 mm^2 according to its diameter of 6 mm (see Equation 3.2). It is important to notice that the velocities occurring in the pathways through the scaffolds are not equal to the overall velocity.

$$Q = A \times v \tag{3.2}$$

The peristaltic pump had to be calibrated before the experiment. The calibration determined the maximal fluid flow Q_{max} which could be pumped by the peristaltic pump. The maximal flow value was necessary to calculate the percentage of pump velocity needed to achieve the intended fluid flow. The function of the cell seeding software was sequentially:

1. Convert the input velocity v [mm/s] to a pump-readable signal [%].

    (a) Input the maximum flow of the pump Q_{max} (e.g. 34.0 ml/min).
    (b) Input the desired velocity v (e.g. 10 mm/s).

    (c) Calculate for the diameter of 6 mm the fluid flow Q (e.g. 16.96 ml/min).

    (d) Calculate the percentage Q_{proz} of the max. flow (e.g. 48.2 %).

    (e) Translate to a compatible signal for the IPC pump (e.g. 48.2 % → `1S00482`).

2. Calculate time t_{half} for a half-cycle.

    (a) Divide volume V (2.25 ml) by the fluid flow Q to get $V/Q = t_{half}$ (e.g. 8 s).

3. Start the perfusion cycles.

    (a) Set the pump counter-clockwise.

    (b) Start pump with Q_{proz} for $t_{half}/2$; This drives the medium levels to start position.

    (c) Stop pump and set it clockwise.

    (d) Start pump with Q_{proz} for t_{half}.

    (e) Stop pump and set it counter-clockwise.

    (f) Start the pump with Q_{proz} for t_{half}.

    (g) Repeat (c) - (f) for desired cycle number n_{cycle}.

    (h) Stop pump.

4. End program.

During the perfusion cycles every signal sent to the pump was written to a text file as a measure for later control. One limitation encountered during the programming in connection with the pump was that the pump had a latency period of approximately 0.5 s which prohibited to send commands non-stop. This limited the perfusion alternating frequency to 1 Hz. The functions of the software are depicted in more detail in the flowcharts presented in Figure 3.14, 3.15 and 3.16.
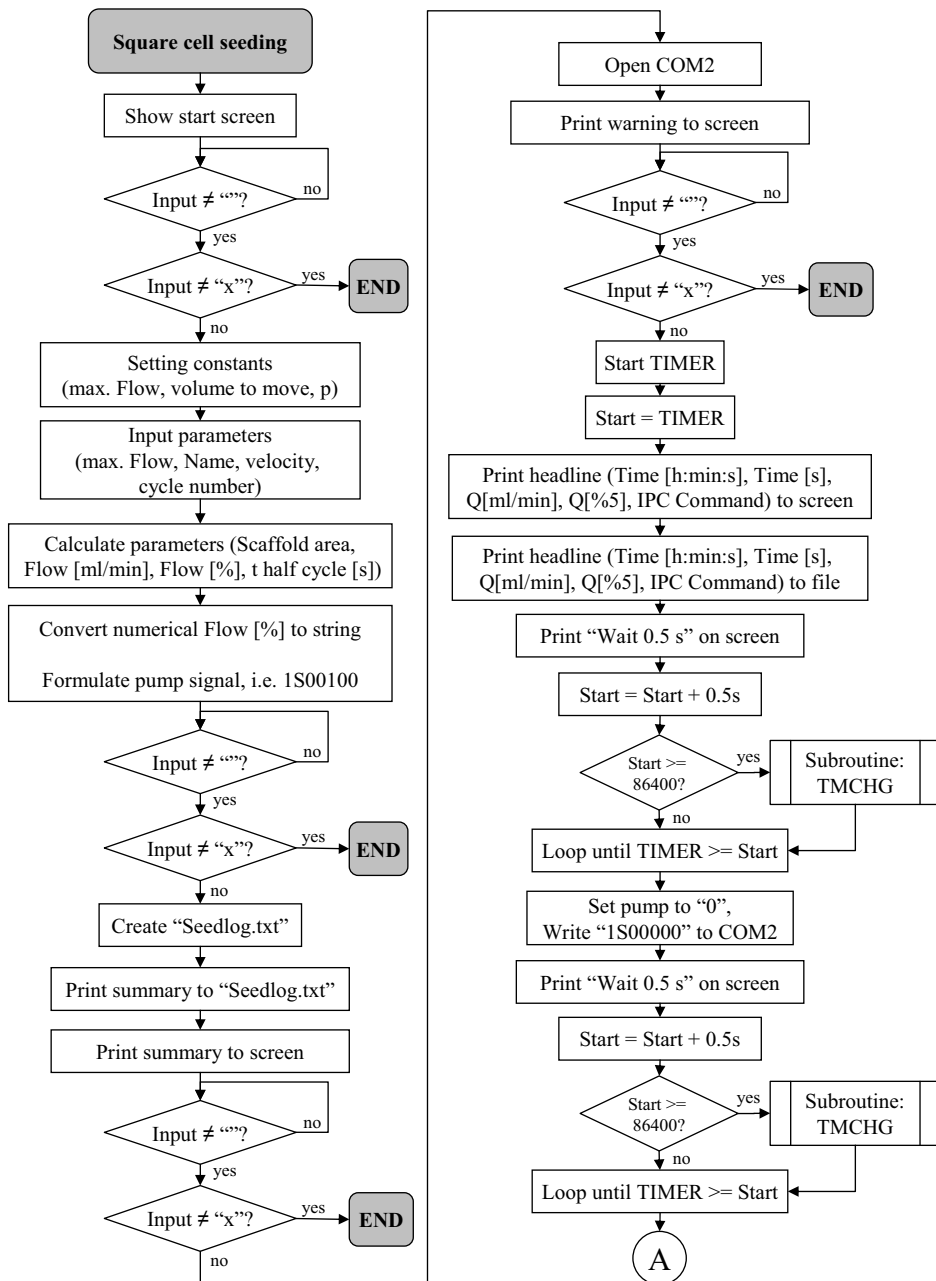
Figure 3.14: Cell seeding software flowchart (1 of 3).
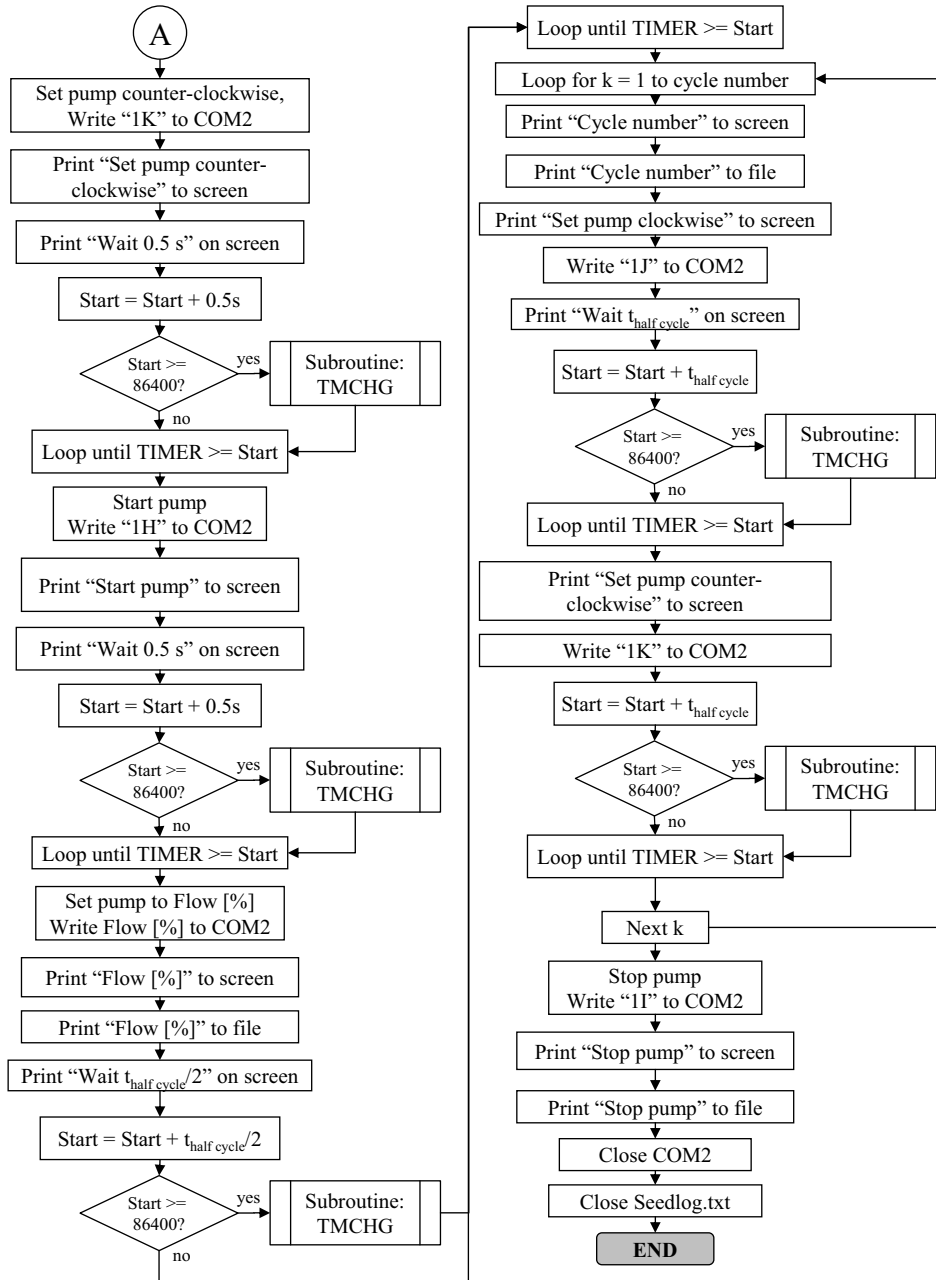
Figure 3.15: Cell seeding software flowchart (2 of 3).
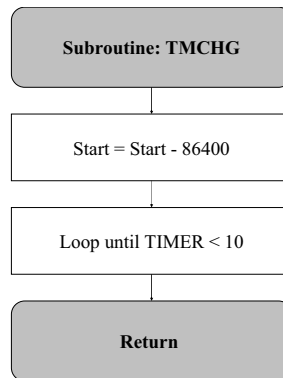
Figure 3.16: Cell seeding software flowchart, subroutine "tmchg" (3 of 3).

The main functions of the software were the establishment of the COM2 connection, the conversion of fluid flow to pump signal and the control of the timer status. The connection to the pump was established by opening the COM2 port by use of the following code.

```
OPEN "COM2:9600,n,8,1,CS,DS,RS" FOR RANDOM AS #1
```

The COM2 port was opened with a baud rate of 9600, no parity bit, 8 data bits, 1 stop bit and assigned it the directory number #1.

The conversion of the desired fluid flow velocity to the pump command was managed by calculating first the percentage of the maximum fluid flow. The percentage fluid flow was rounded to one decimal place and converted to a string. This string was then added to a prefix depending on the size of the percentage. The following excerpt from the source code shows this function.

```
...
y! = INT(Qproz * 10 ^ 1 + .5)
speed$ = STR$(y!)
speed$ = LTRIM$(speed$)
IF y! < 10 THEN GOTO 111
IF y! < 100 THEN GOTO 112
IF y! < 1000 THEN GOTO 113
IF y! < 10000 THEN GOTO 114
111
speed$ = "1S0000" + speed$
```

```
GOTO 115
112
speed$ = "1S000" + speed$
GOTO 115
113
speed$ = "1S00" + speed$
GOTO 115
114
speed$ = "1S0" + speed$
GOTO 115
115
...
```

One problem encountered in the development of the cell seeding software was caused by the use of the `TIMER` function. All timing in the program is achieved by comparing the actual `TIMER` to the time value desired. This caused a problem every time the day changed, because the `TIMER` value counts seconds from 0 (for 00:00:00 in hours:minutes:seconds) to 86399 (23:59:59), representing the number of seconds of the day. After a change from 23:59:59 to 00:00:00 the `TIMER` value changes from 86399 to 0. The overcome this problem, the variable `Start` was set to the actual timer value, the amount of time to wait was added and, in case the sum was bigger or equal to 86399, the program went to the `tmchg` subroutine. In the subroutine, the 86400 was subtracted from the `Start` value followed by a loop until the `TIMER` value changed from 86399 to 0 (see Figure 3.16). The following code illustrates the function:

```
...
Start = TIMER
...
Start = Start + t
IF Start >= 86399 THEN GOSUB tmchg
...
tmchg:
Start = Start - 86400
DO
LOOP UNTIL TIMER <= 10
RETURN
...
LOOP UNTIL TIMER >= Start
...
```

After returning from the subroutine the main routine waited for the remainder of the waiting period. The complete source code of the software is provided in Appendix C.

Use of the cell seeding software   The first screen appearing when running the software was the start screen, showing the name of the program (see Figure 3.17). By pressing the 'x' key the program could be stopped or by pressing any key the program could be continued.

The next screen served to enter the name of the experimenter, the fluid flow velocity and the number of cycles desired. Pressing the 'x' key stopped the program. After pressing any key the entered data as well as calculated parameters were displayed as a summary (see Figures 3.18 and 3.19). Again, pressing the 'x' key stopped the program, pressing any key continued the program.

The user was presented in the next screen with a warning that the pump cycles were going to start. At this point the user was reminded that the pump had to be connected at COM2 of the computer, that the pump was turned on, the power supply should be guaranteed over the duration of the experiment and that the cell suspension levels should have two equal medium levels in the tubing with at least 3.5 cm over the perfusion chambers (see Figure 3.20). Pressing the 'x' key stopped the program, pressing any key started the cell seeding cycles.

The program started then to write commands to the peristaltic pump and to a log file (see Figure 3.21). In this phase the program could not be stopped until all cycles were complete. After ending all cycles the program stopped and asked the user to press any key to close the application.
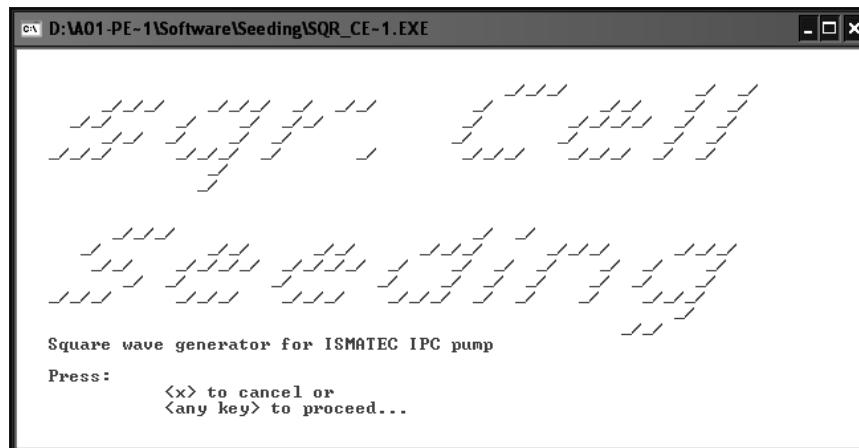
Figure 3.17: Screenshots of the cell seeding program; Start screen.

Figure 3.18: Screenshots of the cell seeding program; Parameter input.

Figure 3.19: Screenshots of the cell seeding program; Summary.

Figure 3.20: Screenshots of the cell seeding program; Warning message.

Figure 3.21: Screenshots of the cell seeding program; Writing to IPC pump.

3.3.3.2 Cell culture software

Function of the cell culture software The software developed for cell culture had to take into account the cell culture perfusion profile. The culture profile consisted of recurring cycles with a duration of 24 hours divided into two periods. The first period was the period for cell stimulation in which medium oscillated through the scaffolds at a high velocity with the intention to stimulate the cells. The second period provided a constant low perfusion velocity to transport nutrients to the cells and eliminate metabolism waste products.

For the stimulation period with oscillating fluid flow the user entered in the program the velocity v_1, the time for every flow direction t_1, which determined the frequency of the stimulation, and the total time for the stimulation period t_{total}, which determined the number of oscillations performed. For the second period the velocity v_2 for the medium transport to the cells was provided by the user (see Figure 3.22). The cell culture software had
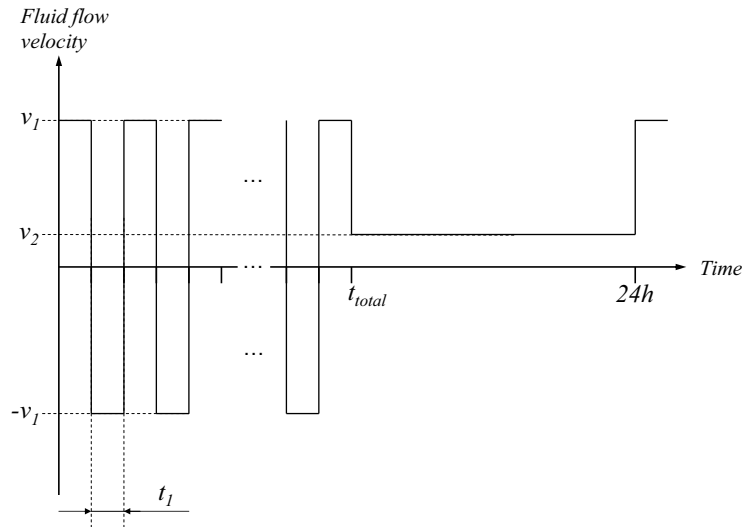
Figure 3.22: Cell culture profile and variables.

the following sequential function:

1. Convert the input velocity to a pump-readable flow.

   (a) Input the maximum flow of the pump Q_{max} (e.g. 34.0 ml/min).

(b) Input velocity v_1 and v_2 (e.g. 10 mm/s and 1 mm/s).

(c) Calculate for the diameter of 6 mm the fluid flow $Q_1 = A \times v_1$ and $Q_2 = A \times v_2$ (e.g. 17.0 ml/min and 1.7 ml/min).

(d) Calculate the percentage of the max. flow Q_{proz1} and Q_{proz2} (e.g. 48.2 % and 4.8 %).

(e) Translate to compatible signal for the IPC pump (e.g. 48.2 % → 1S00482, 4.8 % → 1S00048).

2. Calculate number of stimulation cycles.

(a) Get input for t_1 and t_{total}.

(b) Calculate the rounded number of cycles by $|n_{cycle}| = \dfrac{t_{total}}{2 \times t_1}$.

3. Conduct stimulation period perfusion cycles.

(a) Stop pump, set pump clockwise.

(b) Start pump with Q_{proz1} for t_{half}.

(c) Stop pump, set pump counter-clockwise.

(d) Start pump with Q_{proz1} for t_{half}.

(e) Repeat (a) - (d) for desired cycle number n_{cycle}.

4. Conduct continuous nutrition period.

(a) Stop pump, set pump clockwise.

(b) Start pump with Q_{proz2} for $24h - t_{total}$.

(c) Begin new "Stimulation period" (go to point 3).

During the perfusion cycles every signal sent to the pump was written to a text file as a measure for later control. These 24 hour cycles run until the system was stopped by pressing the 'x' key or paused by pressing the 'p' key for ending or pausing the program. The software for cell culture was written according to the previously defined requirements. The user entered the values for the stimulation period (v_1, t_1 and t_{total}) and the nutrition period (v_2). Figures 3.23, 3.24, and 3.25 depict the detailed flowcharts of the main program function, while Figure 3.26 shows the subroutines for day change and pause mode. The routine for the day change (the change of the `Timer` from 86400 to 0 at midnight) has been described earlier as a subroutine for the cell seeding software. The whole source code is provided in Appendix D.

One of the new key functions in this software was the pause function. This function halted the pump activity until any key is pressed. To achieve

this the remaining waiting period was calculated by subtracting the current `TIMER` value from the `Start` value and the pump was stopped. When resuming the pump process, the remaining time was added to the `TIMER` value to determine the new `Start` parameter. The pump profile was hence shifted by the pause function by the amount of time spent in pause mode.

```
...
Start = TIMER
...
Start = Start + 2
IF Start >= 86399.99 THEN GOSUB tmchg
DO
LOOP UNTIL TIMER >= Start
char$ = INKEY$
SELECT CASE char$
CASE "x"
GOTO 999
CASE "p"
GOSUB pause
...
pause:
PRINT #1, "1I" 'stop perfusion
PRINT
pt = Start - TIMER
PRINT "You are in pause mode!"
PRINT #2, TIME$, TIMER, "*** Perfusion paused ***"
PRINT
PRINT "Hit any key to proceed!"
DO
char$ = INKEY$
LOOP UNTIL char$ <> ""
Start = TIMER + pt
PRINT "Returned from Pause mode..."
PRINT #2, TIME$, TIMER, "*** Returned from pause ***"
PRINT #1, "1K" 'start perfusion again
RETURN
...
```

The pause subroutine is illustrated in Figure 3.26.
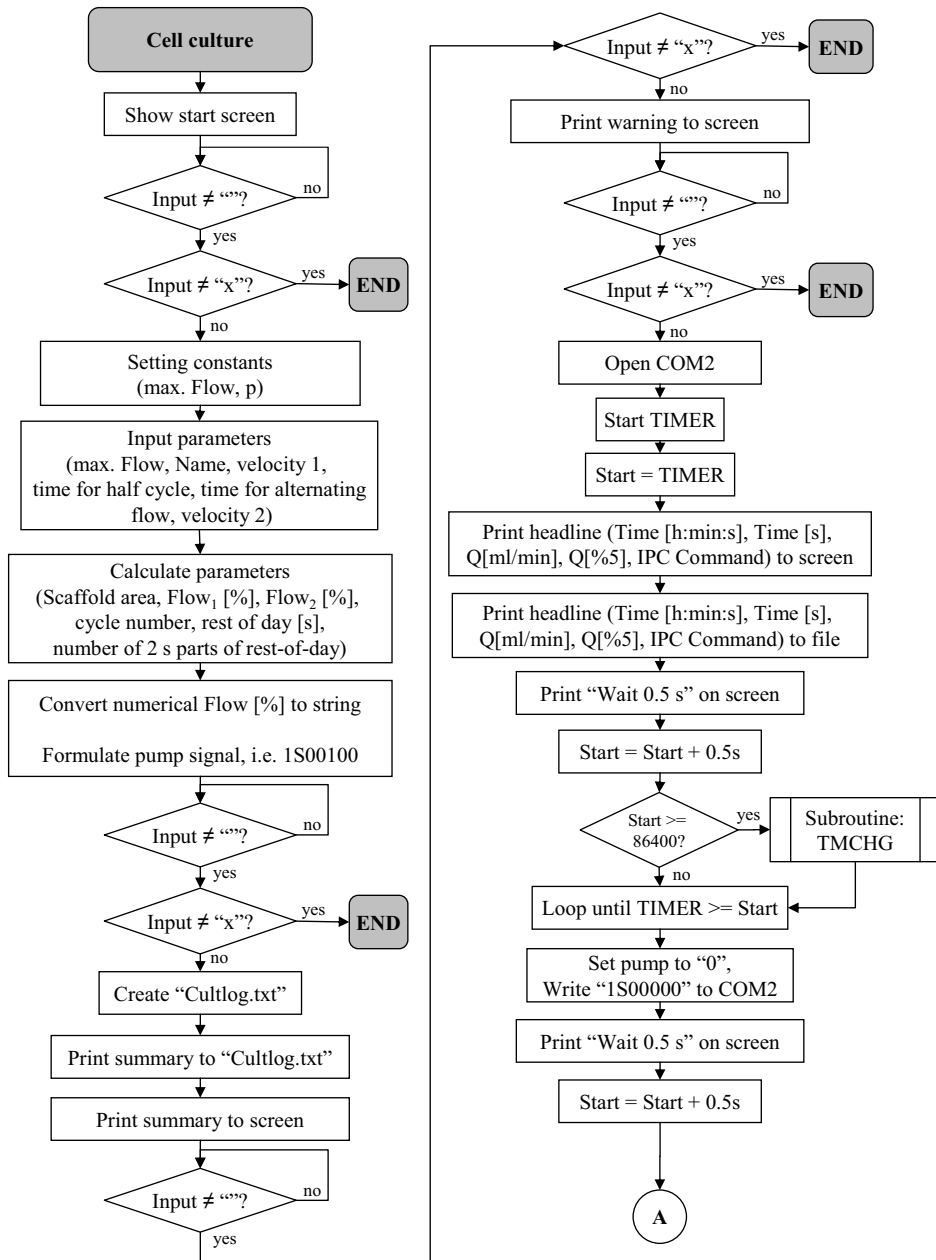
Figure 3.23: Cell culture software flowchart (1 of 4)
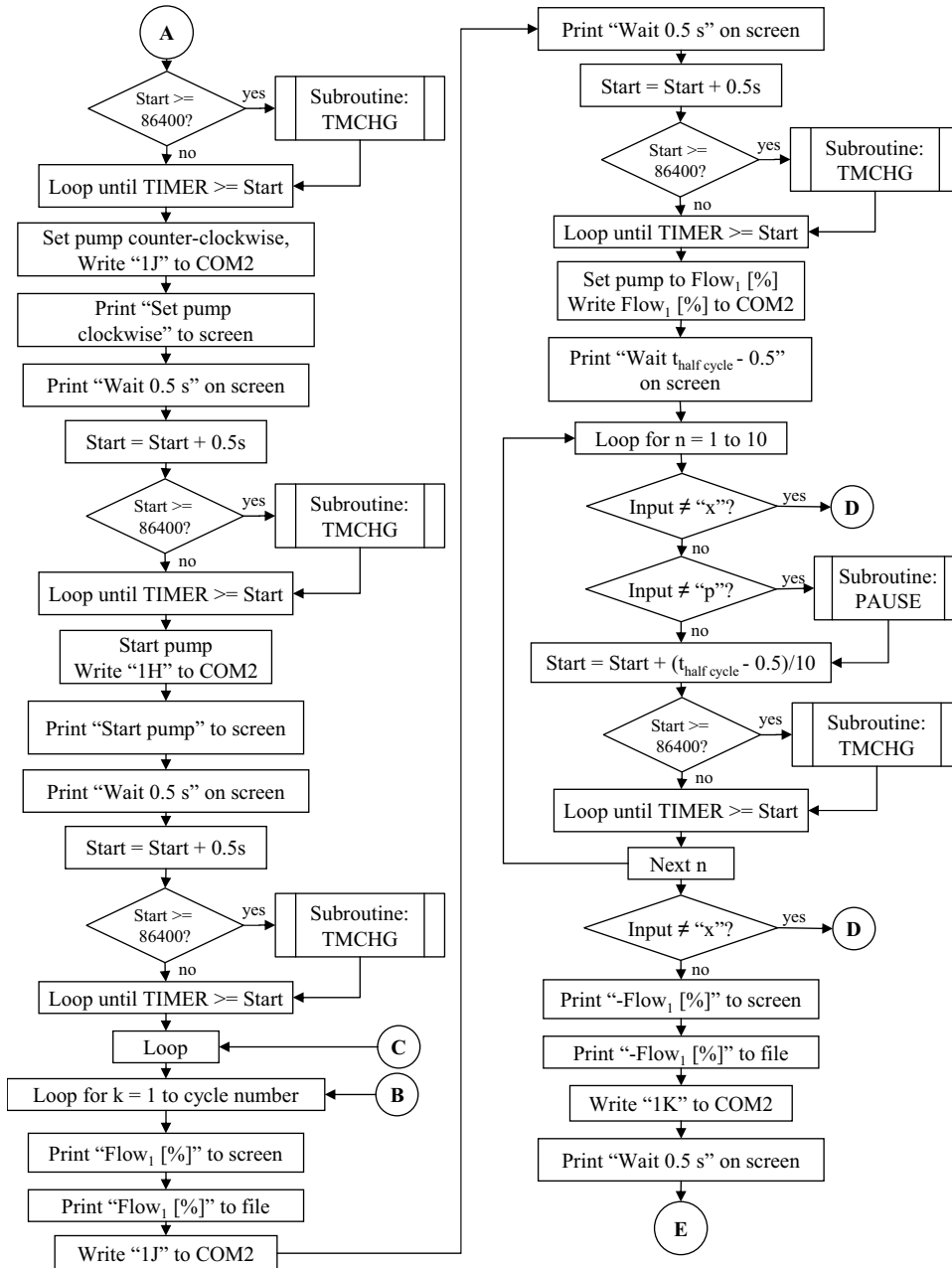
Figure 3.24: Cell culture software flowchart (2 of 4)
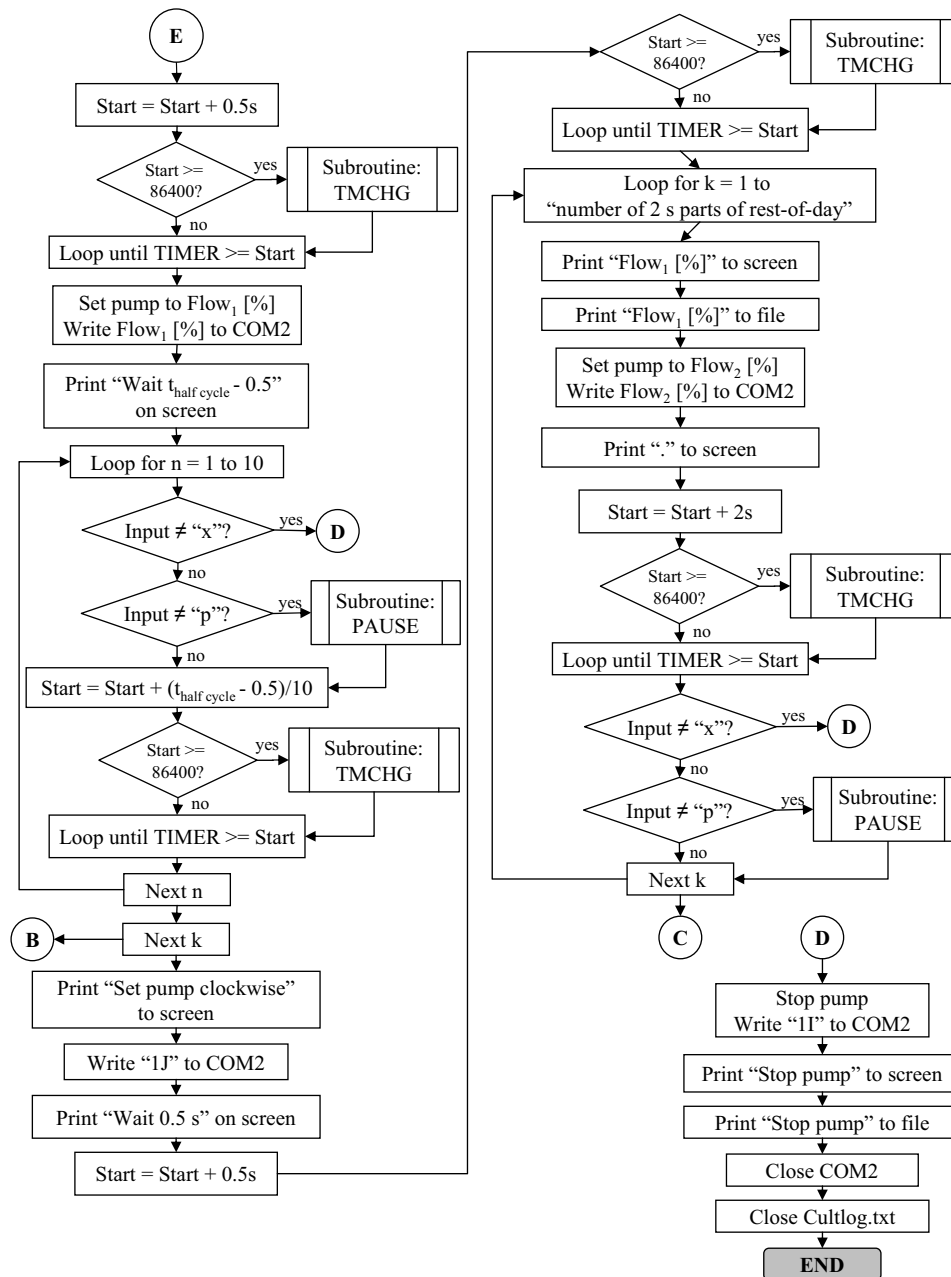
Figure 3.25: Cell culture software flowchart (3 of 4)
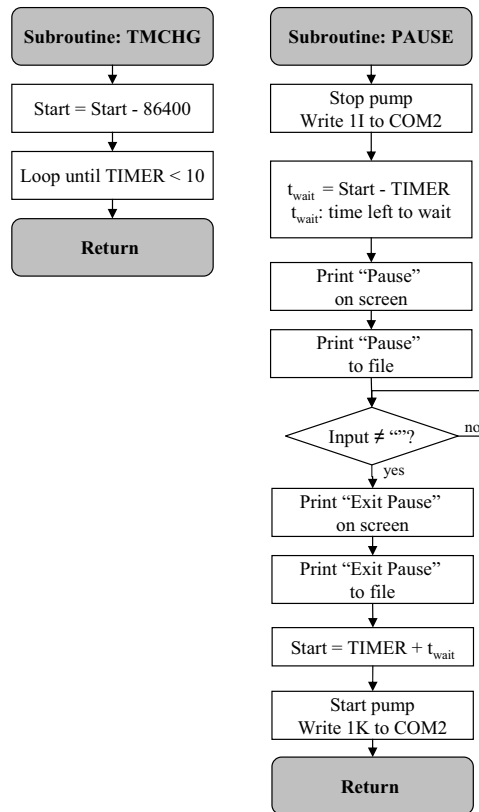
Figure 3.26: Cell culture software flowchart (4 of 4)

Use of the cell culture software   When executed, the software showed
a start screen as presented in Figure 3.27 with the name of the program. By
pressing 'x' the software could be stopped, pressing any other key led the
user to the next screen. The input screen showed a graphic representation
of the variables for the cell culture (see Figure 3.28). The user was asked
to enter values for the variables v_1, t_1, t_{total} and v_2 as explained previously.
After entering the values, the program proceeded to show a summary of all
entered and calculated parameters (see Figure 3.29). The program could
again be cancelled by pressing 'x' or proceeded by pressing any other key.
The user was presented with a warning that the pump has to be connected to
the COM2 port and that power supply should be guaranteed for the duration
of the experiment (see Figure3.30). Pressing 'x' stopped the program at this
point, any other key did start the perfusion profile. During the perfusion
profile the commands were printed on screen and to a log file (see Figure
3.31). By pressing the 'p' key, the software went into pause mode (see Figure
3.32). The pause mode was left by pressing any key and the perfusion profile
was resumed. By pressing the 'x' key the program could be ended (see Figure
3.33).

Figure 3.27: Screenshots of the cell culture program; Start screen.

Figure 3.28: Screenshots of the cell culture program; Parameter input.

Figure 3.29: Screenshots of the cell culture program; Summary.

Figure 3.30: Screenshots of the cell culture program; Warning.

Figure 3.31: Screenshots of the cell culture program; Writing to peristaltic pump.

Figure 3.32: Screenshots of the cell culture program; Pause mode.

Figure 3.33: Screenshots of the cell culture program; End of the program.

3.3.4 Fluid flow velocity validation

The fluid flow profiles applied with the perfusion bioreactor system were validated by determination of the pump accuracy. This included the fluid displacement control by software, as well as the accuracy of the pneumatic displacement of fluid through the scaffolds.

3.3.4.1 Verification of the pump control on the displaced volume

The volume transfer at different pumping velocities was measured to assess the accuracy of the used peristaltic pump in combination with the developed software. For this, a pump tube (Tygon LFL) of 40 cm length and internal diameter of 2.79 mm was inserted into the peristaltic pump cassette. After calibrating the pump according to the manual, the pump tube was immersed in distilled (MilliQ) water on one end, the transported volume was collected on the other end with a beaker. The laptop for control of the pump was connected to the pump via the RS-232 interface and the software for flow control executed. The pump was controlled by the software to pump 2.25 ml at velocities of 1 mm/s, 5 mm/s, 10 mm/s and 15 mm/s. The velocities referred to the 6 mm diameter of the scaffold the fluid would have to pass in the perfusion bioreactor. Before and after each transport the recipient was weighed and the volume of added water calculated (Equation 3.3).

$$\Delta m_{H_2O} = \rho_{H_2O} \times \Delta V \tag{3.3}$$

This test was repeated six times for the four velocities. The four groups were then compared using the Mann-Whitney U test to determine statistical significant differences. This comparison was made to ensure that the volume displacement was not dependent directly on the velocity.

The software used the same algorithm for the calculation of the pump signal and the pumping time for different velocities as in the cell seeding and cell culture software, which calculaed the time of volume transport Δt.

$$\Delta t = \frac{\Delta V}{A \times v} = \frac{2.25ml}{\pi \times 9mm^2 \times v} \tag{3.4}$$

The software provided following functions:

1. Convert the input velocity [mm/s] to a pump-readable flow [%].
   (a) Input the maximum flow of the pump Q_{max} (e.g. 34.0 ml/min).
   (b) Input velocity v (e.g. 1 mm/s).
   (c) Calculate for the diameter of 6 mm the fluid flow Q (e.g. 1.7 ml/min).
   (d) Calculate the percentage of the max. flow Q_{proz} (e.g. 4.8 %).
   (e) Translate to compatible signal for the IPC pump (e.g. 4.8 % → 1S00048).

2. Transport 2.25 ml.
   (a) Stop pump.
   (b) Set pump counter-clockwise.
   (c) Start pump with Q_{proz} for t.
   (d) Stop pump.

3. End program.

The function of the software in detail is presented in flowcharts in Figure 3.34 and 3.35, the source code is provided in Appendix B.
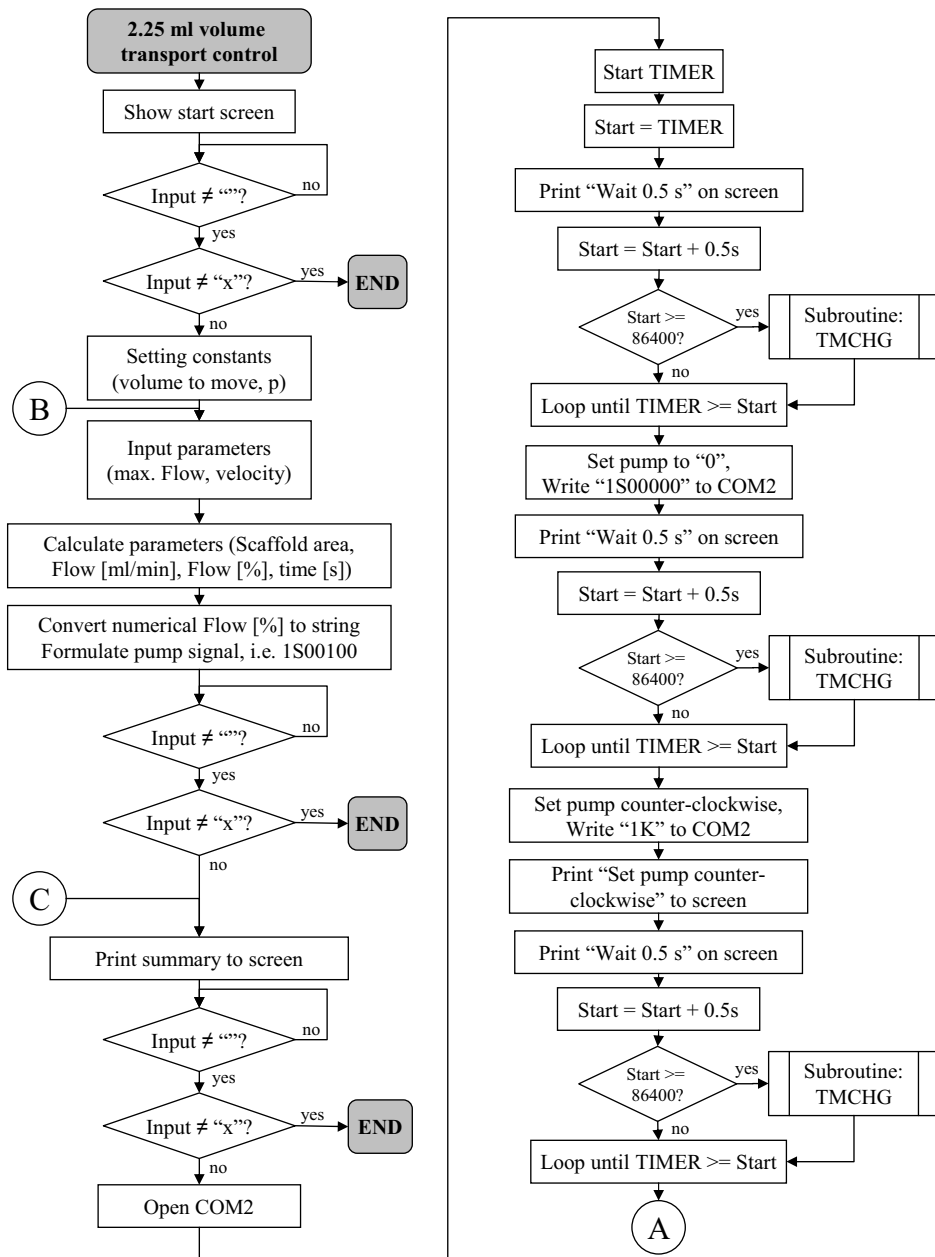
Figure 3.34: Software for volume transport flowchart (1 of 2)
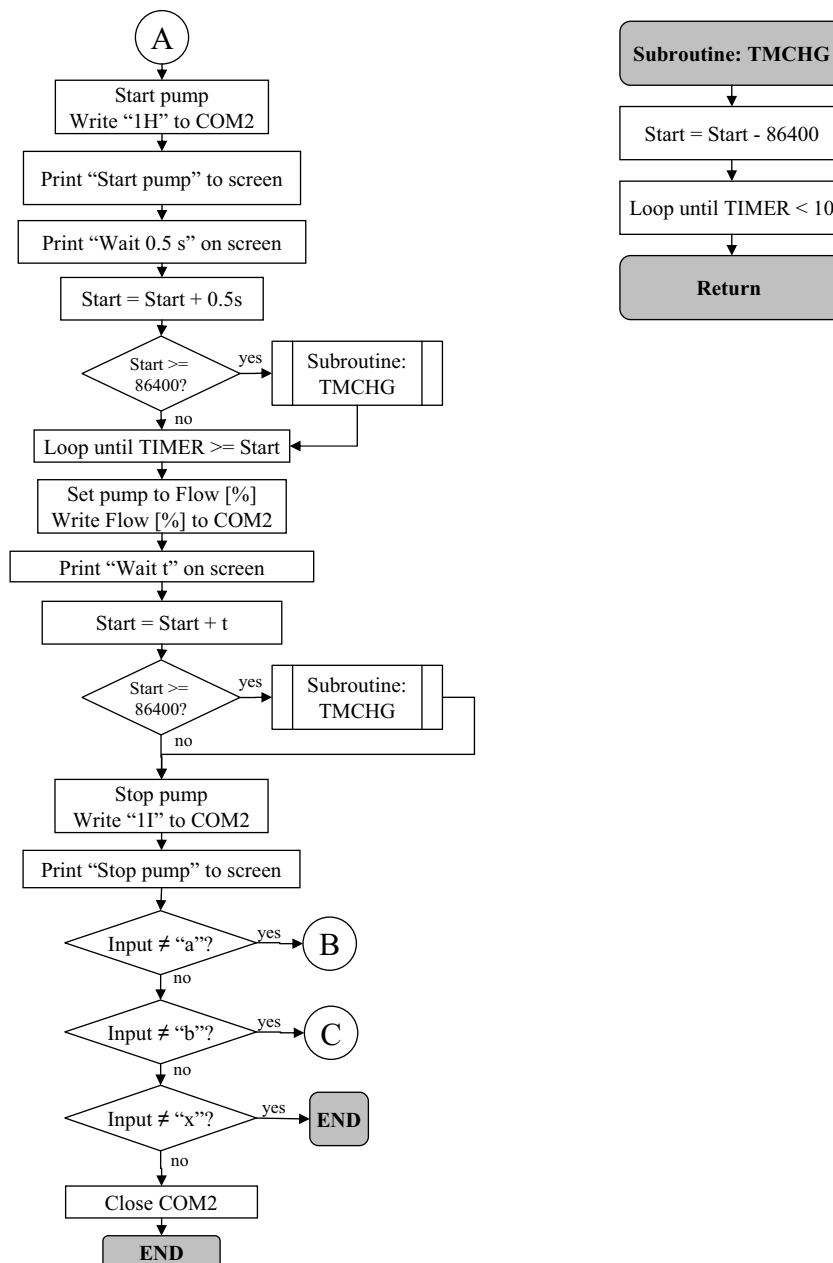
Figure 3.35: Software for volume transport flowchart (2 of 2)

3.3.4.2   Influence of the tubing system on the fluid flow velocity

To verify the fluid flow velocity controlled by the software, one channel of the perfusion system was mounted on a laboratory bench. On one side of the flexible tubing a section of a polystyrene 10 ml pipette (Rubilabor, Ref. 221.1010) was added to determine the displaced volume during the perfusion cycles.

Evaluation of the measurement device   For the determination of fluid flow during several perfusion cycles by use of a 10 ml pipette section, the tolerance of the measurements had to be determined. The pipette section used for the readings was sealed shut on one end and was located vertically on a precision balance (Sartorius CP622, tolerance 0.01 g).

Random volumes between 0.2 ml to 1.2 ml of distilled water were filled into the pipette. The volume on the pipette scale and the weight indicated by the balance were read off before and after adding the water. The scale of the pipette had marks in 0.1 ml steps. A distinction could be made in the pipette reading between volume steps of about 0.05 ml. The weight of added volume was then compared to the measured weight using Equation 3.3 with a water density of ρ_{H_2O} of 0.998 g/cm^3 [23].

Fluid movement profiles in the perfusion system channel   One channel of the perfusion system was assembled to verify the fluid flow velocity controlled by the software. One side of the flexible tubing was expanded with a piece of a polystyrene 10 ml pipette to measure the transported volume (see Figure 3.36). The total length of the tubing remained the same to maintain the elastic properties of the system. The channel was filled with 10 ml of distilled water. Before conducting the experiments the peristaltic pump was calibrated according to its manual. The previously developed cell seeding software was used to apply velocities of 1 mm/s, 5 mm/s, 10 mm/s and 15 mm/s for 5 cycles each. To determine the effect of the tubing assembly on the fluid flow velocity, experiments were conducted with empty perfusion chambers. For the determination of the influence of the PLA/glass composite scaffolds on the fluid flow velocity, three different pairs of pre-wetted scaffolds were inserted into the chambers. The maximum and minimum level of the water in the pipette was read off the scale for every cycle conducted in

Figure 3.36: Setup for measurement of transported volume per half-cycle. Left side of the tubing wass replaced by a 10 ml polystyrene pipette section.

these experiments and used to calculate the transported volume per cycle. Additionally the water level in the pipette section was filmed with a digital camera (Panasonic Lumix DMC-FZ28). The movies in format '.mov' were converted using VLC media player (Version 0.8.6i) using the 'stream/save' feature (output '.avi' file extension, encapsulation method 'MPEG 1', video codec 'mp1v', bitrate 1024 kb/s). The converted movie files were opened with VirtualDub (Version 1.8.1) to observe the movies frame by frame. By advancing frames, the movies were examined to determine the frame number at specific fluid levels. This provided information over form and amplitude of the perfusion cycles.

3.4 Results

3.4.1 Scaffold material

As presented in Chapter 2, scaffold dimensions were subjected to shrinkage during fabrication. By using PTFE moulds of 6.3 mm diameter and 13 mm depth it was expected to compensate this effect on the scaffolds to obtain the desired dimensions. Six scaffolds were measured with a slide calliper (TESA ShopCal, serial number 1K375806) after fabrication, resulting in a mean diameter of 6.2 mm ± 0.1 mm and a mean length of 12.5 mm ± 0.2 mm.

3.4.2 Perfusion bioreactor system

A perfusion bioreactor system for cell seeding and cell culture under fluid flow was developed as presented previously. The design requirements stated in the objectives were accomplished in the development of the perfusion bioreactor system. The only component of this system which could not be obtained commercially were the perfusion chambers, used to contain the scaffolds. The perfusion chambers were applicable to autoclaving, whereas tubing and connectors could be sterilised by gamma rays. The chambers could be mounted by hand without the need of further tools. As could be observed in all conducted experiments the chambers were sealed off tight, ensuring the perfusion of the scaffolds. The sample holder of the chambers showed to be applicable in preliminary tests for scaffolds made of PLA/glass composite and calcium phosphate cement samples.

3.4.3 Software development

As a result of the software development three executable files were obtained, for cell seeding, cell culture and for the volume transport experiments. The executables were tested successfully for their function on the laptop dedicated for the system with the pump connected prior to the validation experiments.

3.4.4   Fluid flow velocity validation

3.4.4.1   Verification of the pump control on the displaced volume

Using the developed software for volume transports of 2.25 ml at different fluid flow velocities, the volume displacement at 1 mm/s, 5 mm/s, 10 mm/s and 15 mm/s was measured to verify the pump algorithm and pump accuracy. The volume was determined by weighing the displaced water and using Equation 3.3 for the volume calculation. The experiments were conducted six times for each velocity. The averages of fluid transport for different fluid flow velocities are listed in Table 3.4.

Comparing the groups using a Mann-Whitney U test, it was found that only the 1 mm/s group was significantly different from the 10 mm/s group ($P < 0.01$, two-tailed test). This showed that the displaced volume did not depend directly on the pump velocity. The average of all values was determined as 2.27 ml $\pm$ 0.04 ml. This was a deviation of about 1 % of the intended volume.

Velocities	Volume [ml]
1 mm/s	2.25 $\pm$ 0.03
5 mm/s	2.26 $\pm$ 0.02
10 mm/s	2.29 $\pm$ 0.01
15 mm/s	2.28 $\pm$ 0.04

Table 3.4: Displaced volumes in the fluid transport validation at different velocities.

3.4.4.2 Influence of tubing and samples on the cell seeding perfusion pattern

Accuracy of the measurement device To determine the reading tolerances of the used pipette section, different water volumes were added to the pipette and compared to the weight readings. The differences of read values before and after adding water are shown in Table 3.5 as well as the differences in measured volume for the 10 conducted measurements.

Deviations of up to 0.04 ml from the measured weight were obtained by this measurement. The determined values and tolerances of volumetric and weight measurements are plotted in Figure 3.37. As can be seen from the graph, the measured volume had a linear relationship to the measured weight as was expected.

calculated V [ml] from weight	measured V [ml] from pipette scale	Difference ΔV [ml]
0.75	0.75	0.00
1.11	1.15	0.04
0.27	0.30	0.03
0.47	0.45	-0.02
0.38	0.40	0.02
0.40	0.41	-0.01
0.47	0.50	0.03
0.34	0.35	0.01
0.27	0.25	-0.02
0.67	0.70	0.03

Table 3.5: The weight added to the pipette section converted to water volume, volume readings and deviation of the volume for the measurement of the measurement tolerance.
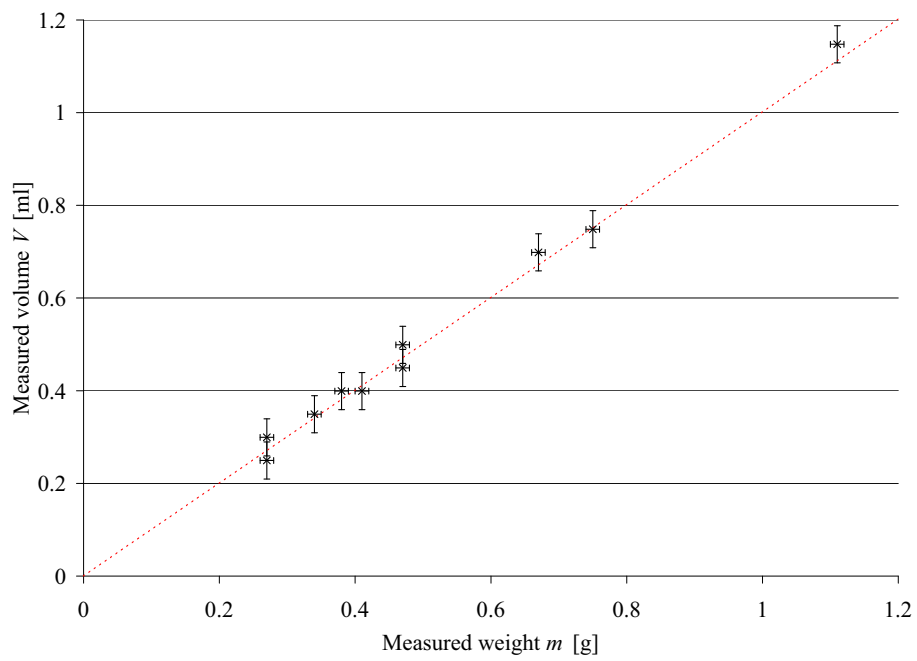
Figure 3.37: Error in volume measurement with a pipette section. The tolerance of measured volume was determined to be 0.04 ml, the tolerance of measured weight was given by the manufacturer with 0.01 g. The dotted line shows the theoretical relationship between weight and volume.

Fluid flow and flow profile validation The developed cell seeding software was used to apply 5 cycles with the velocities of 1 mm/s, 5 mm/s, 10 mm/s and 15 mm/s to an assembled cell seeding channel. Experiments were conducted with empty perfusion chambers and with pre-wetted PLA/glass composite scaffolds in both chambers. Measurements with scaffolds were conducted with three different sample pairs to eliminate the effect of sample heterogeneity. The measured volumes were calculated for every cycle and averaged over five cycles (see Table 3.6). The velocities calculated from those measurements are depicted in Figure 3.38. For the experiments with empty chambers the volume displacement showed to be stable over the whole range of applied velocities, but was decreased in comparison to the intended volume about 8.4 %. When scaffolds were present in the chambers, the displaced volume was decreased about 9.0 %, 13.4 %, 19.6 % and 25.3 % for 1 mm/s, 5 mm/s, 10 mm/s and 15 mm/s respectively.

When the volume displacement in the pipette section was recorded in a movie, the patterns of the fluid level movement could be extracted from the frames. The patterns for experiments with and without scaffolds are depicted in Figure 3.39. In the experiments without scaffolds, a drift of about 0.03 ml/cycle to one side of the channel was observed for all four velocities. This drift occurred in all tested velocities. The triangular pattern of volume displacement was not altered by the channel assembly. Inserting the PLA/glass scaffolds in the perfusion chambers resulted in a higher drift of the fluid to one channel side. During the experiments with scaffolds with 5 cycles with 1 mm/s, 5 mm/s, 10 mm/s and 15 mm/s the drift was 0.025 ml/cycle, 0.035 ml/cycle, 0.04 ml/cycle and 0.08 ml/cycle respectively. The triangular pattern of displacement was kept true for velocities of 1 mm/s and 5 mm/s, whereas the peaks of the pattern were rounded off at high velocities of 10 mm/s and 15 mm/s.

Pump	Volume measured V [ml]		Velocity calculated v [mm/s]	
velocity	no scaffolds	with scaffolds	no scaffolds	with scaffolds
1 mm/s	4.13 ± 0.06	4.09 ± 0.06	0.92 ± 0.01	0.91 ± 0.01
5 mm/s	4.16 ± 0.05	3.89 ± 0.08	4.62 ± 0.06	4.33 ± 0.09
10 mm/s	4.13 ± 0.08	3.61 ± 0.10	9.2 ± 0.2	8.04 ± 0.2
15 mm/s	4.04 ± 0.05	3.37 ± 0.04	13.5 ± 0.2	11.2 ± 0.5

Table 3.6: Transported volumes and calculated velocities with and without PLA/glass composite scaffolds in the velocity validation experiments (n=5).
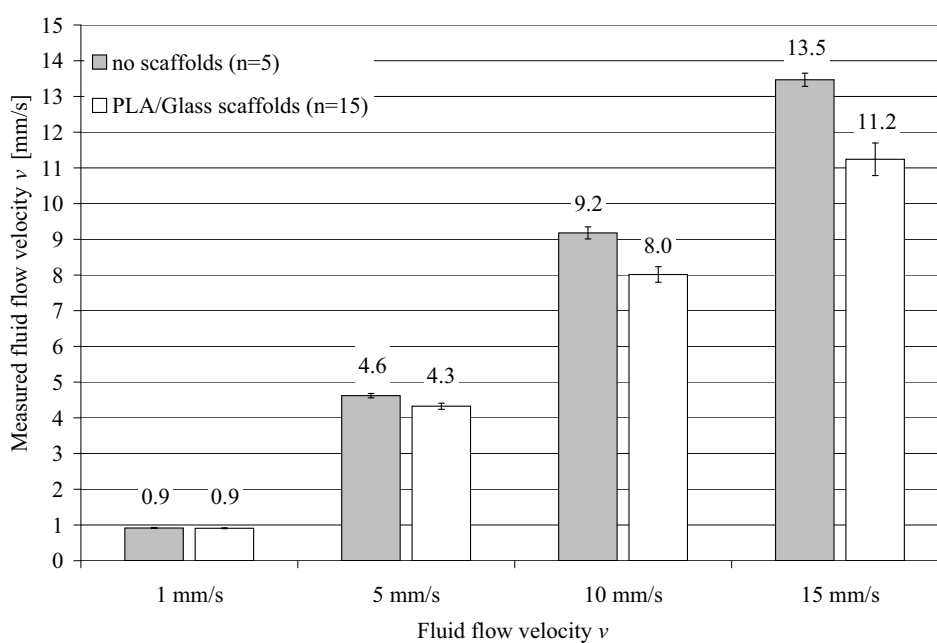
Figure 3.38: Velocity validation of the set fluid flow velocity to the real velocity. Measurements were conducted with and without scaffolds in the perfusion chambers.
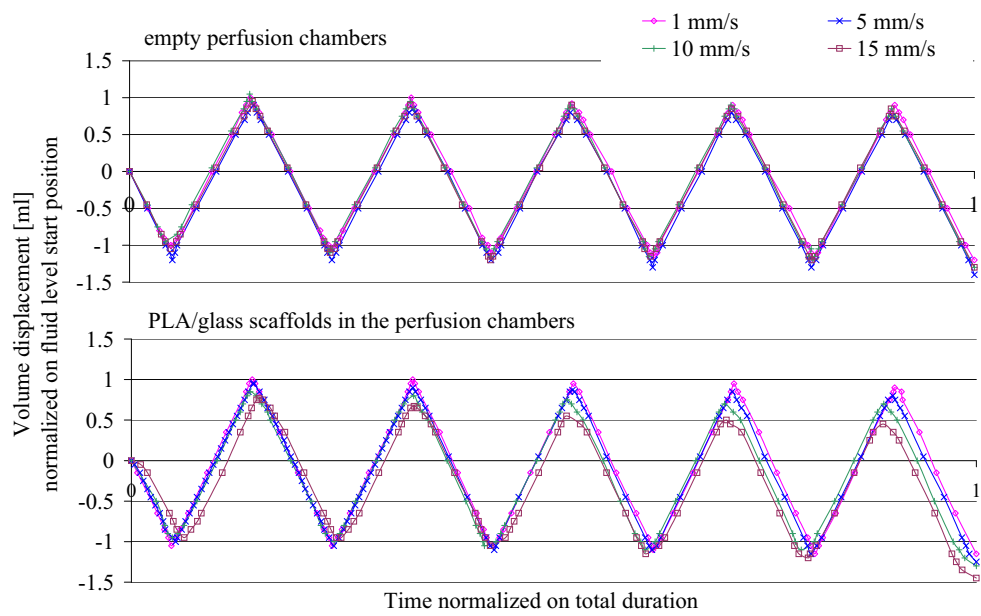
Figure 3.39: Volume drift during alternating perfusion with and without scaffolds. During perfusion without scaffolds, the fluid level drifted to one side of the channel. This effect was enhanced by inserting scaffolds into the perfusion chambers.

3.5   Discussion

PLA/glass composite scaffolds were fabricated for the perfusion bioreactor system validation experiments in PTFE moulds. The porous cylinders were 6.2 mm in diameter and 12.5 mm in length and hence larger than the intended dimensions. This discrepancy did not constitute a disadvantage for the use in the perfusion bioreactor system, because the soft material was pressed against the sample holder walls and hence ensuring the perfusion of the scaffold. Because it is difficult to produce scaffolds which meet exactly the 6.0 mm in diameter and 12.0 mm in length as well as to fabricate scaffold holders with the same dimensions, for samples of harder material it should be considered for further development to incorporate a scaffold holder which adapts to to the actual dimensions of the sample.

A perfusion bioreactor system, including tubing, perfusion chambers, peristaltic pump and computer was developed. As a main component, perfusion chambers for the bioreactor system were developed and tested.

The perfusion pattern of the cell seeding process was validated. This part of use is considered most problematic considering that the fluid levels are driven pneumatically against the resistance of the porous scaffolds inserted. It could be shown that the pump did work with an accuracy of about 1 %, which was considered sufficient for the intended use. The form and amplitude of the cell seeding perfusion was observed, showing that the tubing with empty perfusion chambers diminishes the velocity set to the pump by 8.4 %. This diminishing effect could be determined with a reading tolerance of 0.04 ml as was determined for the measurement device. The lowered fluid flow velocity was most likely caused by compression of air as the driving medium and by tubing elasticity which was buffering the driving pressure. Driving the cell suspension levels pneumatically did imply a loss in fluid flow velocity. Putting PLA/glass composite scaffolds into the chambers lowered the fluid flow velocity up to 25 % depending on the applied velocity in a range up to 15 mm/s. Darcy's law (Equation 2.8) which relates pressure to flow, shows that a higher fluid flow causes a higher pressure difference through the sample. It was suggested that higher pressure enhanced the buffering of transported volume due to tubing elasticity and air compressibility. For cell culture the observed effects of diminished fluid flow velocities

was considered not as severe as in the cell seeding process, because the driving medium in cell culture is the less compressible medium fluid, the amount of elastic tubing is smaller and the applied fluid flow velocities are lower.

Additionally it has to be taken into account that after a long term culture the changes in the scaffolds (material adsorption and tissue development) influence the permeability and hence affect the occurring pressures and perfusion velocities. The impact of this development on the fluid flow velocity cannot be estimated sufficiently. This signifies that tissue development can only be related to the fluid flow set on the pump, not the fluid flow actually occurring in the system.

From these results it can be seen that the main inconvenience of the developed system consists in the missing feedback of actual fluid flow velocity to the pump control. Such feedback allows to measure the actual velocity and correcting the velocity set at the pump. This would have to be monitored very carefully, because the feedback might cause an up-regulation of pump speed which leads to a high pressure in the system which cannot be handled by the pump. So an additional monitoring of the systemic pressure would be appropriate. Implementation of such a feedback loop has not been undertaken in the current system, because of the technical changes implied. These changes would not only consist of adding sensors and changing the software, but also need appropriate electronic for the sensors and a new type of interface connecting the pump and sensors to the laptop. Another type of interface, preferable for parallel data acquisition, implies the change of the programming language. Without any doubt those technical changes in the system can be undertaken in the future and might enhance the function of the perfusion bioreactor system.

Additionally the developed perfusion bioreactor system did not contain measurement mechanisms for cell activity. As Volkmer et al. [24] stated, even in perfusion bioreactor systems it is important to monitor the oxygen gradient in the scaffold. In a future redesign the integration of sensors should be considered to monitor the biological activity of the cultured cells.

The software for controlling perfusion profiles was developed given the required function for cell seeding and cell culture. The user interface was very basic and the input was minimized to the necessary parameters. For further changes, the software can be expanded using the software tools mentioned in

the development description. One major limitation of the software was the command latency of the pump, which did not allow to send two consecutive commands in direct succession, but needed a period between commands. In the case of alternating velocities for the purpose of mechanical stimulation of the cells, this signifies a maximum frequency of 1 Hz.

The selection of BASIC as language limited the application when expanding the systems complexity in the future development. A better combination for further progress would be the use of a hardware interface controlled by software written in a language which supports the interface driver.

3.6 Conclusions

- A perfusion bioreactor system was developed for cell seeding and cell culture experiments including control software. The presence of scaffolds in the perfusion chambers did diminish the fluid flow velocity through the tubing.

- As one of the crucial parts of the bioreactor system a perfusion chamber was developed. The chambers used for the initial tests proved to be usable for the system.

- During cell seeding, the resistance constituted by the scaffolds was diminishing the perfusion velocity and caused a drift to one of the sides. Sensors for control of the fluid flow parameters were not incorporated in the perfusion bioreactor system, but should be considered for further development.

Bibliography

[1] I. Martin, D. Wendt, and M. Heberer. The role of bioreactors in tissue engineering. *Trends Biotechnol*, 22(2):80–86, 2004.

[2] L.E. Freed and G. Vunjak-Novakovic. *Principles of Tissue Engineering*, chapter Tissue Engineering Bioreactors. Academic Press, second edition, 2000.

[3] E.A. Botchwey, M.A. Dupree, S.R. Pollack, E.M. Levine, and C.T. Laurencin. Tissue engineered bone: measurement of nutrient transport in three-dimensional matrices. *J Biomed Mater Res A*, 67:357–367, 2003.

[4] D. Wendt, S. Stroebel, M. Jakob, G.T. John, and I. Martin. Uniform tissues engineered by seeding and culturing cells in 3D scaffolds under perfusion at defined oxygen tensions. *Biorheology*, 43:481–488, 2006.

[5] A.S. Goldstein, T.M. Juarez, C.D. Helmke, M.C. Gustin, A.G. Mikos, and L.V. McIntire. Effect of convection on osteoblastic cell growth and function in biodegradable polymer foam scaffolds. *Biomaterials*, 22(11):1279–1288, 2001.

[6] V. I. Sikavitsas, G. N. Bancroft, J. J. Lemoine, M. A. Liebschner, M. Dauner, and A. G. Mikos. Flow perfusion enhances the calcified matrix deposition of marrow stromal cells in biodegradable nonwoven fiber mesh scaffolds. *Ann Biomed Eng*, 33(1):63–70, 2005.

[7] H.L. Holtorf, T.L. Sheffield, C.G. Ambrose, J.A. Jansen, and A.G. Mikos. Flow perfusion culture of marrow stromal cells seeded on porous biphasic calcium phosphate ceramics. *Ann Biomed Eng*, 33(9):1238–1248, 2005.

[8] H.L. Holtorf, N. Datta, J.A. Jansen, and A.G. Mikos. Scaffold mesh size affects the osteoblastic differentiation of seeded marrow stromal cells cultured in a flow perfusion bioreactor. *J Biomed Mater Res A*, 74:171–180, 2005.

[9] Q.P. Pham, F.K. Kasper, A.S. Mistry, U. Sharma, A.W. Yasko, J.A. Jansen, and A.G. Mikos. Analysis of the osteoinductive capacity and

angiogenicity of an in vitro generated extracellular matrix. *J Biomed Mater Res A*, 88:295–303, 2009.

[10] M. E. Gomes, H. L. Holtorf, R. L. Reis, and A. G. Mikos. Influence of the porosity of starch-based fiber mesh scaffolds on the proliferation and osteogenic differentiation of bone marrow stromal cells cultured in a flow perfusion bioreactor. *Tissue Eng*, 12:801–809, 2006.

[11] M. J. Jaasma, N. A. Plunkett, and F. J. O'Brien. Design and validation of a dynamic flow perfusion bioreactor for use with compliant tissue engineering scaffolds. *J Biotechnol*, 133:490–496, Feb 2008.

[12] L. Fassina, L. Visai, L. Asti, F. Benazzo, P. Speziale, M.C. Tanzi, and G. Magenes. Calcified matrix production by saos-2 cells inside a polyurethane porous scaffold, using a perfusion bioreactor. *Tissue Eng*, 11(5-6):685–700, 2005.

[13] S.H. Cartmell, B.D. Porter, A.J. García, and R.E. Guldberg. Effects of medium perfusion rate on cell-seeded three-dimensional bone constructs in vitro. *Tissue Eng*, 9(6), 2003.

[14] V. Olivier, P. Hivart, M. Descamps, and P. Hardouin. In vitro culture of large bone substitutes in a new bioreactor: importance of the flow direction. *Biomed Mater*, 2(3):174–180, 2007.

[15] D. Du, K. Furukawa, and T. Ushida. Oscillatory perfusion seeding and culturing of osteoblast-like cells on porous beta-tricalcium phosphate scaffolds. *J Biomed Mater Res A*, 86:796–803, 2008.

[16] D.E. Orr and K.J. Burg. Design of a modular bioreactor to incorporate both perfusion flow and hydrostatic compression for tissue engineering applications. *Ann Biomed Eng*, 36(7):1228–41, 2008.

[17] G.N. Bancroft, V.I. Sikavitsas, and A.G. Mikos. Design of a flow perfusion bioreactor system for bone tissue-engineering applications. *Tissue Eng*, 9(3):549–554, 2003.

[18] Saint-Gobain Corp. Tygon LFL long flex life pump tubing. http://tygon.com/Media/Documents/S0000000000000001013/ TygonLFL.pdf. Retrieved: 03-12-2008.

[19] DuPont. Teflon FEP. http://www2.dupont.com/Teflon_Industrial/en_US/ products/product_by_name/teflon_fep. Retrieved: 03-12-2008.

[20] International Organization of Standardization. *ISO 594-1:1986, Conical fittings with a 6 % (Luer) taper for syringes, needles and certain other medical equipment – Part 1: General requirements*, 1986.

[21] Cole-Parmer. Masterflex L/S tubing options. http://www.coleparmer.com/techinfo/techinfo.asp?htmlfile=Tubing_LS-Options.htm&ID=772. Retrieved: 03-03-2009.

[22] American society for testing and materials. *ASTM A176: Standard Specification for Stainless and Heat-Resisting Chromium Steel Plate, Sheet, and Strip*, 2006.

[23] D. Mende and G. Simon. *Physik - Gleichungen und Tabellen.* Fachbuchverlag Leipzig - Köln, 11 edition, 1994.

[24] E. Volkmer, I. Drosse, S. Otto, A. Stangelmayer, M. Stengele, B.C. Kallukalam, W. Mutschler, and M. Schieker. Hypoxia in static and dynamic 3d culture systems for tissue engineering of bone. *Tissue Eng.*, 14(8):1331–40, 2008.

Chapter 4

Cell Seeding in the Perfusion Bioreactor System

4.1 Introduction

One approach in tissue engineering of bone tissue substitutes is the *in vitro* culture on 3D biomaterial matrices or scaffolds. For the development of tissue in the scaffolds it is beneficial to provide a high number of cells and an even cell distribution throughout scaffolds at the start of cell culture. A high cell number can increase bone mineralization in the scaffolds [1] and an even cell distribution is linked to uniform tissue generation during culture in a bioreactor [1, 2]. Additionally a high cell number seeded on scaffolds shortens the time of culture necessary to achieve a sufficiently developed tissue. A high cell seeding efficiency, i.e. the ratio of cells adhered to the scaffold to the total number of cells seeded, can reduce the extent of cell harvesting and *in vitro* cell expansion. Different cell seeding techniques are applied to achieve tissue engineered construct on 3D substrates. Most commonly used methods are static, dynamic and perfusion seeding.

The most applied cell seeding method is static seeding. By pipetting cell suspension on top of a scaffold, cells sink into the pores of the scaffolds by gravity [3]. Even though this is an easy method which does not need special equipment, the number of cells that adhered to the porous scaffolds is relatively small. A cell seeding efficiency between 18 % to 85 % can be obtained by static seeding. The cell seeding densities for this lay in the

magnitude of 10^4 to 10^7 cells/cm^3 [1, 4–11] . It has been shown that most of the cells adhered on the outside of the scaffold, so that only few or no cells were located on the inside [1, 4–6]. This is considered unfavourable for further cell culture.

The most common method for cell seeding under dynamic conditions is the use of spinner flasks. Scaffolds fixated on skewers are immersed into cell suspension [20]. The cell suspension is then agitated by an electromagnetic stirrer and the cells accumulate in the pores of the scaffolds. Seeding in spinner flasks under dynamic conditions yields efficiencies of a wide range, from 17.5 % to 55 %. By rearranging the scaffold placement and changing the wall symmetry of the spinner flask Bueno et al. [12] even achieved seeding efficiencies of 100 %. Cell density in the scaffolds was in the order of 10^4 to 10^8 cells/cm^3 [6, 7, 12] which was in the same range as the static seeding method (see Table 4.1). The cell distribution throughout scaffolds after spinner flask seeding was reported to be non-uniform. While some regions contained aggregations of cells, other regions were found void of cells [6]. Nevertheless dynamic seeding in a spinner flask resulted in better cell distribution compared to static seeding [21, 22].

Perfusion of the scaffolds with cell suspension aims to overcome the shortcoming of cell distribution. By deposition of cells throughout the scaffold by repeated filtering of the suspension through the scaffold the cell number and cell distribution can be enhanced. As presented in the introduction of Chapter 3, different perfusion systems were developed by different research groups. All systems have in common that they allow to push cell suspension through scaffolds, seeding cells throughout the porosity. It has been shown that perfusion seeding results in a high seeding efficiency. The cell seeding efficiencies achieved by this method were 70 to 90 % with cell densities in magnitudes of 10^5 to 10^7 cells/cm^3 [5, 6, 8–10, 13–19] (see Table 4.1). This is comparable to the efficiencies with the dynamic seeding method. But in contrary to the downside of heterogeneous cell distribution, using the perfusion cell seeding method it was possible to distribute cells evenly throughout the scaffold [4–6, 8, 22]. In another form of the perfusion seeding, where scaffolds move through cell suspension instead of the suspension through the scaffolds, Timmins et al.[19] obtained with their T-CUP system a seeding efficiency of 75 % and a high seeding uniformity. Overall perfusion seeding

Type	Reference	Cells	Material	Dimensions (diameter(d) length(l))	Porosity	N_{cells} initial	Efficiency [%]	Efficiency* [cells/cm^3]
static	Holy et al. [1]	BMSC	PLGA 75/25	$5\times7\times7$mm^3	NA	1.5×10^6	25	1.5×10^6
static	Li et al. [4]	Trophoblast-like ED$_{27}$	non-woven PET Matrices	d:1.8mm, l:1mm	85-93%	1×10^7	NA	5.0×10^6
static dynamic	Godbey et al. [7]	HBSMC	PGA	$40\times8\times2.5$mm^3	95%	2×10^5	17.5 15	4.4×10^4 3.8×10^4
dynamic	Bueno et al. [12]	Chondrocytes	PGA	d:5mm, l:2mm	97%	1.0×10^7	100	2.5×10^8
static			Polyactive foam	d:8mm, l:4.3mm	75%	1.3×10^7	85	5.1×10^7
			Hyaff-11 mesh	d:5mm, l:4mm	73%	5.0×10^6	71	4.5×10^7
dynamic	Wendt et al. [6]	Chondrocytes	Polyactive foam	d:8mm, l:4.3mm	75%	1.3×10^7	71	4.3×10^7
			Hyaff-11 mesh	d:5mm, l:4mm	73%	5.0×10^6	66	4.2×10^7
perfusion			Polyactive foam	d:8mm, l:4.3mm	75%	1.3×10^7	87	5.2×10^7
			Hyaff-11 mesh	d:8mm, l:4mm	73%	5.0×10^6	71	2.0×10^7
perfusion	Janssen et al. [13]	BMSC	biphasic calcium phosphate (BCP)	2-6mm granules in 10cm^3 volume	59%	16×10^6	14	2.8×10^5
static perfusion	Zhao et al. [8]	MSC	non-woven PET Matrices	d:12mm, l:1.2mm d:16mm, l:1.2mm	89%	7.5×10^5 1.2×10^5	34 68	1.9×10^6 3.4×10^5
perfusion	Radisic et al. [14]	C2C12, cardiomyocytes	Ultrafoam$^{\circledR}$ collagen hemostat sheet	d:11mm, l:1.5mm	NA	12×10^6	76	6.4×10^7
perfusion	Radisic et al. [15]	C2C12	PGS	d:10mm, l:3mm	90%	12.0×10^6	72.9	3.7×10^7
static perfusion	Alvarez-Barreto et al. [5]	MC3T3-E1	PLLA foams, non-woven polystyrene	d:8mm, l:3mm	95%	2.5×10^5	46 87	7.7×10^5 1.5×10^6
static perfusion	Alvarez-Barreto et al. [9]	MSC	RGD-modified PLA	d:8mm, l:3mm	90%	1×10^6	22 64	1.5×10^6 4.2×10^6
perfusion	Grayson et al. [16]	MSC	decellularized bovine bone	d:4mm, l:4mm	70-80%	3×10^6	24.7	1.5×10^7
perfusion	Chen et al. [17]	Hepatocytes	vegetable sponge	d:8mm, l:112.5mm	90%	7.0×10^7	54	6.7×10^6
static perfusion	Kitagawa et al. [10]	NIH/3T3	PLLA	i.d.:1mm, o.d.: 3mm, l:20mm	95.5%	2.0×10^6	50 100	8.0×10^5 1.6×10^6
static perfusion	Lee et al. [11]	RAEC	poly glycerol sebacate	d:4mm, l:1mm	NA	5.0×10^5 NA	59 66.4	2.4×10^7 NA
perfusion	Shvartsman et al. [18]	C3A hepatocyte	Alginate	d:5mm, l:2mm	90%	6.6×10^5	98	1.6×10^7
perfusion	Timmins et al. [19]	Articular chondrocytes BMSC	Polyactive foam Hyaff 11 ChronOS ceramic foam Hyaff 11	d:8mm, l:4mm	75% 93% 60% 93%	1.0×10^7	86 75 84 80	4.3×10^7 3.7×10^7 4.2×10^7 4.0×10^7

*Cell density was calculated from the reached cell number and scaffold volume which was deduced from the dimensions given by the referenced publications.

Figure 4.1: Cell seeding efficiencies achieved by the three main methods used in tissue engineering.

is attractive, because it allows to perform the cell seeding in the same bioreactor system used for the later perfusion cell culture. Additionally it has been shown that fluid flow movement can enhance the osteogenic potential of the scaffold [22].

The main problem of the cell seeding in perfusion bioreactor systems is the selection of the right fluid flow velocity. As Wendt et al. [6] commented, high velocities do not give to the cells enough time to adhere to the material, whereas low velocities do not move the cells fast enough, so they adhere to the tubing of the perfusion system or sink to the lowest point of the system by the effect of gravity. They found that a fluid flow velocity of 1 mm/s is appropriate for cell seeding in their system. It must be pointed out that the optimal velocity depends highly on the scaffold microstructure. The tortuosity and diameter of the fluid flow pathways in the scaffold affect directly the velocity and hence the occurring forces on the cells in suspension.

Without any doubt more approaches for cell seeding are developed recently, using different principles like centrifugation [7, 23], acoustic waves [24] or vacuum [25]. Other approaches are progressions of the perfusion principle [19, 26], based on the promising results of perfusion bioreactors.

In general, the comparison between different studies is problematic, because cell seeding depends highly on dimensions and structure of the scaffolds, such as porosity, tortuosity, pore size and pore form, the cell density in the suspension used for seeding and the fluid flow fields induced by the perfusion system. The scaffolds used in perfusion seeding and culture studies had diameters ranging from 3 mm to 18 mm and a thickness from 1 mm to 4.3 mm [4–6, 8, 14, 22]. However it is desirable to achieve bigger tissue substitutes if tissue engineering wishes to make a clinical impact. The promising results of previous studies with the perfusion cell seeding approach and the need for larger scaffold culture constitute the basis of the here presented study.

4.2   Objective

The objective of this study was the determination of suitable fluid flow conditions for the perfusion seeding of MG63 cells on porous PLA/glass scaffolds. The cell seeding was conducted using the perfusion bioreactor system as

described in Chapter 3. In this study, the effect of fluid flow velocity and perfusion cycles of the oscillating seeding method on the resulting seeding efficiency and cell distribution had to be determined. The hypothesis of this study was, that it is possible to seed cells throughout a large porous scaffold, with a high length to diameter ratio, by the perfusion seeding approach.

4.3 Materials and methods

4.3.1 Scaffold preparation

The PLA/glass composite scaffolds for this study were fabricated as described in Chapter 2 by solvent cast particle leaching technique. The scaffolds were of 6 mm diameter and 12 mm length with pore diameters of 80-210 μm, porosity of 95.7% and permeability of 1.7×10^{-10} m^2. The scaffolds were then packed in transparent microcentrifuge tubes which were sealed in sterilization bags. The packed scaffolds were sterilized by gamma radiation with a dose of 8 kGy. One day before the seeding experiments the needed number of scaffolds was taken out of the packing under sterile conditions and immersed in 30 % ethanol for less than one minute. The scaffolds were then transferred to a Petri dish with complete medium (high glucose Dulbecco's Modified Eagle Medium (DMEM), 10 % foetal bovine serum (FBS), 1 % penicillin-streptomycin, 1 % sodium pyruvate and 1 % L-glutamine) and incubated overnight. At the beginning of the experiments the scaffolds and the medium were observed under the light microscope to exclude a possible bacterial contamination.

4.3.2 Preliminary test

One of the encountered challenges for this study was to determine the methodology used to obtain an imaging of the cells located in the porous scaffolds. Even though the preliminary tests presented here were not all applicable for the treatment of the samples, those efforts did produce images which show cell morphology and scaffold structure at a more detailed manner than in the cell seeding imagines used in the final experiments.

4.3.2.1   Cell culture on scaffolds

For the preliminary test, cells were seeded into scaffolds. For this, MG63 human osteoblast-like cells were suspended to 500,000 cells per 300 μl complete medium (DMEM, 10 % FBS, 1 % penicillin-streptomycin, 1 % sodium pyruvate and 1 % L-glutamine) and 300 μl injected with a syringe into the scaffolds. The scaffolds were then incubated for 24 hours before preparation for histology.

Preparation of object slides   The object slides used for mounting of the cut samples were silanized to enhance the adhesion of the sample cuts. For this purpose the glass slides were left in soap solution overnight and washed thoroughly with deionized water. The slides were dried and washed with acetone for three minutes. The slides were then immersed in TESPA (3-aminopropiltrietoxysilane) dissolved in acetone in a concentration of 2 % for five minutes. The so treated slides were briefly flushed with distilled water and left for drying overnight protected from dust.

Sample preparation   The scaffolds were taken out of culture and immersed for one hour in formalin and passed into phosphate buffer (PB, 0.1 M at pH 7.4). The samples were then included by immersion in increasing concentrations of ethanol followed by xylol and inclusion in paraffin. Consecutively the samples were transferred for one hour each in 70 % ethanol, two times in 96 % ethanol, two times in 100 % ethanol, two times in xylol, two hours in paraffin at 57 °C and then left in paraffin at 57 °C over night. The prepared samples were put on a metal tray and paraffin poured over them and an embedding cassette was placed over the sample. The samples were left to cool off in a refrigerator at 4 °C until the paraffin was totally hardened. The cassettes were fixed in a rotary microtome (Leica RM2125) and the samples were cut in transverse plane with a thickness of 20 μm under frequent change of the used blade. The best cuts were laid out on silanized object slides and stored overnight at 37 °C.

The sections of the samples were then stained with methylene blue after extraction of the paraffin to make the cell nuclei more visible. To extract the paraffin from the sample sections, the slides were immersed for five minutes in xylol, five minutes in 100 % ethanol, five minutes in 70 % ethanol and

one minute in deionized water. For the methylene blue staining the slides were immersed for 30 to 60 seconds in methylene blue solution. To remove excess dye from the samples, the slides were immersed in deionized water for three minutes, one minute in 95 % ethanol, one minute in 100 % ethanol and lastly for five minutes in xylol. After evaporation of the xylol the samples were mounted with DPX (Di-N-Butyle Phthalate in Xylene). The sections were inspected under light microscope (Nikon Eclipse E-600) and images were taken for documentation.

4.3.3 Perfusion cell seeding

4.3.3.1 Perfusion system

The perfusion bioreactor system was assembled as presented in Section 3.3.2.1. For the experiments three parallel channels where assembled which allowed the use of six perfusion chambers simultaneously. The components of the perfusion chamber were sterilized by autoclave, tubes and plastic connectors were washed thoroughly with ethanol and distilled water and located for 20 minutes under ultraviolet light for sterilization prior to the seeding experiments. At the beginning of the experiment the tubing leading from the pump to the perfusion chambers was assembled under sterile conditions and the connectors closed with sterile caps. The tubing was then transferred to the incubator, guided through an inlet tube on the back of the incubator. The computer and pump were connected and the tubing inserted into the pump. The perfusion chambers were assembled with inserted scaffolds and connected via the large diameter tubing which was closed on top with sterile caps. The perfusion chambers were then transferred to the support rack in the incubator and connected to the previously installed tubing.

4.3.3.2 Cell preparation

The medium used for the cell culture was complete medium (DMEM, 10 % FBS, 1 % penicillin-streptomycin, 1 % sodium pyruvate and 1 % L-glutamine). MG63 human osteoblast-like cells were used for the cell seeding experiments. The cells were cultured in 75 cm^2 culture flasks and trypsinized when reaching confluency. For trypsinization the medium was extracted from the culture flasks, the cells were washed twice with sterile phosphate buffered saline

(PBS). Three millilitre of trypsin (TrypLE Express, Gibco 12605) were added to the cells and the flask incubated over five minutes at 37 °C. Seven millilitre of medium were added to stop the enzymatic activity and the detached cells were extracted from the flask and transferred into a centrifuge tube. The 10 ml suspension was centrifuged at 1000 rpm for five minutes. The supernatant was removed and the cell pellet resuspended in 10 ml medium. The cell number in the suspension was counted in a Neubauer chamber. The suspension was again centrifuged at 1000 rpm for five minutes, the supernatant removed and the cells resuspended in 10 ml medium. Cell density was determined by counting again in the Neubauer chamber to verify the first measurement. The cells were then either transferred to a new culture flask or if used for the experiment diluted to a density of 2×10^6 cells per 10 ml medium. Ten millilitre cell suspension was then injected into the bottom valve of the perfusion bioreactor channels. For the cell seeding experiments MG-63 osteoblast-like cells from pass 8 to 13 were used.

4.3.3.3   Static cell seeding

As a comparison to the perfusion seeding, 10^6 MG63 cells per scaffold suspended in 300 μl complete medium were injected with a syringe (0.9 mm needle) into the composite material. With this method it was intended to bring cells into the interior of the scaffolds. After the injection, the samples were left in complete medium at 37 °C four hours to allow cell adhesion. Four samples were washed with PBS and frozen in serum-reduced medium and used for the determination of the cell number. Two samples were used for the determination of the cell distribution in the interior by acridine orange staining.

4.3.3.4   Perfusion cell seeding

Cell seeding was conducted under oscillating suspension perfusion with varying values for cycle number and fluid flow velocity. The cycle numbers used were 50, 100 and 500 cycles, whereas fluid flow velocities were 1 mm/s, 5 mm/s, 10 mm/s and 15 mm/s. Consequently twelve single experiments were conducted. The combinations of fluid flow velocities and cycle numbers resulted in seeding times from 9 minutes up to 23 hours (see Table 4.1).

Velocity [mm/s]	Cycle number	Cell seeding time
	50	2h19min
1	100	4h36min
	500	23h09min
	50	28min
5	100	55min
	500	4h36min
	50	14min
10	100	28min
	500	2h19min
	50	9min
15	100	19min
	500	1h33min

Table 4.1: Total seeding time for the different perfusion velocities and perfusion cycle numbers.

After completion of the seeding cycles, the system was left undisturbed for four hours to facilitate cell adhesion to the scaffolds. It was ensured that unattached or dead cells were removed from the samples by extraction of the cell suspension supernatant with a syringe and by washing the samples with PBS twice. Two of the six scaffolds were used to determine cell distribution. Four scaffolds were frozen for later determination of the cell number in the scaffolds.

4.3.3.5 Cell distribution

Cell distribution in the scaffolds was assessed directly after four hours of cell adhesion time. The scaffolds were cut longitudinally with a scalpel. All scaffolds were stained with acridine orange to identify living cells. The samples for 50 cycles and 100 cycles were additionally stained with ethidium bromide. Acridine orange (AO) and ethidium bromide (EB) were prepared by diluting a 1 mM stock solution to 10 μM solution which equals a solution of 2.6 μg/ml of acridine orange and 3.9 μg/ml of ethidium bromide. AO and EB were added to the scaffolds and incubated over 5 minutes at 37 °C. The scaffolds were then washed twice with sterile PBS and observed under fluorescence stereoscope (Leica MZ16F) with DSR filter for EB and GFP-3 filter for AO. Pictures were taken of the fluorescence for documentation.

4.3.3.6   Cell number

The cell number present in the scaffolds was measured using a cytotoxicity detection kit (Roche Applied Science) for detection of lactate dehydrogenase (LDH). For the quantification, four scaffolds per experiment were washed twice with serum-reduced medium (DMEM, 1 % FBS, 1 % penicillin-streptomycin, 1 % sodium pyruvate and 1 % L-glutamine), destroyed with tweezers and frozen in 1 ml of serum-reduced medium at -20 °C. The samples were then thawed and frozen three times to destroy all cell membranes. The use of a LDH detection kit for the determination of cell number after cell lysis is an established method [27] and freeze-thawing is an effective method for cell lysis [28]. The samples were prepared in 96 well plates in triplicate. Per well 50 μl of resuspended samples were diluted with 50 μl of serum-reduced medium before adding the test liquid as described in the kit's user manual. The controls were 100 μl of serum-reduced medium. The samples were incubated for 30 minutes at room temperature and kept protected from light. The absorbance of the samples was then measured at 450 nm with a reference wavelength of > 690 nm in a microplate-reader (Biotek Powerwave XS). The cell concentration in the samples was calculated using a standard curve measured on the same 96 well plate. The found seeding efficiencies were compared using the Student's t-test to determine statistically significant differences.

4.4 Results

4.4.1 Preliminary test

The samples used for the preliminary tests were included in paraffin, cut with a rotary microtome and cells were stained with methylene blue. During the preparation it was found that only a few good sections could be preserved, because by cutting, glass particles were dragged by the microtome blade through the sample, slicing the sections into thin strips. Additionally it was found that parts from the usable sections were lost during the various immersions necessary for the staining procedure. The sections treated by the described method were inspected under light microscope and showed the location of MG63 cells inside of the porous material (see Figure 4.2). The cells were lining the pore walls of the composite material and it was observed that cells were adhering preferably to the calcium phosphate glass particles rather than to the PLA polymer.

(a)   *(b)*
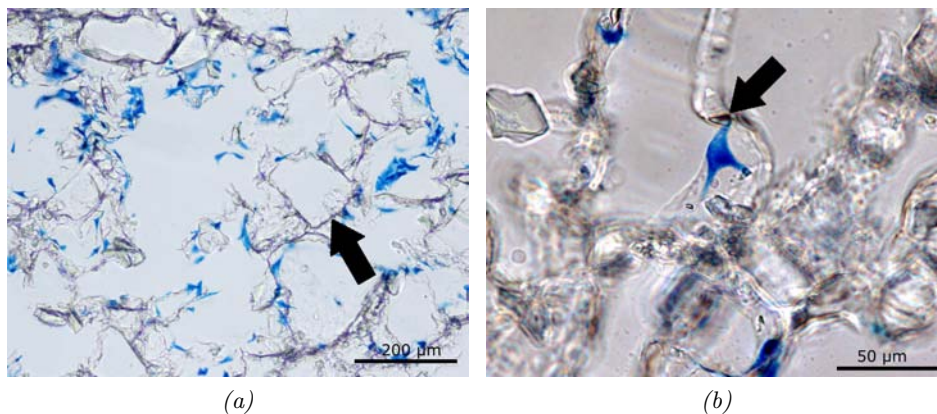
Figure 4.2: Light microscopy images of histological cuts performed with a rotary microtome after methylene blue staining of adhered MG63 cells (thickness 20 μm). *(a)* In lower magnification the cells can be seen distributed in the material. Arrow shows rectangular pores achieved by embedding salt crystals. *(b)* At higher magnifications the morphology of the cells show that cells do adhere preferably to the glass particles (arrow).

4.4.2   Cell seeding

4.4.2.1   Static cell seeding

The measurement of cell seeding efficiency of the cell injection used a quasi-static method resulted in an efficiency of 51.9 % ± 14.3 %.

For the assessment of cell distribution, the scaffolds were cut longitudinally and stained with acridine orange. The fluorescence images taken were converted and stitched together to represent a map of cell distribution over the whole scaffold interior and exterior (see Figure 4.3). The imaging suggested that on the exterior only few cells were located, while in the interior one region contained a high cell density.

Scaffold exterior

Scaffold interior

1 mm
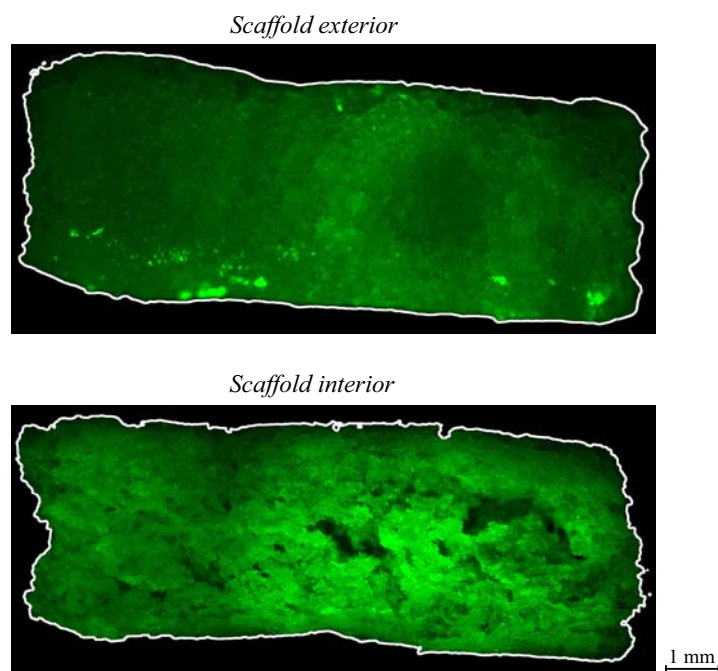
Figure 4.3: Cell staining with acridine orange allowed to observe the distribution of living cells in the scaffold seeded by the static method. The cells are represented as green areas.

4.4.2.2 Perfusion cell seeding

Estimation of shear stress on cells   To estimate the shear stress applied by the fluid flow on adhered cells in the scaffold, a calculation was conducted. Similar to Grayson et al. [16] it was assumed that the pathways through the scaffold were straight tubes of uniform diameter. The diameters were assumed here with 80 and 210 μm according to the size of the pore generating agent. The fluid induced wall shear stress τ_w can be calculated using the culture medium viscosity μ (0.77 cP) and density ρ (1.004 g/ml) [29], the linear fluid flow velocity v and the conduct diameter d. The equation used was derived from the Hagen-Poiseuille relation for laminar flow through a round conduit [16, 30].

$$\tau_w = \frac{4 \times Q \times \mu}{\pi \times r^3} = \frac{8 \times v \times \mu}{d} \tag{4.1}$$

The occurring velocities of 1 mm/s, 5 mm/s, 10 mm/s and 15 mm/s were adjusted to the sample porosity 95.7 % (1.0 mm/s, 5.1 mm/s, 10.3 mm/s and 15.4 mm/s respectively). Additionally for all velocities and diameters, the Reynolds number was calculated to ensure that the flow was laminar [31], which was a prerequisite for the use of the Hagen-Poiseuille relation.

$$R_e = \frac{\rho \times v \times d}{\mu} \tag{4.2}$$

The shear stresses for the four velocities were calculated and are depicted in Figure 4.4. For the diameters of the porosity from 80 to 210 μm shear stresses of up to 1.2 Pa were estimated. Comparing the estimated stresses with the physiological fluid induced shear stresses on bone cells between 0.8 and 3.8 Pa [32, 33], suggested that all fluid flow velocities applied provided a viable stress.
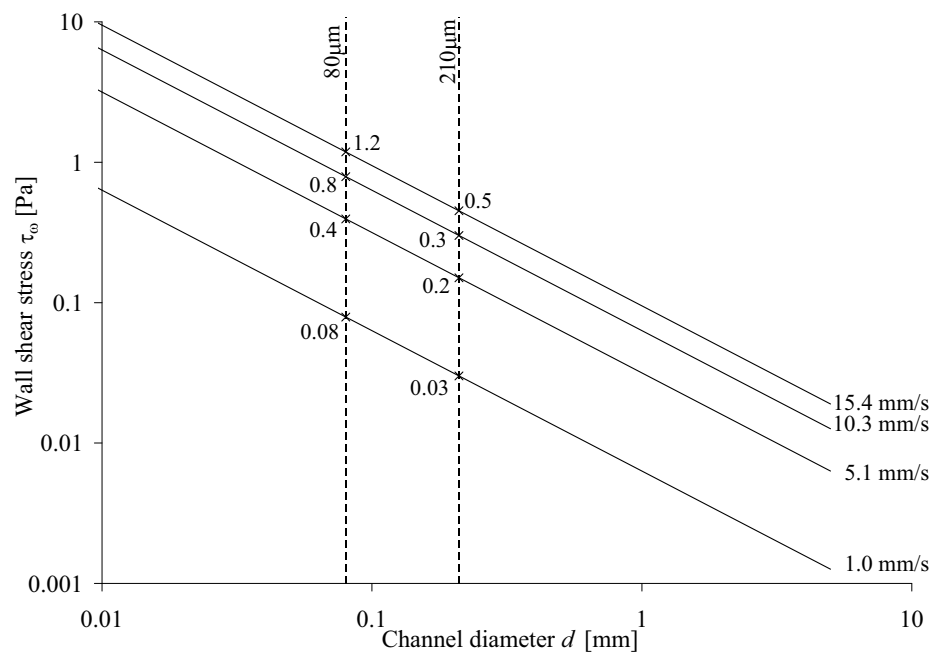
Figure 4.4: The wall shear stresses in tubular conduits was calculated to estimate the shear stresses occurring in the porosity of the PLA/glass composite scaffolds.

Cell distribution After seeding cells in the PLA/glass composite scaffolds using the perfusion bioreactor system with an initial cell number of 10^6 MG63 cells per scaffold, the cells which were present in the scaffolds were stained with acridine orange to determine their distribution on the interior. The staining was observed under fluorescence using a stereoscopic microscope. It was observed that the limited focus plane under the microscope reduced the sharp reproduction of the 3D structure, hence not depicting all stained cells in the images. Additionally, the cutting of the scaffolds affected their structural integrity, because the soft material was partially compressed during preparation. Even though the scaffolds were pulled open with tweezers, the internal structure showed alterations. The images taken under fluorescence were treated by desaturation and adjustment of contrast and brightness to make the cells better visible in print. Single images were stitched together to give a better impression of the overall distribution. Detail images of the perfusion entrance areas and the middle of the samples (see Figure 4.5, 4.6, 4.7 and 4.8) were used to compare the cell distribution at the different perfusion parameters, where the cells can be distinguished as black dots on the lighter background. The images suggested that the cell number inside of the scaffolds did increase with cycle number, showing more cells at 100 and 500 cycle seedings. Likewise an increasing cycle number seemed to improve the distribution throughout the scaffolds providing a more uniform cell distribution inside the scaffold (see Figures 4.5 and 4.6). In a similar way the increasing fluid flow velocity improved cell number and cell distribution up to 10 mm/s. The 15 mm/s experiments showed low cell number present despite the homogeneous cell distribution. Qualitatively the imaging showed that a minimum fluid flow velocity and cycle number had to be used to reach the aim of the perfusion cell seeding, uniform cell distribution and high cell density. The exterior of the scaffolds showed a similar pattern to the uniformity of cell distribution shown in Figures 4.7 and 4.8.

By staining the cut scaffolds with ethidium bromide it was possible to distinguish apoptotic cells from living cells. The obtained images were treated by desaturation and colour inversion and finally coloured red. The images were then overlaid with the green coloured acridine orange staining pictures to achieve maps of cell distributions on the exterior and interior of the scaffolds (see Figures 4.9 and 4.10). The images suggested that the ratio of

apoptotic cells to living cells is low in all cases. With higher cell seeding cycle numbers and higher perfusion flow velocities the amount of apoptotic cells increased. It was observed that one end of every sample bore more apaptotic cells than the other.
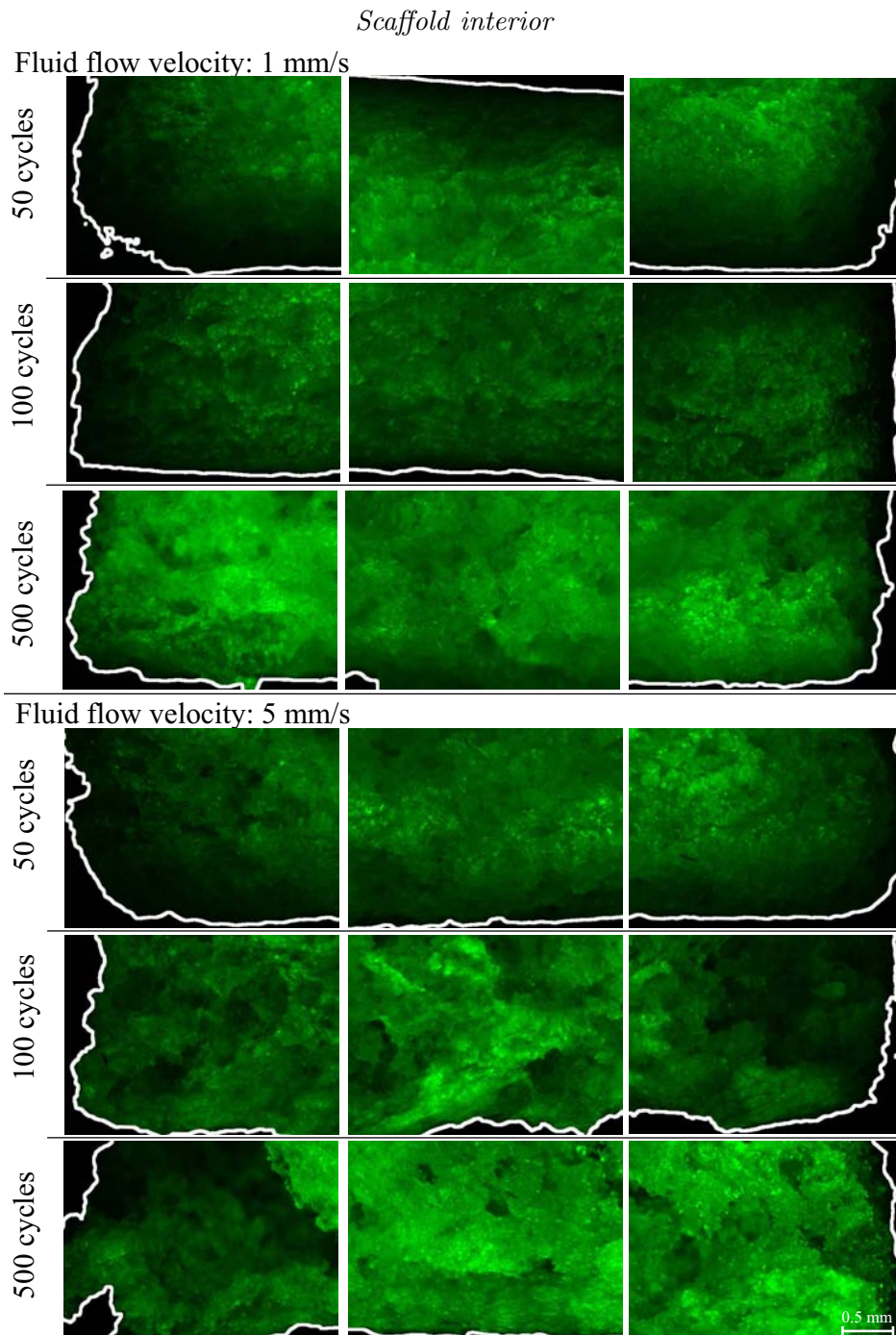
Figure 4.5: Scaffold interior: Cell staining with acridine orange allowed to observe the distribution of living cells on the inside of the scaffold. Shown are sections of both ends and the middle of the scaffolds' insides for 1 mm/s and 5 mm/s fluid flow velocities and 50, 100 and 500 cycles. The cells are represented as green points.
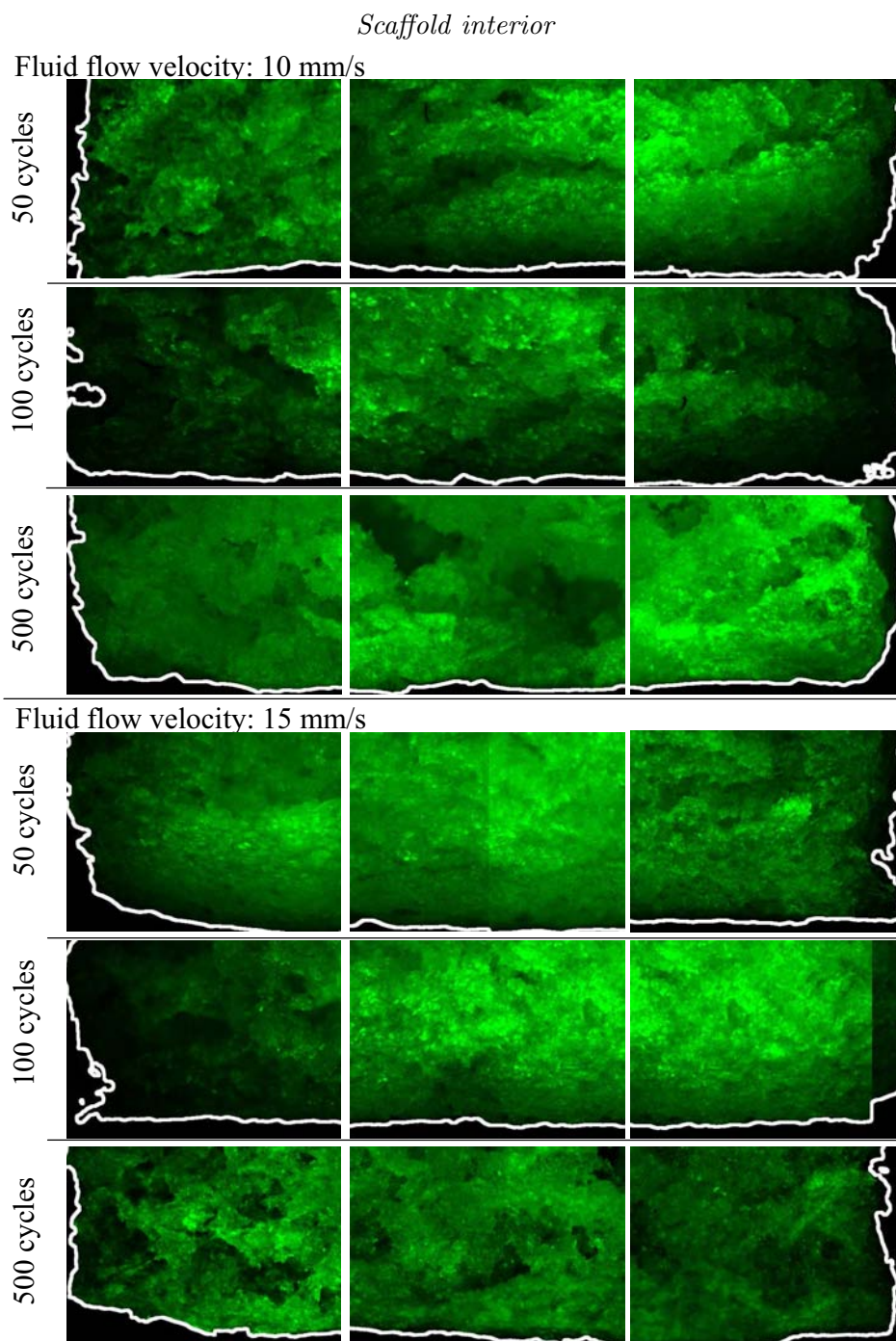
Scaffold interior

Figure 4.6: Scaffold interior: Cell staining with acridine orange allowed to observe the distribution of living cells on the inside of the scaffold. Shown are sections of both ends and the middle of the scaffolds' insides for 10 mm/s and 15 mm/s fluid flow velocities and 50, 100 and 500 cycles. The cells are represented as green points.

Scaffold exterior

Fluid flow velocity: 1 mm/s

Fluid flow velocity: 5 mm/s
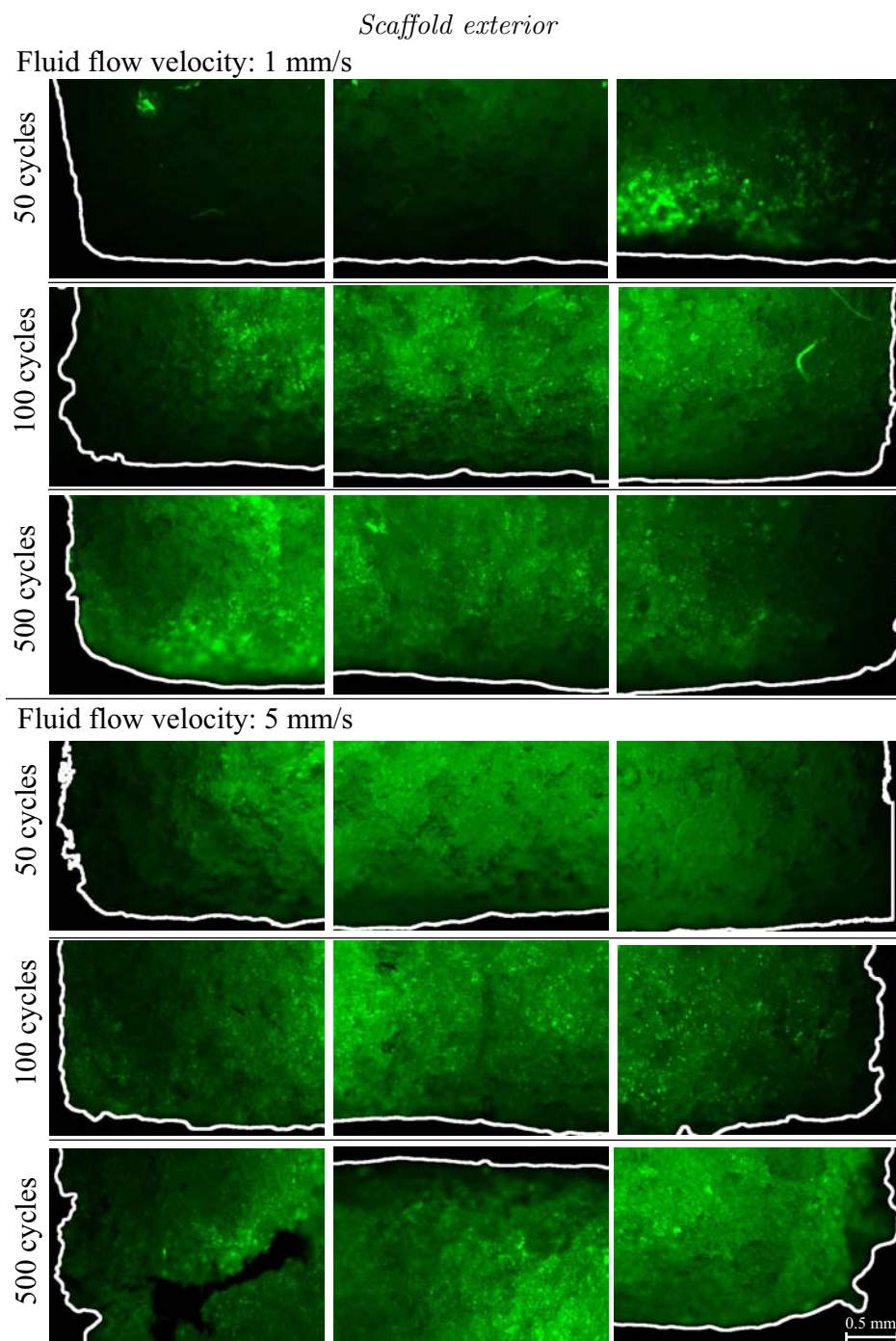
Figure 4.7: Scaffold exterior: Cell staining with acridine orange allowed to observe the distribution of living cells on the exterior of the scaffold. Shown are sections of both ends and the middle of the scaffolds' outsides for 1 mm/s and 5 mm/s fluid flow velocities and 50, 100 and 500 cycles. The cells are represented as black points.

Scaffold exterior

Fluid flow velocity: 10 mm/s

Fluid flow velocity: 15 mm/s
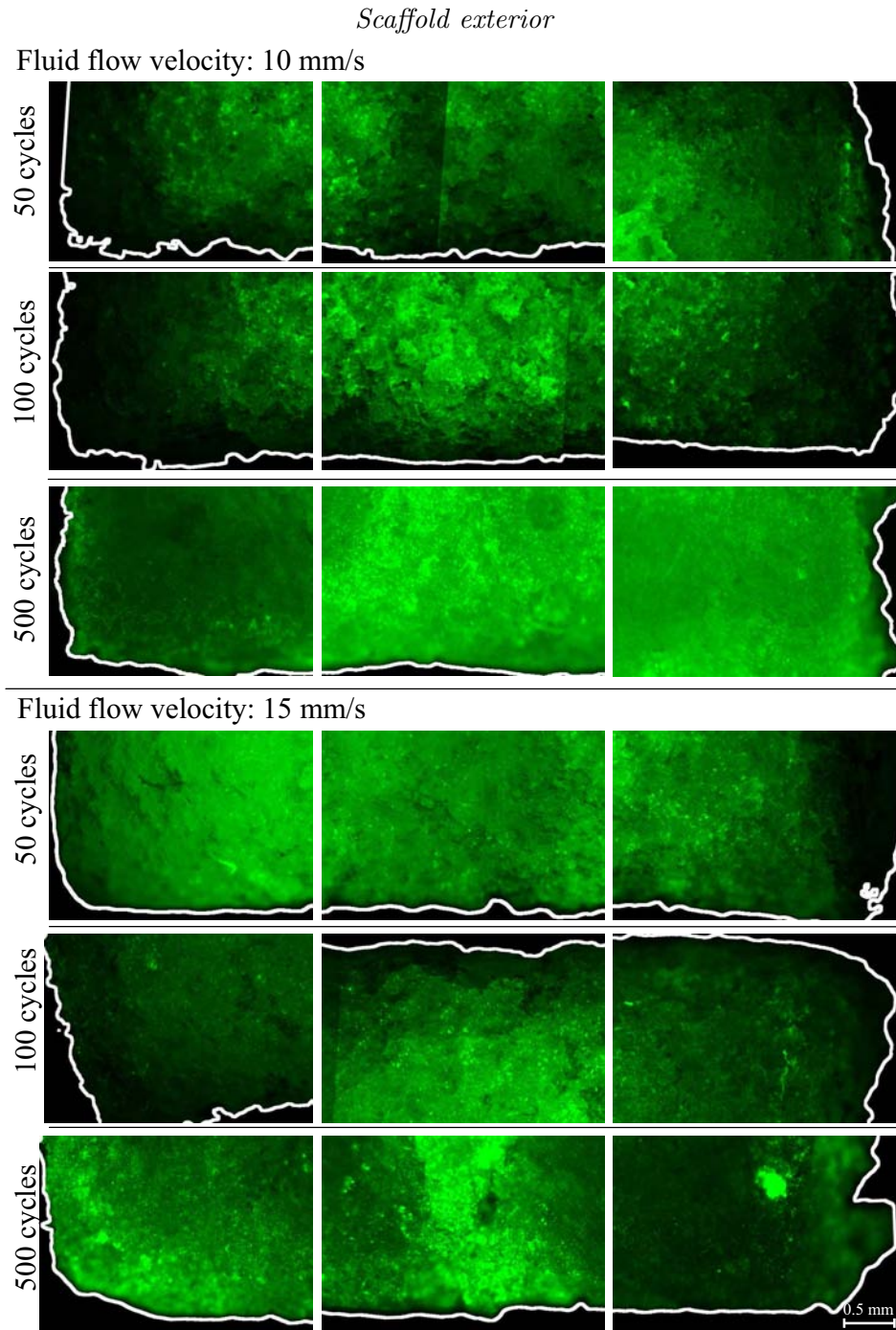
Figure 4.8: Scaffold exterior: Cell staining with acridine orange allowed to observe the distribution of living cells on the exterior of the scaffold. Shown are sections of both ends and the middle of the scaffolds' outsides for 10 mm/s and 15 mm/s fluid flow velocities and 50, 100 and 500 cycles. The cells are represented as black points.

Scaffold interior
Perfusion fluid flow velocity
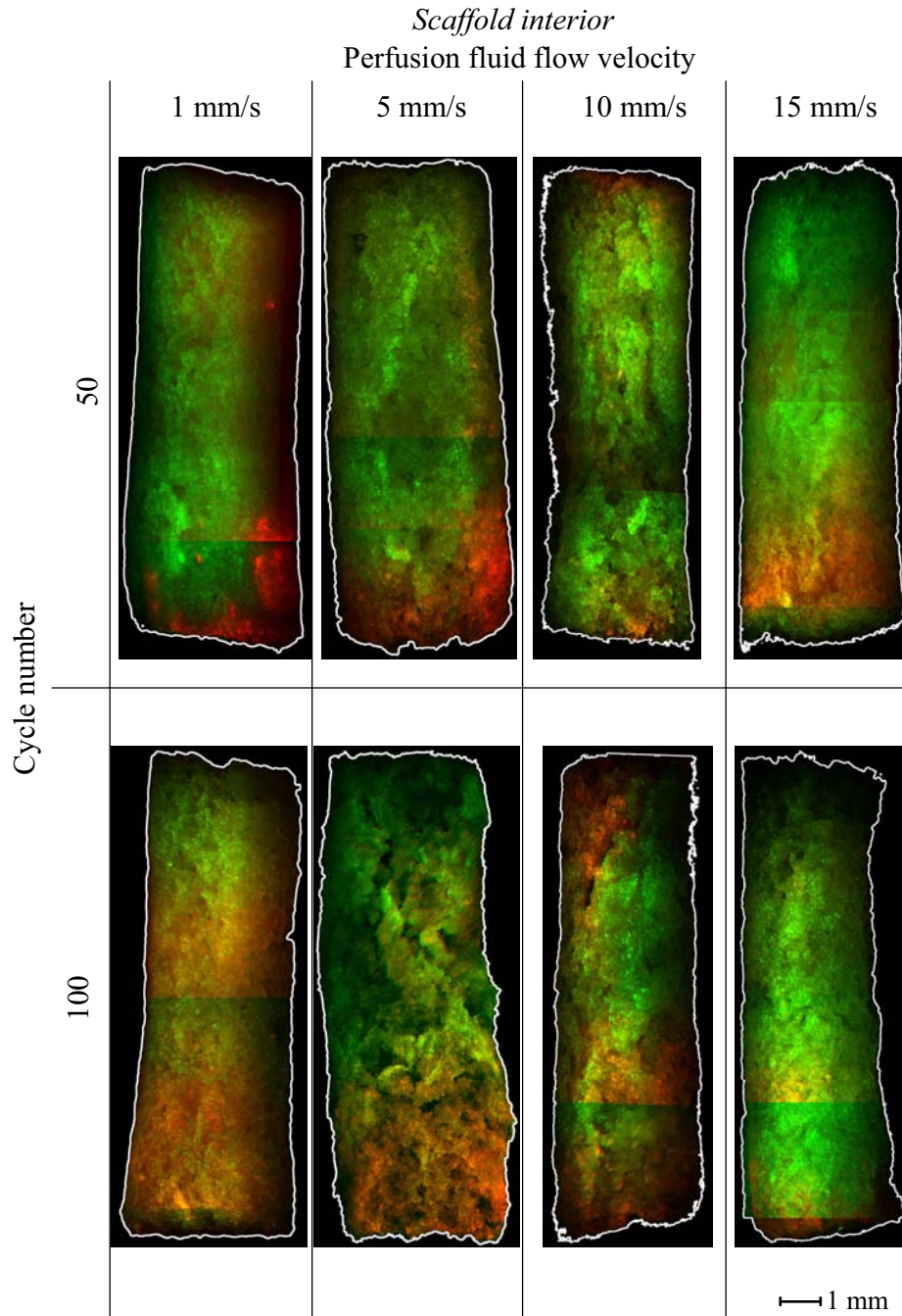
Figure 4.9: Scaffold interior: Cell staining with ethidium bromide and acridine orange allowed to observe the distribution of living and apoptotic cells on the inside of the scaffolds. Shown are longitudinal sections of scaffolds insides for 1 mm/s, 5 mm/s, 10 mm/s and 15 mm/s fluid flow velocities and 50 and 100 cycles. The living cells are represented as green areas, apoptotic cells are coloured red.
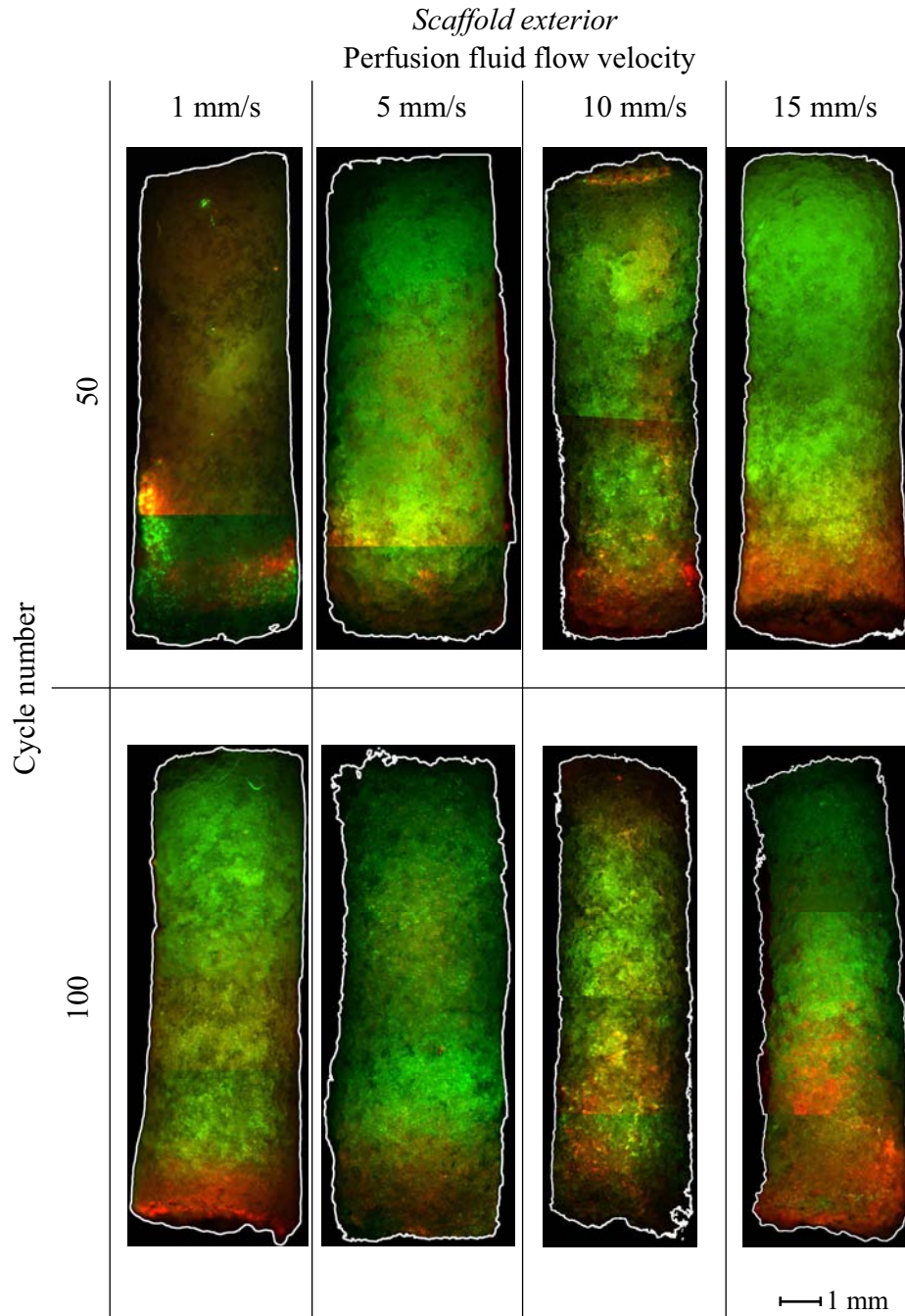
Figure 4.10: Scaffold exterior: Cell staining with ethidium bromide and acridine orange allowed to observe the distribution of living and apoptotic cells on the exterior of the scaffolds. Shown are scaffold outsides for 1 mm/s, 5 mm/s, 10 mm/s and 15 mm/s fluid flow velocities and 50 and 100 cycles. The living cells are represented as green areas, apoptotic cells are coloured red.

Cell seeding efficiency   After seeding cells with 10^6 MG63 cells initially per scaffold using the perfusion bioreactor system, scaffolds were frozen three times to free all incorporated LDH. The samples were diluted 50:50 and the absorbance of the samples was measured at 450 nm wavelength for four samples per perfusion seeding condition. The total cell number was calculated by the use of the standard curves, taking into account the dilution and the total volume of the samples. The cell seeding efficiency was then calculated as ratio of the found cell number to the initial cell number. Figure 4.11 shows the average efficiencies and standard deviations of the samples.
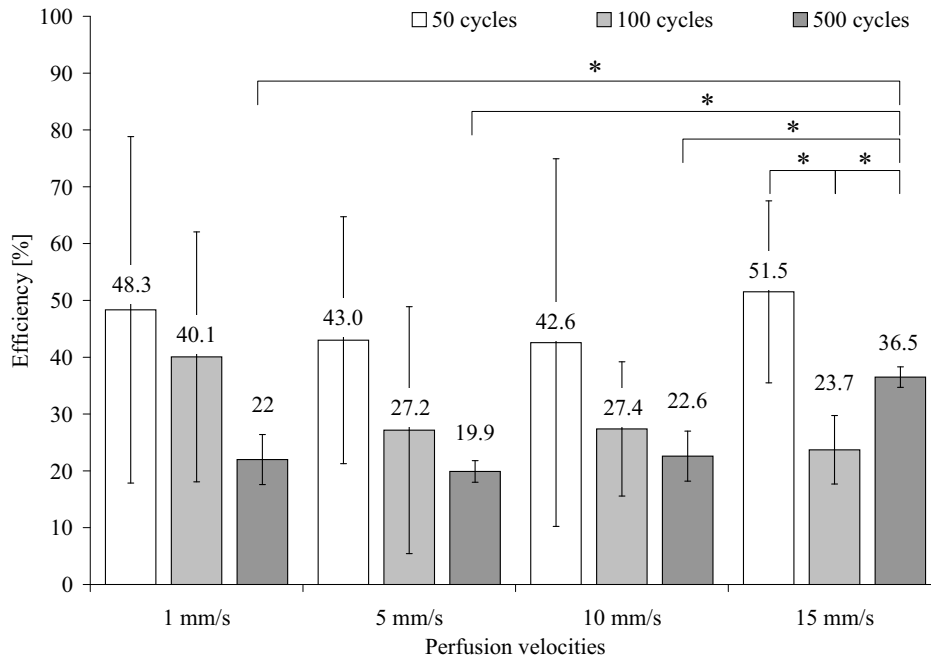
Fluid flow velocity	Perfusion cycle number		
	50 cycles	100 cycles	500 cycles
1 mm/s	48.3±30.5	40.1±22.0	22.0±4.4
5 mm/s	43.0±21.7	27.2±21.7	19.9±1.9
10 mm/s	42.6±32.4	27.4±11.8	22.6±4.4
15 mm/s	51.5±16.0	23.7±6.0	36.5±1.8

Figure 4.11: Cell seeding efficiencies achieved with different fluid flow velocities and varying cycle number with initially 10^6 MG63 cells per scaffold in the perfusion bioreactor system (n=4). Marked groups (*) are statistically significantly different (Student's t-test, $p < 0.05$).

As can be observed in Figure 4.11, the uniformity of seeding between samples increased with the increasing number of perfusion seeding oscillations which can be observed by the narrowing standard deviations. At the

same time higher numbers of seeding cycles did lower the efficiency of the seeding from about 50 % to about 20 %. The changes of fluid flow velocity did not influence the cell seeding efficiency significantly at constant perfusion cycle numbers. An exception to this finding is the case of the 15 mm/s perfusion fluid flow velocity at 500 cycles, which was significantly higher than the efficiencies found at the same cycle number and varying velocity, as was confirmed by Student's t-test ($p < 0.05$).

4.5 Discussion

As was observed during the preliminary test conducted to determine the feasibility of methodology, the sectioning of the microtome sectioning of the samples was not applicable, because only thick partial cuts could be preserved. This was not sufficient to obtain a representation of cell distribution in the interior of the scaffold as was intended. Nevertheless it was possible to examine the structure of the scaffold porosity and the morphology of the cells in the scaffold. It was found that cells adhere better to glass than polymer which is in accordance with the findings of Charles-Harris et al. [34] using the same material and cell type. This behaviour is attributed to the differences in hydrophobicity of both phases. The calcium phosphate glass is more hydrophilic than the PLA [35], which is the most likely cause for a better cell adhesion on the glass particles.

Cell distribution after perfusion cell seeding was observed by cutting open the seeded scaffolds and observing stained cells under fluorescence. This method was found feasible although the structure of the sample was affected by the cutting of the sample. Nevertheless it was possible to observe the distribution of cells throughout the scaffolds. One of the most critical requirements of the perfusion seeding method is the location of cells into the deep porosity of large scaffolds. In this study it was found that for the porous PLA/calcium phosphate glass composite material, velocities over 1 mm/s were needed to press the cells inside of the scaffolds. This is similar to the finding of Wendt et al. [6] which showed that a minimum velocity was needed for a successful cell seeding. It was found that a more uniform distribution of living cells was achieved at 5 mm/s, 10 mm/s and 15 mm/s of fluid flow velocity. The increase in the cell seeding perfusion cycle number did improve the cell distribution throughout the scaffolds. The staining of apoptotic cells suggested that high perfusion cycle numbers had a negative effect on the cell viability, resulting in bigger regions of fluorescence. Higher intensities of the staining were found always on one extreme of the samples. Even though it was not recorded which side of the sample, bottom or top, showed this phenomenon, it was suspected to be on the bottom, being the entry of cells during cell suspension injection and hence the place of high cell densities at the beginning seeding cycles. More apoptotic cells were also

found at high velocities, which also indicated higher stresses on the cells. Hence lower cell seeding fluid flow velocities are better as well as few seeding cycles. The results from this part of the study suggested that a fluid flow velocity of 5 mm/s and 100 cycles of perfusion is sufficient to provide an uniform cell distribution and keeps stress on the cells limited.

To estimate the shear stress on the cells in the scaffolds porosities a calculation was performed based on Hagen-Poisseuille relation. This calculation did not take into account the tortuosities of the fluid flow pathways and the non-uniform structure of the fluid pathways. A computational model realised by Milan et al. [36] for the same PLA/glass composite material showed stresses of 1-8 mPa at 100 μm/s. The estimation applied here gave for this inlet velocity stresses of 3-8 mPa, showing that the estimation was in the same magnitude of the more sophisticated method. The shear stresses estimated for the different fluid flow velocities were in the physiological range of bone cells. This was not consistent with the increasing regions of dying cells at velocities of 10-15 mm/s. It was suggested that the high velocities combined with the numerous direction changes of the fluid flow caused the elevated stress on cells.

The static seeding performed by injecting cells into scaffolds yielded a efficiency comparable to the perfusion seeding. The cell distribution however showed that the cells were concentrated in one area of the scaffold interior, which was less homogeneous than the distribution achieved by perfusion seeding. A region of high cell density was observed at the place of injection of the cell suspension.

The results of the cell seeding efficiencies at different fluid flow velocities and cycle numbers cannot be compared directly, because of the high standard deviations. However a trend can be observed that suggested that the velocity of cell seeding cycles did not have an influence on the number of cells located in the scaffolds. The distribution of cells between samples in the same seeding channel was improved by higher cell seeding cycle numbers as shown by the decreasing standard deviations, whereas at the same time the efficiencies decreased.

Overall the cell seeding was relatively low compared to research mentioned in the introduction [5, 6] with a maximum of about 50 % and high standard deviations. The high standard deviations showed that at low seed-

ing cycles the cells were distributed unevenly between the two scaffolds in one channel. It is important to mention that for this study the efficiency was determined per scaffold instead per channel. A lower deviation might be found when comparing the overall efficiency per channel, but this would exclude information about individual scaffolds. The low efficiency obtained may be caused by the low cell suspension density of 2×10^5 cells/ml. Another parameter possibly responsible for the low cell seeding efficiency can be the volume of moved cell suspension in every cell seeding cycle. This volume was predefined as 4.5 ml in the development of the perfusion bioreactor system.Implementing a higher volume transport would imply the use of longer ascension tubes (or the implementation of a large diameter container above the perfusion chambers) and the further dilution of the cell suspension, which is unfavourable for achieving high cell seeding densities. Even though the cell seeding efficiency was found to be low, when calculating the cell density over the scaffold volume, the magnitude of 10^6 cells/cm^3 was in the range of 10^5 cells/cm^3 [8] to 10^8 cells/cm^3 [6, 14] found in comparable studies. Without any doubt the comparison of different studies is complicated, because of the different materials, perfusion systems and cell suspension densities used. This study has shown that cell seeding in the developed perfusion bioreactor system is feasible and comparable to other existing systems. It was further shown that the cell seeding on scaffolds of large volume and high length to diameter ratio can be achieved by the perfusion approach, which is a very important step towards the cell culture in large scaffolds. Of further interest is the development of cell viability and distribution over longer times after the perfusion cell seeding.

4.6   Conclusions

- It was concluded that the perfusion cell seeding experiments showed the functionality of the developed perfusion bioreactor system. It was possible to bring MG63 cells into the deep pores of the scaffolds, which is essential for the further cell culture. Furthermore the cell seeding of large scaffolds was achieved successfully, opening the way for the culture of large tissue engineered bone substitutes.

- It was determined that a minimum perfusion velocity was needed to push cells into the scaffolds and the most uniform cell distribution was observed at 5 mm/s, 10 mm/s and 15 mm/s and 100 to 500 perfusion cycles.

- Cell viability was determined to be higher at low perfusion velocities, as could be observed in the staining of apoptotic cells, which indicated that high velocities and seeding cycles signified high stress on cells.

- The cell seeding efficiency achieved by the described method was about 50 %. The results suggested that cell seeding efficiency was not influenced by the perfusion seeding velocities, but rather by the perfusion seeding cycle number.

Bibliography

[1] C. E. Holy, M. S. Shoichet, and J. E. Davies. Engineering three-dimensional bone tissue in vitro using biodegradable scaffolds: investigating initial cell-seeding density and culture period. *J Biomed Mater Res*, 51:376–382, Sep 2000.

[2] S. L. Ishaug-Riley, G. M. Crane-Kruger, M. J. Yaszemski, and A. G. Mikos. Three-dimensional culture of rat calvarial osteoblasts in porous biodegradable polymers. *Biomaterials*, 19:1405–1412, Aug 1998.

[3] J. van den Dolder, P. H. Spauwen, and J. A. Jansen. Evaluation of various seeding techniques for culturing osteogenic cells on titanium fiber mesh. *Tissue Eng*, 9:315–325, Apr 2003.

[4] Y. Li, T. Ma, D.A. Kniss, L.C. Lasky, and S.T. Yang. Effects of filtration seeding on cell density, spatial distribution, and proliferation in non woven fibrous matrices. *Biotechnol Prog*, 17(5):935–944, 2001.

[5] J. F. Alvarez-Barreto, S. M. Linehan, R. L. Shambaugh, and V. I. Sikavitsas. Flow perfusion improves seeding of tissue engineering scaffolds with different architectures. *Ann Biomed Eng*, 35:429–442, Mar 2007.

[6] D. Wendt, A. Marsano, M. Jakob, M. Heberer, and I. Martin. Oscillating perfusion of cell suspensions through three-dimensional scaffolds enhances cell seeding efficiency and uniformity. *Biotechnol Bioeng*, 84(2):205–214, 2003.

[7] W. T. Godbey, S. B. Hindy, M. E. Sherman, and A. Atala. A novel use of centrifugal force for cell seeding into porous scaffolds. *Biomaterials*, 25:2799–2805, Jun 2004.

[8] F. Zhao and T. Ma. Perfusion bioreactor system for human mesenchymal stem cell tissue engineering: Dynamic cell seeding and construct development. *Biotechnol Bioeng*, 91(4), 2005.

[9] J. F. Alvarez-Barreto and V. I. Sikavitsas. Improved mesenchymal stem cell seeding on RGD-modified poly(L-lactic acid) scaffolds using flow perfusion. *Macromol Biosci*, 7:579–588, May 2007.

[10] T. Kitagawa, T. Yamaoka, R. Iwase, and A. Murakami. Three-dimensional cell seeding and growth in radial-flow perfusion bioreactor for in vitro tissue reconstruction. *Biotechnol Bioeng*, 93:947–954, Apr 2006.

[11] E. J. Lee, G. Vunjak-Novakovic, Y. Wang, and L. E. Niklason. A biocompatible endothelial cell delivery system for in vitro tissue engineering. *Cell Transplant*, Apr 2009.

[12] E. M. Bueno, G. Laevsky, and G. A. Barabino. Enhancing cell seeding of scaffolds in tissue engineering through manipulation of hydrodynamic parameters. *J Biotechnol*, 129:516–531, May 2007.

[13] F.W. Janssen, I. Hofland, A. van Oorschot, J. Oostra, H. Peters, and C.A. van Blitterswijk. Online measurement of oxygen consumption by goat bone marrow stromal cells in a combined cell-seeding and proliferation perfusion bioreactor. *J Biomed Mater Res*, 79A:338–348, 2006.

[14] M. Radisic, M. Euloth, L. Yang, R. Langer, L. E. Freed, and G. Vunjak-Novakovic. High-density seeding of myocyte cells for cardiac tissue engineering. *Biotechnol Bioeng*, 82:403–414, May 2003.

[15] M. Radisic, A. Marsano, R. Maidhof, Y. Wang, and G. Vunjak-Novakovic. Cardiac tissue engineering using perfusion bioreactor systems. *Nat Protoc*, 3:719–738, 2008.

[16] W. L. Grayson, S. Bhumiratana, C. Cannizzaro, P. H. Chao, D. P. Lennon, A. I. Caplan, and G. Vunjak-Novakovic. Effects of initial seeding density and fluid perfusion rate on formation of tissue-engineered bone. *Tissue Eng Part A*, 14:1809–1820, Nov 2008.

[17] J. P. Chen and C. T. Lin. Dynamic seeding and perfusion culture of hepatocytes with galactosylated vegetable sponge in packed-bed bioreactor. *J Biosci Bioeng*, 102:41–45, Jul 2006.

[18] I. Shvartsman, T. Dvir, T. Harel-Adar, and S. Cohen. Perfusion cell seeding and cultivation induce the assembly of thick and functional hepatocellular tissue-like construct. *Tissue Eng Part A*, 15:751–760, Apr 2009.

[19] N. E. Timmins, A. Scherberich, J. A. Früh, M. Heberer, I. Martin, and M. Jakob. Three-dimensional cell culture and tissue engineering in a T-CUP (tissue culture under perfusion). *Tissue Eng*, 13:2021–2028, Aug 2007.

[20] G. Vunjak-Novakovic, B. Obradovic, I. Martin, P. M. Bursac, R. Langer, and L. E. Freed. Dynamic cell seeding of polymer scaffolds for cartilage tissue engineering. *Biotechnol Prog*, 14:193–202, 1998.

[21] K. J. Burg, W. D. Holder, C. R. Culberson, R. J. Beiler, K. G. Greene, A. B. Loebsack, W. D. Roland, P. Eiselt, D. J. Mooney, and C. R. Halberstadt. Comparative study of seeding methods for three-dimensional polymeric scaffolds. *J Biomed Mater Res*, 51:642–649, Sep 2000.

[22] X. Qi, J.G. Liu, Y. Chang, and X.X. Xu. Comparative study on seeding methods of human bone marrow stromal cells in bone tissue engineering. *Chin Med J*, 117(4):576–580, 2004.

[23] V. A. Kasyanov, J. Hodde, M. C. Hiles, C. Eisenberg, L. Eisenberg, L. E. De Castro, I. Ozolanta, M. Murovska, R. A. Draughn, G. D. Prestwich, R. R. Markwald, and V. Mironov. Rapid biofabrication of tubular tissue constructs by centrifugal casting in a decellularized natural scaffold with laser-machined micropores. *J Mater Sci Mater Med*, 20:329–337, Jan 2009.

[24] M. Bok, H. Li, L. Y. Yeo, and J. R. Friend. The dynamics of surface acoustic wave-driven scaffold cell seeding. *Biotechnol Bioeng*, 103:387–401, Jun 2009.

[25] L. A. Solchaga, E. Tognana, K. Penick, H. Baskaran, V. M. Goldberg, A. I. Caplan, and J. F. Welter. A rapid seeding technique for the assembly of large cell/scaffold composite constructs. *Tissue Eng*, 12:1851–1863, Jul 2006.

[26] M. M. Barthold, I. Majore, S. Fargali, F. Stahl, R. Schulz, S. Lose, H. Mayer, and V. Jäger. 3d-cultivation and characterisation of osteogenic cells for the production of highly viable bone tissue implants. In *Animal Cell Technology Meets Genomics*, volume 2, pages 199–205,

2005. Proceedings of the 18th ESACT Meeting Granada, Spain, May 11-14, 2003.

[27] J. Caviedes-Bucheli, N. Avendaño, R. Gutierrez, S. Hernández, G. C. Moreno, M. C. Romero, and H. R. Muñoz. Quantification of lactate-dehydrogenase and cell viability in postmortem human dental pulp. *J Endod*, 32:183–185, Mar 2006.

[28] M. Q. Tran, Y. Nygren, C. Lundin, P. Naredi, and E. Björn. Evaluation of cell lysis methods for platinum metallomic studies of human malignant cells. *Anal Biochem*, Sep 2009.

[29] J. L. Moreira, P. C. Santana, A. S. Feliciano, P. E. Cruz, A. J. Racher, J. B. Griffiths, and M. J. Carrondo. Effect of viscosity upon hydrodynamically controlled natural aggregates of animal cells grown in stirred vessels. *Biotechnol Prog*, 11:575–583, 1995.

[30] R. S. Reneman, T. Arts, and A. P. Hoeks. Wall shear stress–an important determinant of endothelial cell function and structure–in the arterial system in vivo. Discrepancies with theory. *J Vasc Res*, 43:251–269, 2006.

[31] O. Reynolds. An experimental investigation of the circumstances which determine whether the motion of water shall be direct or sinuous, and of the law of resistance in parallel channels. *Phil Trans R Soc*, 174:935–982, 1883.

[32] S. Weinbaum, S.C. Cowin, and Y. Zeng. A model for the excitation of osteocytes by mechanical loading-induced bone fluid shear stresses. *J Biomech*, 27:339–360, 1994.

[33] S. C. Cowin, S. Weinbaum, and Y. Zeng. A case for bone canaliculi as the anatomical site of strain generated potentials. *J Biomech*, 28:1281–1297, Nov 1995.

[34] M. Charles-Harris, M. A. Koch, M. Navarro, D. Lacroix, E. Engel, and J. A. Planell. A PLA/calcium phosphate degradable composite material for bone tissue engineering: an in vitro study. *J Mater Sci Mater Med*, 19:1503–1513, Apr 2008.

[35] M. Navarro Toro. *Desarrollo y caracterización de materiales biodegradables para regeneración ósea.* PhD thesis, Technical University of Catalonia, 2005.

[36] J. L. Milan, J. A. Planell, and D. Lacroix. Computational modelling of the mechanical environment of osteogenesis within a polylactic acid-calcium phosphate glass scaffold. *Biomaterials*, 30:4219–4226, Sep 2009.

128

Chapter 5

Cell Culture in the Perfusion Bioreactor System

5.1 Introduction

It has been demonstrated that cell culture under fluid flow is a promising approach for the conditioning of bone tissues cultured *in vitro* and the production of clinically relevant engineered tissue volumes [1]. A seeded scaffold can be cultured in perfusion bioreactors over long periods of time, achieving highly cellularised tissue substitutes, containing the tissue specific extracellular matrix. Studies have shown in 2D and 3D culture that a steady flow as well as an alternating fluid flow profile can guide cell differentiation and enhance cell activity [2–18].

The patterns used for perfusion cell culture in scaffolds can be divided into a steady flow, which provides viable conditions, and an alternating flow as a stimulus for cell activity (see Table 5.1). Steady fluid flow rates in the range of 5 μm/s to 400 μm/s [2–12, 19] enhance the distribution, proliferation and osteoblastic differentiation of cells [11, 12, 20, 21], showing the osteoblastic differentiation by enhanced production of alkaline phosphatase (ALP) [7, 8, 13, 22–24], osteopontin [22] and osteocalcin [7, 19] and an increased calcium deposition [10, 13, 18, 22]. Alternating or oscillating fluid flow was studied predominantly in 2D experiments. It was found that alternating fluid flow alters cell activity [17], enhancing prostaglandin E_2 (PGE_2) and intracellular calcium release in comparison to continuous flow

[14–16]. Also pulsatile fluid flow has shown to enhance cell proliferation over longterm treatment [14]. When the cell culture under fluid flow was studied in 3D scaffolds, it was observed that analogue to the 2D experiments, pulsatile perfusion caused enhancement of prostaglandin E_2 (PGE_2) release [4]. Alternating fluid flow through porous scaffolds maintained cell viability and stimulated osteoblast differentiation [6, 25, 26] and resulted in constructs capable of inducing bone formation upon implantation [27]. Also did the application of dynamic fluid flows enhance cellular distribution and osteogenic responses of the scaffold [28].

The alternating fluid flow for cell stimulation for the perfusion culture of bone cells had a frequency of 1-2 Hz with fluid flow velocities of up to 8.5 mm/s and a stimulation duration of 30 minutes daily up to three times 1 hour per day [4, 6, 26, 28] (see Table 5.1).

The flow rate applied to cells in scaffolds is highly important for the cell culture, because even though lower rates increase the proportion of viable cells in the scaffold, high flow rates can result in cell death [5]. As stated for the cell seeding, the scaffold microstructure has an important role on the fluid flow velocities in the fluid pathways and hence on the stimulation of cells.

The beneficial role of fluid flow on the development of engineered tissue in perfusion bioreactors give the basis for the presented study, which aims at the culture of mesenchymal cells on large porous composite scaffolds using the developed perfusion bioreactor system.

Flow	Reference	Cell type	Continuous velocity*	Alternating velocity*	Repetitions	Stimulation duration	Total duration
	Volkmer et al.[29]	MC3T3-E1	5 μm/s	-	-	-	1 week
	Glaum et al. [30]	osteoblast-like cells	6 μm/s	-	-	-	2 weeks
	Zhao et al. [21]	hMSC	10 μm/s	-	-	-	35 days
	Hosseinkhani et al. [31]	rMSC	20 μm/s	-	-	-	3 weeks
	Wang et al. [7]	BMSC	20 μm/s	-	-	-	4 weeks
	Bögel et al. [24]	MG63	30 μm/s	-	-	-	17 days
	Meinel et al. [13]	hMSC	35 μm/s	-	-	-	5 weeks
	Hosseinkhani et al. [19]	rMSC	40 μm/s	-	-	-	2 days
	Li et al. [23]	osteoblast	50 μm/s	-	-	-	16 days
	Freyria et al. [32]	primary chondrocytes	20-60 μm/s	-	-	-	3 weeks
	Zhao et al. [33]	hMSC	10-150 μm/s	-	-	-	20 days
steady	Yang et al. [20]	hMSC	0.1 mm/s	-	-	-	12 days
	Wendt et al. [2]	articular chondrocytes	0.1 mm/s	-	-	-	2 weeks
	Du et al. [25]	MC3T3-E1	0.2 mm/s	-	-	-	6 days
	Goldstein et al. [8]	osteoblasts	0.2 mm/s	-	-	-	2 weeks
	Holtorf et al. [22]	rMSC	0.3 mm/s	-	-	-	16 days
	Holtorf et al. [11]	rMSC	0.3 mm/s	-	-	-	16 days
	Gomes et al. [10]	rMSC	0.3 mm/s	-	-	-	15 days
	Fassina et al. [12]	SAOS-2	0.3 mm/s	-	-	-	16 days
	Grayson et al. [3]	hMSC	0.1-0.4 mm/s	-	-	-	5 weeks
	Du et al. [34]	MC3T3-E1	-	0.1 mm/s	cont.	1/60 Hz	6 days
	Du et al. [25, 35]	MC3T3-E1	-	0.1-0.2 mm/s	cont.	1/120 Hz	6 days
	Timmins et al. [27]	BMSC	-	0.4-1 mm/s	cont.	NA	19 days
alternating	Plunkett et al. [28]	MC3T3-E1	0 mm/s	0.2 mm/s	3× daily	1h, ∼0.04-0.07Hz	14 days
	Plunkett et al. [28]	MC3T3-E1	10 μm/s	0.2 mm/s	3× daily	1h, ∼0.04-0.07Hz	2 days
	Jaasma et al. [6, 26]	MC3T3-E1	20 μm/s	0.2 mm/s	3× daily	1h at 1Hz	1 day
	Vance et al. [4]	MC3T3-E1	5 μm/s	8.5 mm/s	daily	30 min at 1 Hz	2 days

Figure 5.1: Long term cell culture patterns used in cell culture in 3D scaffolds for bone and cartilage tissue engineering.
*Fluid flow velocities were calculated from the fluid flow and scaffold cross-section area given in the respective publications.

5.2　Objectives

The objective of this study was to determine the applicability of the developed perfusion bioreactor system for the long term culture of rat mesenchymal cells (rMSC) on large porous PLA/glass scaffolds. The cell culture was conducted with a steady fluid flow for maintenance of viable cell culture conditions and a daily stimulation by oscillating fluid flow. In this study the cell activity after long culture periods was determined by the resulting cell proliferation, distribution and differentiation. The hypothesis of this study was, that it is possible to maintain viable cells in large porous scaffold using the perfusion bioreactor and influence the differentiation of mesenchymal stem cells by oscillating fluid flow stimulation.

5.3　Materials and methods

5.3.1　Scaffold preparation

For the cell culture experiments the same scaffold type was used as for the cell seeding presented in Chapter 4. The PLA/glass scaffolds were sterilised with gamma rays at 8 kGy prior to the experiments. One day before cell seeding the needed number of scaffolds was taken out of the packing under sterile conditions and immersed in 30 % ethanol for prewetting. The scaffolds were then transferred to a Petri dish with complete advanced medium (Advanced DMEM, 15 % FBS, 1 % penicillin-streptomycin and 1 % L-glutamine) and incubated overnight. At the beginning of the experiments the scaffolds and the medium were observed under a light microscope to exclude possible bacterial contamination.

5.3.2　Cell preparation

Mesenchymal stem cells were isolated from rat bone marrow. For this, Lewis rats (Charles-River) were sacrificed and femora and tibiae were surgically removed. Bone marrow was obtained by flushing the inside of the bones with advanced DMEM (15 % FBS, 1 % penicillin-streptomycin, 1 % L-glutamine, 1 % sodium pyruvate) and 22.5 μg/ml heparin. The obtained cell fraction was transferred to 6-well plates and allowed to adhere. After 24 hours, supernatant was removed and fresh medium was added. 2-3 days after the

initial plating a population of small, elongated, spindle-shaped cells rapidly proliferating could be observed. Cells were trypsinised at subconfluence and passaged 1:3. Cells from passages 3 to 6 were frozen in liquid nitrogen for later cell culture. The cell line for experiments was cultured with complete advanced DMEM (15 % FBS, 1 % penicillin-streptomycin and 1 % L-glutamine) and trypsinised according to protocol described in Chapter 4. rMSC from pass 4 to 8 where used for the experiments.

5.3.3 Static cell seeding

As a comparison to the perfusion seeding method, 300.000 rMSC cells per scaffold suspended in 300 μl complete medium were injected with a syringe (0.9 mm needle) into the composite material. After the injection, the samples were incubated in complete medium for four hours to allow cell adhesion. Five samples were washed with PBS and frozen in serum-reduced medium and used for the determination of the cell number.

5.3.4 Perfusion cell seeding

For the cell seeding, the cell suspension was diluted to a density of 2×10^6 cells per 10 ml medium. Suspended cells were seeded according to the procedure used in the previous cell seeding experiments (see Chapter 4) using the perfusion bioreactor system assembly as presented in Chapter 3. Ten millilitre cell suspension were injected into the side valve of each perfusion bioreactor channel with 10^6 cells per scaffold. The suspension was then oscillated through the scaffolds at 5 mm/s for 100 cycles. After completion of the cell seeding cycles, the cell suspension was left four hours in the system to allow cell adhesion and then extracted from the channel with a syringe.

5.3.5 Cell culture

As presented in Chapter 3, the assembly was changed after completed cell seeding. Reservoirs with 100 ml advanced DMEM medium were put into the channels as shown in Chapter 3 and exchanged weekly for the experiments of two and three weeks period. The stimulation pattern was set to an oscillating fluid flow velocity of 5 mm/s at 0.5 Hz for 30 minutes per day. The rest of the day a steady flow of 0.1 mm/s was applied to exchange continually medium

in the scaffolds. Cell culture was conducted for 1 day, 1 week, 2 weeks and 3 weeks. The samples were analysed for cell distribution, proliferation and differentiation. For the analysis of cell distribution, two samples were used for each culture period, while for the analysis of cell proliferation and differentiation four samples were used for each culture period (40 samples in total) with up to 16 perfusion chambers used in parallel.

5.3.6 Cell distribution

Analogue to the sample treatment in the cell seeding experiments (see Chapter 4) two samples were taken out of the perfusion chambers per culture period after the cell culture period and were cut longitudinally with a scalpel. The samples were stained with 10 μM solution of acridine orange (AO) and ethidium bromide (EB) to visualize under a fluorescence stereoscope (Leica MZ16F) living and apoptotic cells on interior and exterior of the scaffolds. Images of the fluorescence were taken and stitched together to achieve a map of cell distribution.

5.3.7 Cell proliferation

For the measurement of cell proliferation, samples were frozen three times to lyse the cells. Using a LDH cytoxicity test as for the cell seeding presented in Chapter 4, the cell number in the samples was determined. Complete advanced DMEM was used as control and high LDH concentrations in samples were measured by diluting the corresponding sample in advanced medium at dilutions of 1:3 and 1:9. The seeding efficiencies were compared using the Student's t-test to determine statistically significant differences.

5.3.8 Cell differentiation

The cell differentiation of the mesenchymal cells was determined by the gene expression of collagen I, osteocalcin and Runx2. To extract the RNA of the samples, they were taken out of the perfusion chambers and washed in PBS. 350 μl RLT buffer of the RNeasy kit (Qiagen) was added to the samples, which were then destroyed with a homogenizer (Polytron PT 1200 C, Tip: PT-DA 05/2 EC-C 84). The supernatant was then transferred with the sample fragments to a QIAshredder tube (Qiagen) and centrifuged for

two minutes at 13.2×10^3 rpm (Eppendorf Centrifuge 5415R). The lysate of the collection tube was then treated with the RNeasy kit according to the user manual. Per sample 30 μl of RNA suspended in ribonuclease-free water were extracted. As control, rMSCs were trypsinized and put into six well plates (500,000 cells/well) for 24 hours and treated with the RNeasy kit according to the user manual. The concentration of RNA was measured with the nanodrop spectrophotometer (Thermo Scientific) for every sample. The RNA samples were then stored at -20 °C until the further treatment.

The extracted RNA was transcribed to cDNA, using the QuantiTect reverse Transcription Kit (Qiagen) according to the user manual. 500 ng RNA of every sample was used for the transcription. As quality controls one sample was prepared containing all reactants except reverse transcriptase (-RT) and one sample was prepared containing all reactants except the RNA sample (NTC). The concentration of cDNA was measured with the nanodrop spectrophotometer (Thermo Scientific). The gained cDNA was then stored at -20 °C.

For the real time polymerase chain reaction (RT-PCR), the cDNA samples were prepared in an optical reaction 96-well plate. Using Quantitect SYBR green (Qiagen) according to the user manual, a quantity of 75 ng cDNA was analysed for every sample. Primers of collagen I, osteocalcin and RunX-2 as well as β-actin as a comparison (housekeeping gene) were used for the determination of osteoblastic differentiation. The well plate was closed with adhesive film, agitated for 1 minute at 600 rpm and centrifuged for 1 minute at 300 g. The DNA sequences were read out with the Abi Prism 7700 sequence detector (Applied Biosystems). The C_t values for the gene expressions were read out and normalized to the values of β-actin using Equation 5.1, where $C_{t(sample)}$ was the C_t value of the genes (collagen I, osteocalcin or RunX-2) for cells cultured under perfusion, $C_{t(control)}$ was the C_t value of the genes (collagen I, osteocalcin or RunX-2) for cells cultured in a well and $C_{t(\beta-actin)}$ was the C_t value of the housekeeping gene $\beta - actin$ [36].

$$Norm. \, value = 2^{-\Delta\Delta C_t} = \frac{2^{-\Delta C_{t(target)}}}{2^{-\Delta C_{t(norm)}}} = \frac{2^{-(C_{t(sample)}-C_{t(\beta-actin)})}}{2^{-(C_{t(control)}-C_{t(\beta-actin)})}} \quad (5.1)$$

The normalized value determine the up- or down-regulation of gene activity.

5.4 Results

5.4.1 Cell distribution

For the observation of cell distribution after 1 day, 1 week, 2 weeks and 3 weeks of culture, scaffolds were cut open longitudinally and cells were stained with acridine orange (AO) and ethidium bromide (EB). The fluorescence images were treated analogous to the cell seeding presented in Chapter 4. The images taken were stitched together to represent a map of the cell distribution in the whole scaffolds (see Figure 5.2). The cell seeding conducted before the culture provided a cell distribution throughout the scaffolds, as suggested by the AO staining of the samples after 1 day. Up to the longest period culture of 3 weeks, living cells were found on exterior and interior of the scaffolds. The EB staining of the samples suggested an increased part of apoptotic cells at 1 and 2 weeks culture on the interior and it seemed that a maximum of apoptotic cells were found at 2 weeks of culture. The exterior showed in all cases only few apoptotic cells.
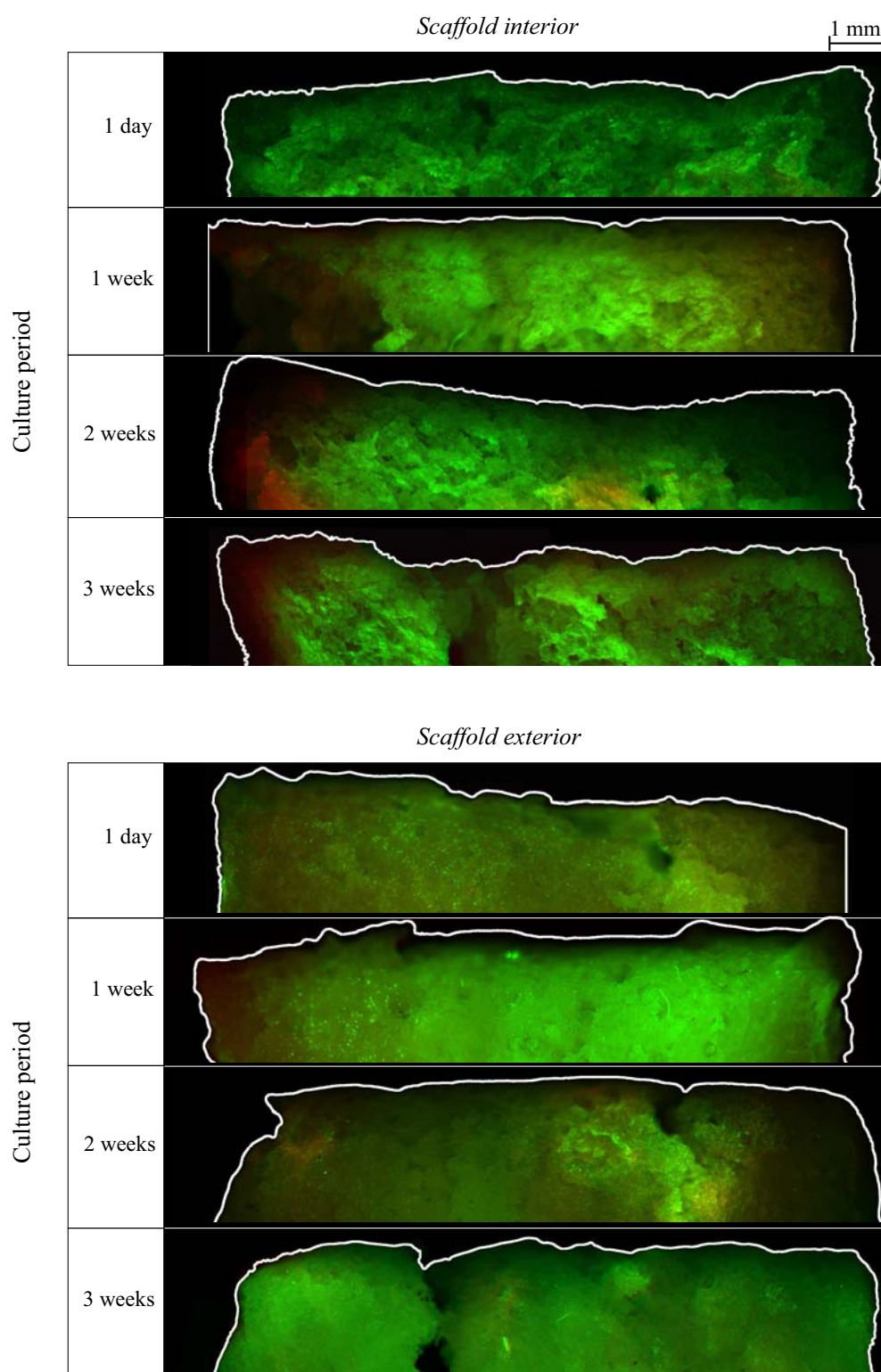
Figure 5.2: Cell distribution after perfusion with daily stimulation for periods up to three weeks. Acridine orange staining for living cells is shown as green areas, ethidium bromide staining for apoptotic cells as red areas.

5.4.2   Cell proliferation

The cell number in the scaffolds at different cell culture periods was assessed by LDH measurement. The results of the measurements showed a low cell number at the beginning of culture, which corresponded to a seeding efficiency of 40.2 % $\pm$ 22.5 % (see Figure 5.3). The cells proliferated over the first two weeks in an exponential manner ($N_{cells} = 0.3 \times e^{0.2t}$), ending up in a 13.5 fold amount of cells in the scaffolds compared to the start of culture. After two weeks, the cell number experienced a severe decrease, which ended after three weeks in a cell number similar to the culture start. Student's t-test showed that the cell number measured after two weeks value had a statistically significant difference the 1 day, 1 week and 3 week measurement. The static seeding method provided a seeding efficiency of 32.1 % $\pm$ 14.0 %, followed by the 3 week culture period in which the cell number did not change significantly as was confirmed by Student's t-test.
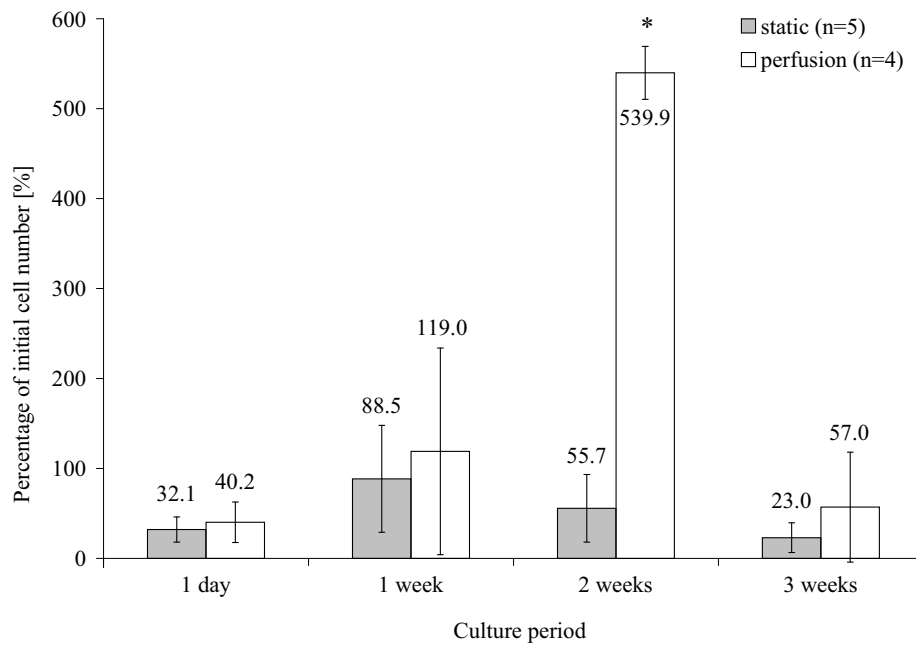
	Cell number as percentage of initial cell number			
	1 day	1 week	2 weeks	3 weeks
static (n=5)	32.1±14.0	88.5±59.4	55.7±37.6	23.0±16.5
dynamic (n=4)	40.2±22.5	119.0±114.9	539.9±29.4	57.0±61.1

Figure 5.3: Cell proliferation under static conditions and perfusion with daily stimulation after up to three weeks culture. The cell number showed an exponential growth up to two weeks, whereas from week two to three the cell number severely decreased. Student's t-test showed that for the perfusion culture, the two weeks value (*) had a statistically significant difference from the other perfusion culture values (p<0.0005).

5.4.3   Cell differentiation

Cell differentiation after 1 day, 1 week, 2 weeks and 3 weeks of cell culture under perfusion was measured by RT-PCR. For the measurement, the highest concentrated RNA samples of every culture period was used. The C_t values of osteocalcin, collagen I and Runx2 were normalized against the control of rMSCs using β-actin as reference gene. No Runx2 and collagen I expression was found in the samples for any culture period. For the osteocalcin expression, high values were found after 1 day (28-fold in comparison to 24 h statistical cultured rMSCs), which decreased to a low level after 1-2 weeks. The upregulation of osteocalcin expression is depicted in Figure 5.4.
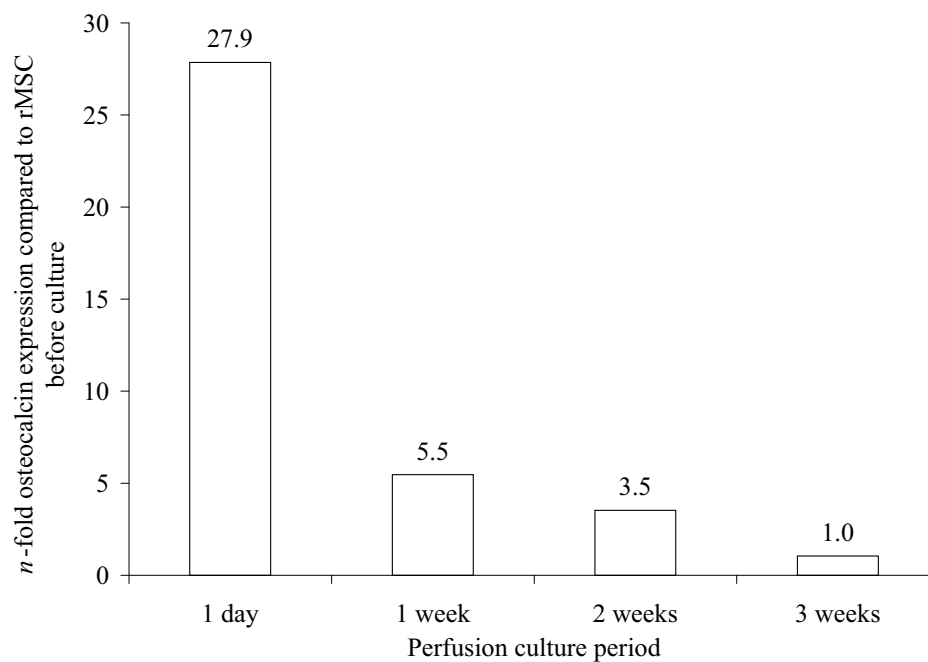
Figure 5.4: Osteocalcin expression in rMSC after 1 day, 1 week, 2 weeks and 3 weeks perfusion culture in the perfusion bioreactor system.

5.5 Discussion

The initial cell distribution throughout the scaffolds seen after the seeding was corresponded to the findings of the previous cell seeding study (see Chapter 4). The pattern used for perfusion culture in the range of similar studies which yielded success in long term cultivation [4, 6, 26, 28]. Similar to the calculation conducted in Chapter 4, the fluid flow shear stress on the cells was estimated to be 150-390 mPa at 5 mm/s and 3-8 mPa at 0.1 mm/s, which was considered well in the physiological range of bone cells [37, 38]. Throughout the long term experiments scaffolds maintained viable inside of the scaffold, even though the imaging indicated an increase of apoptotic cells in the scaffold interior over two weeks. Interestingly the cell viability on the scaffold exterior did not seemed affected by the long term culture under fluid flow perfusion. These results showed that the maintenance of a viable environment in the perfusion bioreactor system was possible, even though the cell mortality in the interior suggested that changes in the fluid flow pattern may yield a better viability.

In the conducted long term cell culture study under medium perfusion through porous scaffolds it was observed that after an initial exponential proliferation of up to 2 weeks, the cell number decreased in the following week. The decrease in cell number indicates a change in the viable environment, which decreased the cell survival in the scaffolds. Comparable studies have shown that it is possible to culture cells in a fluid flow environment over long terms of about two weeks [1, 8, 11, 20–24, 27, 28, 31, 33, 34, 39], but most long term cultures showed similar cell number decreases after an initial cell expansion phase [9–11, 13, 30, 40, 41]. The drop in cell number after an initial proliferation stage was attributed to a prevention of DNA measurement by entrapment of DNA in the ECM [9, 11], a loss of cells due to the loss of scaffold material [13] or the influence of ECM maturation and the late-stage differentiation of osteoblastic cells [10, 30, 40–42]. For the presented study an entrapment of the measured LDH in ECM was excluded, because cells were lysed and the scaffolds totally destroyed. It can be assumed that only little LDH was left in the scaffold fragments after centrifugation in the QIAshredder. It might be considered that cells were lost during culture by material loss. A material loss of about 12.5 % during 3 weeks immersion in

simulated body fluid (SBF) at 37 °C of porous PLA/glass composites under static conditions was reported, showing that a considerable amount of cell adhesion surface was lost during culture [43]. The drop in cell number experienced in this study was not attributed to the late-stage differentiation of the MSCs, because this would rather result in a stabilisation of cell number than a sudden drop in the population. The changes affecting might also be attributed to the 'overpopulation' in the scaffolds after the exponential growth. The amount of cells could have influenced proliferation by altering or blockage of the fluid flow pathways or by elevated nutrient consumption and waste generation. The proliferation of MSCs in the static method showed no statistical significant changes over a long time with an apparent initial proliferation phase up to 1 week, which indicated the limited nutrient supply in the large scaffolds and hence supporting the beneficial influence of the perfusion method on cell culture. One of the most important requirements of cell survival is the availability of oxygen to the cells [2]. The presented set-up did not allow a systemic monitoring of oxygen. Moreover the oxygen consumption rate and the exposure of cells to oxygen is unknown. Nevertheless it can be hypothesised that the growing cell population resulted in an upward trend in oxygen consumption, which was not met with the continuous medium exchange rate applied. Additionally not all cells in the growing cell clusters might have had a direct exposure to the medium, impeding the uptake of oxygen. Because oxygen and nutrient supply and waste removal are crucial for a successful cell culture in large 3D scaffolds, it is for further research of highest interest to incorporate monitoring and control mechanisms for these parameters. This mechanisms should focus on the time-dependent structural changes in the scaffold materials, because those changes can alter the availability of oxygen and nutrients to the cells significantly.

The results of cell differentiation are inconclusive. While the osteocalcin measurements indicate an early cell differentiation into the osteoblast cell line, a lack of Runx2 and collagen I expression as early regulator of differentiation [44–47] indicate the absence of osteoblastic differentiation. Because the cells were cultured prior to the perfusion culture experiments, the cells might have begun the differention. Because Runx2 (or Cbfa1) is early expressed in differentiation [48–50], it might have occured that the cells, when inserted into the perfusion system, were already in the differentiation stage

and Runx2 expression had ceased, which could explain the absence of Runx2 in the conducted measurements. In the case of an osteoblastic differentiation the Runx2 expression continues into the late stage of osteoblast activity [51]. The absence of collagen I however indicates a failure in the measurement procedure, because collagen expression should be present during and beyond the osteocalcin expression [52]. The shown pattern of gene expression leads to the assumption that the primers for collagen I and Runx2 used for the RT-PCR were faulty, while the primer for osteocalcin was able to give an image of cell activity in the long term culture. The verification of these results could not be conducted due to the length of every set of experiments. Taking these results in account, the measurements undertaken were not capable to determine if the applied stimulus was sufficient to provoke the desired reaction of the rMSC to differentiate into osteoblasts. This result has to be deemed preliminar and further studies are required with a more detailed analysis of cell activities before and after the long term perfusion culture. In further studies a comparison experiment should be conducted, applying only a steady flow to allow the distinction of the effect of the stimulation phase on the cells.

The presented study has shown that the developed perfusion bioreactor was capable to provide a viable environment for a long term cell culture on large porous scaffolds. Further studies must be conducted to determine the appropriate stimulus pattern for the osteoblastic differentiation of mesenchymal stem cells and to improve the cell viability.

5.6   Conclusion

- The developed perfusion bioreactor system provided a viable cell culture up to three weeks with cells throughout the large porous scaffolds. Cell number increased exponentially over two weeks and decreased at three weeks, which was attributed to the beginning cell differentiation and the overpopulation of the scaffold.

- The fluorescence imaging of the scaffolds under perfusion culture confirmed the cell population dynamic. Additionally it was observed that cells seemed to be under significantly more stress on the scaffold inte-

rior than on the exterior.

- The cell differentiation analysis did not give a conclusive picture of the differentiation of the rMSCs. Cell activity was indicated by osteocalcin expression. It was concluded that the applied stimulation fluid flow profile was not adequate to induce the desired differentiation. Further detailed studies are necessary to observe the reaction of the cells on the perfusion profile.

Bibliography

[1] F. W. Janssen, J. Oostra, A. Oorschot, and C. A. van Blitterswijk. A perfusion bioreactor system capable of producing clinically relevant volumes of tissue-engineered bone: in vivo bone formation showing proof of concept. *Biomaterials*, 27:315–323, Jan 2006.

[2] D. Wendt, S. Stroebel, M. Jakob, G.T. John, and I. Martin. Uniform tissues engineered by seeding and culturing cells in 3D scaffolds under perfusion at defined oxygen tensions. *Biorheology*, 43:481–488, 2006.

[3] W. L. Grayson, S. Bhumiratana, C. Cannizzaro, P. H. Chao, D. P. Lennon, A. I. Caplan, and G. Vunjak-Novakovic. Effects of initial seeding density and fluid perfusion rate on formation of tissue-engineered bone. *Tissue Eng Part A*, 14:1809–1820, Nov 2008.

[4] J. Vance, S. Galley, D.F. Liu, and S.W. Donahue. Mechanical stimulation of mc3t3 osteoblastic cells in a bone tissue − engineering bioreactor enhances prostaglandin e2 release. *Tissue Eng*, 11(11/12), 2005.

[5] S.H. Cartmell, B.D. Porter, A.J. García, and R.E. Guldberg. Effects of medium perfusion rate on cell-seeded three-dimensional bone constructs in vitro. *Tissue Eng*, 9(6), 2003.

[6] M. J. Jaasma, N. A. Plunkett, and F. J. O'Brien. Design and validation of a dynamic flow perfusion bioreactor for use with compliant tissue engineering scaffolds. *J Biotechnol*, 133:490–496, Feb 2008.

[7] Y. Wang, T. Uemura, J. Dong, H. Kojima, J. Tanaka, and T. Tateishi. Application of perfusion culture system improves in vitro and in vivo osteogenesis of bone marrow-derived osteoblastic cells in porous ceramic materials. *Tissue Eng*, 9(6):1205–1214, 2003.

[8] A.S. Goldstein, T.M. Juarez, C.D. Helmke, M.C. Gustin, A.G. Mikos, and L.V. McIntire. Effect of convection on osteoblastic cell growth and function in biodegradable polymer foam scaffolds. *Biomaterials*, 22(11):1279–1288, 2001.

[9] G.N. Bancroft, V.I. Sikavitsas, and J. van den Dolder. Fluid flow increases mineralized matrix deposition in 3d perfusion culture of marrow

stromal osteoblasts in a dose-dependent manner. *PNAS*, 99(20):12600–12605, 2002.

[10] M. E. Gomes, H. L. Holtorf, R. L. Reis, and A. G. Mikos. Influence of the porosity of starch-based fiber mesh scaffolds on the proliferation and osteogenic differentiation of bone marrow stromal cells cultured in a flow perfusion bioreactor. *Tissue Eng*, 12:801–809, 2006.

[11] H.L. Holtorf, T.L. Sheffield, C.G. Ambrose, J.A. Jansen, and A.G. Mikos. Flow perfusion culture of marrow stromal cells seeded on porous biphasic calcium phosphate ceramics. *Ann Biomed Eng*, 33(9):1238–1248, 2005.

[12] L. Fassina, L. Visai, L. Asti, F. Benazzo, P. Speziale, M.C. Tanzi, and G. Magenes. Calcified matrix production by saos-2 cells inside a polyurethane porous scaffold, using a perfusion bioreactor. *Tissue Eng*, 11(5-6):685–700, 2005.

[13] L. Meinel, V. Karageorgiou, R. Fajardo, B. Snyder, V. Shinde-Patil, L. Zichner, D. Kaplan, R. Langer, and G. Vunjak-Novakovic. Bone tissue engineering using human mesenchymal stem cells: Effects of scaffold material and medium flow. *Ann Biomed Eng*, 32(1):112–122, 2004.

[14] E.A. Nauman, R.L. Satcher, T.M. Keaveny, B.P. Halloran, D.D. Bikle, B.P. Halloran, and D.D. Bikle. Osteoblasts in culture respond to in vitro pulsatile fluid flow with short term increases in pge2 and long term increases in cell proliferation. *J Bone Miner Res*, 15, 2001.

[15] M.R. Kreke, W.R. Huckle, A.S. Goldstein, and et al. Fluid flow stimulates expression of osteopontin and bone sialoprotein by bone marrow stromal cells in a temporally dependent manner. *Bone*, 36(6):1047–1055, 2005.

[16] J. Klein-Nulend, C.M. Semeins, N.E. Ajubi, P.J. Nijweide, and E.H. Burger. Pulsating fluid flow increases nitric oxide (no) synthesis by osteocytes but not periosteal fibroblasts − correlation with prostaglandin upregulation. *Biochem Biophys Res Commun*, 217(2), 1995.

[17] C.R. Jacobs, C.E. Yellowley, B.R. Davis, Z. Zhou, J.M. Cimbala, and H.J. Donahue. Differential effect of steady versus oscillating flow on bone cells. *J Biomech*, 31:969–976, 1998.

[18] V. I. Sikavitsas, G. N. Bancroft, J. J. Lemoine, M. A. Liebschner, M. Dauner, and A. G. Mikos. Flow perfusion enhances the calcified matrix deposition of marrow stromal cells in biodegradable nonwoven fiber mesh scaffolds. *Ann Biomed Eng*, 33(1):63–70, 2005.

[19] H. Hosseinkhani, M. Hosseinkhani, F. Tian, H. Kobayashi, and Y. Tabata. Ectopic bone formation in collagen sponge self-assembled peptide-amphiphile nanofibers hybrid scaffold in a perfusion culture bioreactor. *Biomaterials*, 27:5089–5098, Oct 2006.

[20] J. Yang, C. Cao, W. Wang, X. Tong, D. Shi, F. Wu, Q. Zheng, C. Guo, Z. Pan, C. Gao, and J. Wang. Proliferation and osteogenesis of immortalized bone marrow-derived mesenchymal stem cells in porous polylactic glycolic acid scaffolds under perfusion culture. *J Biomed Mater Res A*, Mar 2009.

[21] F. Zhao, W. L. Grayson, T. Ma, and A. Irsigler. Perfusion affects the tissue developmental patterns of human mesenchymal stem cells in 3D scaffolds. *J Cell Physiol*, 219:421–429, May 2009.

[22] H.L. Holtorf, N. Datta, J.A. Jansen, and A.G. Mikos. Scaffold mesh size affects the osteoblastic differentiation of seeded marrow stromal cells cultured in a flow perfusion bioreactor. *J Biomed Mater Res A*, 74:171–180, 2005.

[23] X. Li, D. Li, L. Wang, B. Lu, and Z. Wang. Osteoblast cell response to beta-tricalcium phosphate scaffolds with controlled architecture in flow perfusion culture system. *J Mater Sci Mater Med*, 19:2691–2697, Jul 2008.

[24] N. Bölgen, Y. Yang, P. Korkusuz, E. Güzel, A. J. El Haj, and E. Piskin. Three-dimensional ingrowth of bone cells within biodegradable cryogel scaffolds in bioreactors at different regimes. *Tissue Eng Part A*, 14:1743–1750, Oct 2008.

[25] D. Du, K. S. Furukawa, and T. Ushida. 3D culture of osteoblast-like cells by unidirectional or oscillatory flow for bone tissue engineering. *Biotechnol Bioeng*, 102:1670–1678, Apr 2009.

[26] M. J. Jaasma and F. J. O'Brien. Mechanical stimulation of osteoblasts using steady and dynamic fluid flow. *Tissue Eng Part A*, 14:1213–1223, Jul 2008.

[27] N. E. Timmins, A. Scherberich, J. A. Früh, M. Heberer, I. Martin, and M. Jakob. Three-dimensional cell culture and tissue engineering in a T-CUP (tissue culture under perfusion). *Tissue Eng*, 13:2021–2028, Aug 2007.

[28] N. A. Plunkett, S. Partap, and F. J. Obrien. Osteoblast response to rest periods during bioreactor culture of collagen-glycosaminoglycan scaffolds. *Tissue Eng Part A*, Oct 2009.

[29] E. Volkmer, I. Drosse, S. Otto, A. Stangelmayer, M. Stengele, B.C. Kallukalam, W. Mutschler, and M. Schieker. Hypoxia in static and dynamic 3d culture systems for tissue engineering of bone. *Tissue Eng.*, 14(8):1331–40, 2008.

[30] R. Glaum, M. Wiedmann-Al-Ahmad, U. Huebner, and R. Schmelzeisen. Tissue engineering of composite grafts: Cocultivation of human oral keratinocytes and human osteoblast-like cells on laminin-coated polycarbonate membranes and equine collagen membranes under different culture conditions. *J Biomed Mater Res A*, Jul 2009.

[31] H. Hosseinkhani, Y. Inatsugu, Y. Hiraoka, S. Inoue, and Y. Tabata. Perfusion culture enhances osteogenic differentiation of rat mesenchymal stem cells in collagen sponge reinforced with poly(glycolic Acid) fiber. *Tissue Eng*, 11:1476–1488, 2005.

[32] A. M. Freyria, Y. Yang, H. Chajra, C. F. Rousseau, M. C. Ronzière, D. Herbage, and A. J. El Haj. Optimization of dynamic culture conditions: effects on biosynthetic activities of chondrocytes grown in collagen sponges. *Tissue Eng*, 11:674–684, 2005.

[33] F. Zhao, R. Chella, and T. Ma. Effects of shear stress on 3-D human mesenchymal stem cell construct development in a perfusion bioreactor system: Experiments and hydrodynamic modeling. *Biotechnol Bioeng*, 96:584–595, Feb 2007.

[34] D. Du, K. Furukawa, and T. Ushida. Oscillatory perfusion seeding and culturing of osteoblast-like cells on porous beta-tricalcium phosphate scaffolds. *J Biomed Mater Res A*, 86:796–803, 2008.

[35] D. Du, K. S. Furukawa, and T. Ushida. Oscillatory perfusion culture of CaP-based tissue engineering bone with and without dexamethasone. *Ann Biomed Eng*, 37:146–155, Jan 2009.

[36] K. J. Livak and T. D. Schmittgen. Analysis of relative gene expression data using real-time quantitative PCR and the 2(-Delta Delta C(T)) Method. *Methods*, 25:402–408, Dec 2001.

[37] S. Weinbaum, S.C. Cowin, and Y. Zeng. A model for the excitation of osteocytes by mechanical loading-induced bone fluid shear stresses. *J Biomech*, 27:339–360, 1994.

[38] S. C. Cowin, S. Weinbaum, and Y. Zeng. A case for bone canaliculi as the anatomical site of strain generated potentials. *J Biomech*, 28:1281–1297, Nov 1995.

[39] V. Olivier, P. Hivart, M. Descamps, and P. Hardouin. In vitro culture of large bone substitutes in a new bioreactor: importance of the flow direction. *Biomed Mater*, 2(3):174–180, 2007.

[40] M. E. Gomes, V. I. Sikavitsas, E. Behravesh, R. L. Reis, and A. G. Mikos. Effect of flow perfusion on the osteogenic differentiation of bone marrow stromal cells cultured on starch-based three-dimensional scaffolds. *J Biomed Mater Res A*, 67:87–95, Oct 2003.

[41] V. I. Sikavitsas, G. N. Bancroft, H. L. Holtorf, J. A. Jansen, and A. G. Mikos. Mineralized matrix deposition by marrow stromal osteoblasts in 3D perfusion culture increases with increasing fluid shear forces. *Proc Natl Acad Sci USA*, 100:14683–14688, Dec 2003.

[42] J. B. Lian and G. S. Stein. Concepts of osteoblast growth and differentiation: basis for modulation of bone cell development and tissue formation. *Crit Rev Oral Biol Med*, 3:269–305, 1992.

[43] M. Charles-Harris Ferrer. *Development and Characterisation of Completely Degradable Composite Tissue Engineering Scaffolds*. PhD thesis, Technical University of Catalonia, 2007.

[44] K. Miyazono, S. Maeda, and T. Imamura. Coordinate regulation of cell growth and differentiation by TGF-beta superfamily and Runx proteins. *Oncogene*, 23:4232–4237, May 2004.

[45] A. Laczka-Osyczka, M. Laczka, S. Kasugai, and K. Ohya. Behavior of bone marrow cells cultured on three different coatings of gel-derived bioactive glass-ceramics at early stages of cell differentiation. *J Biomed Mater Res*, 42:433–442, Dec 1998.

[46] T. Goto, H. Kajiwara, M. Yoshinari, E. Fukuhara, S. Kobayashi, and T. Tanaka. In vitro assay of mineralized-tissue formation on titanium using fluorescent staining with calcein blue. *Biomaterials*, 24:3885–3892, Oct 2003.

[47] H. Declercq, N. Van den Vreken, E. De Maeyer, R. Verbeeck, E. Schacht, L. De Ridder, and M. Cornelissen. Isolation, proliferation and differentiation of osteoblastic cells to study cell/biomaterial interactions: comparison of different isolation techniques and source. *Biomaterials*, 25:757–768, Feb 2004.

[48] K. Y. Choi, S. W. Lee, M. H. Park, Y. C. Bae, H. I. Shin, S. Nam, Y. J. Kim, H. J. Kim, and H. M. Ryoo. Spatio-temporal expression patterns of Runx2 isoforms in early skeletogenesis. *Exp Mol Med*, 34:426–433, Dec 2002.

[49] M. Galindo, J. Pratap, D. W. Young, H. Hovhannisyan, H. J. Im, J. Y. Choi, J. B. Lian, J. L. Stein, G. S. Stein, and A. J. van Wijnen. The bone-specific expression of Runx2 oscillates during the cell cycle to support a G1-related antiproliferative function in osteoblasts. *J Biol Chem*, 280:20274–20285, May 2005.

[50] J. B. Lian, G. S. Stein, A. Javed, A. J. van Wijnen, J. L. Stein, M. Montecino, M. Q. Hassan, T. Gaur, C. J. Lengner, and D. W. Young. Networks and hubs for the transcriptional control of osteoblastogenesis. *Rev Endocr Metab Disord*, 7:1–16, Jun 2006.

[51] P. Ducy, R. Zhang, V. Geoffroy, A. L. Ridall, and G. Karsenty. Osf2/Cbfa1: a transcriptional activator of osteoblast differentiation. *Cell*, 89:747–754, May 1997.

[52] J. E. Aubin, F. Liu, L. Malaval, and A. K. Gupta. Osteoblast and chondroblast differentiation. *Bone*, 17:77S–83S, Aug 1995.

Chapter 6

Development of an *in vivo* Bone Chamber System

6.1 Introduction

One approach of tissue engineering to counter large bone defects consists in the insertion of porous biomaterial into the defect to act as a support and guidance for bone regeneration. The material used should promote the ingrowth and formation of bone tissue and help to bear loads on the bone to reduce recovery time. Prior to *in vivo* tests, biomaterials are thoroughly tested *in vitro* to avoid adverse effects upon implantation. Even though those tests are considerably extensive, they cannot reflect the complex environment of a patient's body, with fully developed tissue interacting with the material and inflammatory and immune responses [1].

Bone chambers are useful tools for skeletal tissue engineering to gain knowledge about the osteoconductive or osteoinductive properties of different scaffold types [2, 3]. By placing a scaffold into the environment of a living organism, the reaction on the implant material and structure can be observed as well as the progress of tissue formation into the material over time. This gives valuable insight into the applicability of a scaffold for its intended purpose. The most common approach to bone chamber systems is the implantation of a hollow metal cylinder into the region of interest (see Figure 6.1). Scaffolds of different materials and fabrication can then be inserted into this cylinder, where apertures allow the ingrowth of tissue

(a)   *(b)*   *(c)*
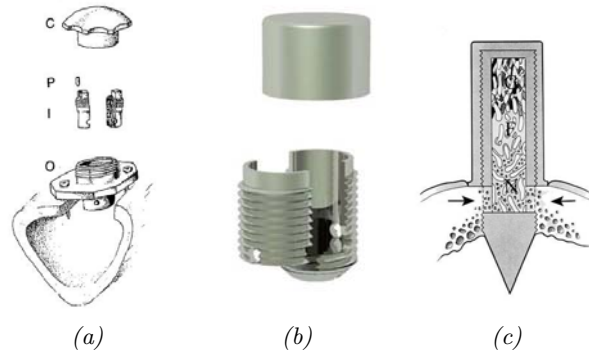
Figure 6.1: Bone chamber designs for the study of bone ingrowth into allografts in goats (a, b) [3, 4] and rats (c) [6].

into the scaffold. After extracting the scaffold or the entire bone chamber, the developed tissue can be analysed histologically to determine the type and amount of present tissue. Even though the application of bone chamber systems is promising for the testing of different scaffold materials, most studies focus on the bone ingrowth in allografts [3–7] or the bone ingrowth into empty chambers [8–11]. Only few used synthetic scaffold material for bone chamber studies [12].

Bone chambers used in animal experiments are either for single use only or reusable for the repeated testing of different samples in the same chamber. Chambers for single use have the advantage of a simpler surgical protocol, but large numbers of samples require also large numbers of animals, which implicates ethical and financial issues. Additionally inter-individual differences may have a severe influence on the measurement results. Reusable bone chambers have the advantage of allowing the test of materials in as few as possible animals and reduce the inter-individual variability [3, 9, 13]. Both bone chamber types can be used in different mammal species, from small animals like rats [6] to big animals as goats [11, 14]. In regard to different animal models and implantation methods it has been shown that bone ingrowth is independent from species [11]. The space inside the bone chambers for bone ingrowth ranges from cylinders of 2 mm in diameter and 7 mm length [6] up to internal diameter of 6 mm, and a length of 8.5 mm [15]. For clinical use however, large defects are of interest for experimentation.

Bone chambers can be constructed to allow application of certain stimuli
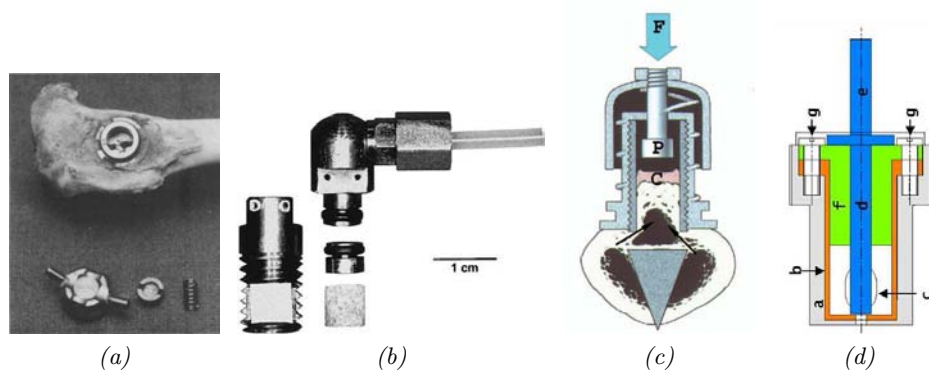
Figure 6.2: Bone chamber designs for the mechanical stimulation of bone formation.(a) Design for the manual compression of ingrowing bone in rabbits [9], (b) hydraulic compression of ingrowing bone in dogs [8], (c) manual compression of allografts in rats [7] and (d) in rabbit shear on titanium implant [13].

to the scaffold for accelerated bone ingrowth. By compression of the ingrowing bone tissue, tissue formation can be stimulated. Using compressive stimulation on samples in bone chambers in rabbits showed the dependency of tissue ingrowth on stimulation amplitude (see Figure 6.2a) [9]. Guldberg et al. [10] developed a bone chamber which allowed a stimulation of a bone graft with a hydraulic piston (see Figure 6.2b), showing an increase of trabecular bone surfaces after a few days of loading [5, 10]. The same hydraulic bone chamber design showed in experiments that mechanical stimulation controlled the pattern of bone cell activity and gene expression [8]. Using another mechanical principle, Tägil et al. [7] used a bone chamber implanted and fully covered by skin, which was used to apply loads on ingrowing bone tissue by pressing from the outside on the incorporated piston (see Figure 6.2c). This study showed dense trabecular bone in the treated bone grafts after manually applying a compressive stimulus. Similar to those bone implants Duyck et al. [13] developed a repeatable bone chamber which used an electromechanical actuator (piezo) to move a titanium implant inside the bone chamber producing shear stress on the adhering tissue to study the effect of movement on osteointegration.

These studies showed the applicability of *in vivo* bone chamber systems. For the study of larger bone defects and the testing of biomaterials with and without compressive load it is necessary to develop a new reusable bone chamber system for large scaffolds. The applicability for large scaffolds of

different compositions constitutes a novelty in this field of application.

6.2 Objectives

The goal of the presented study was the development of a new reusable bone chamber system for large scaffold dimensions (6 mm diameter and 12 mm length) for implantation in the medial side of proximal dog tibia. The bone chamber system was developed for the testing of the integration of different porous biomaterials into a critical bone defect and investigating the role of material properties for tissue ingrowth and development. Additionally a compressive loading device was developed to compress the samples *in situ* to investigate the influence of mechanical stimulation on tissue ingrowth and differentiation. The scope of this work spanned the development of a repeatable implanting system, including tools for implantation and sample extraction and the development of a compression device, which allowed the cyclic compression of the samples. The system was developed for the surgical environment for the *in vivo* animal experiments. The large dimension of the reusable bone chamber used primarily for the testing of synthetic porous materials *in vivo* constitutes a novelty in the field. The results of these studies will be a valuable input for further research in bone regeneration modelling based on the scaffold tissue engineering approach, which was not in the scope of this thesis project.

6.3 Material and methods

6.3.1 Experimental procedure

To develop a bone chamber system for the implantation of large porous scaffolds *in vivo* with the addition of compressive stimulations, the procedure for the system had to be determined as a first step. A priori it was decided that the bone chamber implant system should consist of an external self threading chamber and an internal chamber to hold the implanted scaffold which could be exchanged subsequently. After consulting the surgical team of the Rof Codina foundation (Department of Veterinary Clinical Sciences, University of Santiago de Compostela), the experimental procedure was broken down

into five phases. Consequently the design of the bone chamber system was oriented on this general guideline.

The 5 phases were:

I *Implantation of the external bone chamber.*
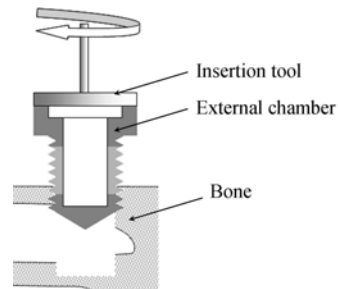
In the first phase, a hole was drilled into the medial side of the proximal dog tibia. The external chamber was then threaded into the bone. This required a special focus on a suitable drill bit, a self-cutting thread and suitable tools for connection of the external chamber to a handle or drill.

II *Osteointegration of the external chamber.*
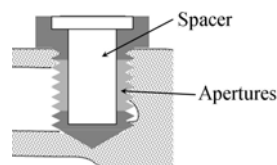
In the second phase, the external bone chamber was left for three month to allow the osteointegration of the chamber. During this time ideally the apertures, which were later used for tissue ingrowth, were closed to prevent the filling of the external chamber with tissue.

III *Insertion of the scaffold and internal cage.*
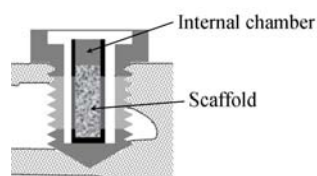
In the third phase, the scaffold was inserted into the external chamber using an internal cage. The internal cage was needed to align the scaffold and to protect the sample during the later extraction procedure.

IV *Stimulation and tissue ingrowth phase.*
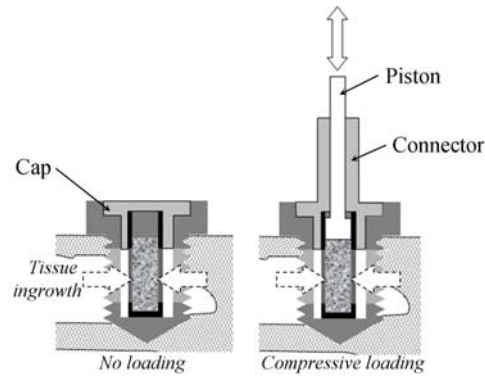
During the fourth phase, the scaffolds were left in the chambers for either 4 or 12 weeks. Part of the samples were compressed cyclically in weekly repetitions.

V *Sample extraction and replacement.*
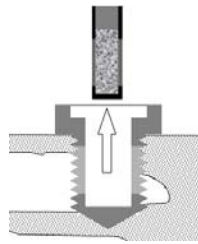
The fifth phase was the extraction of the samples by cutting the ingrown tissue between the internal and external chamber wall with a trepan. The intention was to preserve samples and part of the ingrown tissue during the extraction procedure. Directly after extraction, a new scaffold could be inserted into the external chamber.

The detailed design of the system for the determined phases is explained in the following section. The dimensional plans of the components are presented in Appendix E.

6.3.2   Development of the bone chamber system

6.3.2.1   Implantation of the external bone chamber

The core diameter of the external chamber was determined to be 11 mm. To thread in the chamber into bone, a hole of 11 mm diameter had to be drilled beforehand. In a market research on orthopaedic bone drill burrs, no burr in this

Figure 6.3: The shank of a commercial 11 mm HSS burr was modified to fit into a surgical drill.

size could be found. As shown by a study by Natali et al. [16] it is possible to use commercial available high speed steel (HSS) burrs in orthopaedic surgery. Based on this finding, 11 mm commercial HSS burrs were purchased and modified for use in the planned experiments. The dimensions of the burr shanks were copied from an existing surgical bone drill, which was provided by the surgical team. Because the composition of the burr material was unknown, the modified surfaces were tested on corrosion by immersion in 5 % saline solution for 5 minutes and storage for 1 hour at 37 °C. The concentration of saline solution was lent from standard ASTM B117 [17]. The surfaces were inspected before and after the corrosion test to determine further anti-corrosive treatments.

For the insertion of the external chamber, an assembly was realized consisting of an insertion tool (Material: Stainless steel AISI 01) fixated to the external bone chamber (Material: Ti6Al4V) by two metric screws (Material: Ti6Al4V, M3x6) and a PTFE spacer, which kept debris and ingrowing tissue out of the external bone chamber interior (see Figure 6.4). The insertion tool featured the same shank dimensions as the bone drill burr.
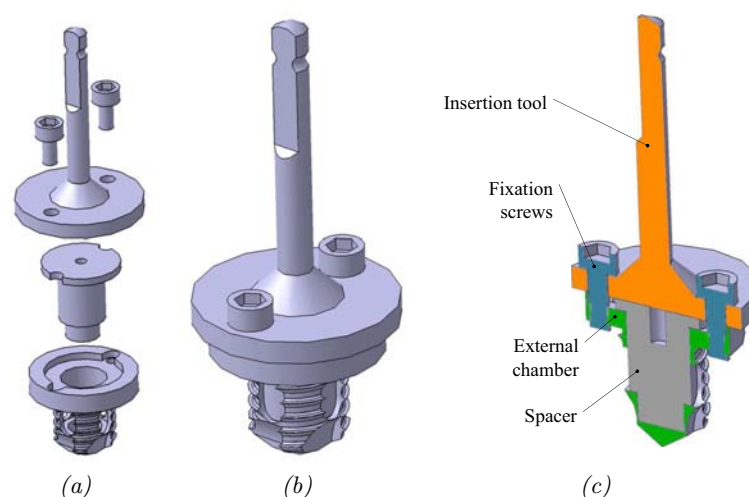
Figure 6.4: Assembly of the components for bone chamber insertion. (a) Explosion, (b) assembly and (c) cross-section of the components.

The external bone chamber had a thread for cortical bone, which was taken from standard ASTM F543 [18] and four cutting flutes on the bottom for threading into the bone. The thread was based on an 11 mm core diameter, which gave a wall thickness of minimal 0.75 mm for the hollow bone chamber. For later tissue ingrowth four apertures were provided in the external chamber wall with 6 mm length and a width of 4 mm. In total the external chamber had a diameter of 22 mm and a length of about 20 mm. The external bone chamber is depicted in Figure 6.5 with the four different development stages.

The drilling of the hole and the threading of the external chamber was tested in dog cadaver tibia at the veterinary hospital Rof Codina.

(a)   *(b)*   *(c)*

(d)
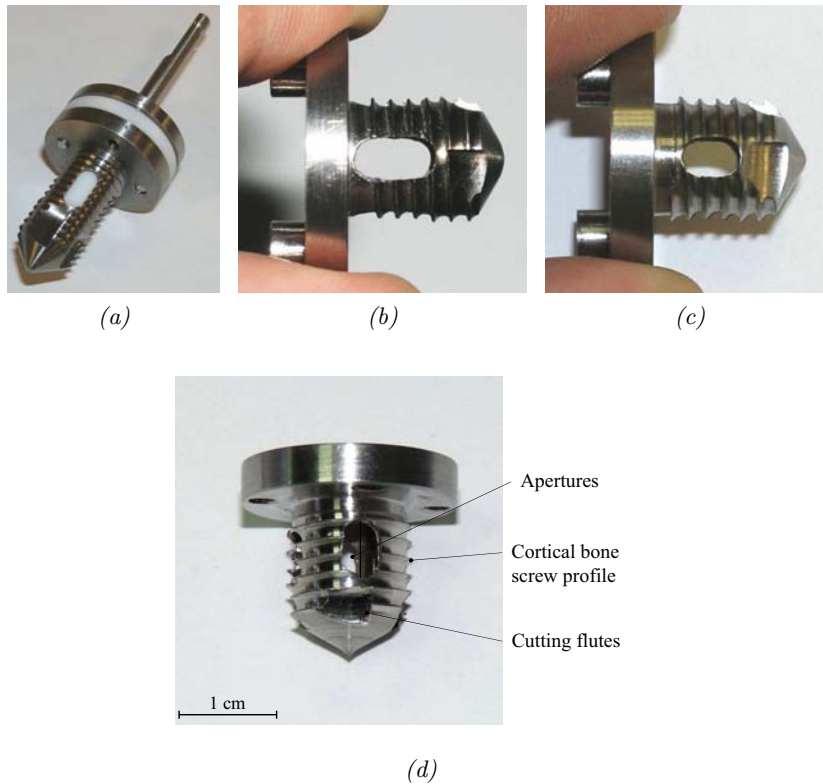
Figure 6.5: The four different development versions of the external chamber. (a) The first version, shown here with the insertion tool attached, proofed to be too long. The second version (b) was shortened. In the third version (c) the apertures were positioned further down. For the fourth and final version (d) the dimensions of the head were minimized.

6.3.2.2   Osteointegration of the external chamber

The insertion tool was taken off the bone chamber and the wound was closed over the implant for the osteointegration of the external bone chamber. As pictured in Figure 6.6 the external chamber was located in the tibia with the apertures on the level of trabecular bone. The contained spacer had a metric thread on its top to facilitate the extraction if needed.
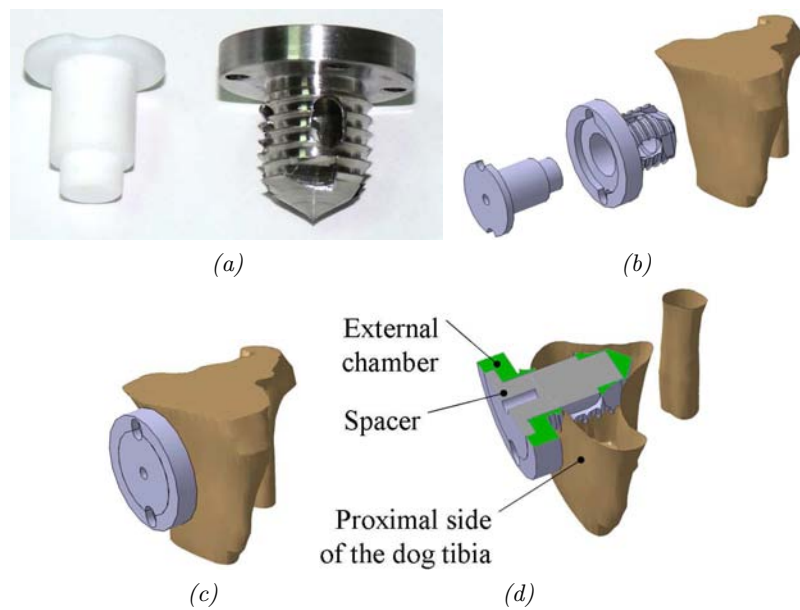
Figure 6.6: The assembly and location of the external bone chamber in the dog tibia during osteointegration. (a) The fabricated components, (b) explosion view, (c) assembly of the components and (b) cross-sectional view.

6.3.2.3   Insertion of the scaffold and internal cage

For the insertion of scaffolds after the osteointegration phase, two different assemblies were developed, depending on whether compressive stimuli were to be applied or not. For scaffolds which were not subjected to compression, the assembly consisted of the internal cage, which contained the scaffold, and a cap to close the scaffold compartment (see Figure 6.7).
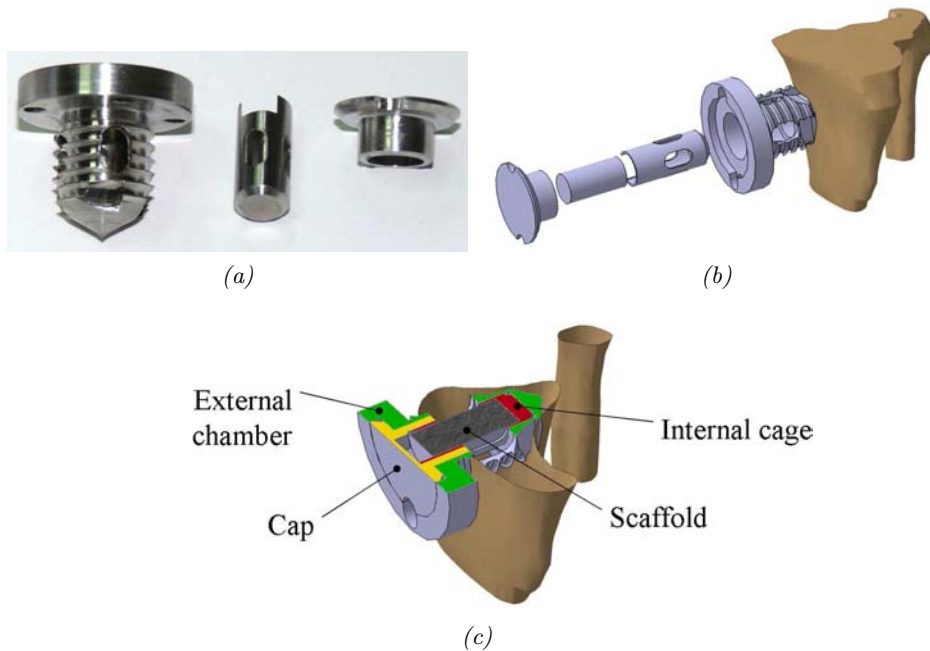
Figure 6.7: Assembly of components for the insertion of scaffolds without compressive stimulus. (a) The fabricated components, (b) explosion and (c) cross-sectional view of the assembly.

Both cap and internal cage were fabricated from titanium (Ti6Al4V). The internal cage had a profile on the top, which was aligned with its counterpart in the cap. The cap itself had notches on the top, so that aligning the notches of the cap with the threaded holes on top of the external chamber aligned the apertures of the internal cage with the apertures of the external chamber (see Figure 6.8). The internal cage had an internal diameter of 6.2 mm, a wall thickness of 0.4 mm and apertures matching the dimensions of the external chamber. The total opening was giving access to about 36 % of the lateral surface of the scaffold. The distance of scaffold surface to core diameter of the external chamber thread was about 2.5 mm, a gap that had to be bridged by ingrowing tissue. This assembly was left covered by skin tissue for the 4 or 12 weeks of planned tissue ingrowth.

The assembly for the compression of scaffolds *in vivo* contained the same internal cage as previously described. Instead of the cap, a connector (Material: Ti6Al4V) was fixated with two metric titanium screws to the external chamber. The connector aligned the apertures of the internal cage in the same manner as the previously described cap. Additionally the connector incorporated a piston consisting of a pole (Material: Ti6Al4V) screwed to a PTFE head or a titanium piston head for compression of stiff materials. The piston could be held in position with

(a)   *(b)*   *(c)*   *(d)*

Figure 6.8: Alignment of the apertures for tissue ingrowth. The internal cage (a) had a profile on its top which corresponded to the profile in the cap (b). The cap and internal cage (c) was then inserted into the external cage. The cap notches aligned with the holes did ensure the alignment of the apertures (d).

a plastic clip (1.5 mm rings of FEP tubing, cut open on one side). The connector penetrated the skin tissue for the connection of a compression device. The connector could be closed off for the periods of no stimulation with a protective cap, where the cap was secured with a headless screw (see Figure 6.9).

6.3.2.4 Stimulation and tissue ingrowth phase

After the insertion of the scaffolds into the bone chamber, it was intended to leave them for 4 or 12 weeks. In the case of compression of the scaffolds, a compresion device was coupled to the bone chamber weekly. The development of the compression device is broken down in Sections 6.3.3 and 6.3.5, to explain in depth the function of its electronics, hardware and software.

(a)

(b)

(c)
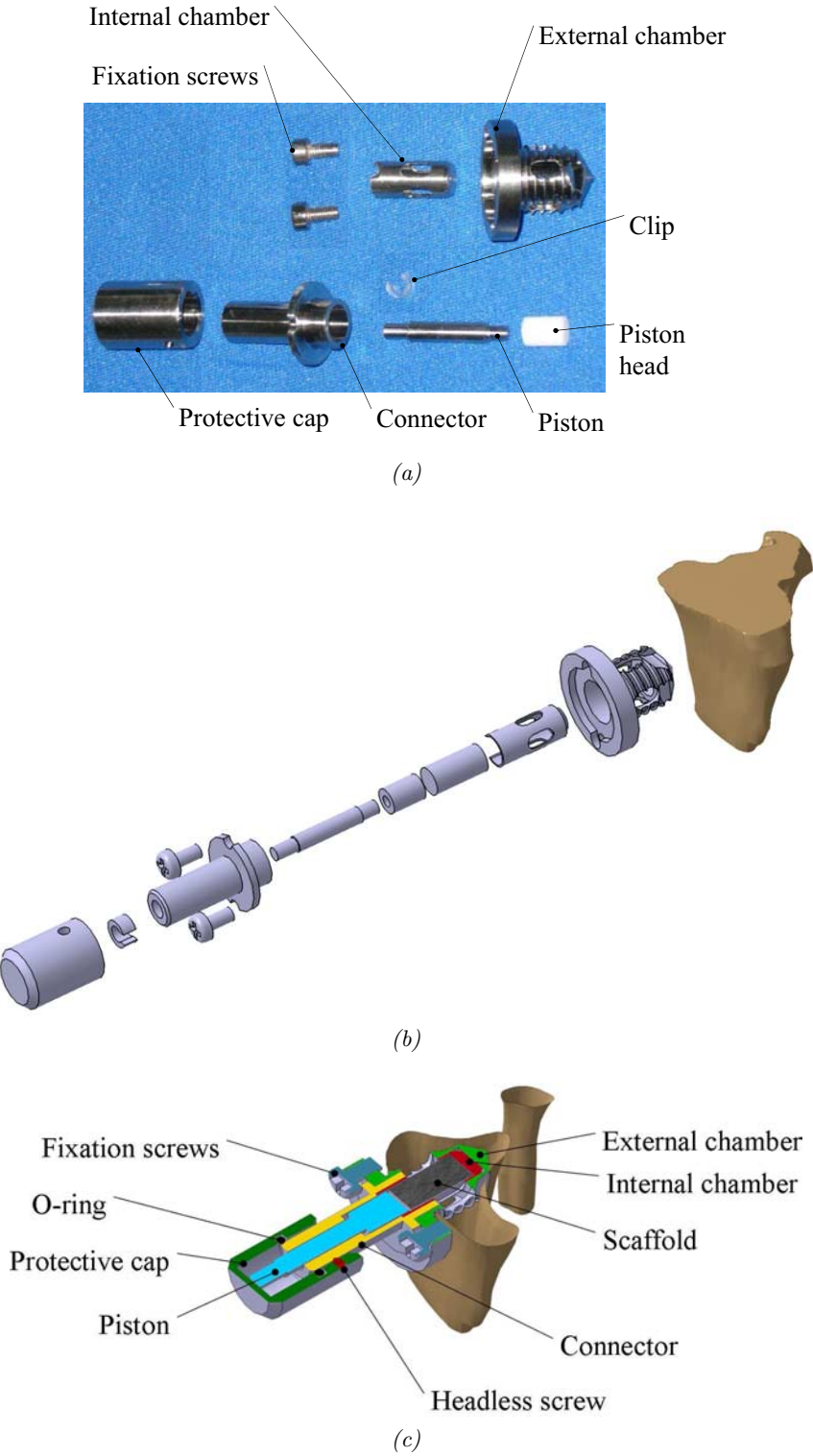
Figure 6.9: Assembly of the components for scaffolds intended for compressive stimulation. (a) Fabricated components, (b) explosion and (c) cross-sectional view of the assembly.

6.3.2.5   Sample extraction and replacement

After the desired period of tissue ingrowth, the skin over the implant was opened and the cap or connector taken off. With a dental trepan (Art.Nr. 227B.204.090 from Komet Dental, internal height 12 mm, internal diameter 7.9 mm, external diameter of 9 mm) it was possible to cut between internal and external chamber to extract the sample (see Figure 6.10). After trepanation a new internal cage containing a scaffold could be inserted.

(a)   (b)
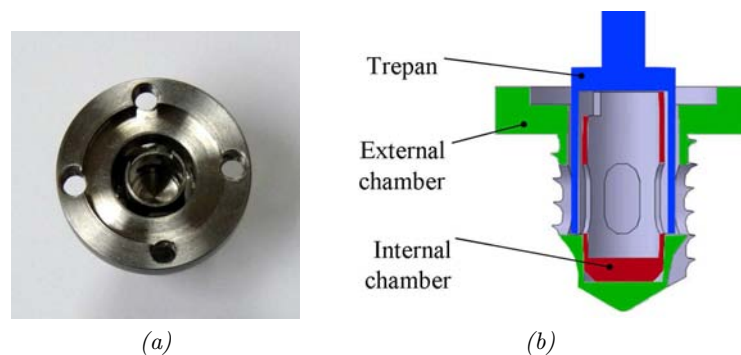
Figure 6.10: Trepanation of the sample for the extraction and insertion of a new scaffold.(a) The gap between internal cage and external chamber was used to insert a dental trepan. (b) The trepan cut with a depth of 12 mm down to the bottom of the gap.

6.3.3   Electronics and hardware development

The *in vivo* compression system for the bone chamber consisted of the compression device, a metal casing containing electronic control and measurement components and a laptop computer running custom developed software. The software on the laptop was controlling the movement of the linear stepper motor by giving out digital signals over a data I/O interface to the motor controller board. The displacement resulted in a compression which was measured with a force sensor. The resulting force signal was then amplified and read out by the data I/O interface. All components implicated in these processes are depicted in Figure 6.11. The function of the components are explained in the subsequent sections.
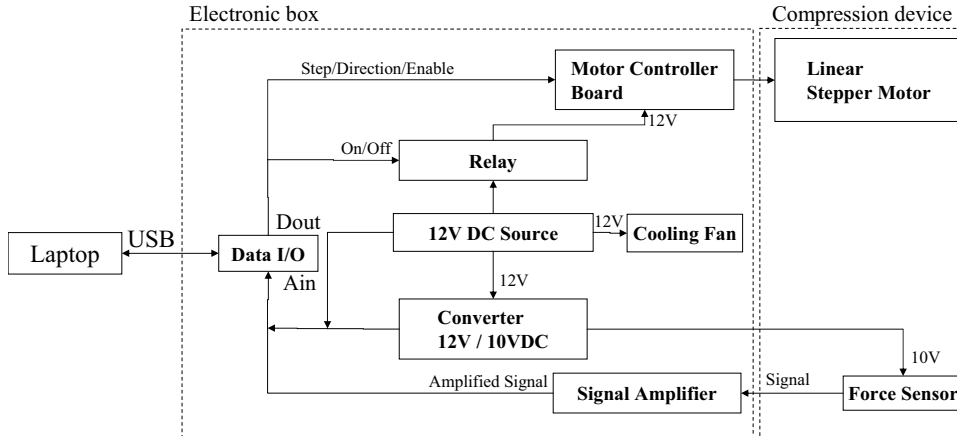
Figure 6.11: Block diagram of the electronics components. A laptop controls over the digital output (Dout) and analogue input (Ain) of a data interface the linear stepper motor and force measurement.

6.3.3.1 Control and measurement electronics

All electronic components were contained in a metal casing, shielding the measurement equipment against external noise and protecting the user against electrical damages. The exterior of the box is depicted in Figure 6.12a. The user had access from the exterior to a 4-pin connector to connect the force sensor, a 6-pin connector for the stepper motor, a switch to turn on or off the power source and a connector for the main power. An air inlet at the top allowed to move air through the box to the air outlet on the side to cool off the electronic components. The box contained a signal amplifier for the force sensor signal, a voltage source for all components, a voltage converter for the force sensor and amplifier, a motor controller board for the driving of a stepper motor, a relay for switching on and off motor and controller board, an USB digital analogue interface and a cooling fan. The location of the components is indicated in Figure 6.12b.
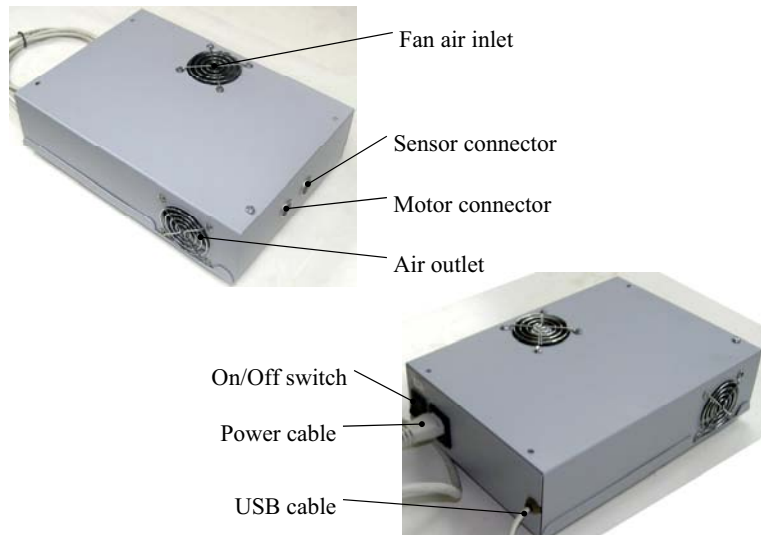
(a) External view of the electronics box, holding control and measurement components.
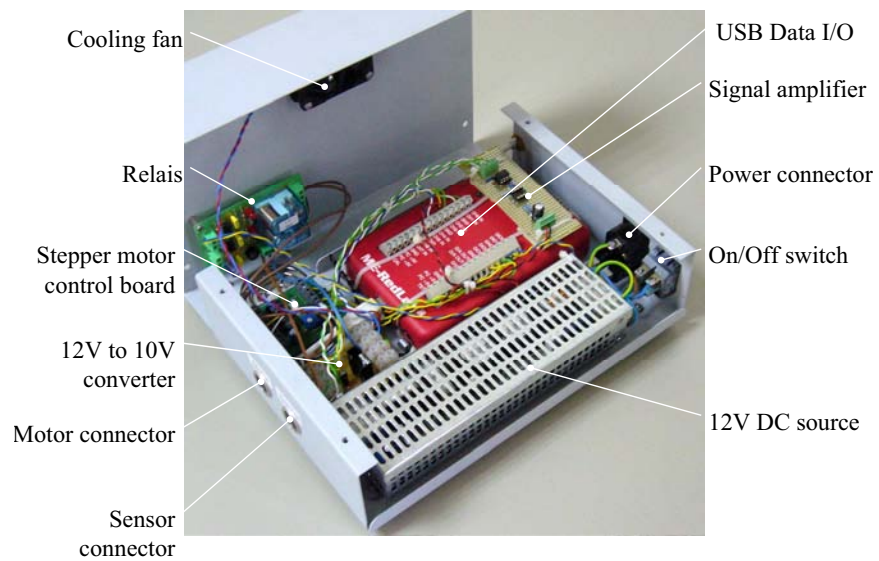
(b) View of the internals of the electronics box. The location of the individual electronic components is indicated.

Figure 6.12: Metal casing containing electronic components to control motor movement and measure force signals.

Stepper motor controller board   The stepper motor controller board (RSSM2, RS-online, Art. No.: 240-7920) used was appropriate to drive an unipolar stepper motor with four phases. The board was supplied with 12 VDC and was able to drive up to 2 A through the motor windings. The connections of the controller board are listed in Table 6.1.

Pin	Description	Connected to:
Control panel		
+5V	5V output (logic high)	Not connected
ENB	Enables the CKl input	DO3 on USB interface
H/F	Half or full step	GND
DIR	Direction	DO2 on USB interface
WAV	Wave mode	GND
DIS	Disables the CKl input	GND
CK0	Clock output	Not connected
CKl	Step rate input	DO0 on USB interface
Motor panel		
0VL	Ground of the motor	GND
+VL	Controller power supply	+12V of the power supply
PHD	Motor winding 'D'	Phase Q2 on motor
PHB	Motor winding 'B'	Phase Q4 on motor
PHC	Motor winding 'C'	Phase Q1 on motor
PHA	Motor winding 'A'	Phase Q3 on motor
+VM	Motor voltage	VM on motor
0VM	Logic low	Not connected

Table 6.1: Connections of the motor controller board.

Relay   It was observed that the stepper motor run hot, when it was left in stand-by. By using a relay (T-5, Cebek Electronics Circuits) it was possible to turn off the power supply of the motor and the motor controller board. The relay was powered by the 12 VDC source and the signal for switching was taken from the DO1 port of the data I/O interface. The connections of the relay are depicted in Figure 6.13.
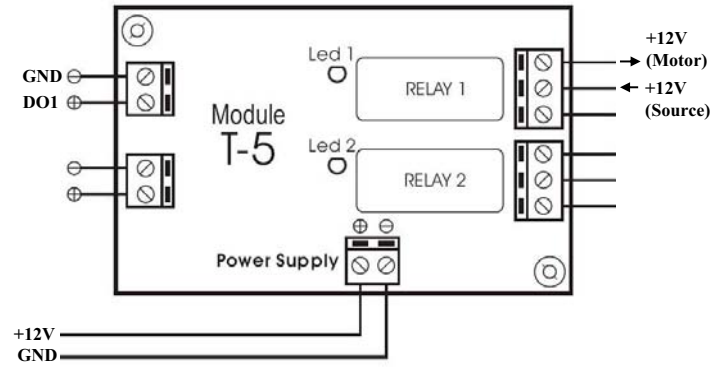
Figure 6.13: The connections of the power supply relay. Schematic modified from the user manual of the relay board.

Data I/O interface   For controlling the actuator movements and measuring voltages, an interface (Meilhaus RedLab 1008) was chosen which was connected to the designated laptop using a USB connection. With a resolution of 11 bits in differential mode, a voltage resolution of 0.48 mV ($\frac{1V}{2^{11}}$) could be achieved by the analogue input of the interface. The analogue input was used to control the function of the 12 VDC source and the 10 VDC converter and to measure the output of the amplified force sensor signal. The digital output was used to set the logic levels on the relay and motor controller board. The connections of the Redlab data I/O interface are listed in Table 6.2. LabView drivers were provided by the manufacturer, which facilitated the later software development. For the correct function of the interface, the Meilhaus software InstaCal (Version 5.7.2) had to be installed on the laptop.

Pin	Connected to:	Description
Differential analogue inputs		
CH0-CH1	Signal amplifier	Measures the voltage output of the force signal amplifier.
CH2-CH3	10VDC converter	Measures the correct function of the 10VDC output.
CH4-CH5	12VDC power supply	Measures the correct function of the power supply.
Digital outputs		
DO0	Motor controller board 'CKl'	Step rate of the motor.
DO1	Relay	Switching motor power supply.
DO2	Motor controller board 'DIR'	Direction of the motor movement.
DO3	Motor controller board 'ENB'	Enables the step rate input.

Table 6.2: Connections of the data I/O interface.

12 VDC power supply   The motor and motor controller board were supplied by a 12 VDC source. Because the motor had a specified current per winding of 0.42 A, which sums up to 1.7 A when windings are active, the power supply had to provide more than 20 W power ($P = 1.7 \text{ A} \times 12 \text{ V} = 20.2 \text{ W}$). For this reason a 50 W supply was purchased (ZWS50-12, Coutant Lambda). The connection to the mains connector was secured by two fuses (Schurter, 5A). A flip switch was inserted into the circuitry to turn the power supply on and off (see Figure 6.14). The power supply was covered with a metal casing, which was connected to common ground, to prevent influence on other electronic components. The metal casing of the electronics was connected to the common ground as a security measure.
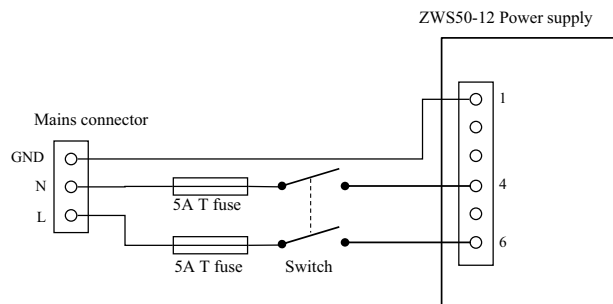
Figure 6.14: Connection of the 12 VDC power supply to the mains connector. The connection was secured by two fuses.

Voltage converter To achieve a stable 10 V direct current source for the force sensor and signal amplifier a voltage converter was built. The converter was based on a LM2940 regulator (National Semiconductor) which could drive up to 1 A. The input voltage was 12 VDC directly connected from the power supply. The 10 VDC output was stabilized with a 22 μF capacitor as suggested in the regulator manual. The LM2940 chip was equipped with a cooling sink (Aavid Thermalloy PF720, 28.9 K/W), to protect it from overheating. The voltage converter circuitry is depicted in Figure 6.15. The voltage converter was tested by connecting the 12 VDC power supply to the input and measuring the voltage on the output with a multimeter (Noru, NR-908-140).
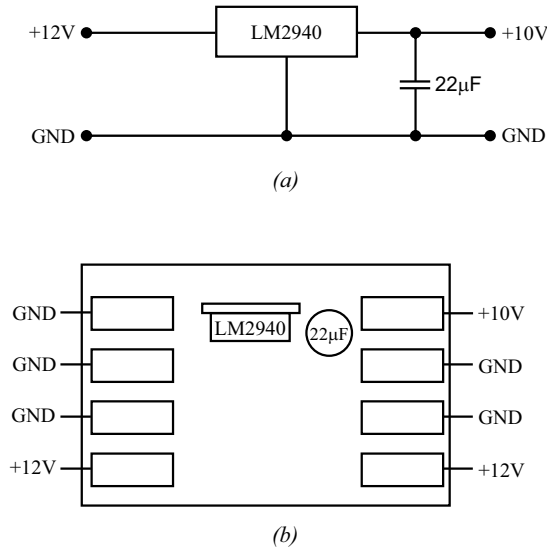
Figure 6.15: Voltage converter for the stable regulation of 10 VDC from a 12 VDC source. (a) Wire diagram of the voltage converter. (b) Connections of the voltage converter board.

Cooling fan To move air over the electronic components for cooling, a fan (ebm-pabst, 612FH) was installed. The fan was connected directly to the 12 VDC power supply taking up a power of 1.4 W. The fan run whenever the power supply was switched on. The fan sucked in air from the top of the electronics box which exited through the side. The air inlet and outlet were placed in a manner which guided the airflow over the power supply, voltage converter, motor controller board and the relay board. These components were suspected to generate the most heat inside the electronics box.

Signal amplifier   The force sensor used in the compression device had a signal output of 0 mV - 100 mV corresponding to applied forces of 0 N to 100 N. To improve the signal for the later conversion from analogue voltage to a digital value, a signal amplifier was used. It was intended to amplify the sensor signal to up to 1 V. The advantage of this was the use of the whole measurement range of ±1 V of the USB data I/O device, which allowed a voltage resolution of 0.48 mV. Higher amplifications would force the use of the next higher measurement range of ±10 V, which would result in a lower resolution of 4.8 mV. A basic inverting amplifier was implemented using an 8-pin TL071 operational amplifier (Texas Instruments) (see Figure 6.16). The amplifier was connected to 10 VDC as a power source which was stabilized on the same circuitry board by a 220 μF capacitor. This amplifier had an amplification factor of -10 (Equation 6.1) [19].

$$G = -\frac{R_2}{R_1} = -\frac{100k\Omega}{10k\Omega} = -10 \tag{6.1}$$

The signal amplifier was tested by applying a direct current voltage at the input with a 1.5 V battery connected to a potentiometer. The input and output voltage was measured with a multimeter (Noru, NR-908-140).
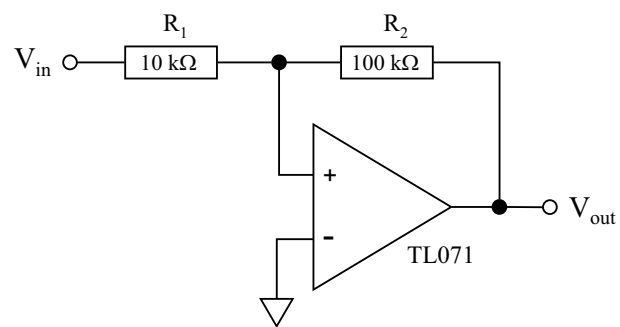
(a)
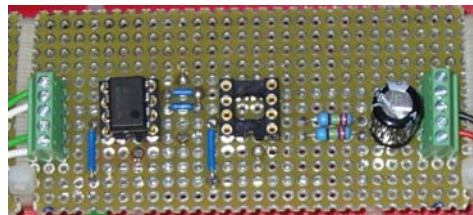
(b)
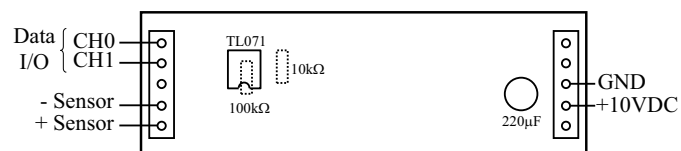
(c)

Figure 6.16: Signal amplifier realized for the amplification of the force sensor signal voltage. (a) Circuit diagram of the signal amplifier based on the TL071 operational amplifier with an amplification of -10. (b) Actual build of the amplifier on prototyping board. (c) Indication of the connections of the circuit and the situation of the electronic parts. The resistors are on the backside.

6.3.3.2   Device for *in vivo* compression of scaffolds

For the compression of the implanted scaffolds in the bone chamber, a device was developed which was coupled weekly to the implant. The device consisted of a handle, which was fixated on the bone chamber and a moving axis, which was fixated on the piston of the assembly. The device contained a linear stepper motor for movement of the piston and a force sensor for the measurement of the occurring forces .

Linear actuator   A stepper motor was chosen as linear actuator, allowing a large displacement at high forces. The stepper motor (Danaher motions, 42DBL10C2U-L12) was a unipolar motor with four windings (see Figure 6.17) which could move a force of 100 N at a step rate or 300 steps per second. The displacement of every step was 25.4 μm. The power consumption of the motor was specified with 10 W at 12 VDC supply. According to its datasheet, the motor had an axial backlash of 150 μm.

(a)   *(b)*
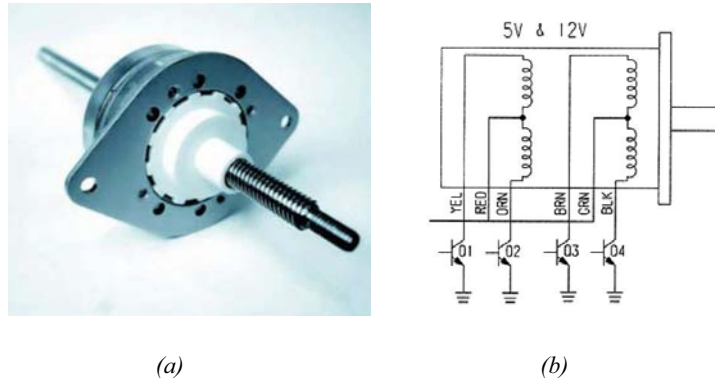
Figure 6.17: The stepper motor used for linear displacement. A picture of the stepper motor (a) taken from the manufacturers datasheet. The wire diagram (b) shows the four windings of the motor and the connection of the six wires.

Force sensor   The force sensor of the device (XFTC310, FPG Sensors and Instrumentations) was appropriate for a maximal force measurement of 100 N. The output signal of the sensor ranged from 0 mV to 100 mV, depending on the applied force. The sensor worked as a Wheatstone bridge (see Figure 6.18), where force and output voltage had a linear relation. The sensor needed a stabilized voltage source of 10 VDC to function correctly.

(a) *(b)*
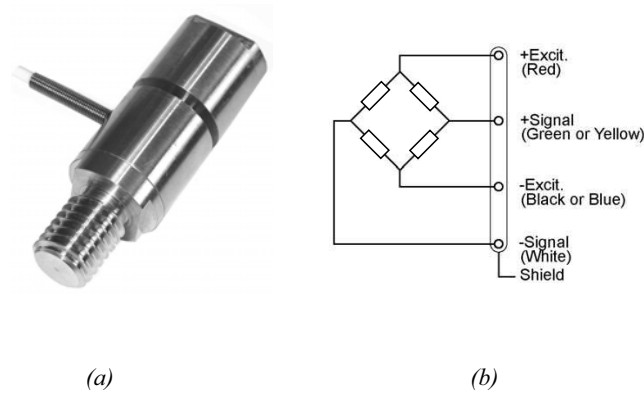
Figure 6.18: Miniature force sensor XFTC310 used in the compression device. (a) Picture of the force sensor from the manufacturer datasheet. (b) Representation of the sensor as Wheatstone bridge with the four connections.

Compression device   The device used for the *in vivo* compression of scaffolds incorporated the linear stepper motor and force sensor described beforehand. The linear stepper motor pushed down its threaded axis, which was connected to the force sensor. The axis was prevented from turning around the length axis by tightening a fixation nut which pushed against the force sensor. The force sensor itself was threaded into a stainless steel (ASTM A176 [20]) block, mounted on a precision linear slide (IKO Nippon Thompson, BSR1540SL). A fixation nut secured the threading of the force sensor to the block. The block provided on the opposed end a bolt thread for threading of a miniature drill chuck, which by turning could be closed or opened. To minimize the backlash of the stepper motor, a spring loaded tension system was implemented on the top of the motor (see Figure 6.19). A compression spring (Springmasters, D12030, free length 56 mm, 0.81 N/mm) hidden in an aluminium casing was pulling the motor axis upwards, so that no backlash occurred when the motor changed directions. By tightening the axis fixation nuts

on top of the mechanism the pull up force could be adjusted.

The aluminium handle, which held the components, was used to fixate the stepper motor and the linear guide. The handle was used by the user to hold the device while fixating it to the bone chamber implant. Additionally the handle did serve as a heat sink for the stepper motor which did dissipate heat during activation. At the tip of the handle a hole was provided for the fixation for the bone chamber implant. The handle was slid over the implant connector. A threaded 'L'-shaped fixation screw was then used to press the cleft end of the handle together against the cylindrical connector.

Axis fixation nut

Spring pressing upwards

Threaded axis

Spring

Axis thread pressed upwards against rotating thread

Rotating thread inside the stepper motor
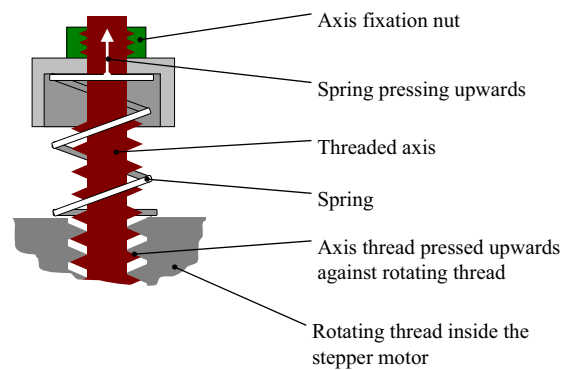
Figure 6.19: Working principle of the mechanism for the reduction of axial backlash of the linear stepper motor. A spring pushes the thread of the motor axis against the thread of the rotating part of the motor. (Not all components of the compression device design are shown here.)

The parts of the compression device are depicted schematically in cross-section in Figure 6.20a. The connection to the implanted bone chamber is shown in Figure 6.20b. Figure 6.21 shows the assembled compression device.
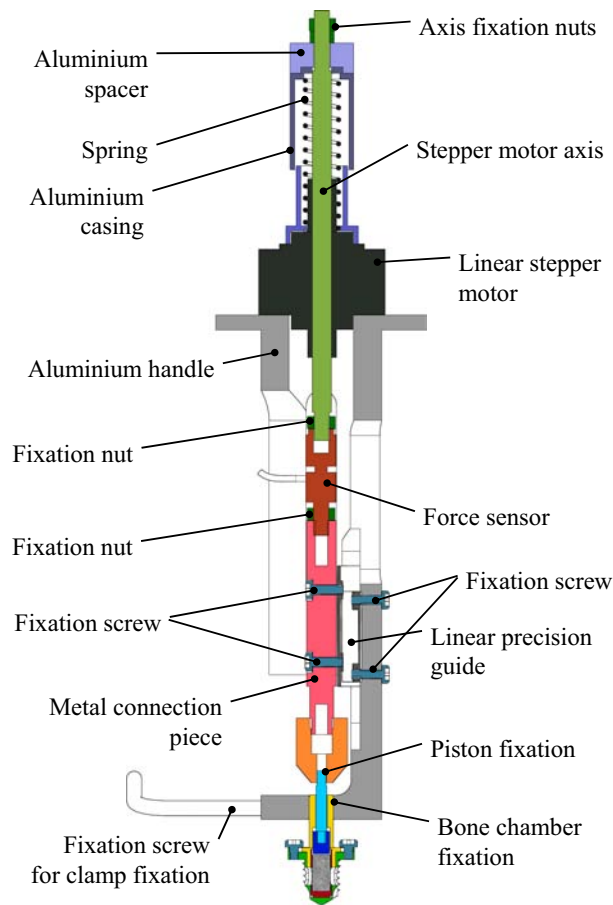
(a) Schematic cross-section through the compression device, connected to the bone chamber implant.
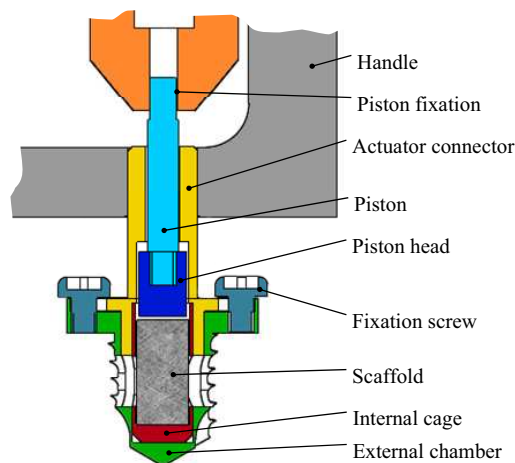
(b) Close-up of the fixation of the bone chamber implant to the compression device.

Figure 6.20: Schematic cross-section of the compression device, depicting its components.
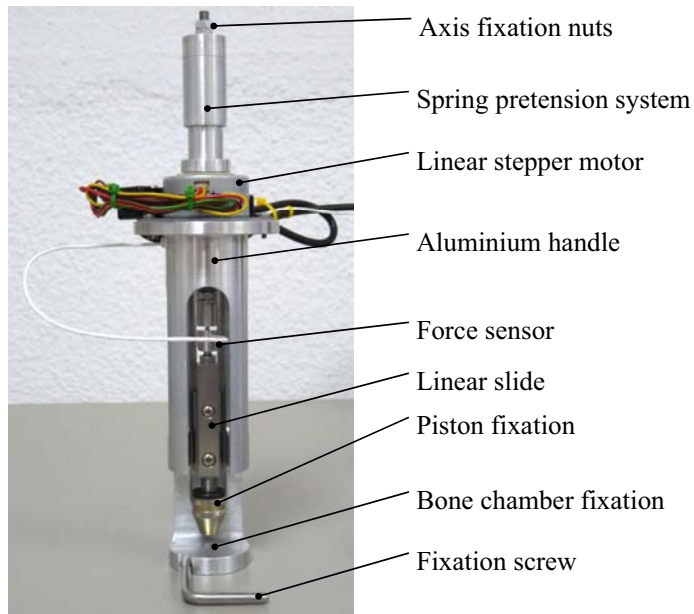
(a) The assembled compression device with indication of the components.
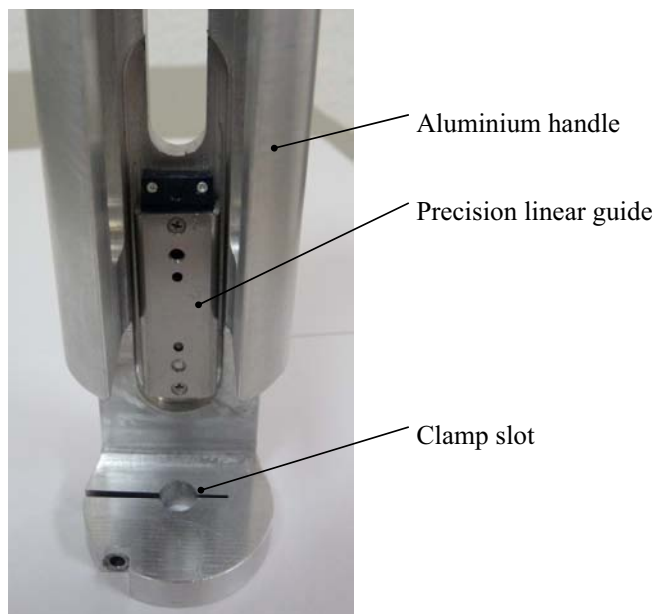
(b) Close-up of the cleft end of the handle and the linear guide in a partial assembled device.

Figure 6.21: Photographs of the compression device used to compress scaffolds *in vivo*.

6.3.4 Validation of the compression device

6.3.4.1 Minimal time step

One critical parameter for the compression device was the minimum time needed for one step, where one step included the output of two digital signals (a '1' followed by a '0' to activate the step) and the input of the analogue force signal. LabView programs were written to measure the time needed for digital output and analogue input. Both programs measured 100 times the time needed for the respective functions. The programs are depicted in Figure 6.22.
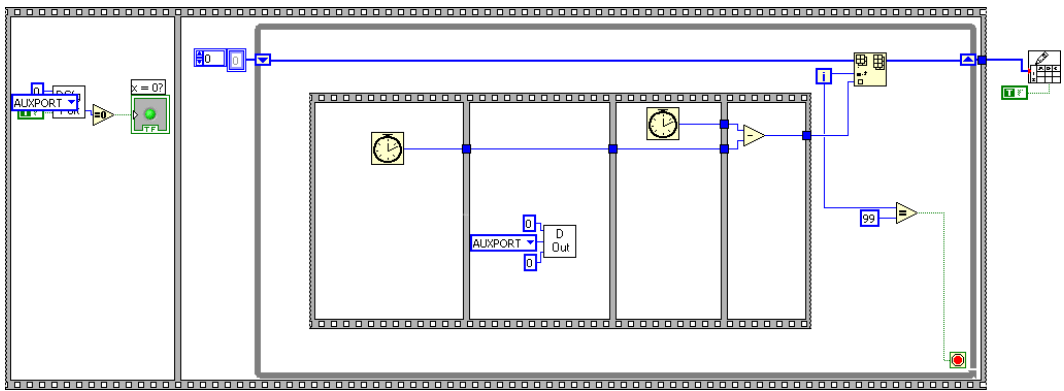
(a) LabView program used to determine the time for digital output.
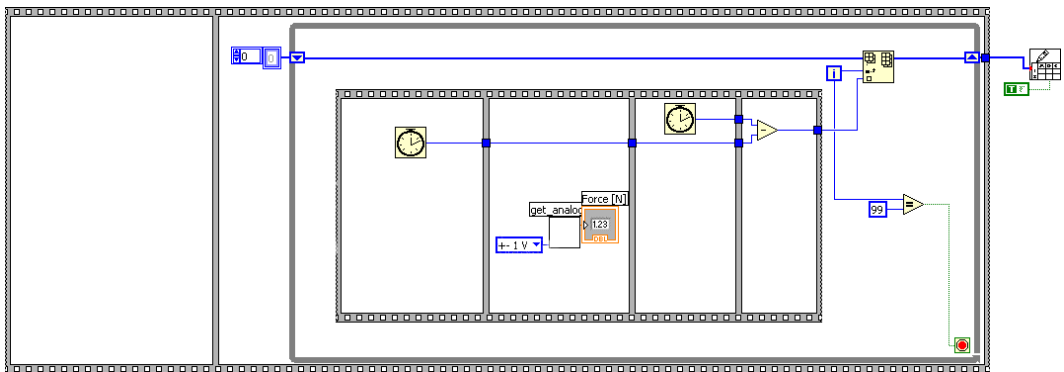
(b) LabView program used to determine the time for analogue input.

Figure 6.22: LabView programs to measure 100 times the time needed for digital output or analogue input.

6.3.4.2   Calibration of the force measurement

To calibrate the force measurement of the force sensor, the resulting voltage was measured at different loadings. For the measurements the force sensor was mounted in a test rig (see Figure 6.23). The rig consisted of an acrylic base plate (1.5 mm thick) on which the force sensor was mounted vertically with a stainless steel screw. Guided by four rods, a movable stage was rested on the force sensor. On top of the movable stage, weights could be positioned to apply loads to the sensor.
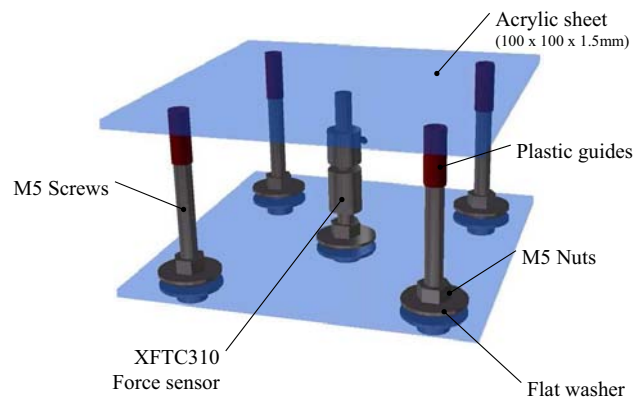
Figure 6.23: The test rig used to test the force measurement consisted of a movable stage guided by 4 rods and resting in a right angle on the force sensor. Weights were placed on the movable stage to apply force on the sensor. The force sensor was mounted on a base plate and a movable stage rested on top of the force sensor.

The motor and force sensor were connected to the electronics, which was connected via USB to the laptop computer. A LabView program was written, using the algorithm for reading the analogue data from the data I/O. The software read out the analogous signals on three ports every 50 ms and displayed them on screen (see Figure 6.24). The first port was connected to the signal amplifier and its range was set to ± 1 V. The setup of the force measurement included all electronics used in the final device. This ensured that the measurements were made in the configuration of later use.

For the application of loading on the force cells, weights were purchased (2×0.5 kg, 5×1 kg and 2×2 kg). The exact weight was determined by weighing on a scale (Measure Tech MB-2610). The weights were then placed on the movable stage of the test rig in approximately 10 N steps. The resulting voltage measurements were read of the display. Measurements were conducted in triplication.
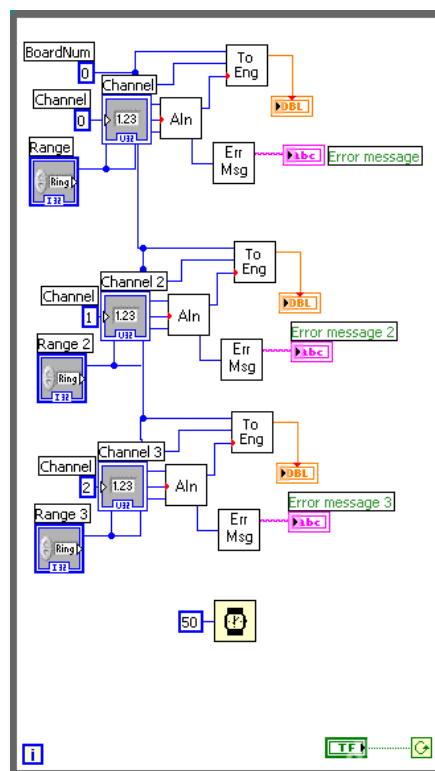
Figure 6.24: Software for the measurement of voltages for different forces applied to the test rig.

6.3.4.3   Displacement validation

To verify the software control of the piston movement, the displacement was measured as a function of the step number controlled by the software. A software was written in LabView to displace the piston (see Figure 6.25). The user had the possibility to enter the number of steps for displacement and select the direction. A displacement of 5 to 25 steps was measured with a micrometer (NSK, resolution 0.01 mm), displacements of 25 to 250 steps were measured with a caliper (TESA Shopcal, resolution 0.01 mm). All measurements were done in triplicate.

6.3.4.4   Motor temperature

One of the concerns of the developed compression device was the heat dissipation of the used linear stepper motor. To measure developing temperatures, a temperature sensor was applied to the metal motor casing. The sensor was a K-type thermocouple connected to a thermometer (RS1313). For the measurement, the compression device was used for 10 minutes of linear compression of 508 μm at 0.5 Hz. After the compression the system was left five minutes to allow the cooling of the motor. This procedure was repeated four times, while the temperature was measured every minute.
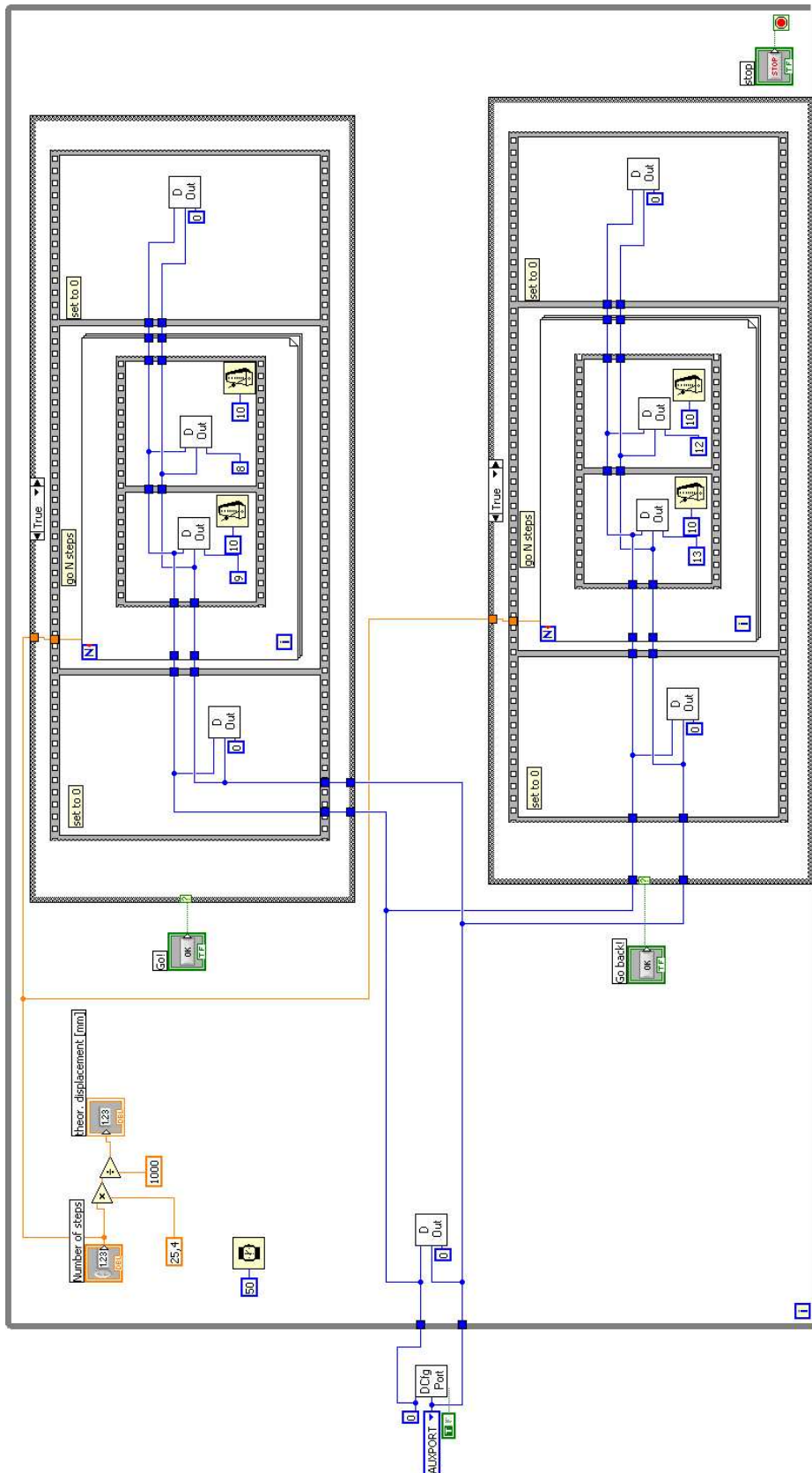
Figure 6.25: Software for the evaluation of the displacement in dependency of the step numbers.

6.3.4.5   Compression of different scaffold materials

For the validation of the compression device, different compression tests were conducted to ensure the function of the device with the porous materials intended to implant. For this purpose the device was used to measure forces under compression with no sample, PLA/glass composite, glass ceramic and nickel-titanium in the internal chamber. The fabrication of the materials is explained in further detail in Chapter 7.

Interference in force measurement during compressive movement
To measure the effect of friction on the measurements with materials, a measurement was conducted without materials. A bone chamber was mounted with internal chamber and compression device connector including the piston. The compression device was then fixated on the connector and the piston. Three tests were conducted with different assemblies of piston, internal cage and connector. Ten cycles were completed of 508 μm compression at 0.5 Hz. Force measurements at every step were obtained.

PLA/glass composites   Three samples of the PLA/glass composites were tested under cyclic compression. The sample dimensions were measured with a calliper (TESA Shopcal) before, directly after, 3 hours after and 24 hours after compression to determine if the samples experienced a permanent deformation. The samples were compressed 609.6 μm for 450 cycles at 0.5 Hz. Force measurements were documented at every step.

Glass ceramics   To measure the elastic modulus and the maximal stress of the glass ceramics, eight samples were tested on a commercial mechanical testing equipment (Adamel Lhomargy, DY-34) with a 10 kN force cell and a compression velocity of 1 mm/min. To test the developed compression device, five glass ceramics samples were compressed 127 μm in 450 cycles at 0.5 Hz with a titanium piston head. The sample length and diameter was determined before and after compression with a calliper (TESA Shopcal). Of these compressive tests, the elastic modulus was determined and compared to the previously determined modulus.

Nickel-titanium   Of the porous nickel-titanium scaffolds supplied, only one was available for testing the developed compression device for the cyclic compression. The piston head used was fabricated of titanium. The sample dimension was measured with a calliper (TESA Shopcal) and compressed three times for 10 cycles at 0.5 Hz with compressions of 25.4 μm, 50.8 μm, 76.6 μm, 101.6 μm and, 127 μm.

The resulting maximum and minimum forces were used to calculate the compressive modulus.

6.3.5 Software development

For the compression device a software was developed for control the linear stepper motor movement and the measurement of occurring forces, using LabView (Version 8.0). The software provided a graphical user interface to give easy access to the functions of the device to the surgical team, which was meant to use the compression device without supervision after an introductory training. The software showed the compression parameters, the state of the system for the compression procedure, a real-time graph with the displacement and the measured force and the software generated a file with all measurements.

Compression procedure The function of the software was integrated in the procedure for the *in vivo* sample compression:

1. To start, the laptop was turned on.

2. The electronics box was connected to the mains and via USB to the computer.

3. The software was started.

4. The electronics box was turned on, after connecting motor and sensor of the compression device.

5. In the software settings, the material type to be compressed was selected.

6. The protective cap was removed from the implanted bone chamber.

7. The piston fixation was opened.

8. The compression device was connected to the implanted bone chamber by use of the clamping mechanism.

9. The piston fixation was driven down to the piston by the software.

10. The piston fixation was closed.

11. The compression was started by the software.

12. The measured forces were saved in a '.txt' file.

13. After the compression procedure, the piston fixation and handle clamp was opened and the compression device taken off the implant.

14. When all compressions were finished, the software was closed.

15. Finally the electronics box was turned off and the computer shut down.

While the software had to comply to the selected procedure of application, it also had to ensure the safety of user and the equipment itself. Therefore during the manual positioning of the linear actuator and the automatic compression the software protected the device from overloading. During movement of the linear stepper motor, the occurring force was monitored and, when a force larger than a set limit was detected, the motor moved two steps (50.8 μm) in the opposite direction of the actual movement and finally stopped. The software also monitored the correct function of the 12 VDC source and the 10 VDC converter by measuring the voltages. If an unexpected failure occurred during the automatic compression phase, the user had the possibility to cancel the compression. Whenever the linear stepper motor was not used, the software turned the voltage source for the linear stepper motor off, to protect the motor and controlling electronics from electric surge and to let the motor cool off.

Compression movement The movement of the piston for the compression was broken down into different phases to guarantee the same positions and offset measurements for different bone chamber assemblies. When the compression was started, the piston was in the position in which the piston was fixated to the compression device. In this position the offset force was measured. The piston was then moved upwards to the mechanical limit. This was considered the defined start position for all compression sessions. The piston was then moved down to the surface of the scaffold either by sensing the resistive force of the scaffold or by a fixed displacement. When the scaffold was reached, the cyclic compression was initiated according to the compression protocol. After completing the compressions, the piston was moved up to the initial position, in which the piston was fixated. A schematic of the piston movement is depicted in Figure 6.26.
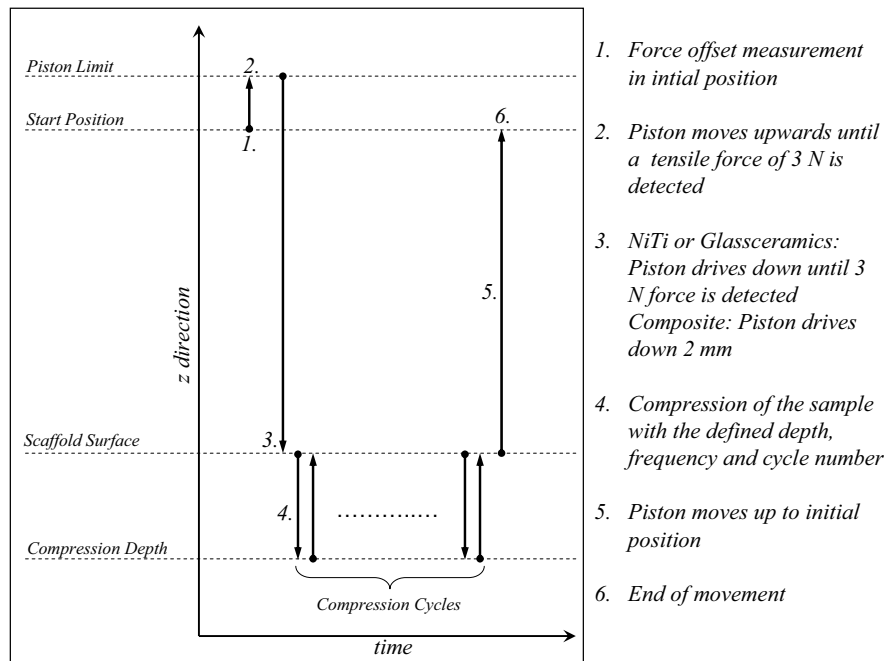
Figure 6.26: Movement of the compression device piston realized by the developed software.

Parameters of the compression   To have the possibility of adjusting parameters for the compression after compilation of the executable software, a `settings.ini` file was provided containing the following content:

    #maxforce:100;[N]
    #uplimit:3;[N]
    #stepsize:25.4;[um]
    'Calibration Values of Sensor + Amplifier
    #slope:14.4;[mV/N]
    #maxwayup:200;[steps]
    #maxwaydown:200;[steps]

Additionally parameters for the different compressed materials were provided in their respective protocol files, which are presented in Table 6.3.

Parameters	Scaffold materials			Unit
	Nickel-titanium	PLA/glass composite	Glass-ceramics	
File name	niti.txt	pla.txt	glass.txt	-
#Waveform	triangle	triangle	triangle	-
#Frequency	0.5	0.5	0.5	Hz
#Cycle number	450	450	450	-
#Compression	127	508	127	μm
#touchforce	5	999*	5	N
#waytogo	2	2	2	mm

Table 6.3: Protocol files for the different material-dependent compressions. * When the touchforce parameter was over 50 N, the piston was moved towards the sample with a discrete displacement instead of depending on the measured force.

These parameters had the following significance in the compression procedure. When the compression device was fixated to the implant and the compression was started, the piston was pulled up until a force bigger then the specified parameter '#uplimit' from the 'settings.ini' file was reached. At this point the piston was at the upper mechanical limit, which was considered the start position for every compression. If the force was not detected until step number '#maxwayup', a warning was shown and the procedure cancelled, because it was considered that the piston was not fixated on the linear actuator.

Depending on the protocol selected previously, the piston moved then down for a fixed displacement ('#waytogo' from the protocol file), or the piston was moved down until a certain force ('#touchforce' from the protocol file) was detected, indicating the touching of the sample. If the force was not detected until step number '#maxwaydown', a warning was shown and the procedure cancelled, to protect the compression device.

When the piston was touching the sample, the compression cycles began, with a cycle number defined as '#Cycle number' in the protocol file with a displacement

of '#Compression' at a frequency of '#Frequency'. The waveform was chosen by the '#Waveform' parameter. The developed software supported triangular and sinusoidal waveforms. When the cycle number was completed or the compression cancelled, the piston was moved up to its start position.

During the compression and the manual positioning of the compression, the device was protected from overloading. During movements of the linear stepper motor, the occurring force was monitored and, when a force larger than '#maxforce' from the 'settings.ini' file was detected, the motor was moved two steps into the opposite direction of the actual movement.

Software structure   The software was organized into routines which are listed with a short description in Table 6.4. For the comprehension of the detailed function, screenshots of all subroutines are provided in Appendix F as well as flowcharts showing the logical operation and dependencies of the subroutines in Appendix G.

main.vi: Main application; Windows of the GUI.			
Input:	-	*Output:*	-
2stepsback.vi: Drives the actuator two steps upwards.			
Input:	-	*Output:*	-
2stepsdown.vi: Drives the actuator two steps downwards.			
Input:	-	*Output:*	-
calcsinus.vi: Generates a sinus value at a given timepoint for the displacement.			
Input:	- Displacement l	*Output:*	Time t
	- Max. displacement l_{max}		
	- Frequency f		
choose_protocol.vi: GUI menu for choosing a protocol and input animal ID.			
Input:	-	*Output:*	- Protocol name
			- Protocol path
			- Patient ID
			- Touch force [N]
			- Frequency [Hz]
			- Cycle number
			- Compression [μm]
			- Waveform
control10V.vi: Tests if the voltage source of 10V is within a range of $\pm$ 0.25 V.			
Input:	-	*Output:*	- "Voltage in range?" (T/F)
control12V.vi: Tests if the voltage source of 12V is within a range of $\pm$ 0.25 V.			
Input:	-	*Output:*	- "Voltage in range?" (T/F)
controltmin.vi: Measures 25 times the time needed to set DO twice and read AI once and gives out the average.			
Input:	-	*Output:*	- Smallest timestep t_{min}
convert_mV_to_N.vi: Converts the measured voltage to force, taking in account the offset and slope of the calibration.			
Input:	- Analog input signal [V]	*Output:*	- Force [N]
	- Offset [mV]		
	- From settings.ini: #slope		
generate dt.vi: Converts a consecutive time array into differential time.			
Input:	- Time Array [s] (1D)	*Output:*	- dt Array [s] (1D)
generatesinus.vi: Generates a time point for every displacement step (uses calcsinus.vi for calculation) for a wave.			
Input:	- Compression [μm]	*Output:*	- Time array [s] (1D)
	- Frequency [Hz]		- Step array [μm] (1D)
generatetotalwave.vi: Generates the overall waveform for all cycles (uses generatesinus.vi and generatetriangle.vi).			
Input:	- Compression [μm]	*Output:*	- Total time array [s] (1D)
	- Frequency [Hz]		- Total step array [μm] (1D)
	- Number of Cycles		
	- Waveform		
continued on next page			

continued from previous page			
generatetriangle.vi: Generates a time point for every displacement step for a triangle wave.			
Input:	- Compression [μm] - Frequency [Hz]	*Output:*	- Time array [s] (1D) - Step array [μm] (1D)
get_analog.vi: Reads the analog input voltage, converts it to force (using convert_mV_to_N.vi).			
Input:	- Offset [mV] - Voltage range	*Output:*	- Voltage [V] - Force [N] - Error Message
getoffset.vi: Measures 10 times the momentary force signal and calculates the average.			
Input:	- Analogue measurement range	*Output:*	- Offset [mV] - Offset [V]
limitsensoric.vi: Moves piston up, until the piston head hits its upper limit or a certain number of steps have been exceeded.			
Input:	- #maxforce from settings.ini - #uplimit from settings.ini - #maxwayup from settings.ini - Offset [mV] - Analogue measurement range	*Output:*	- "Overload?" (T/F) - Number of done steps
pistontosample.vi: Moves the piston downwards for a certain number of steps.			
Input:	- #maxforce from settings.ini - #waytogo from settings.ini - Offset [mV] - Analogue measurement range	*Output:*	- "Overload?" (T/F) - Number of done steps
pistonup.vi: Drives the piston up to its start position.			
Input:	- Number of steps - Offset [mV] - Voltage range	*Output:*	- "Piston is at start position?" (T/F)
timearray.vi: Takes a 1D array of half-wave time points and completes it to a full-wave time point array.			
Input:	- First half time array [s] (1D)	*Output:*	- Time array for one cycle [s] (1D)
touchsensoric.vi: Moves the piston downwards, until the sample is touched or a certain number of steps have been exceeded.			
Input:	- Offset [mV] - Voltage range	*Output:*	- Number of steps - "Touching sample?" (T/F) - "Overload ?" (T/F)
up_down.vi: GUI: Allows user to drive the piston up and down manually.			
Input:	- Offset [mV] - Voltage range	*Output:*	- "Overload ?" (T/F)

Table 6.4: List of software subroutines, their function, input and output.

Use of the software   The software was provided to the user as an executable file with the 'settings.ini' file in the same directory, the protocol files in a 'protocols' folder and a 'results' folder containing the saved measurements. For the easy use, links were provided on the desktop to the application and the 'results' folder. Executing the compression device control software prompted to the user the main panel, which included the display of protocol parameters, actual phase of the compression procedure and a graph of displacement and measured force. The control buttons at the bottom of the screen allowed the user to access the settings panel, the manual displacement control, start the compression procedure and exit the software (see Figure 6.27a). When the 'Change Settings' button was pressed, the settings panel opened up (see Figure 6.27b). This panel allowed to choose the protocol used for the compression (which depended on the scaffold material) and to enter the patient identifier. The panel was closed by pushing the 'OK' button. When the 'Manual Actuator Control' button was pressed on the main panel, a control panel appeared which gave control over the movement of the linear actuator (see Figure 6.27c). By holding the 'UP' button pressed, the actuator moved upwards, when 'DOWN' was held pressed, the actuator moved downwards. The control panel was closed by pushing the 'OK' button. When the 'Compress' button on the main panel was pushed, the compression procedure started. The actual phase of the procedure as well as the compression and force were indicated in the main panel. After completing or cancelling by pushing the 'Cancel' button of the compression procedure, the measured forces were saved in a file. The location of the file was displayed for the user (see Figure 6.27d). When the 'EXIT' button of the main panel was pushed, a reminder was shown that the electronics box had to be turned off before disconnecting the motor and sensor (see Figure 6.27e). By pressing 'OK' the software was then closed. The generated result file from the force measurement was structured as presented in Table 6.5. Beneath the experiment date, the protocol used and the Patient ID, four columns contained the time of every displacement and the displacement value, as well as the time of force measurement and the force value. The file name itself consisted of the start date and time of the compression and the patient ID (e.g. 090310-13_24_43-Dummy.txt was created on March 10th 2009 at 13:24:43 for the patient 'Dummy').
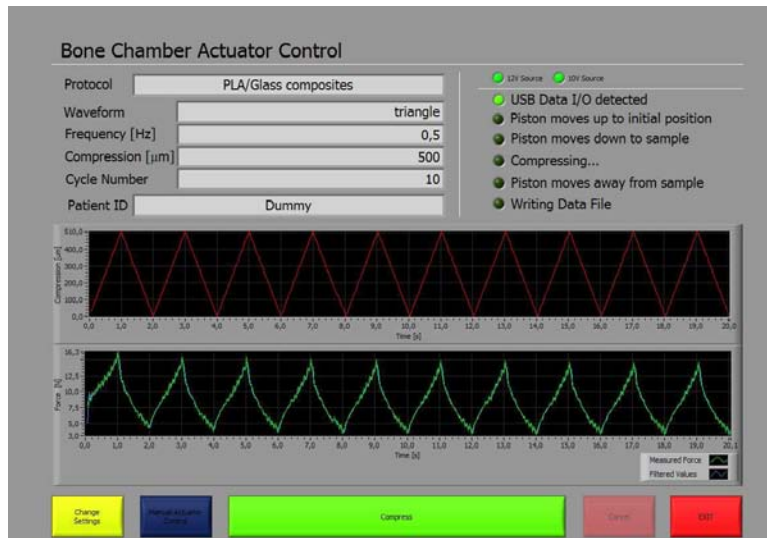
(a) Main screen of the software. Top left: Parameters of the chosen protocol and patient ID. Top right: Indicator of the phase of the compression procedure. Middle: Indications of the compression and measured force over time. Bottom: Control buttons.
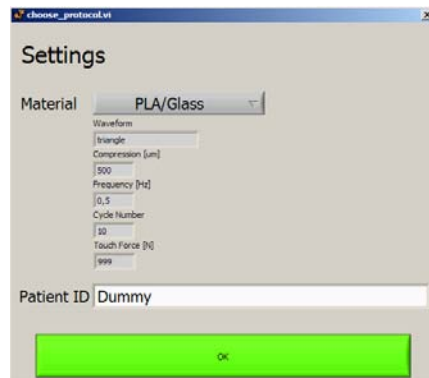
(b) The settings panel allowed to select the protocol, displayed the protocol parameters and allowed to insert the patient ID.
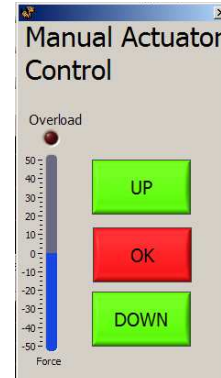
(c) Manual control over linear actuator movement.
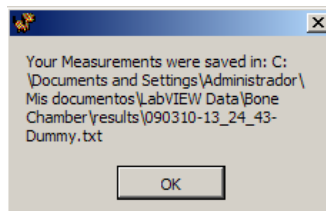
(d) The notification of the directory of the saved result file.
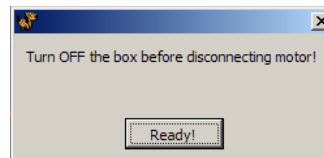
(e) Reminder appearing before exiting the program.

Figure 6.27: Screenshots of the developed software for control of the compression device.

10/03/2009 13:24
Protocol Name:PLA/Glass composites
Patient ID:Dummy

Step Time [ms]	Displacement [μm]	Force Time [ms]	Force [N]
50	25.4	61	7.8566
100	50.8	117	8.8399
150	76.2	165	8.5686
...	...	...	...

Table 6.5: The result file generated after the compression contained information about the date, patient ID and protocol used.

6.4 Results

6.4.1 Implantation of the bone chamber

Surgical drill burr   To provide a 11 mm burr for the bone chamber implantation, a commercial HSS burr was modified. It was found that the modified surfaces tended to corrode heavily after immersion for 5 min in 5 % saline solution and 1 hour at 37 °C (see Figure 6.28). To counter corrosion, newly modified burrs were treated with physical vapour deposition with Chrome Nitrate at the modified surface prior to sterilization and use.
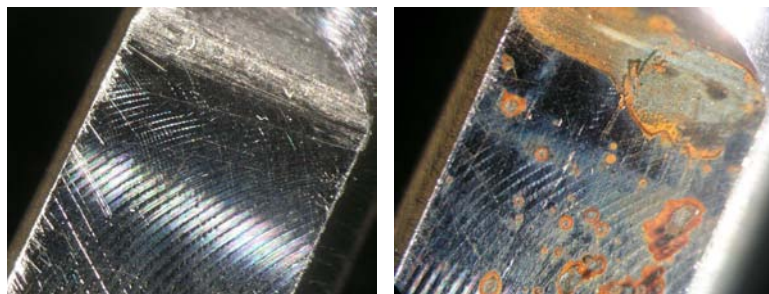
(a) Surface of the modified drill shank.

(b) Surface after corrosion test.

(c) Drill treated with chrome nitrate by PVD.

Figure 6.28: Modified drill burr without surface treatment. (a) shows the surface before, (b) shows the surface after the corrosion treatment. Even after a short period of 1 hour after wetting with 5% saline solution corrosion is observable. (c) shows the burr shank treated by physical vapour deposition.

Use of the bone chamber system in the surgical environment   The implantation tools for the developed bone chamber systems were tested successfully in dog cadaver tibia before the implantation of the chamber in the animal experiments. Finally the function of the system was verified by implantation in dogs. The protocol for the animal experiments is explained in detail in Chapter 7. The bone chamber was implanted as shown in Figure 6.29. Before drilling the appropriate hole for the bone chamber, a small diameter hole was drilled into the tibia. The modified HSS drill was used to expand the hole and the bone chamber was threaded in using the insertion tool. After taking off the tool, the wound was closed over the

implant for the osteointegration phase.

After osteointegration, the implantation site was opened up, a scaffold was inserted into an internal chamber, the protective cap was assembled on the internal cage and the assembly inserted into the bone chamber (see Figure 6.30). The wound was then closed over the chamber. When inserting the samples for later compression, the actuator connector was assembled instead of the protective cap (see Figure 6.9). This connector was protruding from the wound, which allowed the compression device to be connected to the implant and the piston (see Figure 6.31).

When the sample was implanted for the intended period, the wound was opened up again and the protective cap or actuator connector taken off. Cutting between internal cage and external chamber with a trepan, the sample was taken out, leaving the empty chamber ready for a new sample (see Figure 6.32).
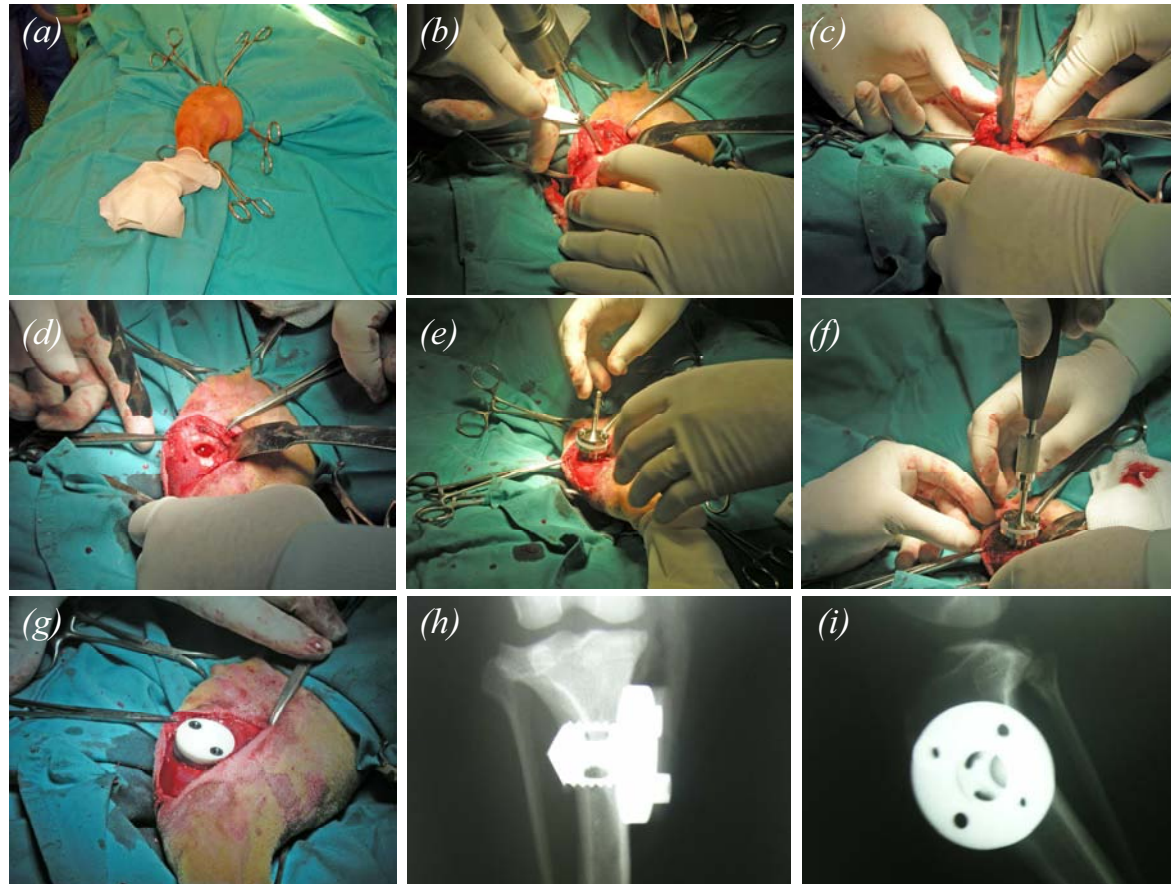
Figure 6.29: Implantation of the bone chamber. (a) Preparation of the dog leg for the implantation. (b) A small hole is drill for guidance in the tibia. (c)+(d) The hole for the threading of the bone chamber was produced with the modified HSS drill. (e) The bone chamber with the attached insertion tool was inserted in the hole and (f) threaded into the bone. The insertion tool was detached. (g) The skin was closed over the implant. (h)+(i) Location of the implanted chamber in the medial side of the proximal tibia.
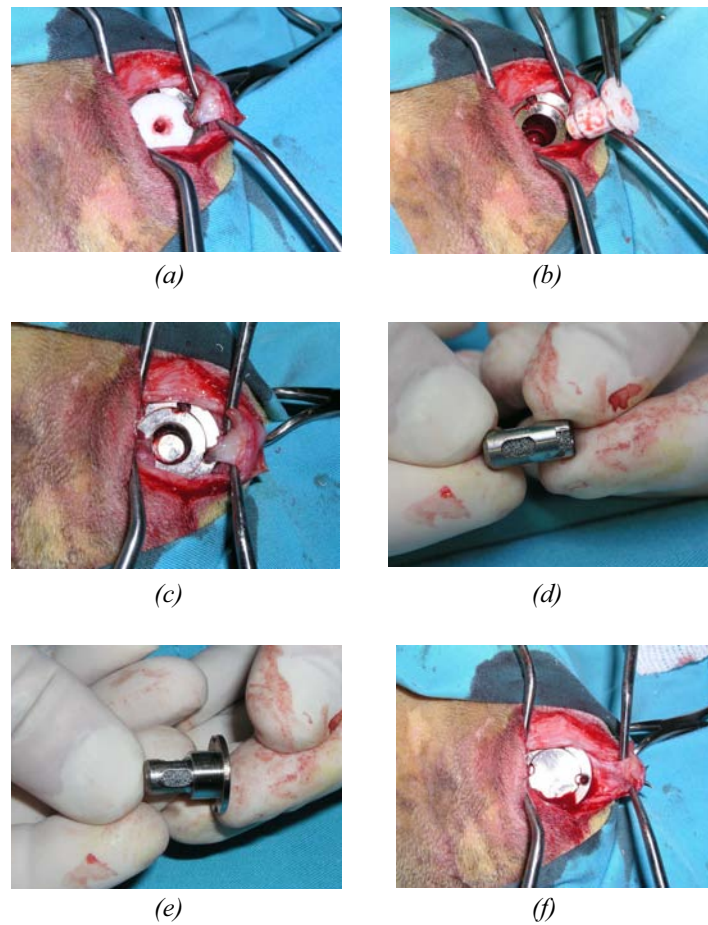
Figure 6.30: For the insertion of the scaffolds, the implantation site was opened (a) and the Teflon spacer taken out (b). The sample compartment was held free of ingrowing tissue (c). The scaffold was inserted into the internal cage (d), the protective cap assembled (e). The assembly was inserted into the bone chamber and the wound closed (f). For the experiments with compressive load, the actuator connector and piston was assembled instead of the protective cap.

Figure 6.31: For the *in vivo* compression of implanted scaffolds, the developed compression device was connected to the piston from the exterior.
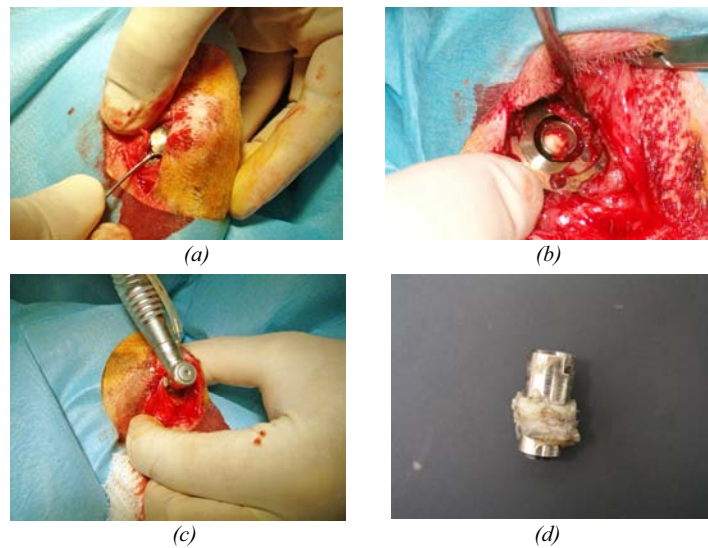
Figure 6.32: After the experiments, the samples were extracted from the bone chambers. (a) The protective cap or actuator connector was taken off. (b) Between internal cage and external chamber a gap was provided to (c)+(d) cut the samples with a trepan out. The sample was then prepared for the histology.

6.4.2   Electronics and hardware development

6.4.2.1   Signal amplifier

The signal amplifier realised for the amplification of the force sensor was tested by application of constant voltages to its input. The resulting output voltage was measured and is depicted in Figure 6.33. After application of a linear regression, an amplification of -10.01 was observed. This was practically identical to the theoretic amplification of -10 of the circuitry.
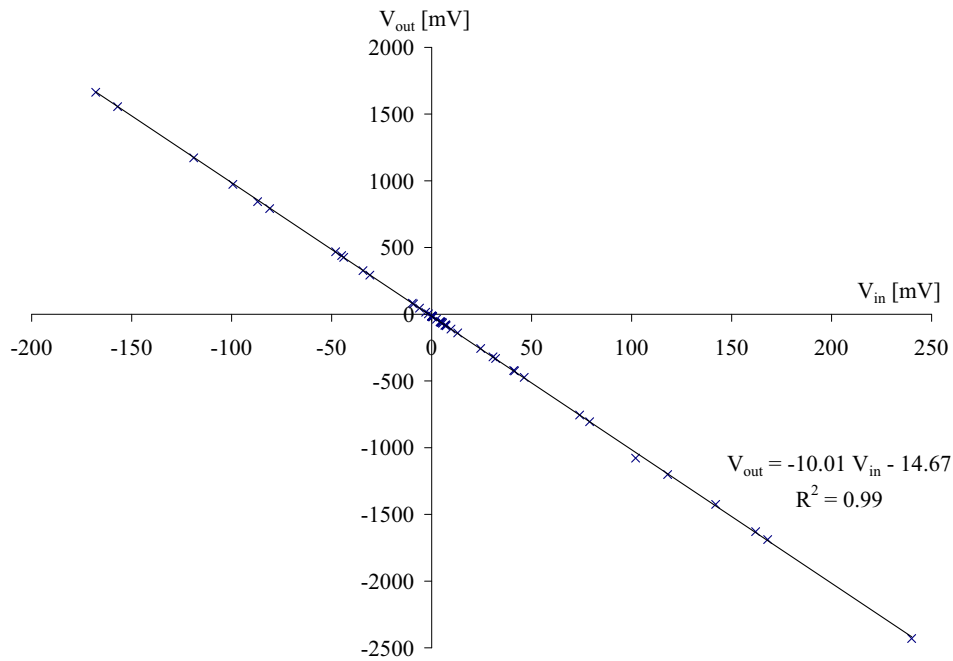
Figure 6.33: Amplification measurement of the implemented inverting amplifier circuitry.

6.4.3   Validation of the compression device

After development of the software for the compression device, several tests were conducted with the device.

6.4.3.1   Minimal time step

Using the described method the time needed for setting the digital port and reading out the analogue input was averaged over 100 measurements. It was determined that the setting of the digital port needed 8 ms in average and the reading of the analogue port needed 16 ms. For the compression device in every step, the

step signal had to be set two times and the analogue input had to be read one time, summing the time for one step up to 32 ms. The fixed minimal displacement velocitiy (25.4 μm per 32 ms) was significantly limiting the possible frequencies and amount of compression (see Figure 6.34). The frequency was calculated as a function of the step number N_{steps}, which depends on the linear displacement $s_{compression}$ (see Equation 6.2).

$$f = \frac{1}{N_{steps} \times 32ms}; N_{steps} = 2 \times \frac{s_{compression}}{25.4\mu m} \tag{6.2}$$

In the final software for the compression device, the smallest possible time step was measured for every protocol to validate the applicability of the frequency and compression parameters.
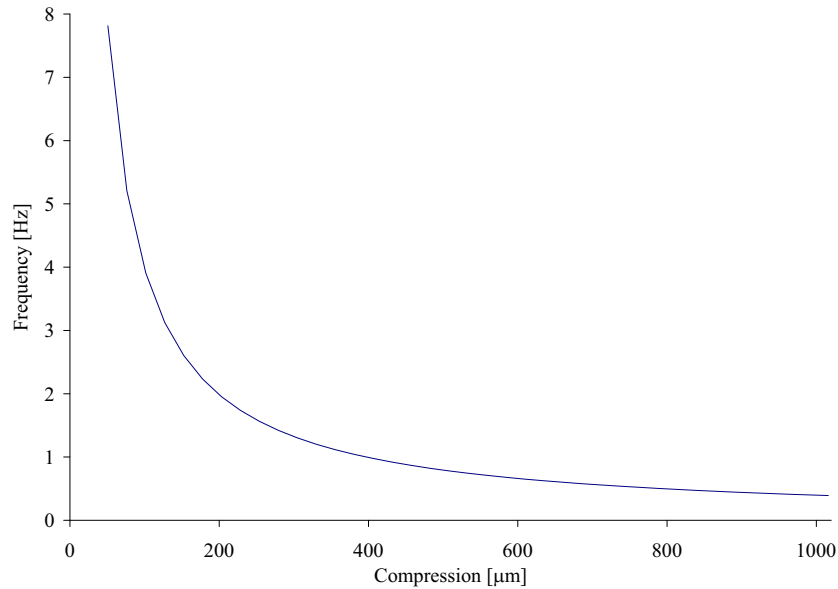
Figure 6.34: The possible compression depth and frequency with a fixed minimum time step of 32 ms and steps of 25.4 μm.

6.4.3.2   Calibration of the force measurement

The voltage resulting from the application of different forces on the force sensor was measured for the calibration of the signal chain of force sensor, signal amplifier and USB data I/O interface. The applied weight and the resulting voltage is listed in Table 6.6.

The resulting voltage was related linear to the applied force (see Figure 6.35). The sensitivity of of the force measurement system was determined with 0.0144 V/N.

Weight [g]	Force [N]	Voltage [V]
0	0	-0.0822 ± .001
1030.2	10.1	0.0498 ± .006
1998.5	19.6	0.215 ± 0.025
3003.3	29.5	0.351 ± 0.014
3934.0	38.6	0.508 ± 0.050
4938.8	48.4	0.636 ± 0.047
5981.5	58.7	0.787 ± 0.044
6964.2	68.3	0.921 ± 0.024
7981.4	78.3	1.05 ± 0.02
9017.7	88.5	1.18 ± 0.01
10047.9	98.6	1.35 ± 0.04

Table 6.6: List of weights applied to the force sensor and the corresponding voltage readings (n=3).

Taking into account the voltage measurement resolution of 0.48 mV, this implied a force measurement resolution of 0.03 N ($\frac{0.48mV}{14.4mV/N}$).
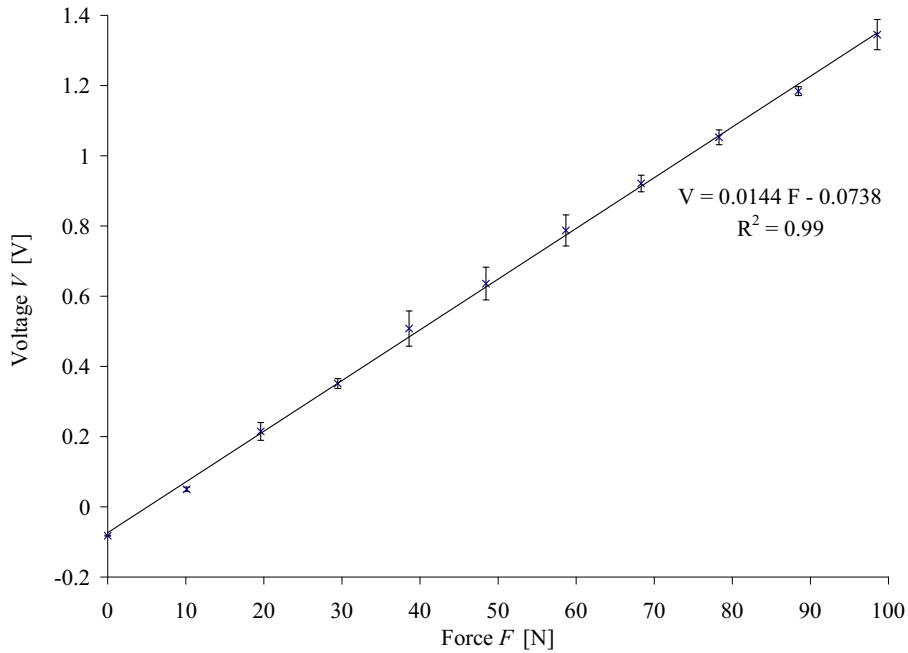
Figure 6.35: Voltage resulting from the loading of the force sensor after amplification (n=3). The slope of the regression line shows a sensitivity of 0.0144 V/N for the measurement.

6.4.3.3 Displacement validation

The displacement of the linear stepper motor at increasing step numbers was measured between 5 and 250 steps. The correlation between step number and displacement can be seen in Figure 6.36. The measured displacement was determined to be 25.0 μm/step. This was 1.5 % smaller than the theoretical displacement of 25.4 μm/step.
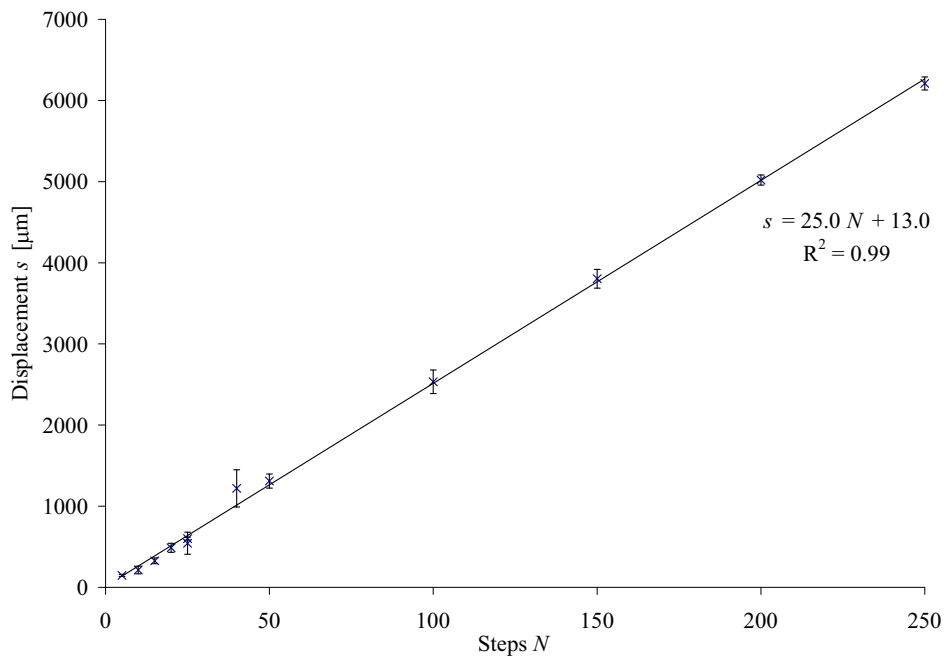
Figure 6.36: The measured displacement showed a linear correlation to the steps proceeded with the stepper motor.

6.4.3.4 Motor temperature

The motor temperature was measured over one hour, with the motor being active for 10 minutes and cooling off for 5 minutes repeatedly. As can be seen from the measurements (see Figure 6.37), the motor temperature rose steeply from room temperature when the motor was activated for the first time. When the motor stopped, the temperature dropped exponentially. By repeating the motor movements and cooling phases, the maximum temperature of every activity was stabilizing at about 55 °C.
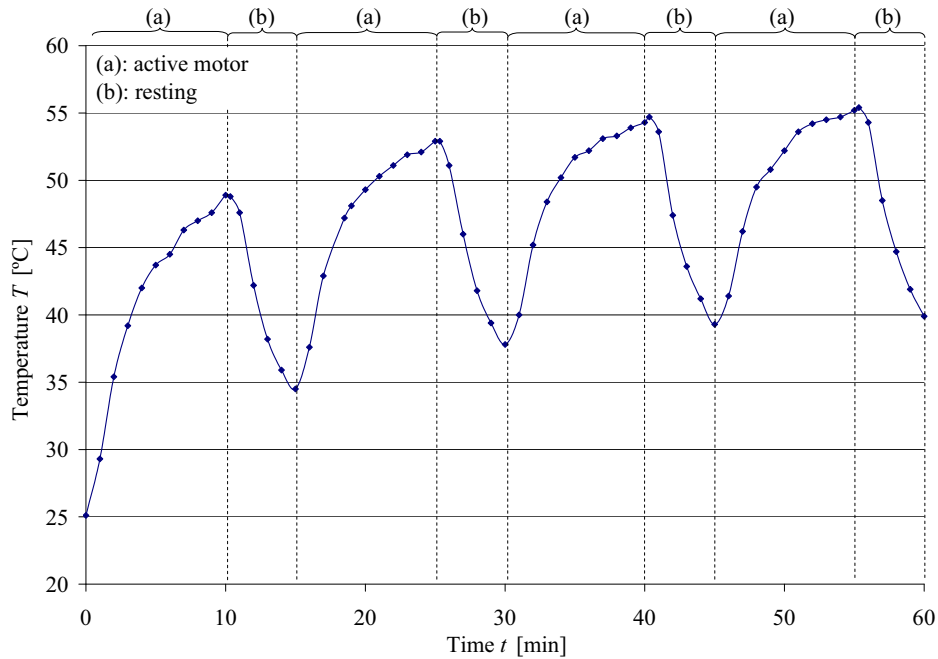
Figure 6.37: The temperature measured directly on the motor casing measured over one hour. The motor was active for 10 minutes and left for cooling for 5 minutes.

6.4.3.5   Compression of different scaffold materials

Interference in force measurement during compressive movement
Measurements of the occurring forces at compressive movements at 0.5 Hz frequency and 508 μm displacement without scaffolds showed an interference signal. The force signal was alternating synchronously with the piston movement and had a range of about 5 N peak to peak (see Figure 6.38). The force wave form depended on the different component assemblies which indicated that friction was the cause of the signal.

PLA/glass composite   After compression of the PLA/glass composites (at 0.5 Hz, 609.6 μm compression and 450 cycles) the force measurements were plotted and compared to pure offset measurements (see Figure 6.39). The forces occurring during compression of the composites could not be distinguished from the signal of the measurement without sample. The expected force value at a compression of 0.6 mm (equaling 5 %) with a elastic modulus of the material of 130 kPa [21] was 0.2 N, too small to be determined reliably with the developed compression device.

Diameter and length of the PLA/glass composite scaffolds were measured before, directly after, 3 hours after and 24 hours after the compression cycles. The
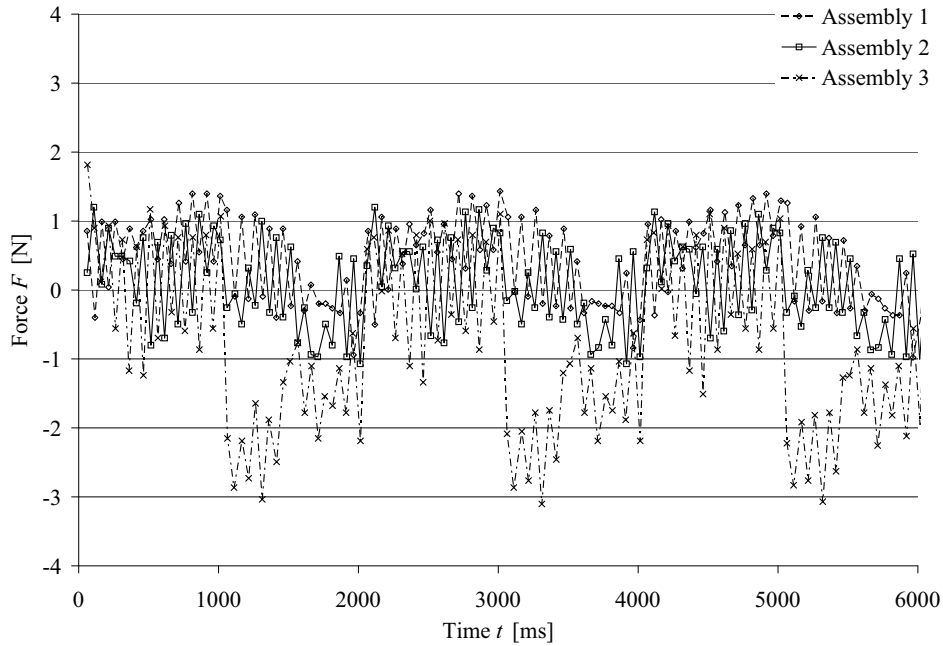
Figure 6.38: Three cycles of three measurements with different piston assembly without a sample in the internal cage. The force signal is alternating with the piston movement of 0.5 Hz frequency and 508 μm displacement.

three samples had a length of 11.6 mm $\pm$ 0.1 mm and diameter 5.9 mm $\pm$ 0.1 mm before the compression. The dimensions were normalized to the initial values and depicted in Table 6.7. Directly after compression, the samples were deformed about 1 %, but regained their length after 3 hours of rest. The diameter of the scaffolds did not change significantly during compression.

| | Time after compression | | |
	0h	3h	24h
length	99.0 % $\pm$ 0.6 %	99.7 % $\pm$ 0.2 %	99.7 % $\pm$ 0.2 %
diameter	99.7 % $\pm$ 0.8 %	100.6 % $\pm$ 0.8 %	100.3 % $\pm$ 1.3 %

Table 6.7: PLA/glass composite scaffold length and diameter measured after cyclic compression. Values are normalized to the dimensions before compression (n=3).
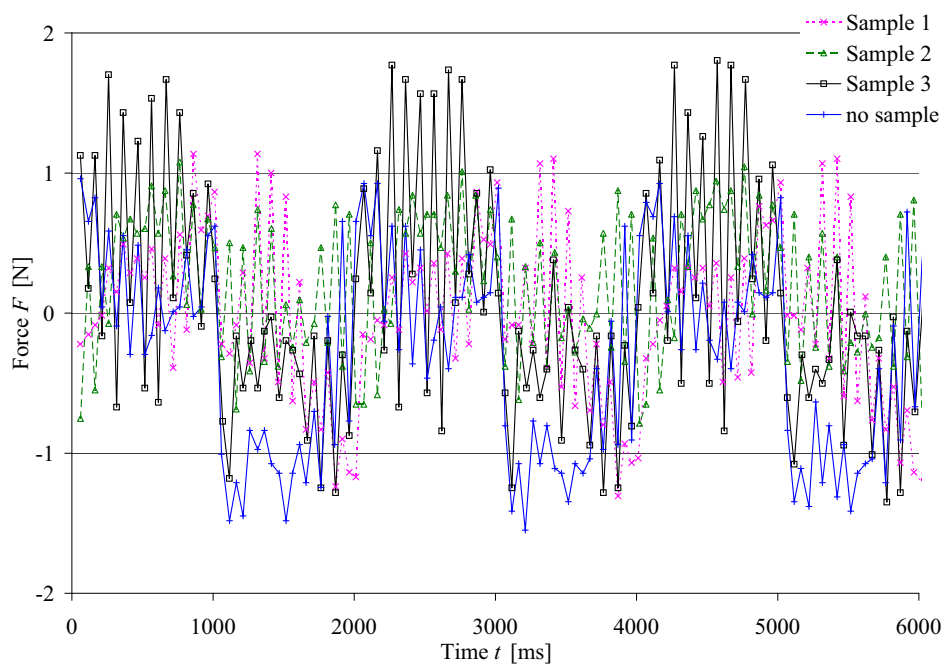
Figure 6.39: Force measurements of three PLA/glass composites under compression of 609.6 μm at 0.5 Hz in comparison to compression of an empty internal cage. Only three of 450 cycles are shown. The resulting force measurements cannot be distinguished from the interference signal in force measurement.

Glass ceramics   Eight samples of the porous glass ceramics were tested with the Adamel test equipment. The samples had a diameter of 7.7 mm $\pm$ 0.5 mm and a length of 12.5 mm $\pm$ 1.2 mm. The compressive modulus derived from the stress-strain curves was 273.0 MPa $\pm$ 156.2 MPa, showing a wide range of moduli. The yield stress was determined to be 6.3 MPa $\pm$ 1.4 MPa.

Five porous glass ceramic samples were compressed in the developed compression device (at 0.5 Hz, 127 μm compression and 450 cycles) and the resulting forces were determined (see Figure 6.40a). Using the force measurements for every sample at compressions of 76.2 μm, 101.6 μm and 127 μm of the first 10 cycles, it was possible to calculate the compressive modulus for every sample. The stress-strain curves of all samples are depicted in Figure 6.40b. From those curves a modulus of 244.9 MPa $\pm$ 42.8 MPa could be determined, which was about 10 % smaller that the previous measured modulus. This result showed that the developed compression device reproduced reliably the measurements of the commercial test equipment.

It was observed that over the course of 450 compression cycles the measured force decreased (see Figure 6.41). The decrease of force is possibly caused by destruction of the micro-structure of the samples, even though it was ensured that the compression of 127 μm kept the theoretic strain of the sample under the yield point of 6.3 MPa with a maximal strain of 2.9 MPa (see Equation 6.3).

$$\sigma = E \times \varepsilon = 273\,MPa \times \frac{0.127\,mm}{12\,mm} = 2.9\,MPa \tag{6.3}$$

The partial destruction of the samples was confirmed by the measurements of the scaffold dimensions before and after cyclic compression. Table 6.8 shows the decrease in sample length about 1.7 %. The diameter of the samples was the same after compression compared to the value before compression.

	before compression		after compression	
	length [mm]	diameter[mm]	length [mm]	diameter[mm]
Sample 1	9.98	5.37	9.77	5.35
Sample 2	10.40	5.31	10.30	5.34
Sample 3	10.42	4.96	10.06	4.86
Sample 4	10.15	5.32	9.98	5.47
Sample 5	10.22	5.96	10.19	5.83
Mean	10.23	5.38	10.06	5.37
SD	0.18	0.36	0.20	0.35

Table 6.8: Length and diameter of the glass ceramics samples measured before and after 450 compression cycles.
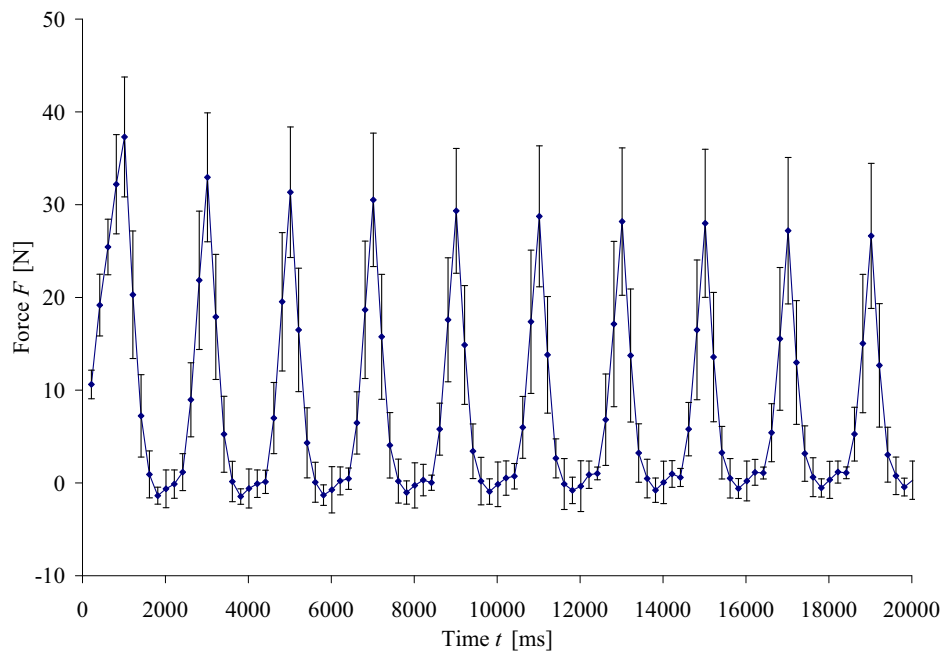
(a) The average of force measurement for the first 10 of 450 compression cycles of 5 glass ceramic samples.
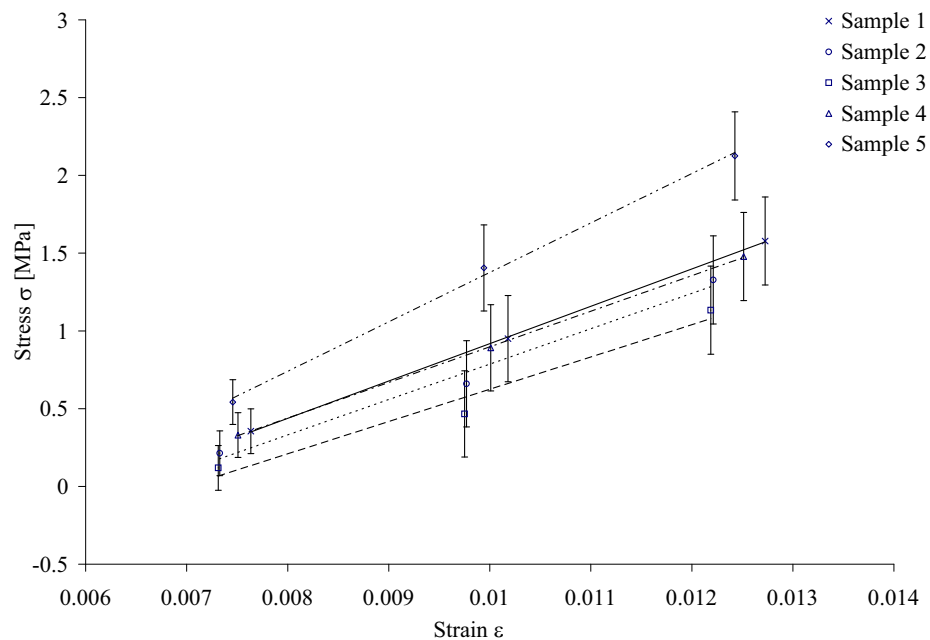
(b) Stress-strain diagram for the three largest compressions (up to 127 μm) for 5 samples compressed in the developed device (n=10).

Figure 6.40: Force measurements and stress-strain curves resulting from the cyclic compression of glass ceramics scaffolds.
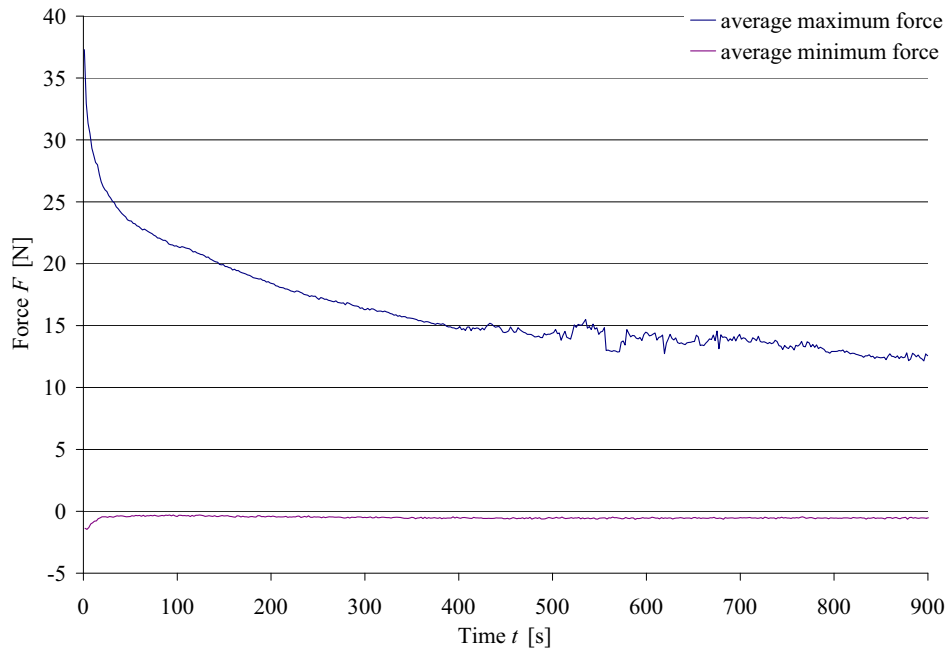
Figure 6.41: Graph of the average maximum forces achieved in every cycle of the compression of glass ceramics samples (n=5). The maximum force decreased over time.

Nickel titanium scaffolds   One nickel titanium sample (11.8 mm length, 5.9 mm diameter) was compressed cyclically for 10 cycles with compressions of up to 127 μm. These compressions were repeated three times (see Figure 6.42a). The low standard deviations showed the high repeatability of force measurements with the same component assembly. From the force measurements stress-strain curves were calculated and the compressive modulus was determined with 370.7 MPa (see Figure 6.42b). This value was only a third of the literature value of 1.2 GPa $\pm$ 0.4 GPa given by the provider of the material [22].
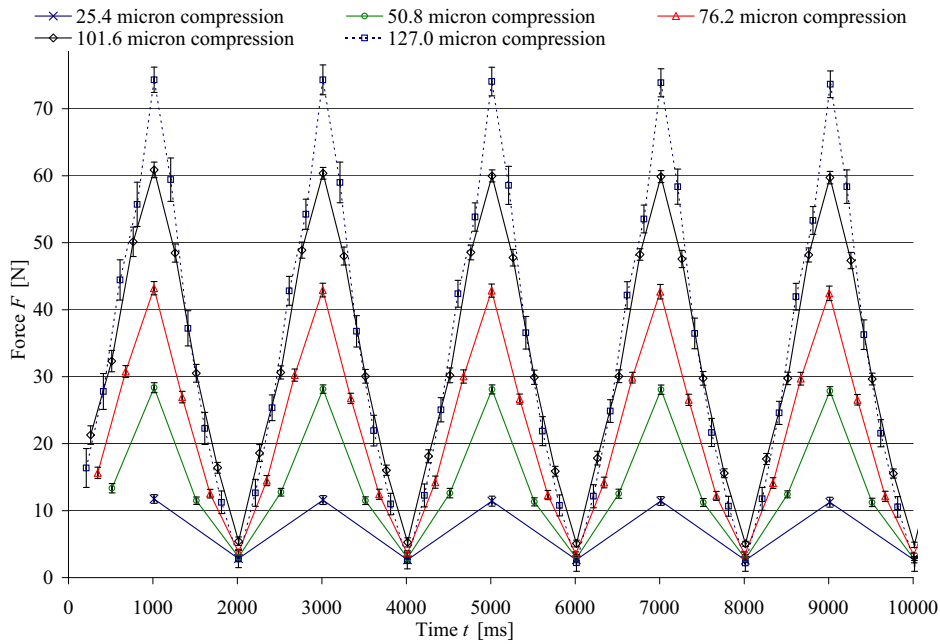
(a) Average force signals of sample compressions with nickel titanium (n=3). The measurements showed a high repeatability at different compression displacements. Five cycles of ten are shown.
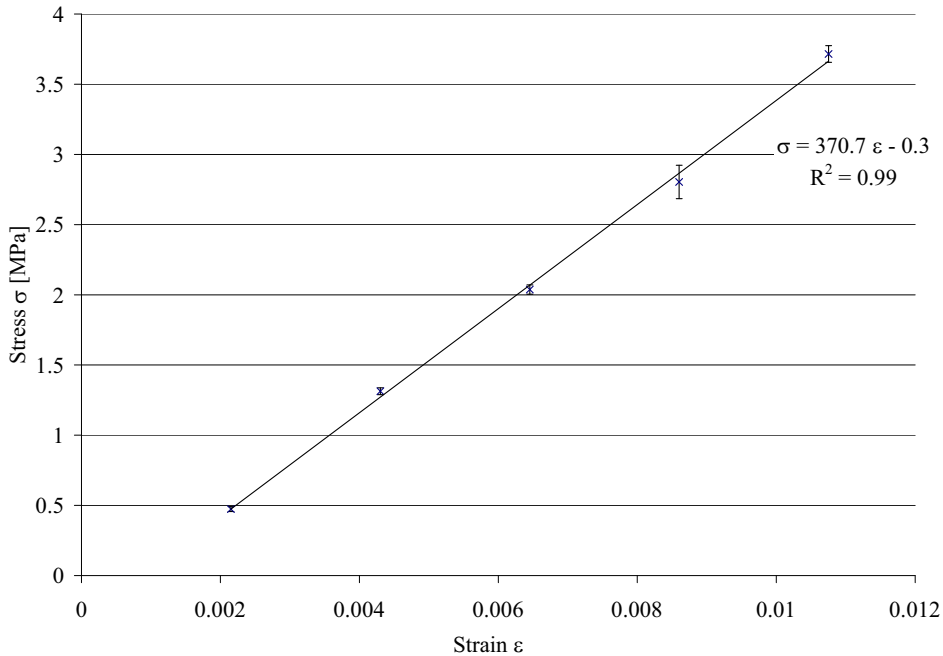
(b) Stress-strain curve for the compressions of nickel titanium scaffold (n=3).

Figure 6.42: Compression of nickel titanium scaffold.

6.5   Discussion

In the presented study, a bone chamber system for repeatable implantation of large scaffolds and additional mechanical stimulation was developed. The implantation of the bone chamber system in the dog tibia showed feasible with the developed tools and the selected procedure. The design took in consideration that the bone ingrowth apertures were as big as possible to enhance the mass of ingrowing tissue as has been shown in similar bone chamber design studies [15]. One limiting dimension of the bone chamber design was the gap between internal cage and external chamber which caused a distance of tissue to scaffold of 2.5 mm. In the subsequent study (see Chapter 7) it has to be shown that tissue has the ability to cross this distance and grow into the scaffold.

The bone chamber system was made as a portable device, which was an advantage for the use and manipulation in the operating theatre. The system was equipped with a compression device with a displacement resolution of 25.4 μm, a velocity of 0.79 mm/s, a maximal force of 100 N and a force measurement resolution of 0.03 N. The compression pattern applied with the device was programmable and hence presented a high flexibility of the system, adapting the protocol to the material properties of the used samples. Additionally, the software for the device provided a graphical user interface, which made the use of the system easy for the user. The system design allowed the easy transport and setup in the operating theatre. It had been shown, that the custom made circuitry was functioning correctly. The signal amplifier was considered a crucial component, because it was treating the force sensor signal before measurement and hence had to amplify reliably the signal.

The testing device was tested to determine functionality and limitations. It was found that the time needed for one step of the motor and the measurement of the resulting force was limited to 32 ms. This limited the frequencies of compression depending inversely on the maximum compression. The compression device could compress samples up to 762 μm at 0.5 Hz, equalling 6.4 % of the 12 mm scaffolds. The force of compression was limited to 100 N by the stepper motor. Hence the compression displacement has to be adjusted to the stiffness of the scaffold materials. The comparison of the range of compression with previous studies is difficult, because the used systems applied rather forces than displacement on the implants [5, 7, 8, 10].

The force measurement resolution of 0.03 N was deemed to be sufficient for the measurement of occuring forces of the materials intended for the implantation (PLA/glass composites, glass ceramics and nickel titanium). The testing with the materials however had shown that the force measurement was limited by interferences during cyclic compression, which was attributed to friction during piston

movement. The signal impeded the measurement of small force values, which were expected for the PLA/glass composite materials. For the much stiffer glass ceramics and nickel titanium the interference was negligible in comparison to the resulting high force signals even at small compressions. In the case of the composite scaffolds, it was suggested to use the force measurement to detect the ingrowing tissue, which would constitute a higher resistance to compression.

After cyclic compression the composite scaffolds showed a deformation about 1 %, which disappeared within three hours. This showed that the material behaved viscoelastic, whereas the deformation was small in comparison to the compression (5 %).

The test measurements with the glass ceramics material have shown that the developed system measured forces comparable to a commercial material testing equipment. The cyclic compression showed a permanent deformation of the samples in the range of the overall compression, which might have been caused by damage of the microstructure. The measured force during the cyclic compression was decreasing with preceding cycles, which indicated that the destruction of the sample appeared as fatigue. The forces at the last cycles indicated that the samples were still compressed.

The measurements with nickel titanium have shown the reproducibility of the force measurements. An elastic modulus of 370 MPa was determined which was a third of the value given by the provider [22]. The specified value of 1.2 GPa $\pm$ 0.4 GPa for the Young's modulus was in the range of similar porous titanium materials [23–25]. It was suggested that the material properties were altered due to the machining required to obtain scaffolds in the desired dimensions. The material was not cooled during the treatment in the turning lathe, to prevent contamination with the coolant. The generated heat might have influenced the mechanical properties of the nickel-titanium. It was excluded that other parts of the bone chamber experienced larger deformation during compression than the sample and hence partially prevent the compression of the sample. It was suggested that the weakest part of the chamber was the area of the apertures, where four flat struts connect the bottom of the top of the implant. The deformation in this region was estimated to be two magnitudes smaller than in the sample assuming the specified Young's modulus for the materials. Because only one sample was available for testing, no conclusion can be drawn about the material properties.

The developed bone chamber system has shown to be reliable and functional. The application of large scaffold dimensions and the overall design constitute a novelty in the field of bone chamber systems.

6.6   Conclusions

- A reusable bone chamber system for the testing of large porous scaffolds in large bone defects in dog tibia was developed. The bone chamber system proved to be applicable for the implantations.

- For the *in vivo* loading of implanted scaffolds a programmable compression device with force measurement was developed and validated.

- The functionality of the system must be validated subsequently *in vivo* experiments.

Bibliography

[1] C. J. Kirkpatrick, V. Krump-Konvalinkova, R. E. Unger, F. Bittinger, M. Otto, and K. Peters. Tissue response and biomaterial integration: the efficacy of in vitro methods. *Biomol Eng*, 19:211–217, Aug 2002.

[2] P. Buma, W. Schreurs, and N. Verdonschot. Skeletal tissue engineering-from in vitro studies to large animal models. *Biomaterials*, 25:1487–1495, Apr 2004.

[3] N. Lamerigts, P. Aspenberg, P. Buma, D. Versleyen, and T. J. Slooff. The repeated sampling bone chamber: a new permanent titanium implant to study bone grafts in the goat. *Lab Anim Sci*, 47:401–406, Aug 1997.

[4] G. Hannink, B. W. Schreurs, and P. Buma. Irradiation has no effect on the incorporation of impacted morselized bone: a bone chamber study in goats. *Acta Orthop*, 78:31–38, Feb 2007.

[5] A.O. Duty, N.D. Case, and R.E. Guldberg. Cyclic compressive loading of trabecular bone allografts in an in vivo rabbit bone chamber model. *BED-Vol. 50, 2001 Bioengineering Conference, ASME*.

[6] M. Tägil and P. Aspenberg. Fibrous tissue armoring increases the mechanical strength of an impacted bone graft. *Acta Orthop Scand*, 72:78–82, Feb 2001.

[7] M. Tägil, J. Åstrand, L. Westman, and P. Aspenberg. Alendronate prevents collapse in mechanically loaded osteochondral grafts. *Acta Orthop Scand*, 75(6):756–761, 2004.

[8] M.R. Moalli, N.J. Caldwell, P.V. Patil, and S.A. Goldstein. An in vivo model for investigations of mechanical signal transduction in trabecular bone. *J Bone Miner Res*, 15(7):1346–1353, 2000.

[9] S. B. Goodman. The effects of micromotion and particulate materials on tissue differentiation. Bone chamber studies in rabbits. *Acta Orthop Scand Suppl*, 258:1–43, Jun 1994.

[10] R.E. Guldberg, N.J. Caldwell, X.E. Guo, R.W. Goulet, S.J. Hollister, and S.A. Goldstein. Mechanical stimulation of tissue repair in the hydraulic bone chamber. *J Bone Miner Res*, 12(8):1295–1302, 1997.

[11] S. van der Donk, P. Buma, P. Aspenberg, and B. W. Schreurs. Similarity of bone ingrowth in rats and goats: a bone chamber study. *Comp Med*, 51:336–340, Aug 2001.

[12] G. Hannink, B. W. Schreurs, and P. Buma. No positive effects of OP-1 device on the incorporation of impacted graft materials after 8 weeks: a bone chamber study in goats. *Acta Orthop*, 78:551–558, Aug 2007.

[13] J. Duyck, M. D. Cooman, R. Puers, H. Van Oosterwyck, J. V. Sloten, and I. Naert. A repeated sampling bone chamber methodology for the evaluation of tissue differentiation and bone adaptation around titanium implants under controlled mechanical conditions. *J Biomech*, 37:1819–1822, Dec 2004.

[14] S. van der Donk, N. Verdonschot, B. W. Schreurs, and P. Buma. Soft tissue movement and stress shielding do not affect bone ingrowth in the bone conduction chamber. *Comp Med*, 52:328–331, Aug 2002.

[15] G. Hannink, P. Aspenberg, B.W. Schreurs, and P. Buma. Development of a large titanium bone chamber to study in vivo bone ingrowth. *Biomaterials*, 27:1810–1816, 2006.

[16] C. Natali, P. Ingle, and J. Dowell. Orthopaedic bone drills-can they be improved? temperature changes near the drilling face. *J Bone Joint Surg*, 78(B):357–362, 1996.

[17] American society for testing and materials. *ASTM B117-B287: Standard practice for operating salt spray apparatus*, 1995.

[18] American society for testing and materials. *ASTM F543: Standard specification and test method for metallic medical bone screws*, 2007.

[19] J. Hoffmann. *Taschenbuch der Messtechnik*. Fachbuchverlag Leipzig, 2000.

[20] American society for testing and materials. *ASTM A176: Standard Specification for Stainless and Heat-Resisting Chromium Steel Plate, Sheet, and Strip*, 2006.

[21] M. Charles-Harris Ferrer. *Development and Characterisation of Completely Degradable Composite Tissue Engineering Scaffolds*. PhD thesis, Technical University of Catalonia, 2007.

[22] M. Barrabés, A. Michiardi, C. Aparicio, P. Sevilla, J. A. Planell, and F. J. Gil. Oxidized nickel-titanium foams for bone reconstructions: chemical and mechanical characterization. *J Mater Sci: Mater Med*, 18:2123–2129, 2007.

[23] X. Li, C. T. Wang, W. G. Zhang, and Y. C. Li. Properties of a porous Ti-6Al-4V implant with a low stiffness for biomedical application. *Proc Inst Mech Eng H*, 223:173–178, Feb 2009.

[24] J. Y. Xiong, Y. C. Li, X. J. Wang, P. D. Hodgson, and C. E. Wen. Titanium-nickel shape memory alloy foams for bone tissue engineering. *J Mech Behav Biomed Mater*, 1:269–273, Jul 2008.

[25] X. Wang, Y. Li, P. D. Hodgson, and C. Wen. Biomimetic Modification of Porous TiNbZr Alloy Scaffold for Bone Tissue Engineering. *Tissue Eng Part A*, Aug 2009.

Chapter 7

In vivo Application of the developed Bone Chamber System

7.1 Introduction

Biomaterials for bone tissue engineering must be examined thoroughly *in vitro* and *in vivo* concerning their biocompatibiliy and their capacity of osteoinduction or osteoconduction before they can be used in the clinical field. As described in the previous chapter, bone chamber systems are useful tools for the study of *in vivo* performance of biomaterials. Besides the technical development of the bone chamber system, it is important to test the system *in vivo*, because the implantation procedure and the reaction of the tissue to the implant cannot be anticipated entirely beforehand. For the success of the implantation, the period of implantation is crucial as well as the protocol for the compressive stimulation. In previous studies, bone chambers were implanted for compressive stimulation of bone growth in different animal models (see Table 7.1). In those studies, the bone chambers were left for up to four weeks before beginning the cyclic compression [1–5]. After this period, compressions of up to 20 N were applied cyclically to the ingrown tissue. The cycle number of the compressive stimulation ranged from 10 to 3600 cycles per session [1–8] and the frequencies applied were in a range of 0.1 Hz to 1 Hz. The compressions were repeated in intervals of twice per week up to daily [1–8]. In these studies the compressions were applied by force rather than displacement [1–8]. In general strains in bone *in vivo* are considered smaller than 0.2 % [9–11]. *In vitro* studies have shown to require strains of a magnitude higher than *in vivo* to achieve

the adequate intracellular biochemical response [12–14]. The duration of cyclical loadings were up to 12 weeks until sample extraction [3–8], whereas some studies allowed an additional tissue growth time after the loading up to 12 weeks [1, 2].

The dog model is used frequently in the field of bone tissue engineering, because of the similar bone mineral density compared to humans [15, 16]. Dogs withstand stress situations and anaesthesia which is important for the daily treatment [17]. Studies have shown that results of the dog model in bone tissue engineering can be extrapolated to humans, which validates the selection of the model for this study of histocompatibility [18]. The tibia was chosen as implantation site, because surgery and later treatment of the chambers were easy to achieve. The medial side of the proximal tibia lies subcutaneous, so no important functional tissue (muscles, nerves, large blood vessels) was put at risk in the implantation process. Overall the tibia is considered as an adequate implantation site because of the high amount of trabecular bone in its interior [17].

Based on the promising results of *in vivo* bone chamber studies, it was intended in the presented study to use the developed bone chamber system (see Chapter 6) for the implantation of large porous scaffolds into dog tibia.

Description	Rest before loading	Displacement or Force	Frequency	Repetitions	Cycle number	Duration	Reference
Hydraulic, subcutaneous in rats	3 days	13.3 N	1 Hz	3× per week	1800	2 weeks of loading and 4 weeks resting	[1]
Hydraulic, in canine femoral and tibial metaphyses	4 weeks	18 N	1 Hz	daily	1800	8 weeks loading and 12 weeks resting	[2]
Hydraulic, in canine femoral and tibial metaphyses	4 weeks	17.8 N	1 Hz	daily	1800	8 weeks resting and 6 days loading	[3]
Pneumatic, in goat distal femur	1 week	78.4 N	1 Hz	daily	3600	12 weeks	[4, 5]
Direct displacement, in rabbit distal femur	-	19.6 N	0.5 Hz	daily	50	8 weeks	[7]
Piezo-electric, in rabbit proximomedial tibia	-	50 μm	1 Hz	2× per week	800	4 weeks	[6]
Direct displacement, in rat proximal tibia	-	6.2 N	0.16 Hz	daily	10	4 weeks	[8]

Table 7.1: Compression patterns of *in vivo* experiments with systems similar to the developed bone chamber system.

7.2   Objectives

The objective of the conducted *in vivo* experiments was to study the tissue response to the implanted bone chamber previously developed. The bone chamber was filled with scaffolds consisting of PLA/glass composite, glass ceramics and nickel-titanium, to study the osteoconductivity or osteoinductivity of the materials. Scaffolds of PLA/glass composites and glass ceramics were compressed to stimulate the development of ingrowing tissue. The integration of the chambers and the tissue ingrowth into scaffolds was evaluated by analysis of histological cuts and radiographies.

7.3   Materials and methods

7.3.1   Scaffold materials

The scaffold materials for the implantation in the bone chamber were porous cylinders of PLA/glass composites, glass ceramics and nickel-titanium (see Figure 7.1) with dimensions of 6 mm diameter and 12 mm length.

(a) PLA/glass composite   *(b)* Nickel-titanium   *(c)* Glass ceramic
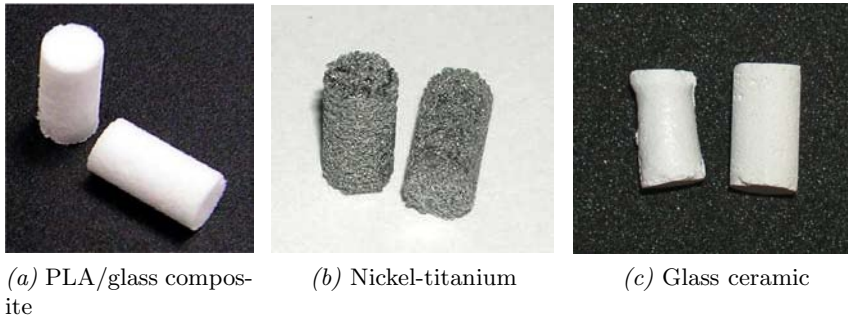
Figure 7.1: Examples of porous material cylinders used as scaffolds in the *in vivo* implantation experiments.

PLA/glass composites were fabricated as described in Chapter 2. The composite scaffolds were sterilized by gamma radiation (8 kGy) prior to the implantations. Glass ceramic scaffolds were produced by foaming glass particles (0.1 μm - 100 μm, Na_2O-CaO-P_2O_5-TiO_2) with egg white and sintering with a resulting porosity of about 30 % [19]. The glass ceramics scaffolds were sterilized by gamma radiation (8 kGy). Cylinders of porous nickel-titanium were produced by self-propagating high-temperature synthesis (SHS) as described by Barrabés et al. [20] with porosities of 62 - 65 %. Because the cylinders provided were too big, they were mechanized on a lathe to match the dimension requirements. The titanium scaffolds were cleaned in ultrasonic bath in acetone, ethanol and distilled water for 5 min-

utes each and sterilized by autoclave. The dimensions of the different scaffolds were measured with a calliper (see Table 7.2). As can be observed in Figure 7.1, the cylindrical form of the scaffolds could be obtained in composite and nickel-titanium scaffolds, whereas the glass ceramic scaffolds showed irregularities in form duie to the manufacturing process.

Scaffold Type	n	Diameter [mm]	Length [mm]
PLA/glass composite	6	6.2 ± 0.1	12.5 ± 0.2
Nickel-titanium	8	6.0 ± 0.1	12.0 ± 0.1
Glass ceramic	12	5.7 ± 0.2	10.2 ± 0.7

Table 7.2: Dimensions of the scaffolds fabricated for the *in vivo* experiments.

7.3.2 *In vivo* experiments

The described surgical interventions and histological analysis were conducted by the surgical unit of the University Veterinary Hospital Rof Codina in Lugo (Spain).

7.3.2.1 Experiment animals

Six female Beagle dogs (*canis familiaris*) were enrolled for the bone chamber study. The dogs were three years old, had an average weight of 15 kg and were treated in conformity with the 'Directive for the Protection of Vertebrate Animals used for Experimental and other Scientific Purposes (86/609/EEC)' of the European Union. The *in vivo* study protocol was approved by the Regional Ethics Committee for Animal Research.

7.3.2.2 Surgical procedure

For the implantation of the bone chambers, the dogs were prepared for anaesthesia with acepromazine (Calmo Neosan, 0.01 mg/kg intramuscular) and morphine (0.5 mg/kg intramuscular). Anaesthesia was induced with propofol (Propovet, 2-4 mg/kg intravenous). Dogs were intubated to maintain the anaesthesia during the operation with isoflurane (2.5 %) and oxygen (100 %). After making an incision and spreading the the skin and subcutaneous tissue on the medial side of the proximal tibia, a hole of 11 mm diameter was drilled through both cortical surfaces. To prevent fracture of the bone, smaller diameter holes were drilled before using the 11 mm drill. The bone chamber was then threaded manually into the hole, using the insertion tool developed for this purpose. The Teflon spacer was inserted and the wound closed over the implant. To ensure the correct implantation, the implantation sites were x-rayed in the latero-lateral and posteroanterior projection. After the operations, the dogs were kept under close observation in individual

cages. They received antibiotics (cefovecin sodium), analgesics, anti-inflammatories (Meloxicam) and gastric protection (Omeprazole) as post-operative treatment.

After three month of osteointegration, the dogs received a general anaesthesia for the insertion of the scaffolds. The skin over the implant was opened, the Teflon spacer extracted and the scaffold in the internal cage inserted. To minimize the development of scar tissue by repeated opening of the tissue over the bone chamber, incisions were made parallel, moving the skin over the chamber for access. A total of 56 samples were used for implantation in the bone chambers, with 24 PLA/glass composites, 24 glass ceramic and 8 nickel-titanium (see Table 7.3).

| | Sample number | | |
| | Implantation period | | |
Scaffold Type	4 weeks	12 weeks	Total
Without mechanical stimulation			
PLA/glass composite	6	6	12
Glass ceramic	6	6	12
Nickel-titanium	6	2	8
Mechanical stimulation			
PLA/glass composite	6	6	12
Glass ceramic	6	6	12

Table 7.3: Number of different scaffold types used in implantations with and without compressive stimulation.

The samples were extracted after 4 or 12 weeks implantation, which required the general anaesthesia of the dogs. The protective cap of the implant was taken off and the sample cut out with a dental trepan burr connected to a dental drill. The samples were immediately immersed in 10 % formaldehyde for the further histological preparation.

When cyclic compressions were applied to the scaffolds weekly, the medication of the dogs had to be augmented with antibiotics of the lincosamid group to prevent infections. The wounds were cleaned with physiological serum and povidone-iodine three times daily. When the compressions were applied, the dogs were sedated with medetomidine and medicated with butorphanol as analgesic. The applied cyclic compressions consisted of 450 cycles of linear compression (triangular waveform) of 508 μm for the PLA/glass composites and 127 μm for the glass ceramics. The detection of the samples by force was only applied for the glass ceramics samples with a sensor force of 5 N. After the compression, the dogs were medicated with atipamezole to eliminate the effects of the anaesthetic.

7.3.2.3   Euthanasia

The sacrifice of the animals after the experiments was conducted by an intravenous injection of sodium pentobarbital. This substance suppresses the central nervous system and causes death in a few seconds. This method is commonly used and does not imply suffering of the animal [21].

7.3.3   Sample preparation

The extracted samples were included in glycol methacrylate as described by Donath [22]. The samples were fixated by immediate immersion in 10 % formaldehyde after extraction for two weeks. After fixation the samples were dehydrated by immersion in increasing ethanol concentrations of 70 % to 100 % for three days for each concentration. The samples were then infiltrated with glycol methacrylate (Technovit 7200) and benzoyl peroxide diluted with ethanol. For three days each, the samples were immersed in benzoyl peroxide dilutions of 30 % to 100 %. The last immersion was done in vacuum to ensure the correct intrusion of the polymer. The samples were then included in a block of Technovit 7200. Sections of 200 μm of the block were cut with a band saw and the cuts were polished down to 70 μm thickness. The samples were stained with Levai-Laczko stain and examined under light microscope (Olympus CH30) and loupe (Olympus SZX9). The samples were analysed for tissue and cells based on standard ISO 10993-6 [23].

7.3.3.1   Microscopic evaluation

The quantitative histology was performed for an average of 15 histological sections per sample. After determining the tissue types present in the samples, the bone-implant contact and new bone volume for all sections was calculated. The bone-implant contact (BIC) (%) was the ratio of histological sections displaying bone-implant contact with respect to the total number of sections (see Figure 7.2a). The amount of BIC representing the fraction of mineralized bone tissue in direct contact with the implant could not be determined, because a very low value for this parameter was observed in the histological sections. The new bone volume (NBV) (%) was the percentage of new bone tissue in the sample. The values were calculated using MicroImage 1.0, where new bone matrix was coloured violet (stereoscopic microscope)(see Figure 7.2b).
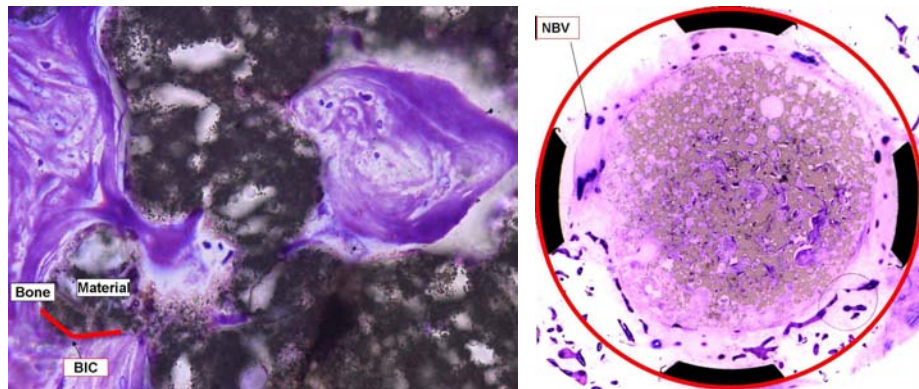
(a) The measurement of bone-implant contact (BIC) includes the detection of bone-material interfaces. Bone is stained purple with Levai-Laczko stain.

(b) New bone volume (NBV) was measured by the amount of purple stain inside the internal cage (red circle).

Figure 7.2: Illustration of the histomorphometrical measurement of BIC and NBV.

7.3.3.2   Statistical analysis

The histomorphometrical data was analysed statistically using SPSS 15.0 software. The two-way analysis of variance was chosen, followed by the Tukey's post hoc test. A p-value <0.05 was considered statistically significant.

7.4 Results

7.4.1 Surgical procedure

The surgical procedures were conducted as planned in the development of the bone chamber system. The animals did not show any alteration after the operations and no problems in anaesthesia and surgical practice were experienced. After the application of the compressions, the dogs showed signs of pain in the treated extremities. The pain was classified using the Melbourne scale for pain in dogs [24–26]. The dogs scored 6 out of 24 of the scale, which was considered a slight pain, relieved with the administration of meloxicam.

7.4.1.1 Complications

Delayed wound healing and fractures Directly after implantation of the bone chambers two types of complications were observed, insufficient wound healing and bone fractures. In 14 of 37 incisions the wound did not close properly immediately after operation. In most cases this was caused by dogs licking the wound. The wound healing was also delayed by the appearance of fibrous tissue due to the repeated opening of the implantation site. The first implant, which was realized with a bone chamber version previous to the final version provoked severe wound healing problems. The cause of the problem was most likely the large dimensions of the implant head of this version and the large Teflon area presented by the spacer. The wound healing was finally accomplished after taking out the Teflon spacer.

Two of the six dogs enrolled in this study experienced fractures around one implant after implantation, which caused the loss of two chambers. The fractures were fixated to save the dogs from early euthanasia, because both still presented working implants in the opposite tibia (see Figure 7.3).

(a) First case of fracture (left: fixation after fraction; middle and right: fracture fully healed around the implant).

(b) Second case of fracture (left: fixation after fraction; middle: the bone chamber fell out of the tibia ; right: fracture healed after fixation).

Figure 7.3: Two cases of bone fractures of dog tibia after the bone chamber implantation.

Infections One of the bone chambers with application of cyclic loading showed a severe loosening associated with suppuration and pain. A radiography of the bone chamber showed no bone remodelling around the implant (see Figure 7.4). To exclude microfractures, which might have been overseen in the radiography after implantation, a Computer Assisted Tomography scan of the chamber was conducted. The extracted chamber was examined bacteriologically, which showed an infection with *Pseudomona spp.*

Figure 7.4: Radiographs of the bone chamber affected by infection showed no bone remodelling around the external chamber.

Implant loosening After loosening and loss of one bone chamber in the compression experiments, all bone chambers were examined on loosening. It was found that 5 of the 10 bone chambers showed a slight loosening at some point, which was confirmed by radiolucent areas around the implants in radiographies, similar to the lost bone chamber.

7.4.2   Histological findings

Out of 56 samples used in this study, 32 were extracted and examined histologically. The implantation of samples with cyclical loading was not conducted further, because it was suspected that the further use might lead to an implant loosening. All samples presented ingrown tissue, whereas directly at the extraction of the samples it was observed that the tissue resembled soft tissue rather than bone. Even though tissue was found in all samples, it was observed that three of 12 glass ceramic samples had pores too small to allow tissue ingrowth, resulting in areas lacking any tissue.

In 16.1 % of the histological sections, signs of infection were observed. These sections were excluded from data analysis, because of the influence on tissue formation in the bone chamber lumen. After both implantation periods, most of the samples presented newly formed tissue consisting of a mixture of newly formed bone, bone marrow and fibrous tissue (see Figures 7.5a, 7.5c and 7.5e).

The results of the histomorphometry are presented in Table 7.4. No statistically significant differences were found between samples regarding NBV and BIC. There were no statistically significant differences between different periods of time. However all materials showed an increasing trend of BIC and NBV over time.

Scaffold type	n	BIC [%]		NBV [%]	
		4 weeks	12 weeks	4 weeks	12 weeks
PLA/glass composite	12	2.5±0.2	4.2±0.7	7.3±1.1	11.4±3.1
Nickel titanium	8	3.2±0.6	4.4±0.9	6.6±2.1	11.0±2.8
Glass ceramics	12	2.1±0.4	4.0±0.8	6.0±1.3	12.0±3.1

Table 7.4: Results of histomorphometric measurements. Values represent the mean percentage (± SD).
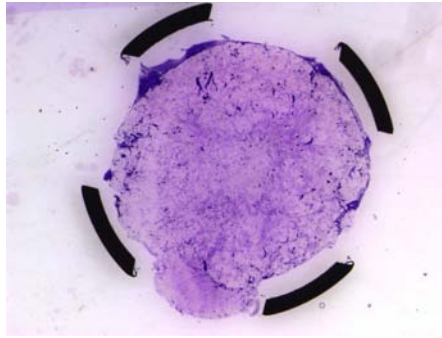
(a) Histological section of PLA/glass composite samples after 4 weeks of implantation. The material was partly absorbed and the chamber filled with fibrous tissue.
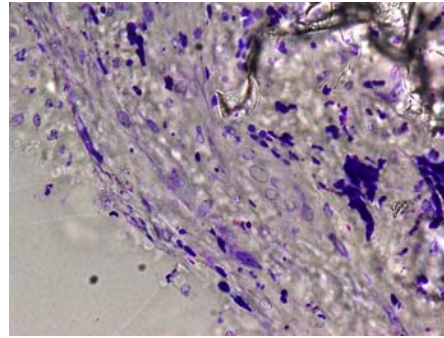
(b) Histological section of PLA/glass composite samples after 12 weeks of implantation.
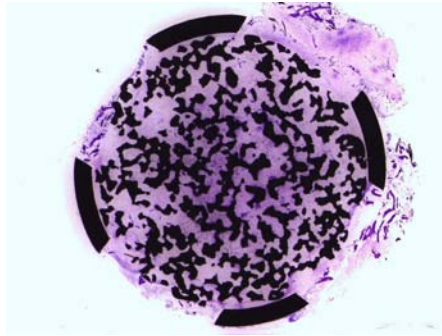
(c) Histological section of nickel-titanium sample after 4 weeks implantation.
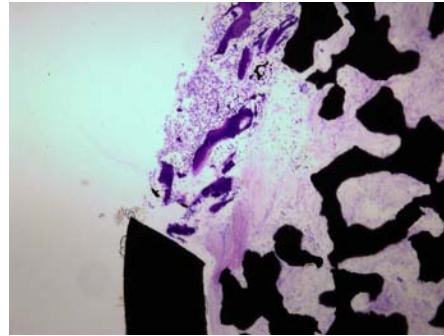
(d) Histological section of nickel-titanium sample after 4 weeks implantation. Beginning ossification in the internal cage aperture was observed, whereas the scaffold was surrounded and intruded by fibrous tissue.
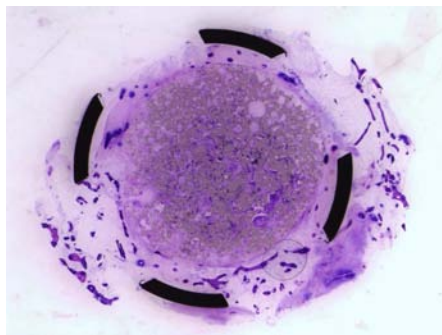
(e) Histological section of glass-ceramic sample after 12 weeks of implantation. Bone tissue can be seen on the exterior of the scaffold, which is covered in a layer of fibrous tissue.
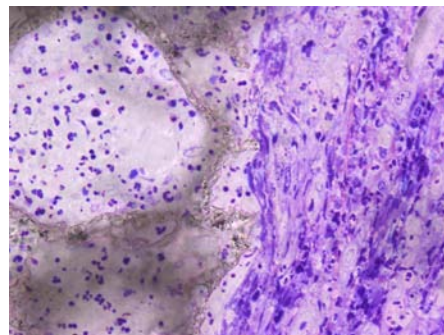
(f) Histological section of glass-ceramic sample after 12 weeks of implantation.

Figure 7.5: Histological sections of extracted samples after Levai-Laczko staining.

PLA/glass composite scaffolds were more absorbed than glass ceramic scaffolds, while the nickel-titanium scaffolds showed no signs of resorption (as expected). Bone marrow found in the samples was well organized and contained large numbers of adipocytes and blood vessels (see Figure 7.6a). Between the graft and the newly formed bone and between the bone chamber and the newly formed bone a fibrous layer was present, which consisted of a mixture of mineralized bone and immature woven bone in a fibrovascular stroma (see Figure 7.6b). Histology suggested that new bone originated from bone outside of the bone chamber. In the newly formed bone, trabeculae were lined with osteoblasts and osteocytes, extending up to the implant (see Figure 7.6b). Less bone trabeculae were observed at the implant surface for the 4 week experiments.

(a) Bone marrow found in the samples contained large numbers of adipocytes (Ad) and blood vessels ($\leftarrow$)(x100 magnification).
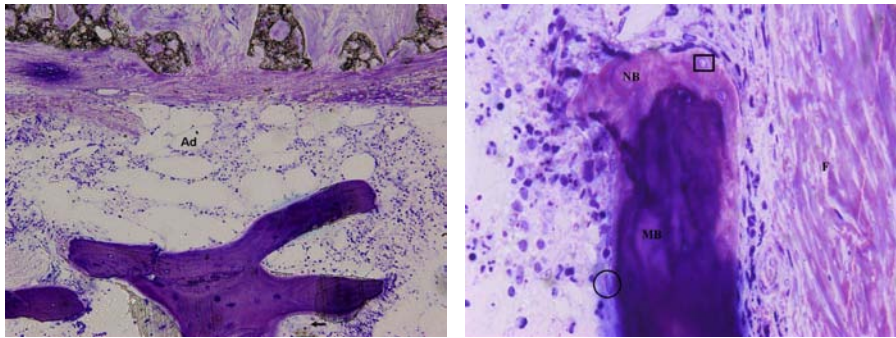
(b) Illustration of mineralized bone (MB) and immature woven bone (NB) in a fibrovascular stroma (F). Trabeculae were lined with osteoblasts ($\circ$) and osteocytes ($\square$) were found within the newly formed bone tissue and extended up to the implant (x100 magnification).

Figure 7.6: Histological sections of newly formed tissue, found in implanted samples.

7.5   Discussion

With this study it was intended to experimentally prove the function of the developed bone chamber system and to test the osteointegration of materials deemed suitable for the application in bone tissue regeneration in a repeatable *in vivo* environment. For this, bone chambers were implanted into the medial side of the proximal tibia in dogs.

The compression pattern chosen for the developed bone chamber system was in the range of comparable studies, which yielded successful enhancement of bone growth and tissue mineralization [1–8]. A weekly stimulation of 0.5 Hz and 450 cy-

cles was selected with compressions of 1 % and 5 % for glass ceramics and PLA/glass composites respectively. However, the compressed samples were not analysed at the time of this writing. The compression experiments was delayed to the end of the study when the described implant mobility was observed to prevent an influence on the implantations without compression.

The design of the bone chamber, which was based on the 6 mm diameter and 12 mm long scaffolds, made it inevitable to choose a species of appropriate proportions for the implantation in the tibia. The chosen dog animal model made it difficult to compare the study with other bone chamber studies, because of different implantation sites or different species of the experiment animal and different experimental protocols. Because the bone chamber system developed for the studies was never used before, no direct comparison to other studies could be drawn.

The surgical procedure for the bone chamber system used in this study appeared to be appropriate, showing no complications during surgery and anaesthesia. The bone chamber system needed an 11 mm diameter hole for implantation, which was considered to be a critical size defect (CSD). Comparable studies in rabbit [6] with 10 mm diameter defects were conducted successfully, which was the basis for the assumption of the possible success of this study.

One of the experienced post-surgery complications was the delayed or insufficient wound healing after implantation of the bone chambers. This was caused by the dogs licking the wounds, the repeated opening of the wound and the exposure of PTFE surfaces. It has been shown that PTFE implants can cause pronounced, persistent inflammations [27], which might have cause the severe adverse reaction. The exposition of the skin flap to the PTFE spacer over a long time period was an inadequate design choice and has to be revised in further designs to avoid the problems in wound healing. In this sense, the bone chamber might be left empty during the osteointegration phase, which then has to be freed of ingrown tissue before the insertion of the first scaffold.

Another complication of the experiments were the occurrence of fractures due to the large defects created in the tibia. The remaining bone left by the large dimensions of the bone chamber was in two cases not enough to support the weight of the dogs. The diameter of the bone chamber was determined by the scaffold dimensions and the trepan available for the sample extraction. Exchanging the trepan for a thin walled cutting device could make the bone chamber diameter smaller and hence safer.

The third complication encountered were infections on the implant site. The most frequent symptom for an infection in traumatologic implants is the loss of the implant [28]. In the occurring case, the lost bone chamber was examined for bacteria and *Pseudomona spp* was identified as source of the infection. *Pseudomona spp*

is a resistant gram negative bacteria, which is considered to be highly pathogenic and can be found amongst others in the hospital environment and is resistant to antibiotics and antiseptics. Even a thorough medication and cleaning of the implantation site cannot guarantee a prevention of an infection. It can be excluded that the infection found was caused by the implantation or the implant itself, because symptoms arouse for the first time after the application of the cyclic compressions. It was suggested that the space between actuator connector and piston was open to allow influx of air, which might have been the way of infection. For a further design of the compression device and the chamber, it would be desirable to have a implantable chamber, totally closed off to the surrounding. Without any doubt, a severe change in the design might lead to a limitation in types of scaffolds usable and the programmability of the device. Such limitations call for a very well defined catalogue of design requirements for the device before development which cannot be changed easily in the subsequent realisation of the system.

At the beginning of the compression phase of the experiments the observed implant loosening occurred. It was suggested that the loosening was effected by the mechanical stress of the compression, because the bone chambers were mechanically fixed in the implantation site, rather then really integrated in the bone. The mobility of the implanted bone chambers indicated that the chambers were integrated by fibrous integration or fibro-osteointegration [29, 30] rather than by osteointegration. The non-bony integration of the bone chamber might be caused by the size of the bone defect produced, letting the defect fill up with fibrous tissue because of the limited amount of cells for bone regeneration in the surrounding area. The bone chamber integration might also have been affected by the compression device or by the compression itself. The weight of the device could have caused microfracture during the connection, which led finally to the loosening. The compression device was not fixated sufficiently to assure a stress-free application against the dog's leg. When moving the piston, the stepper motor imposed an impulse to the whole device, which certainly was transmitted to the connected bone chamber. Even though the amplitude of the impulses is not known, the amount of impulses per cyclic compression session is suspected to be sufficient to provoke an implant loosening by step-by-step fraction of the bone-implant connection. In the case of PLA/glass composites, the bone chamber received 18.000 impulses per session, the glass ceramics received 4.500 impulses.

Without any doubt, a series of studies could be undertaken, trying to optimize the bone chamber surface for the osteointegration. It has been reported that nickel-titanium materials can be bioinert, causing a delayed healing time until reaching osteointegration and formation of a fibrous capsule around the implant [31–33]. A treatment of the titanium surface by coating with hydroxyapatite or collagen can

enhance the integration in bone significantly [34, 35]. Even though such a treatment has to be tested in *in vivo* experiments to ensure the suitability for the used animal model, a surface treatment should be considered for a further bone chamber re-design.

The materials chosen for the bone chamber and scaffolds were deemed applicable for the implantation, based on the *in vivo* behaviour of comparable materials (nickel-titanium [36, 37] and calcium phosphate glass ceramics [38]) and their *in vitro* biocompatibility (PLA/glass composite [39–42]). Additionally the total duration of 12 weeks for implantations with and without compressive loading should have permitted a sufficient amount of newly formed bone. The histology of the extracted samples showed tissue ingrowth into the bone chambers. The tissue was a combination of newly formed bone, bone marrow and fibrous tissue. There was no significant difference in new bone volume and bone-implant contact found between different materials and implantation times. The found tissue indicated that new bone formation in the scaffolds was beginning, but the presence of not absorbed PLA/glass composite and glass ceramic material, as well as the nickel-titanium scaffolds, affected the velocity and structure of ingrowing tissue and bone formation.

Analogue to the experienced problems in wound healing caused by the present PTFE surface, it can be considered that the apertures of the bone chamber were closed by fibrous tissue as an initial reaction to the spacer. The fibrous tissue was hence the first tissue to intrude the scaffolds and delayed the appearance of bone tissue.

As has been shown by the results, the bone chamber system did not work sufficiently to allow conclusions about the osteoinductive or osteoconductive properties of the implanted scaffolds. Further revision of the design is necessary to achieve a better integration of the external chamber and ingrowth of bone tissue.

7.6 Conclusions

- The evaluation of the reusable bone chamber system in beagle dog tibia has been conducted. Several complications were encountered including problems in wound healing, fractures, infections and implant loosening.

- Histological analysis of the implanted samples without loading after 4 and 12 weeks showed tissue ingrowth, composed of newly formed bone, bone marrow and fibrous tissue into the bone chambers. The new bone volume (NBV) and bone-implant contact (BIC) were not significantly different between the different scaffold materials and implantation times. The present tissue indicated a favourable environment for bone formation, but the bone formation seemed to be delayed by material left in the chambers.

- In the current configuration the compression device of the bone chamber system cannot be used for the *in vivo* loading of scaffolds. As suggested by the experimental data, the application of the device might cause loosening of the bone chambers by impacts of the stepper motor moving or infection of the bone chambers due to the design of the actuator connector assembly.

- The implantation of the bone chambers did cause unpredictable complications and could not provide the desired results reliably. Nevertheless did the study provide an insight into the problems of the current bone chamber design. A redesign of the bone chamber system and the surgical protocol are crucial for further experiments, to ensure better clinical results.

Bibliography

[1] A. O. Duty, M. E. Oest, and R. E. Guldberg. Cyclic mechanical compression increases mineralization of cell-seeded polymer scaffolds in vivo. *J Biomech Eng*, 129:531–539, Aug 2007.

[2] R.E. Guldberg, N.J. Caldwell, X.E. Guo, R.W. Goulet, S.J. Hollister, and S.A. Goldstein. Mechanical stimulation of tissue repair in the hydraulic bone chamber. *J Bone Miner Res*, 12(8):1295–1302, 1997.

[3] M.R. Moalli, N.J. Caldwell, P.V. Patil, and S.A. Goldstein. An in vivo model for investigations of mechanical signal transduction in trabecular bone. *J Bone Miner Res*, 15(7):1346–1353, 2000.

[4] N. M. Lamerigts, P. Buma, R. Huiskes, W. Schreurs, J. Gardeniers, and T. J. Slooff. Incorporation of morsellized bone graft under controlled loading conditions. A new animal model in the goat. *Biomaterials*, 21:741–747, Apr 2000.

[5] S. van der Donk, P. Buma, N. Verdonschot, and B. W. Schreurs. Effect of load on the early incorporation of impacted morsellized allografts. *Biomaterials*, 23:297–303, Jan 2002.

[6] J. Duyck, M. D. Cooman, R. Puers, H. Van Oosterwyck, J. V. Sloten, and I. Naert. A repeated sampling bone chamber methodology for the evaluation of tissue differentiation and bone adaptation around titanium implants under controlled mechanical conditions. *J Biomech*, 37:1819–1822, Dec 2004.

[7] M. C. van der Meulen, X. Yang, T. G. Morgan, and M. P. Bostrom. The effects of loading on cancellous bone in the rabbit. *Clin Orthop Relat Res*, 467:2000–2006, Aug 2009.

[8] M. Tägil, J. Åstrand, L. Westman, and P. Aspenberg. Alendronate prevents collapse in mechanically loaded osteochondral grafts. *Acta Orthop Scand*, 75(6):756–761, 2004.

[9] C. T. Rubin and L. E. Lanyon. Limb mechanics as a function of speed and gait: a study of functional strains in the radius and tibia of horse and dog. *J Exp Biol*, 101:187–211, Dec 1982.

[10] S. P. Fritton, K. J. McLeod, and C. T. Rubin. Quantifying the strain history of bone: spatial uniformity and self-similarity of low-magnitude strains. *J Biomech*, 33:317–325, Mar 2000.

[11] *Bone mechanics handbook*, chapter In vivo measurement of bone deformations using strain gauges, pages 8–10ff. Boca Raton, FL: CRC Press,, 2001.

[12] J. You, C. E. Yellowley, H. J. Donahue, Y. Zhang, Q. Chen, and C. R. Jacobs. Substrate deformation levels associated with routine physical activity are less stimulatory to bone cells relative to loading-induced oscillatory fluid flow. *J Biomech Eng*, 122:387–393, Aug 2000.

[13] E. H. Burger, J. Klein-Nulend, and J. P. Veldhuijzen. Mechanical stress and osteogenesis in vitro. *J Bone Miner Res*, 7 Suppl 2:397–401, Dec 1992.

[14] S. M. Tanaka. A new mechanical stimulator for cultured bone cells using piezoelectric actuator. *J Biomech*, 32(4):427–430, 1999.

[15] A. I. Pearce, R. G. Richards, S. Milz, E. Schneider, and S. G. Pearce. Animal models for implant biomaterial research in bone: a review. *Eur Cell Mater*, 13:1–10, 2007.

[16] J. Aerssens, S. Boonen, G. Lowet, and J. Dequeker. Interspecies differences in bone composition, density, and quality: potential implications for in vivo bone research. *Endocrinology*, 139:663–670, Feb 1998.

[17] J. C. Reichert, S. Saifzadeh, M. E. Wullschleger, D. R. Epari, M. A. Schütz, G. N. Duda, H. Schell, M. van Griensven, H. Redl, and D. W. Hutmacher. The challenge of establishing preclinical models for segmental bone defect research. *Biomaterials*, 30:2149–2163, Apr 2009.

[18] M. A. Liebschner. Biomechanical considerations of animal models used in tissue engineering of bone. *Biomaterials*, 25:1697–1714, Apr 2004.

[19] G. Àvila, S. Martínez, S. del Valle, M. P. Ginebra, J. A. Planell, and X. Alcobé. Study of porous glass ceramic made by foaming egg white. In *Proceedings of the international conference on porous ceramic materials*, 2005. Belgium.

[20] M. Barrabés, A. Michiardi, C. Aparicio, P. Sevilla, J. A. Planell, and F. J. Gil. Oxidized nickel-titanium foams for bone reconstructions: chemical and mechanical characterization. *J Mater Sci: Mater Med*, 18:2123–2129, 2007.

[21] J. Donovan and P. Brown. Euthanasia. *Curr Protoc Immunol*, Chapter 1:Unit 1.8, Jul 2006.

[22] K. Donath. *Preparation of histologic sections*. Norderstedt: EXAKT-Kulzer Publication, 1995.

[23] International Organization of Standardization. *ISO 10993-6, Biological evaluation of medical devices – Part 6: Tests for local effects after implantation*, 2007.

[24] A. M. Firth and S. L. Haldane. Development of a scale to evaluate postoperative pain in dogs. *J Am Vet Med Assoc*, 214:651–659, Mar 1999.

[25] P. Hellyer. *Handbook of veterinary pain management*, chapter Objective categoric methods for assessing pain and analgesia, pages 82–107. Mosby, St Louis, 2002.

[26] B. D. Hansen. Assessment of pain in dogs: veterinary clinical studies. *ILAR J*, 44:197–205, 2003.

[27] A. Rosengren, B. R. Johansson, N. Danielsen, P. Thomsen, and L. E. Ericson. Immunohistochemical studies on the distribution of albumin, fibrinogen, fibronectin, IgG and collagen around PTFE and titanium implants. *Biomaterials*, 17:1779–1786, Sep 1996.

[28] A. D. Pye, D. E. Lockhart, M. P. Dawson, C. A. Murray, and A. J. Smith. A review of dental implants and infection. *J Hosp Infect*, 72:104–110, Jun 2009.

[29] W. E. Roberts. Bone tissue interface. *J Dent Educ*, 52:804–809, Dec 1988.

[30] P. Schaffner, J. Meyer, M. Dard, R. Wenz, B. Nies, S. Verrier, H. Kessler, and M. Kantlehner. Induced tissue integration of bone implants by coating with bone selective RGD-peptides in vitro and in vivo studies. *J Mater Sci Mater Med*, 10:837–839, Dec 1999.

[31] S. Nishiguchi, T. Nakamura, M. Kobayashi, H. M. Kim, F. Miyaji, and T. Kokubo. The effect of heat treatment on bone-bonding ability of alkali-treated titanium. *Biomaterials*, 20:491–500, Mar 1999.

[32] J. B. Nebe, L. Müller, F. Lüthen, A. Ewald, C. Bergemann, E. Conforto, and F. A. Müller. Osteoblast response to biomimetically altered titanium surfaces. *Acta Biomater*, 4:1985–1995, Nov 2008.

[33] W. Ma, J. H. Wei, Y. Z. Li, X. M. Wang, H. Y. Shi, S. Tsutsumi, and D. H. Li. Histological evaluation and surface componential analysis of modified micro-arc oxidation-treated titanium implants. *J Biomed Mater Res Part B Appl Biomater*, 86:162–169, Jul 2008.

[34] R. S. Faeda, H. S. Tavares, R. Sartori, A. C. Guastaldi, and E. Marcantonio. Biological performance of chemical hydroxyapatite coating associated with implant surface modification by laser beam: biomechanical study in rabbit tibias. *J Oral Maxillofac Surg*, 67:1706–1715, Aug 2009.

[35] B. Stadlinger, S. Bierbaum, S. Grimmer, M. C. Schulz, E. Kuhlisch, D. Scharnweber, U. Eckelt, and R. Mai. Increased bone formation around coated implants. *J Clin Periodontol*, 36:698–704, Aug 2009.

[36] G. S. Leventhal. Titanium, a metal for surgery. *J Bone Joint Surg Am*, 33-A:473–474, Apr 1951.

[37] D. F. Williams. Titanium: epitome of biocompatibility or cause for concern. *J Bone Joint Surg Br*, 76:348–349, May 1994.

[38] A. S. Monem, H. A. ElBatal, E. M. Khalil, M. A. Azooz, and Y. M. Hamdy. In vivo behavior of bioactive phosphate glass-ceramics from the system P2O5-Na2O-CaO containing TiO2. *J Mater Sci Mater Med*, 19:1097–1108, Mar 2008.

[39] M. Charles-Harris, M. A. Koch, M. Navarro, D. Lacroix, E. Engel, and J. A. Planell. A PLA/calcium phosphate degradable composite material for bone tissue engineering: an in vitro study. *J Mater Sci Mater Med*, 19:1503–1513, Apr 2008.

[40] M. Navarro, E. Engel, J. A. Planell, I. Amaral, M. Barbosa, and M. P. Ginebra. Surface characterization and cell response of a PLA/CaP glass biodegradable composite material. *J Biomed Mater Res A*, 85:477–486, May 2008.

[41] M. Navarro, M. P. Ginebra, J. A. Planell, C. C. Barrias, and M. A. Barbosa. In vitro degradation behavior of a novel bioresorbable composite material based on PLA and a soluble CaP glass. *Acta Biomater*, 1:411–419, Jul 2005.

[42] M. Navarro, S. del Valle, S. Martínez, S. Zeppetelli, L. Ambrosio, J. A. Planell, and M. A. Ginebra. New macroporous calcium phosphate glass ceramic for guided bone regeneration. *Biomaterials*, 25:4233–4241, 2004.
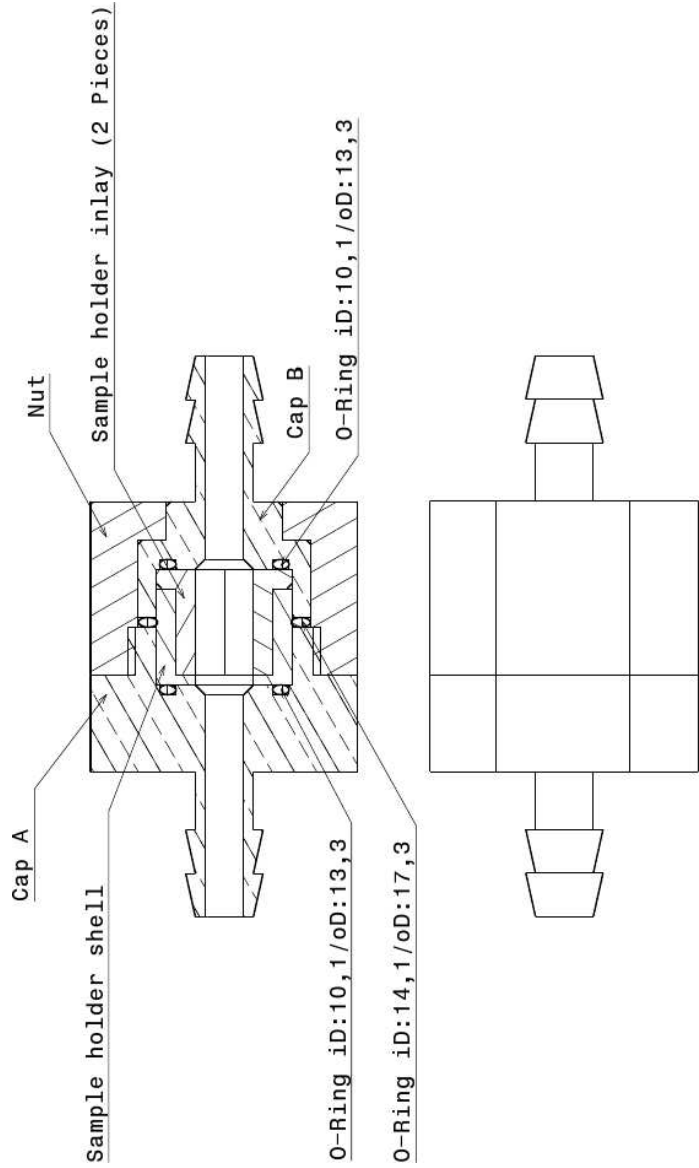
Chapter 8

Conclusions

- For the cell seeding and culture on large porous scaffolds for bone tissue engineering, an *in vitro* perfusion bioreactor system was developed. Studies for the determination of appropriate cell seeding parameters were conducted, as well as long term cell culture experiments under steady fluid flow with stimulation by oscillating fluid flow. The studies have shown that it was possible to seed cells throughout large porous scaffolds, which is deemed a crucial step for the further cell culture. The results with osteoblast-like cells suggested that an increasing fluid flow velocity improved cell distribution on the interior of the scaffolds, while an increase in cycle number of the oscillatory perfusion enhanced the uniformity between samples. The bioreactor system provided a viable environment for long term cell culture of mesenchymal stem cells. Cells proliferated up to two weeks in an exponential manner, followed by a severe decrease at three weeks, which was attributed to the beginning of cell differentiation and limitation of cell population size by the nutrient transport. The cell differentiation analysis conducted showed cell activity, but the differentiation into the osteoblast cell line could not be observed due to inconclusive test results. Further detailed studies are necessary to observe the reaction of the cells on the perfusion profile. For future experiments, the developed perfusion bioreactor system can be used with different scaffold materials, to provide different structures for cell culture. Additionally different stimulation patterns can be applied to find the ideal parameters for cell differentiation into bone forming cells. Further development of the system, including application of sensors, might give a more detailed view on cell activity in real-time.

- For the testing of large porous scaffolds *in vivo*, a bone chamber system was developed. The system allowed the repeated implantation of large porous

scaffolds of different material compositions in a large bone defect in dog tibia. The ingrowing tissue was observed to allow conclusions about the osteoconductive or osteinductive properties of the scaffold materials. Additionally a compression device was developed to apply cyclic loading on the scaffolds *in vivo* to study the effect of mechanical stimulation on tissue development. The functionality of the bone chamber system was evaluated by implantation. Histology showed that the chambers were integrated into the bone by fibro-osteointegration, causing the loosening of the chambers during the application of loads. This made the *in vivo* mechanical compressive stimulation of the samples impossible. After 4 and 12 weeks newly found tissue was found in all samples, indicating an ongoing formation of bone. A delay of bone ingrowth was attriuted to the created bone defect size and the formation of a predominantly fibrous layer.Even though the experienced complications did not allow final conclusions about scaffold material properties, the study provided input for further development of the device and clinical protocol.

- The presented studies constituted a novelty in the field of bone tissue engineering, regarding the creation of bioreactors for the study of large porous scaffolds *in vitro* and *in vivo*. The developed systems established the basis for further studies in mechanobiology of cells and tissues, including the use of scaffolds produced by Rapid Prototyping. The results of the cell culture on well-defined structures can be complemented by numerical simulation, which constitutes an promising approach in modern tissue engineering.

- For the future more long term cell culture experiments have to be conducted in the perfusion bioreactor system under a range of perfusion profiles to determine the ideal culture conditions. A focus has to be laid on cell differentiation and restructuring of the engineered tissue. Furthermore it would be interesting to establish conditions under which the engineered tissue becomes stable over a long term, representing an *in vitro* model of bone tissue, which can be used for e.g. drug testing. For the developed *in vivo* bone chamber system a redesign must be conducted to minimise the caused defect in the experiment animal bone. The compression device has to be changed to incorporate a coupling system, which minimises the risk of infection during loading. With only a few changes the compression device might be used for *in vitro* mechanical stimulation of cells in scaffolds or for measurement of mechanical properties of engineered tissue.
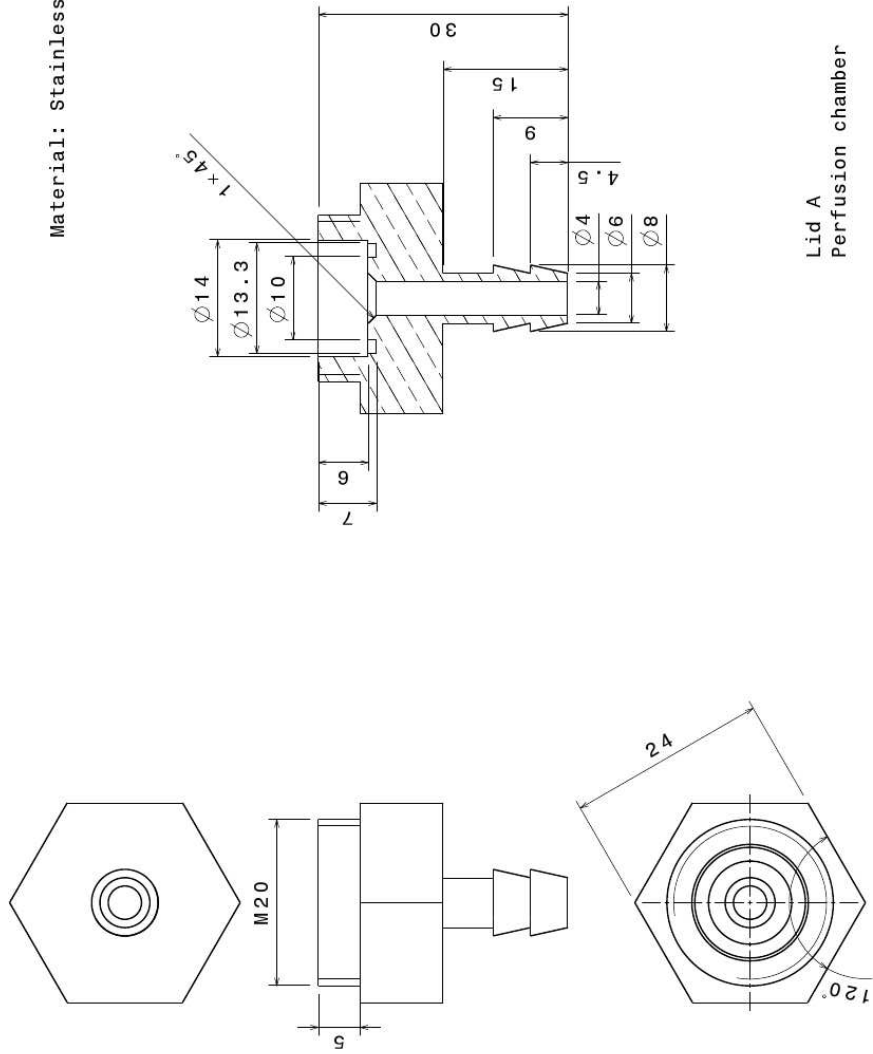
Appendix A

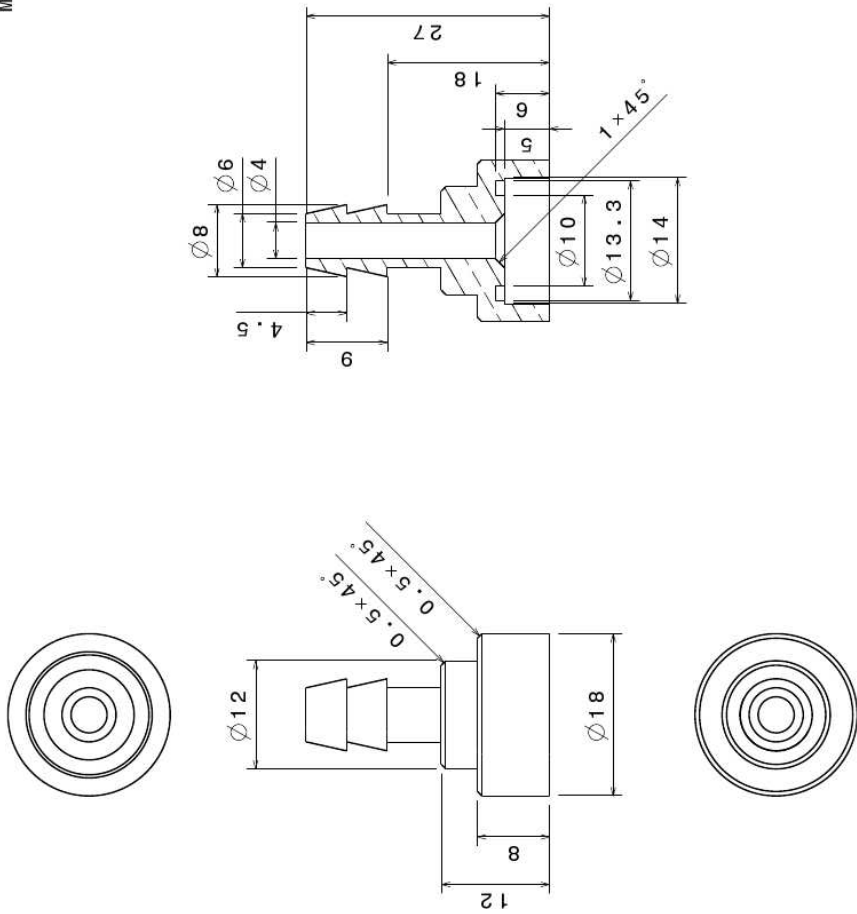# Technical Drawings of the Perfusion Bioreactor Chamber

Nut

Sample holder inlay (2 Pieces)

Cap B

O-Ring iD:10,1/oD:13,3

Cap A

Sample holder shell

O-Ring iD:10,1/oD:13,3

O-Ring iD:14,1/oD:17,3

Perfusion chamber

Material: Stainless steel

Lid A
Perfusion chamber
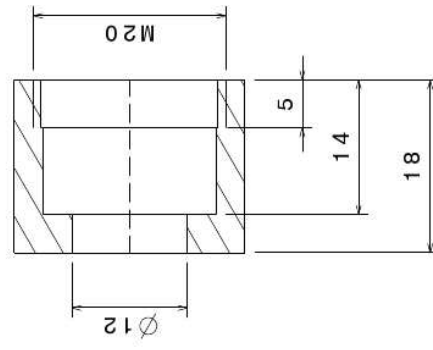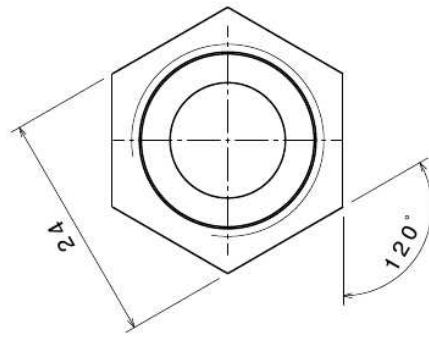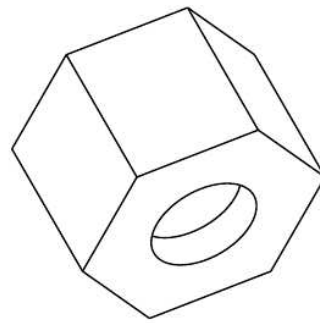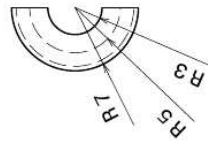
30

15

9

4.5

1×45°

Ø14
Ø13.3
Ø10

Ø4
Ø6
Ø8
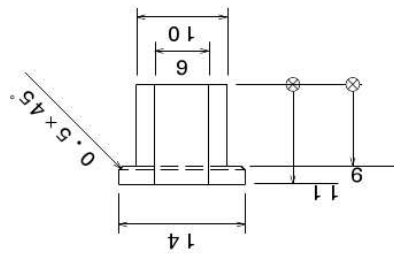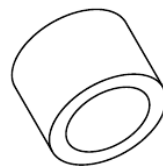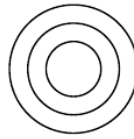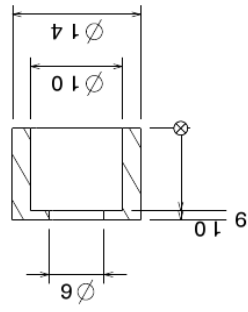
6

7

M20

5

24

120°

Material: Stainless steel

Lid B
Perfusion chamber

M20

5

14

18

⌀12

Nut
Perfusion chamber

24

120°

Material: Stainless steel

Sample holder inlay

Material: PTFE

R7

R5

R3

10

9

14

11

6

0.5×45°

$\varnothing 14$

$\varnothing 10$

$\varnothing 6$

10

6

Sample holder shell
Perfusion chamber

Material: Stainless steel

Appendix B

Source Code for Volume Transport Validation

```
CLS

PRINT
PRINT "*********************************************"
PRINT "*                                           *"
PRINT "*      2.25 ml Volume Transport Control      *"
PRINT "*                                           *"
PRINT "*********************************************"
PRINT
PRINT
PRINT
PRINT
PRINT
PRINT
PRINT
PRINT
PRINT
PRINT
PRINT
PRINT
PRINT "   Press:"
PRINT , "<x> to cancel or"
PRINT , "<any key> to proceed..."
DO
char$ = INKEY$
LOOP UNTIL char$ <> ""
SELECT CASE char$
CASE "x"
END
END SELECT
```

```
'*********************** Constants *************************
vol = 2.25      'moved Volume in ml
pi = ATN(1) * 4
'*********************** Input values *********************
200
CLS
GOSUB header
PRINT
PRINT "Please calibrate the pump before going on..."
PRINT
PRINT
PRINT "Set pump to Flow pressing <MODE> and push the <^> button to maximum."
INPUT "max. Fluid flow of the pump [ml/min]*: ", Qmax
'input of max. Flow [ml/min]
PRINT
INPUT "...Fluid Flow Velocity [mm/s]: ", v
IF Qmax = 0 THEN GOTO 200
IF v = 0 THEN GOTO 200
PRINT
A = pi * 3 ^ 2            'scaffold area [mm^2]
Q = A * v                 'Flow [mm^3/s]
Q = 60 * Q / 1000         'Flow [ml/min]
Qproz = Q / Qmax * 100    ' input of max. Flow [%]
t = vol / Q * 60               'time half-cycle [s]
t1 = INT(t * 100 + .5)         'rounded time
t = t1 / 100
PRINT
PRINT "Calculating..."
'*********************** convert Q to IPC signal *********
y! = INT(Qproz * 10 ^ 1 + .5)
speed$ = STR$(y!)
'conversion to Pump signals (i.e. 1S00100 for 10%)
speed$ = LTRIM$(speed$)

IF y! < 10 THEN GOTO 111
IF y! < 100 THEN GOTO 112
IF y! < 1000 THEN GOTO 113
IF y! < 10000 THEN GOTO 114
111
speed$ = "1S0000" + speed$
GOTO 115
112
speed$ = "1S000" + speed$
GOTO 115
113
speed$ = "1S00" + speed$
GOTO 115
114
speed$ = "1S0" + speed$
GOTO 115
```

```
115
PRINT "Done!"
PRINT
300
PRINT
PRINT "SUMMARY"
PRINT "-------"
PRINT "Fluid Flow velocity [mm/s]: "; v
PRINT
PRINT "Fluid Flow [ml/min]: "; Q
PRINT
PRINT "Flow [%]: "; Qproz
PRINT
PRINT "IPC signal: "; speed$
PRINT
PRINT "Duration [s]: "; t
PRINT
PRINT
PRINT "OPTIONS:"
PRINT , "<x> to cancel or"
PRINT , "<any key> to start pump."
DO
char$ = INKEY$
LOOP UNTIL char$ <> ""
SELECT CASE char$
CASE "x"
END
END SELECT
'*********************** Initiation ************************
OPEN "COM2:9600,n,8,1,CS,DS,RS" FOR RANDOM AS #1
'*********************** WARNING ************************
CLS
GOSUB header
PRINT
PRINT
PRINT "Writing to IPC"
PRINT
TIMER ON
Start = TIMER
PRINT TIME$, TIMER, "*** Wait .5s ***"
Start = Start + .5
IF Start >= 86399.99 THEN GOSUB tmchg
DO
LOOP UNTIL TIMER >= Start
PRINT TIME$, TIMER, "*** Set Pump to 0 ***"
PRINT #1, "1S00000"
PRINT TIME$, TIMER, "*** Wait .5s ***"
Start = Start + .5
IF Start >= 86399.99 THEN GOSUB tmchg
DO
LOOP UNTIL TIMER >= Start
```

```
PRINT TIME$, TIMER, "*** Set pump counter-clockwise ***"
PRINT #1, "1K"
PRINT TIME$, TIMER, "*** Wait .5s ***"
Start = Start + .5
IF Start >= 86399.99 THEN GOSUB tmchg
DO
LOOP UNTIL TIMER >= Start
PRINT TIME$, TIMER, "*** Start Pump ***"
PRINT #1, "1H"
PRINT TIME$, TIMER, "*** Wait .5s ***"
Start = Start + .5
IF Start >= 86399.99 THEN GOSUB tmchg
DO
LOOP UNTIL TIMER >= Start
PRINT TIME$, TIMER, "*** Set Pump to "; Qproz; "% ***"
PRINT #1, speed$
PRINT TIME$, TIMER, "*** Wait "; t; "s ***"
Start = Start + t
IF Start >= 86399.99 THEN GOSUB tmchg
DO
LOOP UNTIL TIMER >= Start
PRINT TIME$, TIMER, "*** Stop Pump ***"
PRINT #1, "1I"
TIMER OFF
CLOSE #1
PRINT
PRINT "DONE!"
PRINT
PRINT "OPTIONS:"
PRINT , "<a> Enter new velocity."
PRINT , "<b> Same velocity."
PRINT , "<x> End program."
DO
char$ = INKEY$
LOOP UNTIL char$ <> ""
SELECT CASE char$
CASE "x"
END
CASE "a"
GOTO 200
CASE "b"
GOTO 300
END SELECT
END
'*** Header Graphic ***
header:
PRINT "*********************************************"
PRINT "*                                           *"
PRINT "*      2.25 ml Volume Transport Control      *"
PRINT "*                                           *"
PRINT "*********************************************"
```

```
RETURN
'*********** day changes ********
tmchg:
Start = Start - 86399.99
DO
LOOP UNTIL TIMER <= 10
RETURN
```

254

Appendix C

Source Code for Cell Seeding in the Perfusion Bioreactor System

```
CLS
PRINT
PRINT
PRINT
PRINT
PRINT "                                          _/_/_/          _/  _/    "
PRINT "     _/_/_/    _/_/_/  _/  _/_/        _/          _/_/  _/ _/     "
PRINT "    _/_/    _/    _/  _/_/            _/          _/_/_/_/ _/ _/      "
PRINT "     _/_/  _/    _/  _/              _/          _/        _/ _/       "
PRINT "  _/_/_/      _/_/_/  _/          _/          _/_/_/    _/_/_/  _/ _/        "
PRINT "            _/                                                      "
PRINT "           _/                                                       "
PRINT
PRINT
PRINT "      _/_/_/                      _/  _/                        "
PRINT "     _/          _/_/      _/_/      _/_/_/      _/_/_/      _/_/_/   "
PRINT "    _/_/    _/_/_/_/ _/_/_/_/ _/    _/ _/ _/    _/ _/    _/    "
PRINT "      _/  _/      _/        _/    _/ _/ _/ _/    _/ _/    _/     "
PRINT "  _/_/_/      _/_/_/    _/_/_/    _/_/_/ _/  _/    _/    _/_/_/    "
PRINT "                                                  _/     "
PRINT "                                                 _/_/      "
PRINT "    Square wave generator for ISMATEC IPC pump"
PRINT
PRINT "   Press:"
PRINT , "<x> to cancel or"
PRINT , "<any key> to proceed..."
```

```
DO
char$ = INKEY$
LOOP UNTIL char$ <> ""

SELECT CASE char$
CASE "x"
END

END SELECT


'*********************** Constants ***********************
vol = 2.25       'moved Volume in ml
pi = ATN(1) * 4
'*********************** Input values ********************
CLS
GOSUB header
PRINT
PRINT
PRINT "Input values"
PRINT "------------"
PRINT "Set pump to Flow pressing <MODE> and push the <^> button to maximum."
INPUT "max. Fluid flow of the pump [ml/min]: ", Qmax        'input of max. Flow
PRINT
INPUT "Please type in your name: ", name$
PRINT
PRINT "Fluid Flow "
PRINT "-------------"
INPUT "Fluid Flow Velocity [mm/s]: ", v
INPUT "Number of Cycles [-]: ", c
PRINT
A = pi * 3 ^ 2            'scaffold area [mm^2]
Q = A * v                'Flow [mm^3/s]
Q = 60 * Q / 1000        'Flow [ml/min]
Qproz = Q / Qmax * 100   ' input of max. Flow [%]
t = vol / Q * 60             'time half-cycle [s]
t1 = INT(t * 100 + .5)          'rounded time
t = t1 / 100
'*********************** convert Q to IPC signal *********
y! = INT(Qproz * 10 ^ 1 + .5)
speed$ = STR$(y!)
'conversion to Pump signals (i.e. 1S00100 for 10%)
speed$ = LTRIM$(speed$)
IF y! < 10 THEN GOTO 111
IF y! < 100 THEN GOTO 112
IF y! < 1000 THEN GOTO 113
IF y! < 10000 THEN GOTO 114
111
speed$ = "1S0000" + speed$
GOTO 115
112
```

```
speed$ = "1S000" + speed$
GOTO 115
113
speed$ = "1S00" + speed$
GOTO 115
114
speed$ = "1S0" + speed$
GOTO 115
115
PRINT
PRINT "OPTIONS:"
PRINT , "<x> to cancel or"
PRINT , "<any key> to proceed..."
PRINT
DO
char$ = INKEY$
LOOP UNTIL char$ <> ""
SELECT CASE char$
CASE "x"
END
END SELECT
'************************ Print Summary ********************
OPEN "Seedlog.txt" FOR OUTPUT AS #2
CLS
PRINT #2, "Name: "; name$
PRINT #2, "Date [m/d/y]: "; DATE$
PRINT #2, "Time [h:m:s]: "; TIME$
PRINT #2, "Fluid Flow velocity [mm/s]: "; v
PRINT #2, "max. Fluid Flow [ml/min]: "; Q
PRINT #2, "max. Flow [%]: "; Qproz
PRINT #2, "IPC signal: "; speed$
PRINT #2, "cycle duration [s]: "; 2 * t
PRINT #2, "Number of cycles: "; c
PRINT #2,
GOSUB header
PRINT
PRINT
PRINT "SUMMARY"
PRINT "-------"
PRINT "Name: "; name$
PRINT "Date [m/d/y]: "; DATE$
PRINT "Time [h:m:s]: "; TIME$
PRINT "Fluid Flow velocity [mm/s]: "; v
PRINT "max. Fluid Flow [ml/min]: "; Q
PRINT "max. Flow [%]: "; Qproz
PRINT "IPC signal: "; speed$
PRINT "cycle duration [s]: "; 2 * t
PRINT "Number of cycles: "; c
PRINT
PRINT
PRINT "OPTIONS:"
```

```
PRINT , "<x> to cancel or"
PRINT , "<any key> to proceed..."
DO
char$ = INKEY$
LOOP UNTIL char$ <> ""
SELECT CASE char$
CASE "x"
END
END SELECT
'*********************** Initiation ************************
OPEN "COM2:9600,n,8,1,CS,DS,RS" FOR RANDOM AS #1
'*********************** WARNING ************************
200
CLS
GOSUB header
PRINT
PRINT
PRINT "CAUTION!"
PRINT "--------"
PRINT "                                                 "
PRINT "This will start the pump process which will durate "; 2 * t * c;
" second(s)"
PRINT "Be sure that:"
PRINT
PRINT "- The pump is connected at COM2 of the computer"
PRINT "- Power supply is guaranteed over the duration of the experiment"
PRINT
PRINT "- Be sure to have two equal medium levels in the U-Tube
(at least 3,5cm over Perfusion Chambers!)"
PRINT
PRINT
PRINT "OPTIONS:"
PRINT , "<x> to cancel or"
PRINT , "<any key> to proceed..."
DO
char$ = INKEY$
LOOP UNTIL char$ <> ""
SELECT CASE char$
CASE "x"
END
END SELECT
'******************** write to IPC ************************
CLS
GOSUB header
PRINT
PRINT
PRINT "Writing to IPC"
PRINT
TIMER ON
Start = TIMER
PRINT "Time [h:m:s]", "Time [s]", "Q [%]", "Q [ml/min]", "IPC Comand"
```

```
PRINT #2, "Time [h:m:s]", "Time [s]", "Q [%]", "Q [ml/min]", "IPC Comand"
PRINT TIME$, TIMER, "*** Wait .5s ***"
Start = Start + .5
IF Start >= 86399.99 THEN GOSUB tmchg
DO
LOOP UNTIL TIMER >= Start
PRINT TIME$, TIMER, "*** Set Pump to 0 ***"
PRINT #1, "1S00000"
PRINT TIME$, TIMER, "*** Wait .5s ***"
Start = Start + .5
IF Start >= 86399.99 THEN GOSUB tmchg
DO
LOOP UNTIL TIMER >= Start
PRINT TIME$, TIMER, "*** Set pump counter-clockwise ***"
PRINT #1, "1K"
PRINT TIME$, TIMER, "*** Wait .5s ***"
Start = Start + .5
IF Start >= 86399.99 THEN GOSUB tmchg
DO
LOOP UNTIL TIMER >= Start
PRINT TIME$, TIMER, "*** Start Pump ***"
'PRINT #2, TIME$, TIMER, "*** Start Pump ***"
PRINT #1, "1H"
PRINT TIME$, TIMER, "*** Wait .5s ***"
'PRINT #2, TIME$, TIMER, "*** Wait .5s ***"
Start = Start + .5
IF Start >= 86399.99 THEN GOSUB tmchg
DO
LOOP UNTIL TIMER >= Start
PRINT TIME$, TIMER, "*** Set Pump to "; Qproz; "% ***"
PRINT #1, speed$
PRINT "Driving medium levels to start position"
'gets the levels in "start position"
PRINT TIME$, TIMER, "*** Wait "; t / 2; "s ***"
PRINT TIME$, TIMER, "-"; Qproz, "-"; Q, speed$
PRINT #2, TIME$, TIMER, "-"; Qproz, "-"; Q, speed$
Start = Start + t / 2
IF Start >= 86399.99 THEN GOSUB tmchg
DO
LOOP UNTIL TIMER >= Start
FOR k = 1 TO c
char$ = INKEY$
IF char$ = "x" THEN END
PRINT "Cycle "; k; " of "; c
PRINT #2, "Cycle "; k; " of "; c
PRINT TIME$, TIMER, "*** Set pump clockwise ***"
PRINT TIME$, TIMER, Qproz, Q, speed$
PRINT #2, TIME$, TIMER, Qproz, Q, speed$
PRINT #1, "1J"
PRINT TIME$, TIMER, "*** Wait "; t; "s ***"
Start = Start + t
```

```
IF Start >= 86399.99 THEN GOSUB tmchg
DO
LOOP UNTIL TIMER >= Start
PRINT TIME$, TIMER, "*** Set pump to counter-clockwise ***"
PRINT TIME$, TIMER, "-"; Qproz, "-"; Q, speed$
PRINT #2, TIME$, TIMER, "-"; Qproz, "-"; Q, speed$
PRINT #1, "1K"
PRINT TIME$, TIMER, "*** Wait "; t; "s ***"
Start = Start + t
IF Start >= 86399.99 THEN GOSUB tmchg
DO
LOOP UNTIL TIMER >= Start
NEXT k

PRINT TIME$, TIMER, "*** Wait .1s ***"
Start = Start + .1
IF Start >= 86399.99 THEN GOSUB tmchg
DO
LOOP UNTIL TIMER >= Start
PRINT TIME$, TIMER, "*** Stop Pump ***"
PRINT #2, TIME$, TIMER, "*** Stop Pump ***"
PRINT #1, "1I"
TIMER OFF
SOUND 440, 5
PRINT #2, "Pump cycle complete."
CLOSE #1
CLOSE #2
PRINT
PRINT
PRINT "Pump cycle complete."
PRINT
PRINT "A log file <Seedlog.txt> has been created."
PRINT
PRINT
PRINT
PRINT "Press <any key> to end program"
DO
char$ = INKEY$
LOOP UNTIL char$ <> ""
END
'*** Header Graphic ***
header:
PRINT "*********************************************"
PRINT "*                Cell Seeding               *"
PRINT "*-------------------------------------------*"
PRINT "*                                           *"
PRINT "*  Square wave generator for ISMATEC IPC pump  *"
PRINT "*                                           *"
PRINT "*********************************************"
RETURN
'*********** day changes ********
```

```
tmchg:
Start = Start - 86399.99
DO
LOOP UNTIL TIMER <= 10
RETURN
```

Appendix D

Source Code for Cell Culture in the Perfusion Bioreactor System

```
CLS
PRINT
PRINT
PRINT
PRINT
PRINT "      _/_/_/          _/  _/    "
PRINT "     _/            _/_/    _/  _/    "
PRINT "    _/          _/_/_/_/  _/  _/      "
PRINT "   _/          _/        _/  _/        "
PRINT "    _/_/_/    _/_/_/  _/  _/        "
PRINT
PRINT
PRINT "      _/_/_/          _/    _/                                    "
PRINT "     _/          _/    _/  _/  _/_/_/_/  _/    _/  _/  _/_/    _/_/    "
PRINT "    _/          _/    _/  _/  _/        _/    _/  _/_/      _/_/_/_/  "
PRINT "   _/          _/    _/  _/    _/      _/    _/  _/        _/        "
PRINT "    _/_/_/    _/_/_/  _/      _/_/    _/_/_/  _/          _/_/_/    "
PRINT
PRINT "   Culture pattern generator for ISMATEC IPC pump"
PRINT
PRINT
PRINT "   Press:"
PRINT , "<x> to cancel or"
PRINT , "<any key> to proceed..."

DO
char$ = INKEY$
```

```
LOOP UNTIL char$ <> ""
SELECT CASE char$
CASE "x"
END
END SELECT
'************************* Constants *************************
'When changing the type of pump tube you have to change
'parameters dtube and Qmax here!
dtube = 2.79     'pump tube diameter [mm]
pi = ATN(1) * 4
'************************* Input values *********************
CLS
GOSUB header
PRINT "This program is for use with 2.79 mm pump tubing!"
PRINT
PRINT "Input values"
PRINT "============"
PRINT
PRINT "Set pump to Flow pressing <MODE> and push the <^> button to maximum."
INPUT "max. Fluid flow of the pump [ml/min]: ", Qmax       'input of max. Flow
PRINT
INPUT "Please type in your name: ", name$
CLS
GOSUB header
PRINT
PRINT "Fluid Flow Pattern"
PRINT
PRINT " v1|---      ---                              ---"
PRINT "   |   |   |   |                          |   |"
PRINT " v2|   |   |   |    ------------------------   |"
PRINT "   |___|___|___|___|_____|___"
PRINT "   |   |   |   |   |                      '   |"
PRINT "   |   |   |   |   |                   24h    |"
PRINT "   |   |   |   |   |                          |  "
PRINT "-v1|    ---      ---                              ---"
PRINT
PRINT "   <-t->"
PRINT "    <----Period 1---><--------Period 2--------->"
PRINT
PRINT
PRINT "Period 1 - Alternating fluid flow"
PRINT "--------------------------------"
PRINT
INPUT "Fluid Flow Velocity v1 [mm/s]: ", v1
INPUT "Time for every direction t [s]: ", tdir
INPUT "Total time for alternating flow [min]: ", taf
PRINT
PRINT "Period 2 - Continuous fluid flow"
PRINT "-------------------------------"
PRINT
INPUT "Fluid Flow Velocity v2 [mm/s]: ", v2
```

```
PRINT
'*************** Calculating Values ********************
A = pi * 3 ^ 2              'scaffold area [mm^2]
Q1 = A * v1                 'Flow Period 1 [mm^3/s]
Q2 = A * v2                 'Flow Period 2 [mm^3/s]
Q1 = 60 * Q1 / 1000         'Flow Period 1 [ml/min]
Q2 = 60 * Q2 / 1000         'Flow Period 2 [ml/min]
Q1proz = Q1 / Qmax * 100    ' input of max. Flow Period 1 [%]
Q2proz = Q2 / Qmax * 100    ' input of max. Flow Period 2 [%]
taf = taf * 60      'Total time for alternating flow [s]
c = taf / tdir       'Get the number of cycles
c! = INT(c / 2) * 2 'Round the number of cycles
taf = c! * tdir
c = c! / 2
rday = 86400 - taf  'rest of day [s]
dday = rday / 2      'break down rest of day into 2s pieces
'************************** convert Q1 and Q2 to IPC signal **********
y! = INT(Q1proz * 10 ^ 1 + .5)
speed1$ = STR$(y!) 'conversion to Pump signals for 1st period
speed1$ = LTRIM$(speed1$)

IF y! < 10 THEN GOTO 111
IF y! < 100 THEN GOTO 112
IF y! < 1000 THEN GOTO 113
IF y! < 10000 THEN GOTO 114
111
speed1$ = "1S0000" + speed1$
GOTO 115
112
speed1$ = "1S000" + speed1$
GOTO 115
113
speed1$ = "1S00" + speed1$
GOTO 115
114
speed1$ = "1S0" + speed1$
GOTO 115
115
y! = INT(Q2proz * 10 ^ 1 + .5)
speed2$ = STR$(y!)   'conversion to Pump signal for 2nd period
speed2$ = LTRIM$(speed2$)
IF y! < 10 THEN GOTO 211
IF y! < 100 THEN GOTO 212
IF y! < 1000 THEN GOTO 213
IF y! < 10000 THEN GOTO 214
211
speed2$ = "1S0000" + speed2$
GOTO 215
212
speed2$ = "1S000" + speed2$
GOTO 215
```

```
213
speed2$ = "1S00" + speed2$
GOTO 215
214
speed2$ = "1S0" + speed2$
GOTO 215
215
PRINT
PRINT "OPTIONS:"
PRINT , "<x> to cancel or"
PRINT , "<any key> to proceed..."
PRINT
DO
char$ = INKEY$
LOOP UNTIL char$ <> ""
SELECT CASE char$
CASE "x"
END
END SELECT
'*********************** Print Summary *******************
OPEN "Cultlog.txt" FOR OUTPUT AS #2
CLS
PRINT #2, "Name: "; name$
PRINT #2, "Date [m/d/y]: "; DATE$
PRINT #2, "Time [h:m:s]: "; TIME$
PRINT #2,
PRINT #2, "Period 1 - Alternating fluid flow"
PRINT #2, "-------------------------------"
PRINT #2, "Fluid Flow Velocity [mm/s]: "; v1
PRINT #2, "IPC signal: "; speed1$
PRINT #2, "Time for every direction [s]: "; tdir
PRINT #2, "Number of cycles: "; c
PRINT #2, "Duration [min]: "; taf / 60
PRINT #2,
PRINT #2, "Period 2 - Continuous fluid flow"
PRINT #2, "-------------------------------"
PRINT #2, "Fluid Flow Velocity [mm/s]: "; v2
PRINT #2, "IPC signal: "; speed2$
PRINT #2, "Duration [h]: "; rday / 3600
PRINT #2,
PRINT #2, "-----------------------------------------"
PRINT #2,
GOSUB header
PRINT
PRINT "SUMMARY"
PRINT "-------"
PRINT "Name: "; name$
PRINT "Date [m/d/y]: "; DATE$
PRINT "Time [h:m:s]: "; TIME$
PRINT
PRINT "Period 1 - Alternating fluid flow"
```

```
PRINT "-------------------------------"
PRINT "Fluid Flow Velocity [mm/s]: "; v1
PRINT "IPC signal: "; speed1$
PRINT "Time for every direction [s]: "; tdir
PRINT "Number of cycles: "; c
PRINT "Duration [min]: "; taf / 60;
PRINT
PRINT "Period 2 - Continuous fluid flow"
PRINT "-------------------------------"
PRINT "Fluid Flow Velocity [mm/s]: "; v2
PRINT "IPC signal: "; speed2$
PRINT "Duration [h]: "; rday / 3600
PRINT
PRINT "OPTIONS:"
PRINT , "<x> to cancel or"
PRINT , "<any key> to proceed..."
DO
char$ = INKEY$
LOOP UNTIL char$ <> ""
SELECT CASE char$
CASE "x"
END
END SELECT
'************************* WARNING *************************
CLS
GOSUB header
PRINT
PRINT "We will begin the perfusion now. Please assure that:"
PRINT "- The pump is connected at COM2 of the computer"
PRINT "- Power supply is guaranteed over the duration of the experiment"
PRINT
PRINT "While running you can CANCEL the operation with the <x> key."
PRINT "The software stops after the time for one direction in period 1
or after 2s in period 2."
PRINT "PAUSE with the <p> key!"
PRINT
PRINT "Do not close the lid of the laptop, it may cause the program to go
to sleep!"
PRINT
PRINT
PRINT "OPTIONS:"
PRINT , "<x> to cancel or"
PRINT , "<any key> to proceed..."
DO
char$ = INKEY$
LOOP UNTIL char$ <> ""
SELECT CASE char$
CASE "x"
END
END SELECT
'************************* Initiation *************************
```

```
OPEN "COM2:9600,n,8,1,CS,DS,RS" FOR RANDOM AS #1
'********************* write to IPC ************************
CLS
char$ = ""
GOSUB header
PRINT
PRINT
PRINT "Writing to IPC"
PRINT
'Initiate Pump
TIMER ON
Start = TIMER
PRINT "Time [h:m:s]", "Time [s]", "Q [%]", "Q [ml/min]", "IPC Comand"
PRINT #2, "Time [h:m:s]", "Time [s]", "Q [%]", "Q [ml/min]", "IPC Comand"
PRINT TIME$, TIMER, "*** Wait .5s ***"
Start = Start + .5
IF Start >= 86399.99 THEN GOSUB tmchg
DO
LOOP UNTIL TIMER >= Start
PRINT TIME$, TIMER, "*** Set Pump to 0 ***"
PRINT #1, "1S00000"
PRINT TIME$, TIMER, "*** Wait .5s ***"
Start = Start + .5
IF Start >= 86399.99 THEN GOSUB tmchg
DO
LOOP UNTIL TIMER >= Start
PRINT TIME$, TIMER, "*** Set pump clockwise ***"
PRINT #1, "1J"
PRINT TIME$, TIMER, "*** Wait .5s ***"
Start = Start + .5
IF Start >= 86399.99 THEN GOSUB tmchg
DO
LOOP UNTIL TIMER >= Start
PRINT TIME$, TIMER, "*** Start Pump ***"
PRINT #1, "1H"
PRINT TIME$, TIMER, "*** Wait .5s ***"
Start = Start + .5
IF Start >= 86399.99 THEN GOSUB tmchg
DO
LOOP UNTIL TIMER >= Start
888
PRINT "Beginning perfusion period 1."
FOR k = 1 TO c
PRINT "Cycle Number "; k; "of"; c
PRINT TIME$, TIMER, Q1proz, Q1, speed1$
PRINT #2, TIME$, TIMER, Q1proz, Q1, speed1$
PRINT #1, "1J"
PRINT TIME$, TIMER, "*** Wait .5s ***"
Start = Start + .5
IF Start >= 86399.99 THEN GOSUB tmchg
DO
```

```
LOOP UNTIL TIMER >= Start
PRINT #1, speed1$
PRINT TIME$, TIMER, "*** Wait "; tdir-0.5; "s ***"
FOR n = 1 TO 10
char$ = INKEY$
SELECT CASE char$
CASE "x"
GOTO 999
CASE "p"
GOSUB pause
END SELECT
Start = Start + ((tdir-0.5) / 10)
IF Start >= 86399.99 THEN GOSUB tmchg
DO
LOOP UNTIL TIMER >= Start
NEXT n
char$ = INKEY$
SELECT CASE char$
CASE "x"
GOTO 999
END SELECT
PRINT TIME$, TIMER, "-"; Q1proz, "-"; Q1, speed1$
PRINT #2, TIME$, TIMER, "-"; Q1proz, "-"; Q1, speed1$
PRINT #1, "1K"
PRINT TIME$, TIMER, "*** Wait .5s ***"
Start = Start + .5
IF Start >= 86399.99 THEN GOSUB tmchg
DO
LOOP UNTIL TIMER >= Start
PRINT #1, speed1$
PRINT TIME$, TIMER, "*** Wait "; tdir-0.5; "s ***"
FOR n = 1 TO 10
char$ = INKEY$
SELECT CASE char$
CASE "x"
GOTO 999
CASE "p"
GOSUB pause
END SELECT
Start = Start + ((tdir-0.5) / 10)
IF Start >= 86399.99 THEN GOSUB tmchg
DO
LOOP UNTIL TIMER >= Start
NEXT n
NEXT k

PRINT "Beginning perfusion period 2."
PRINT TIME$, TIMER, "*** Set pump to clockwise ***"
PRINT TIME$, TIMER, Q2proz, Q2, speed2$
PRINT #2, TIME$, TIMER, Q2proz, Q2, speed2$
PRINT #1, "1J"
```

```
PRINT TIME$, TIMER, "*** Wait .5s ***"
Start = Start + .5
IF Start >= 86399.99 THEN GOSUB tmchg
DO
LOOP UNTIL TIMER >= Start
FOR k = 1 TO dday
PRINT #1, speed2$
PRINT ".";
Start = Start + 2
IF Start >= 86399.99 THEN GOSUB tmchg
DO
LOOP UNTIL TIMER >= Start
char$ = INKEY$
SELECT CASE char$
CASE "x"
GOTO 999
CASE "p"
GOSUB pause
END SELECT
NEXT k
GOTO 888
999
PRINT TIME$, TIMER, "*** Stop Pump ***"
PRINT #2, TIME$, TIMER, "*** Stop Pump ***"
PRINT #1, "1I"
TIMER OFF
CLOSE #1
CLOSE #2
PRINT
PRINT
PRINT "Software stopped."
PRINT
PRINT "A log file <Cultlog.txt> has been created."
PRINT
PRINT
PRINT
PRINT "Press <any key> to end program"
DO
char$ = INKEY$
LOOP UNTIL char$ <> ""

END

'***************** SUBROUTINES *********************
'*** Header Graphic ***
header:
PRINT "**********************************************"
PRINT "*              Cell Culture                  *"
PRINT "*    Pattern generator for ISMATEC IPC pump  *"
PRINT "**********************************************"
RETURN
```

```
'*********** day changes ********
tmchg:
Start = Start - 86399.99
DO
LOOP UNTIL TIMER <= 10
RETURN

'********** pause **************
pause:
PRINT #1, "1I" 'stop perfusion
PRINT
pt = Start - TIMER
PRINT "You are in pause mode!"
PRINT #2, TIME$, TIMER, "*** Perfusion paused ***"
PRINT
PRINT "Hit any key to proceed!"
DO
char$ = INKEY$
LOOP UNTIL char$ <> ""
Start = TIMER + pt
PRINT "Returned from Pause mode..."
PRINT #2, TIME$, TIMER, "*** Returned from pause ***"
PRINT #1, "1K" 'start perfusion again
RETURN
```

Appendix E

Technical Drawings of the Bone Chamber System
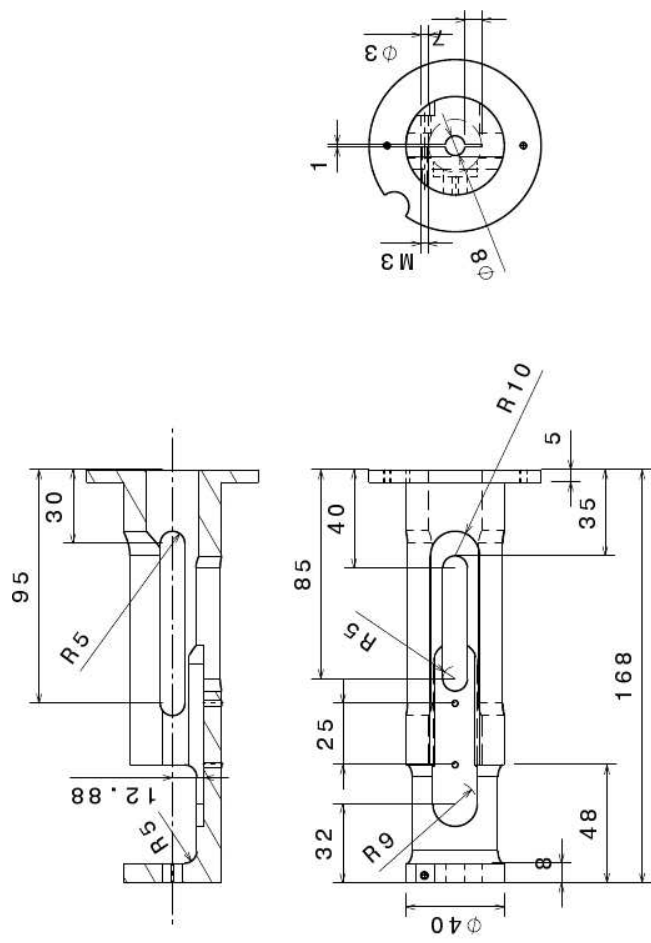
Material: Aluminium
Bone Chamber
Actuator Handle
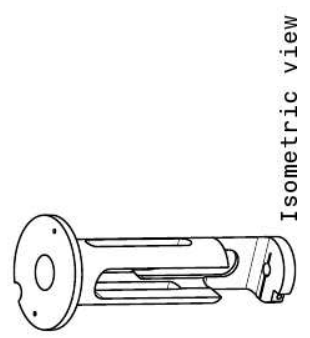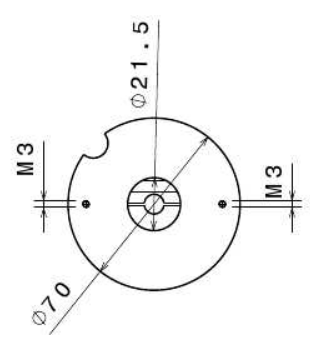
Isometric view
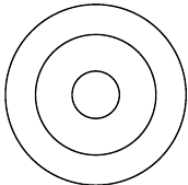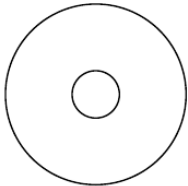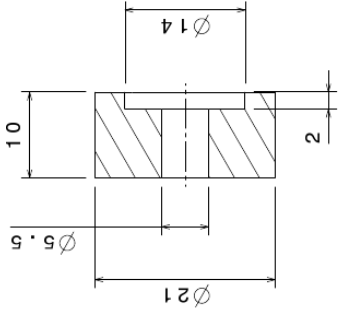
Material: Aluminium
Spring Load Spacer

∅14

10

2

∅5.5

∅21
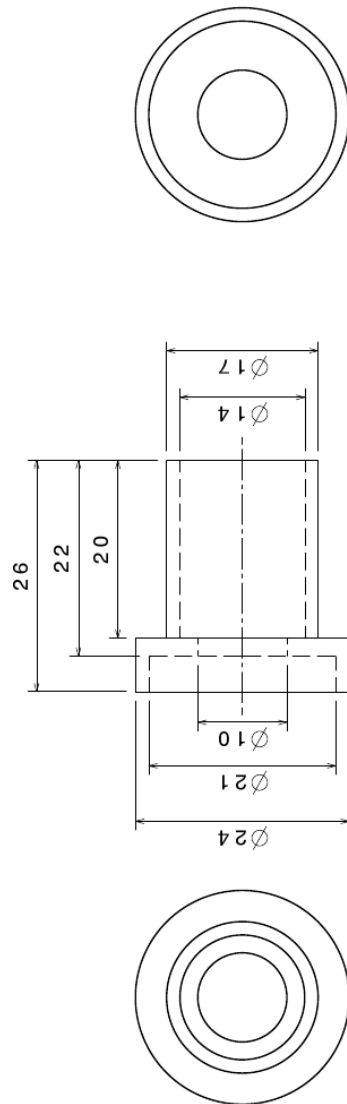
Material: Aluminium
Bone Chamber
Spring load shell 1
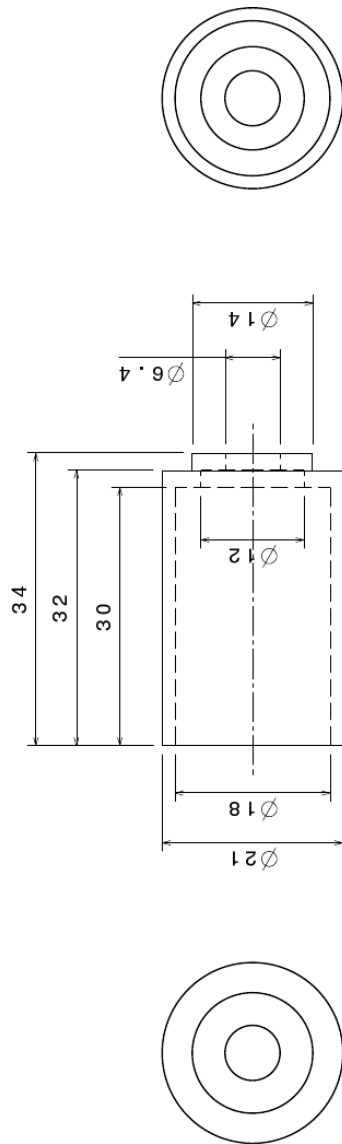
Material: Aluminium
Bone Chamber
Spring load shell 2

⌀14
⌀6.4
⌀12
⌀18
⌀21
34
32
30
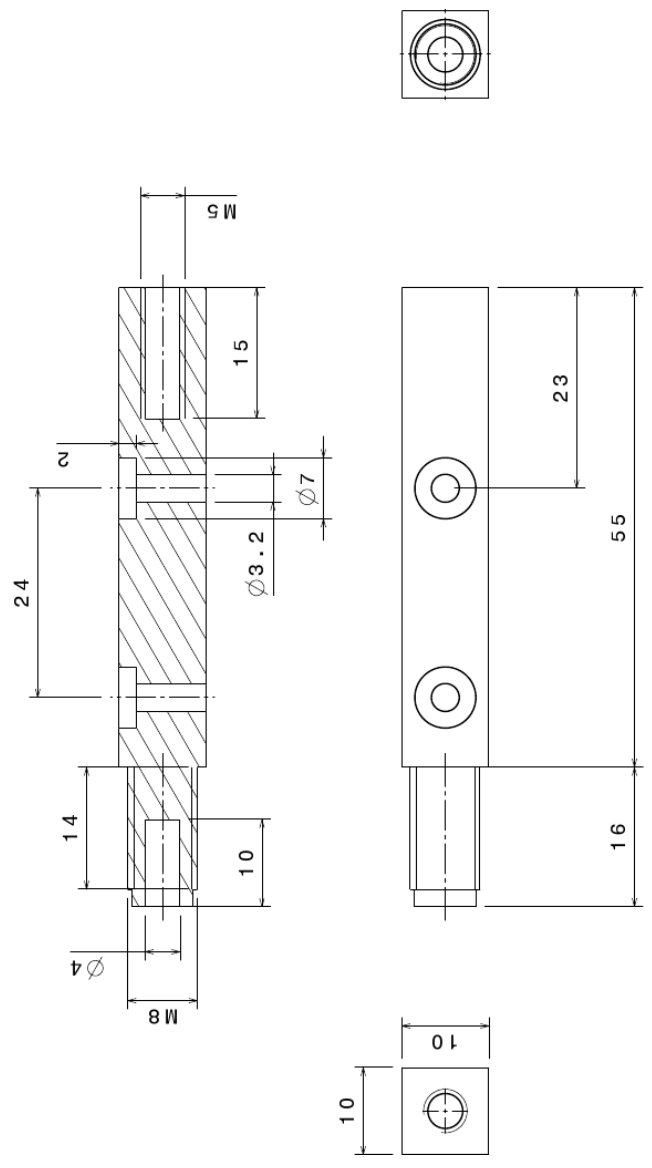
Material: Stainless steel
Bone Chamber
Connector Block
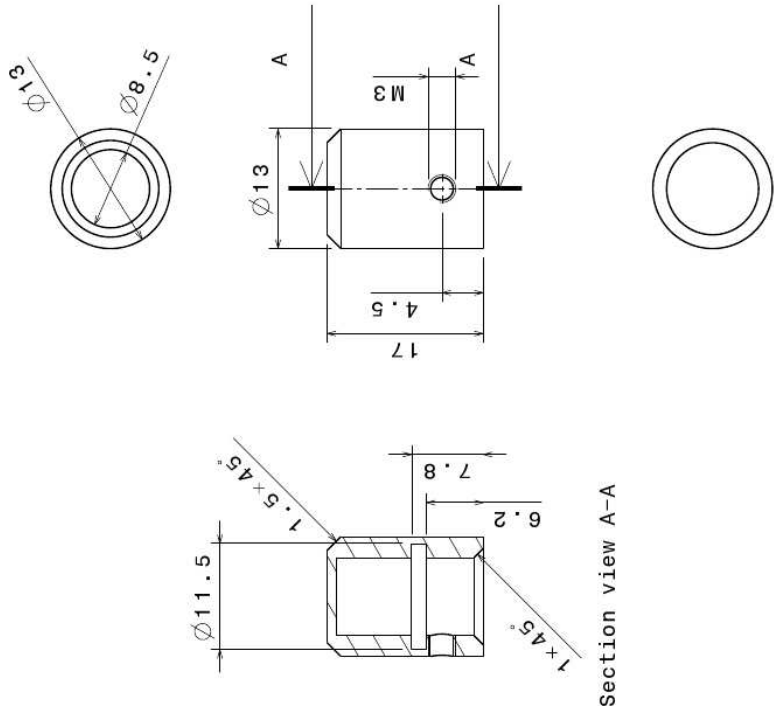
Section view A-A

Material: Ti6Al4V
Bone Chamber
Protection Cap

Material: Ti6Al4V
Bone Chamber
Cap
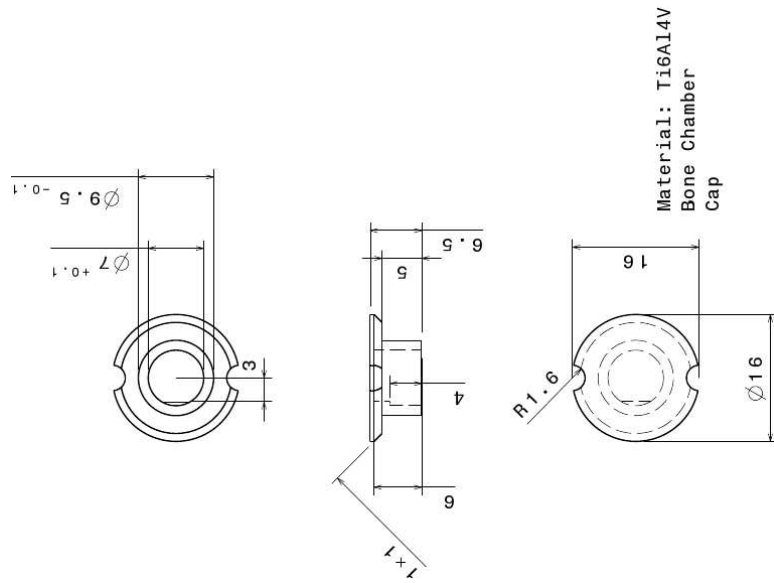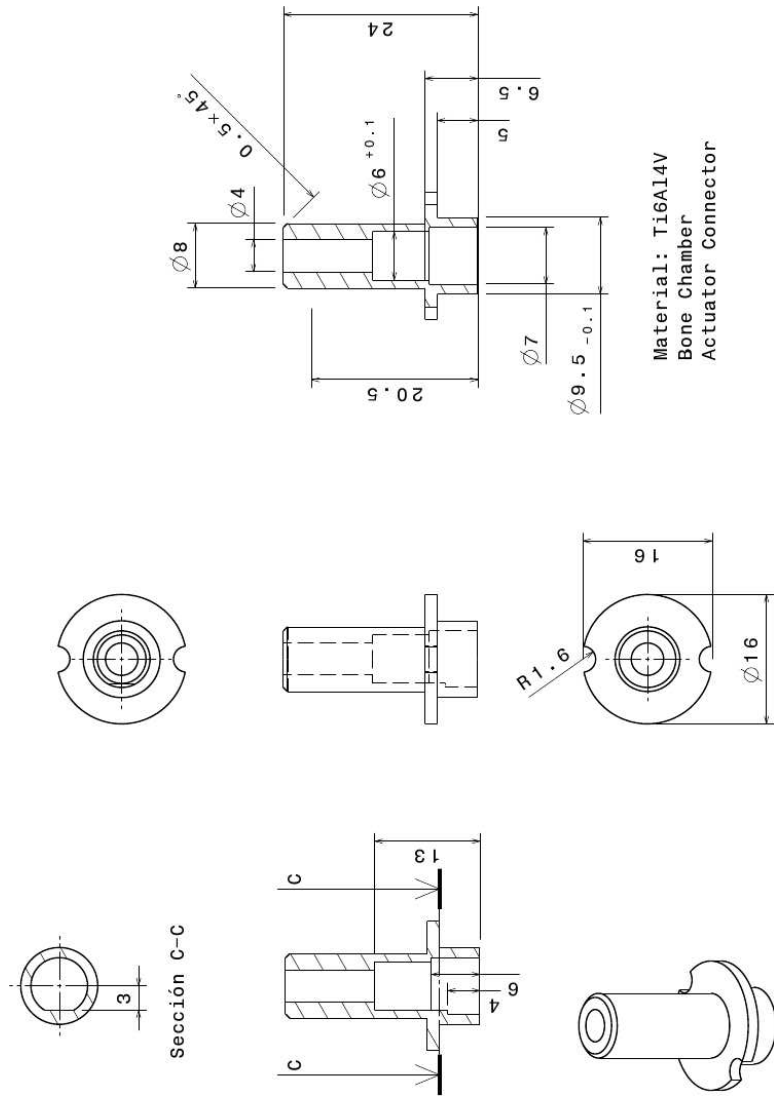
Material: Ti6Al4V
Bone Chamber
Actuator Connector

Sección C-C

Section view A-A

Ø9.5
Ø7
R2
R5
120°
4
2
1.5
12.5
16.5

Material: Ti6Al4V

Bone Chamber
External chamber

3.73
1.62
18
Ø11

Thread ASTM F543-02
Profile type HA5.0; Pass 2mm

Ø22
3.2
A
A
Ø16
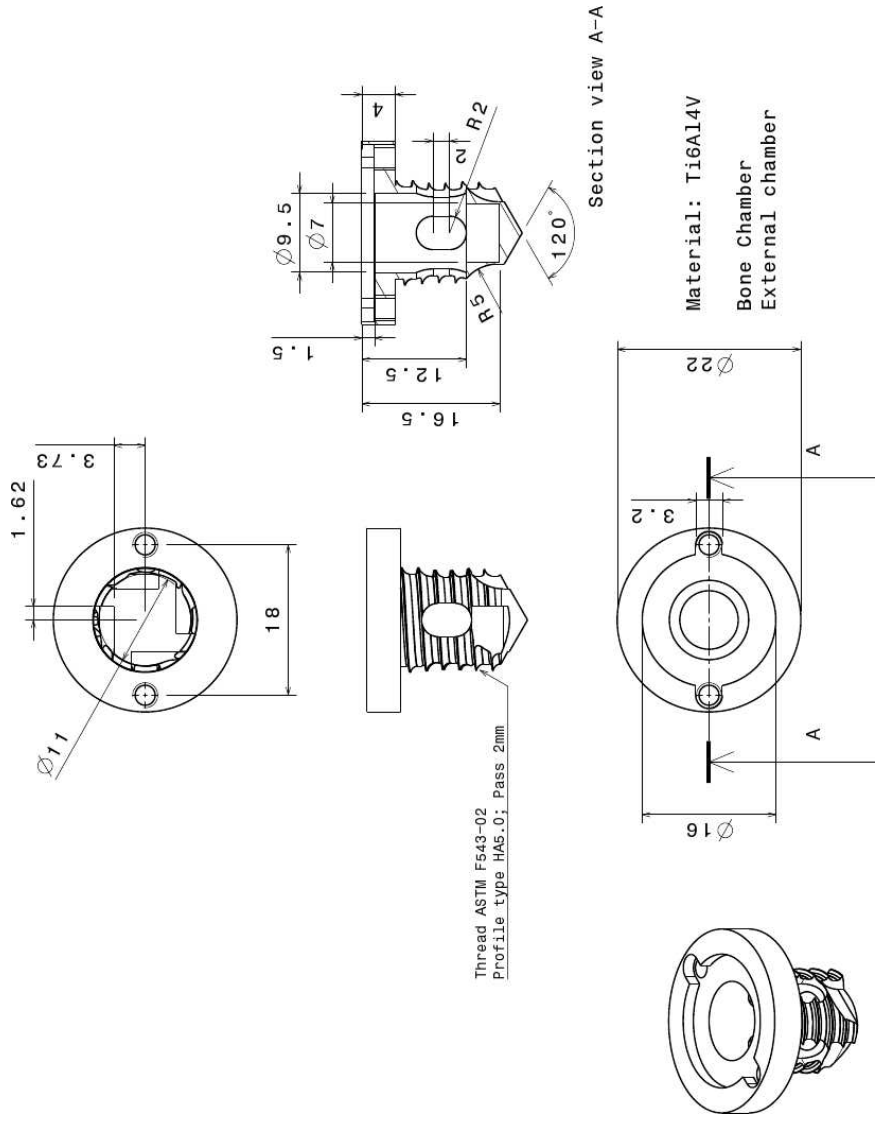
Material: Ti6A14V
Bone Chamber
Internal Cage

R1.5

1×45°

⌀7 −0.1

3

4

5.5

8.5

16

5

⌀9.2

14
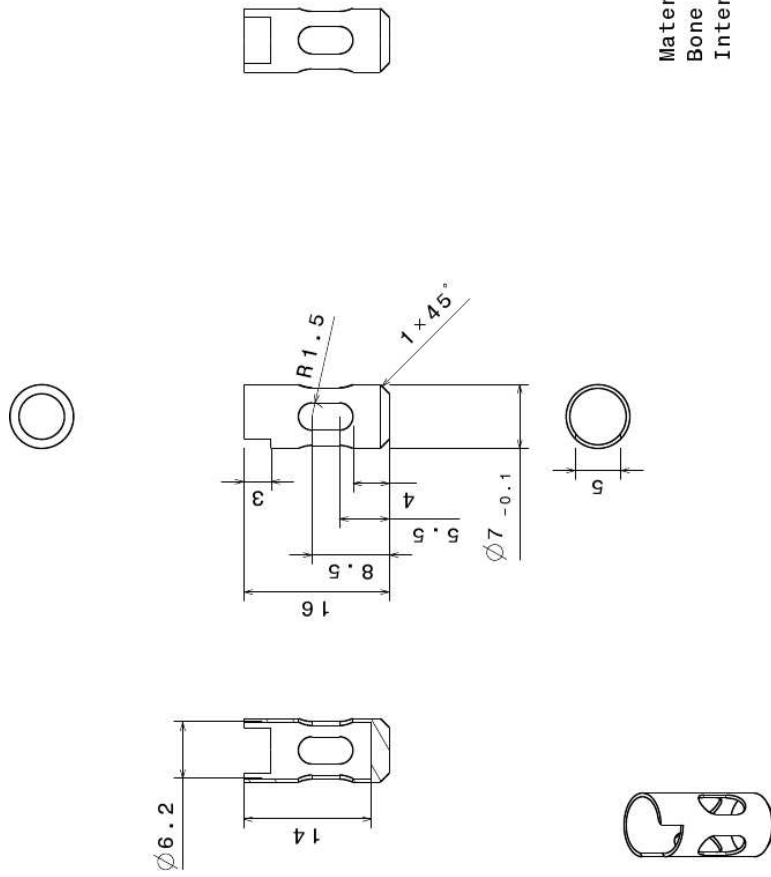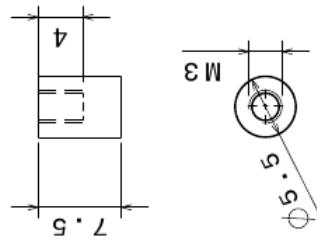
Piston part II

Material: PTFE

Bone Chamber
Piston

4

7.5

M3

Ø5.5

Piston part I

24

5

4

Ø3

Ø3.5

M3
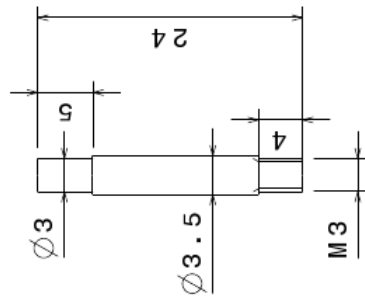
Material: Ti6Al4V
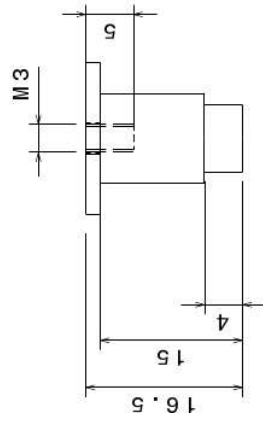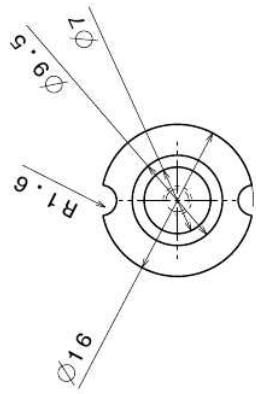
Material: PTFE
Bone Chamber
Chamber spacer

∅7
∅9.5
R1.6
∅16

M3
5
4
15
16.5

Material: AISI 01 steel
Bone Chamber
Insertion tool

39.75

36.75

45°

33

16

3

R3.03

1

R1.25

2

1

4.5

R1.6

R6

18
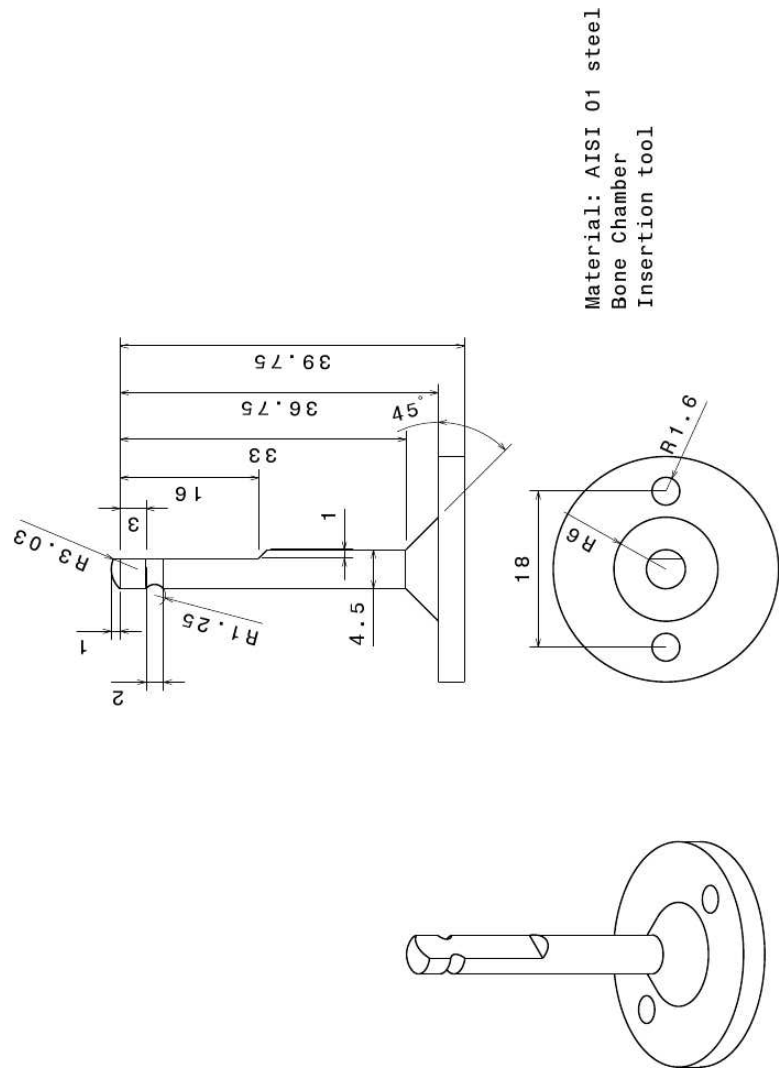
Appendix F

LabView Software for the Bone Chamber System
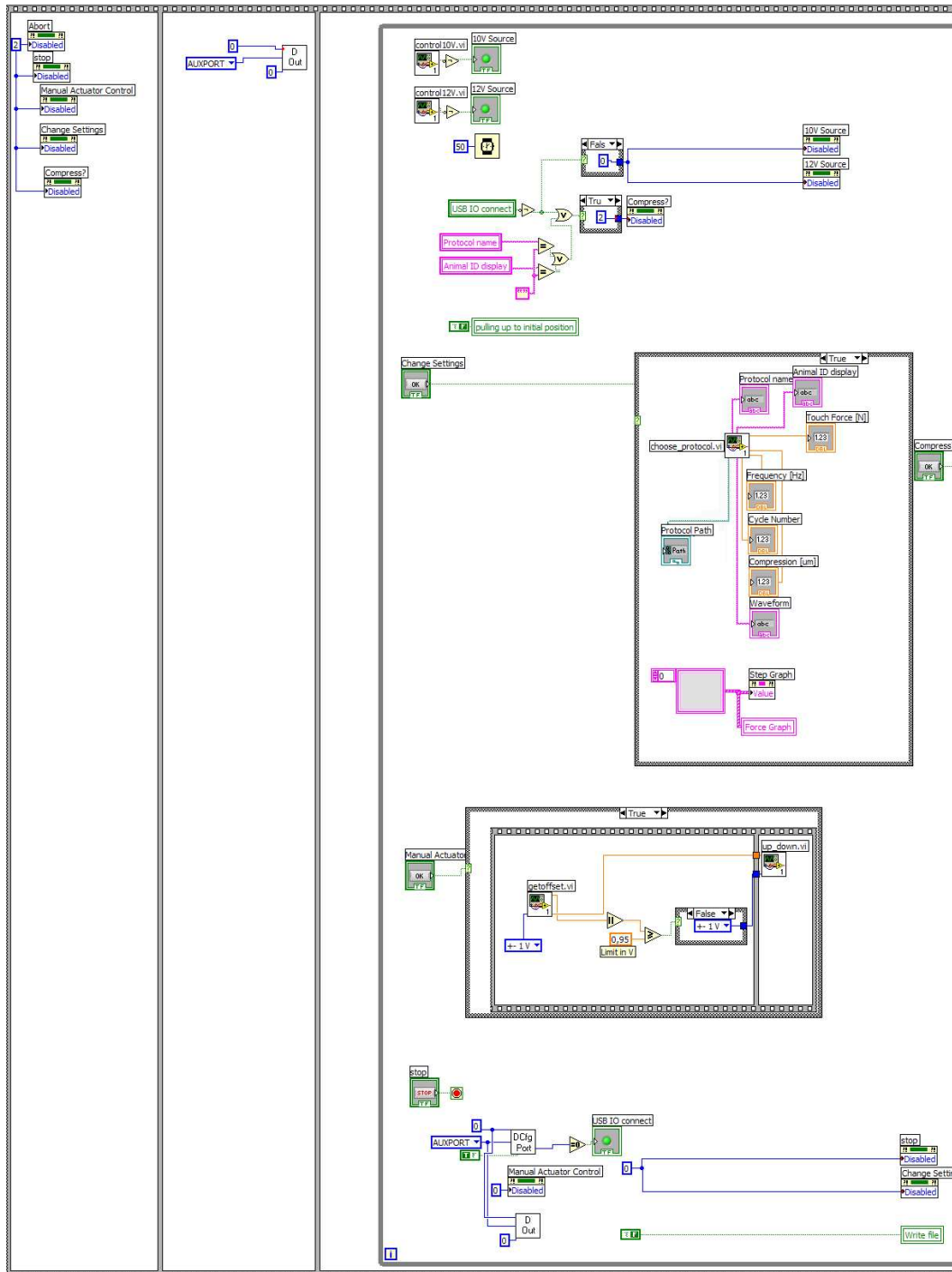
Figure F.1: Main.vi program of the bone chamber system. Continued in Figure F.2.
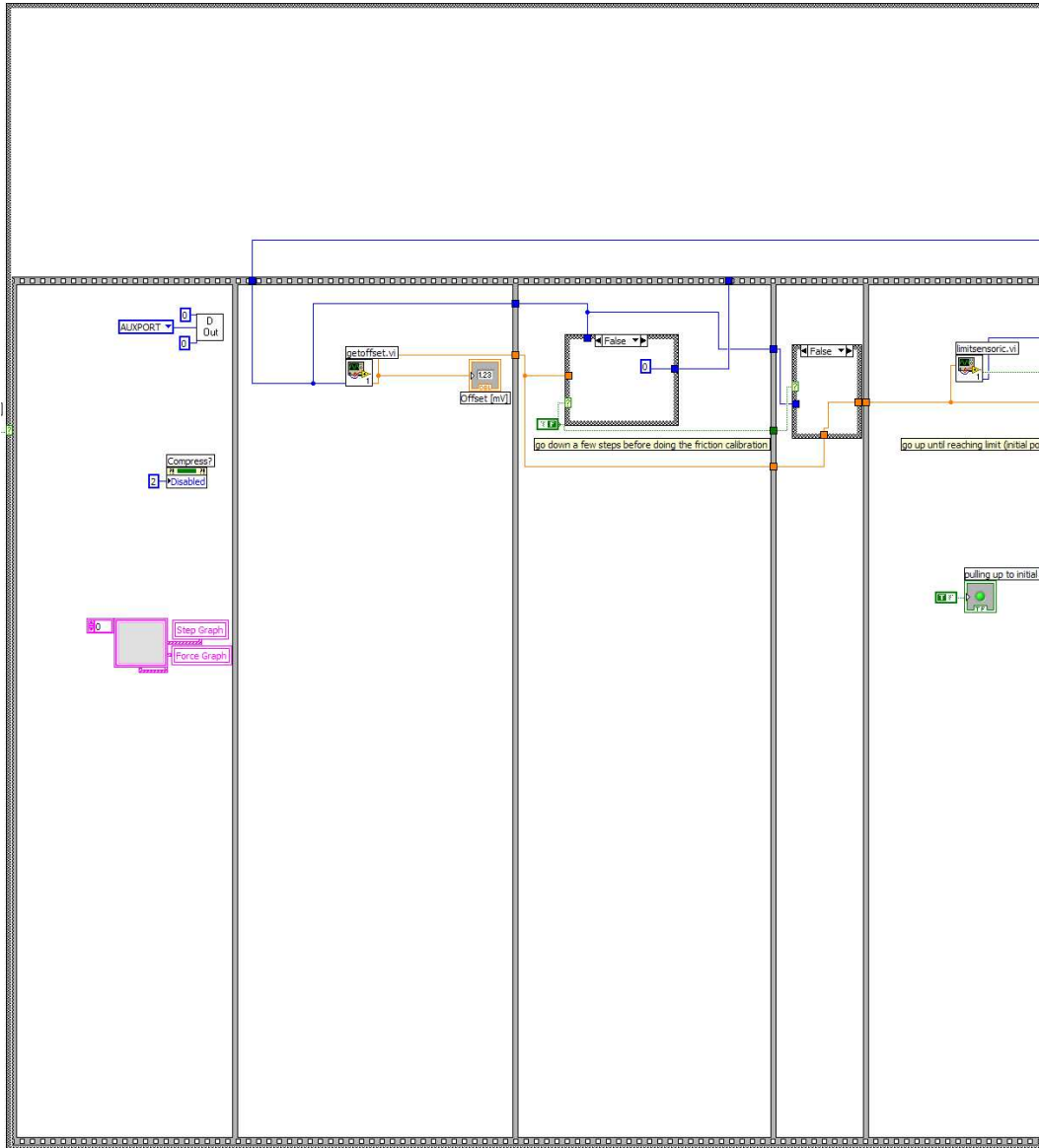
Figure F.2: Main.vi program of the bone chamber system. Continuation of Figure F.1, continued in Figure F.3.
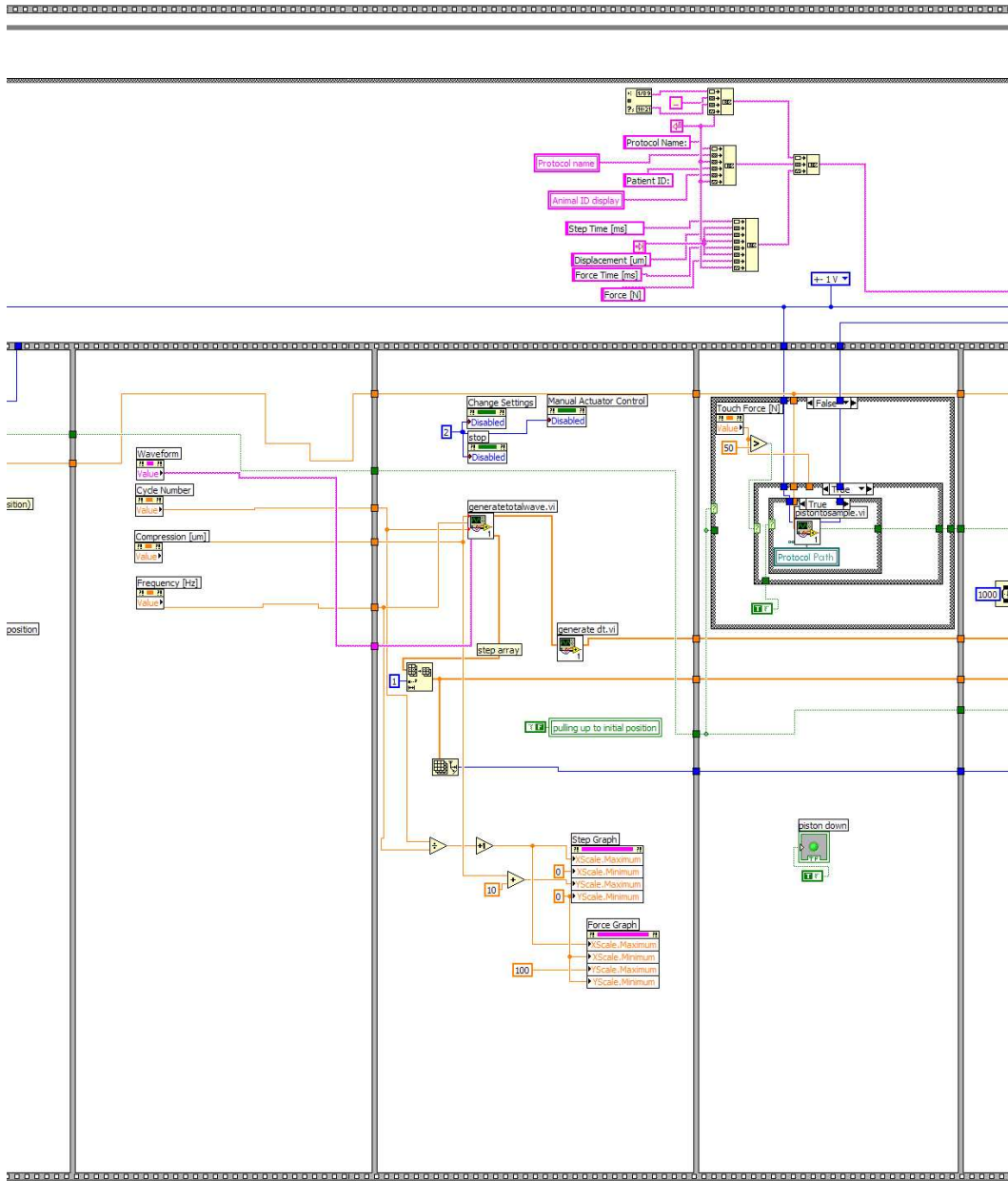
Figure F.3: Main.vi program of the bone chamber system. Continuation of Figure F.2, continued in Figure F.4.
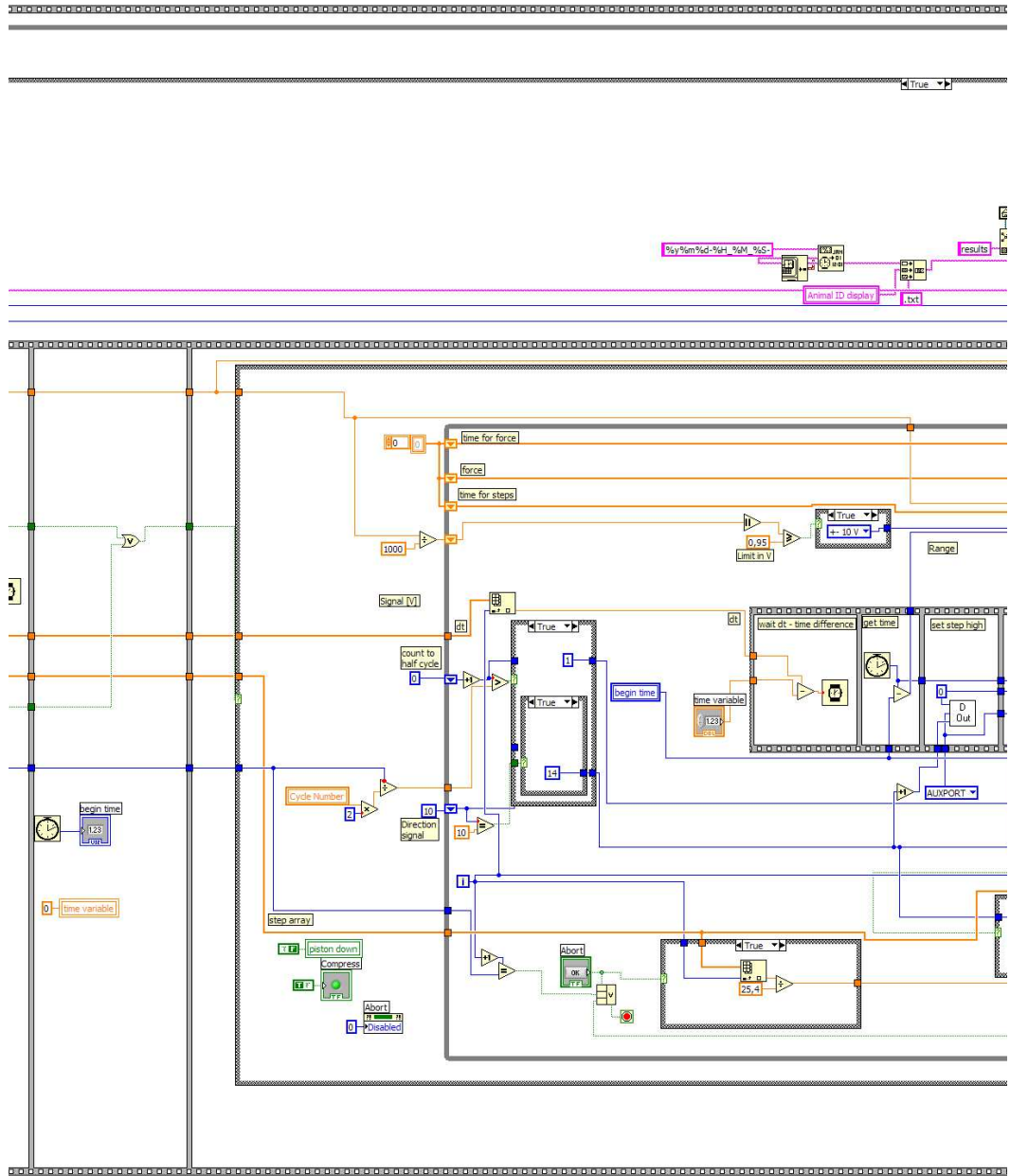
Figure F.4: Main.vi program of the bone chamber system. Continuation of Figure F.3, continued in Figure F.5.
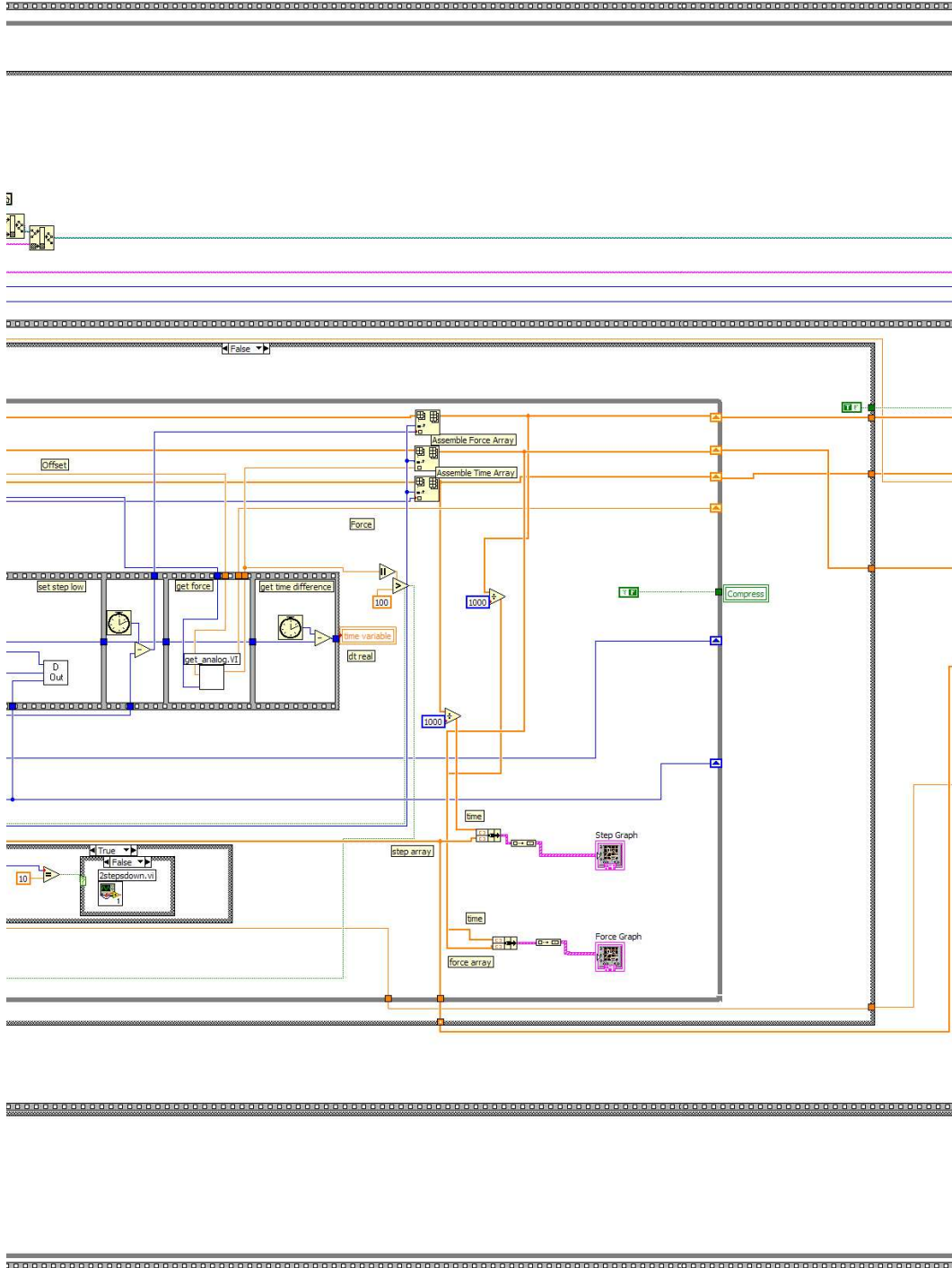
Figure F.5: Main.vi program of the bone chamber system. Continuation of Figure F.4, continued in Figure F.6.
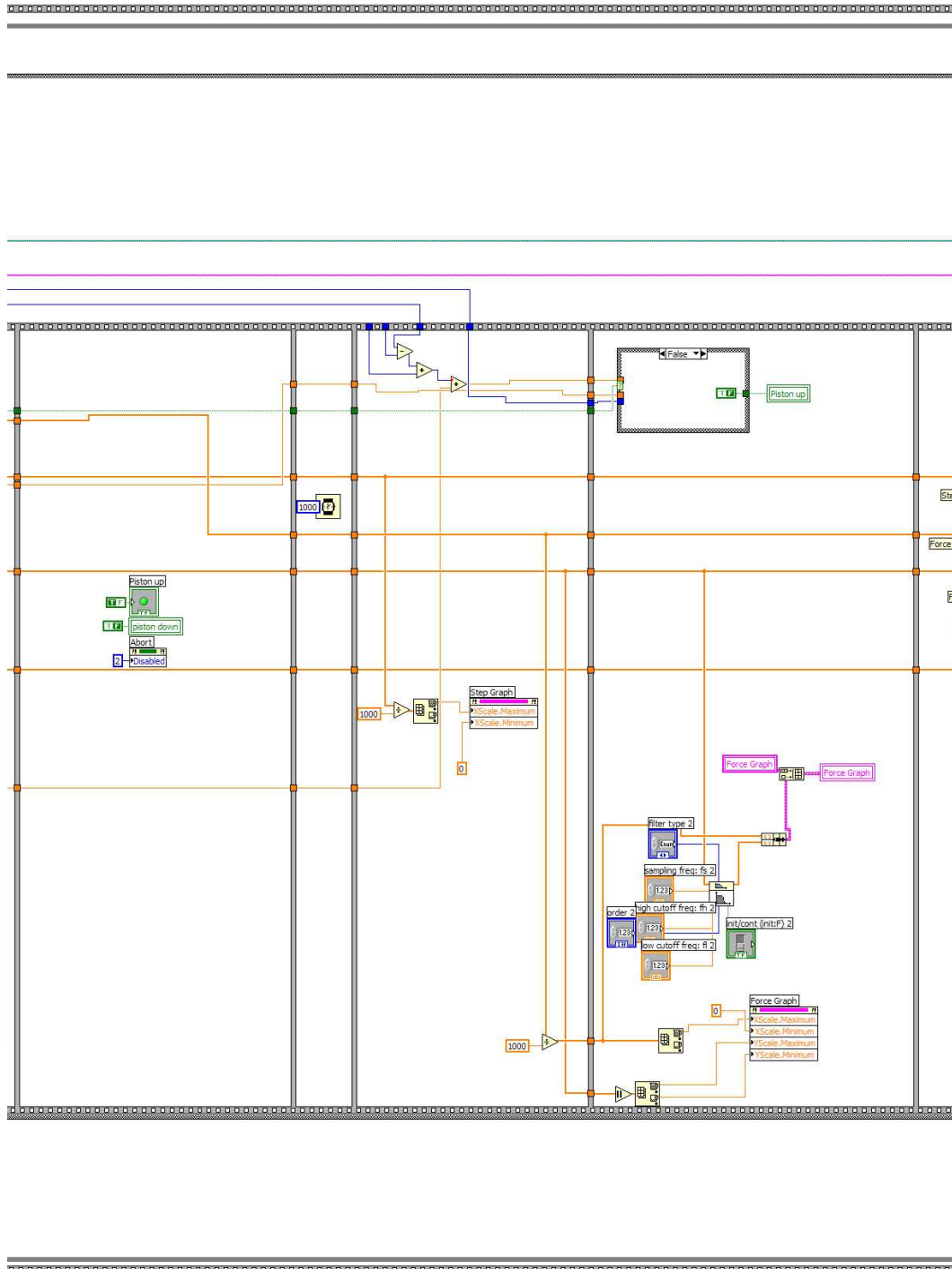
Figure F.6: Main.vi program of the bone chamber system. Continuation of Figure F.5, continued in Figure F.7.
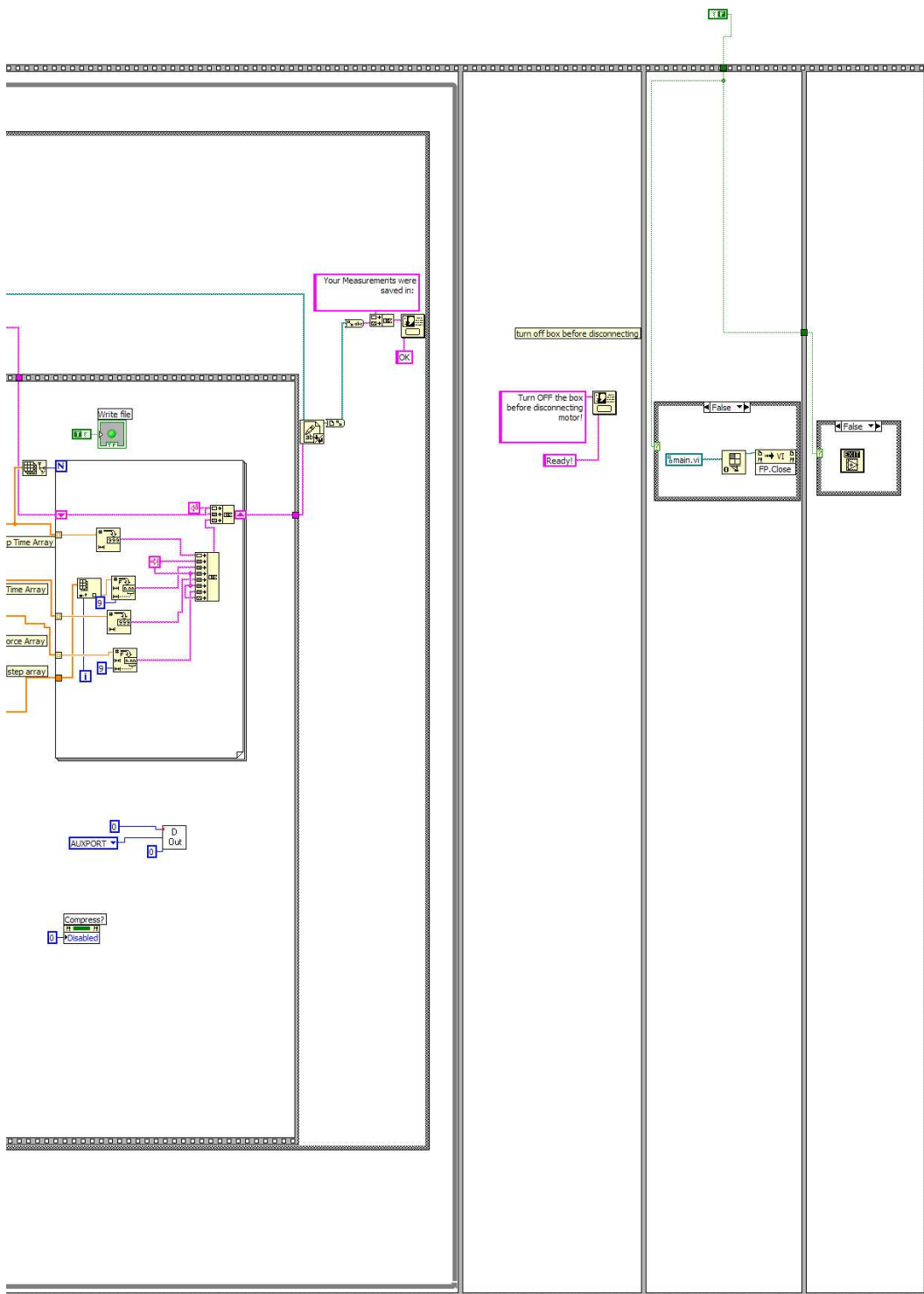
Figure F.7: Main.vi program of the bone chamber system. Continuation of Figure F.6.
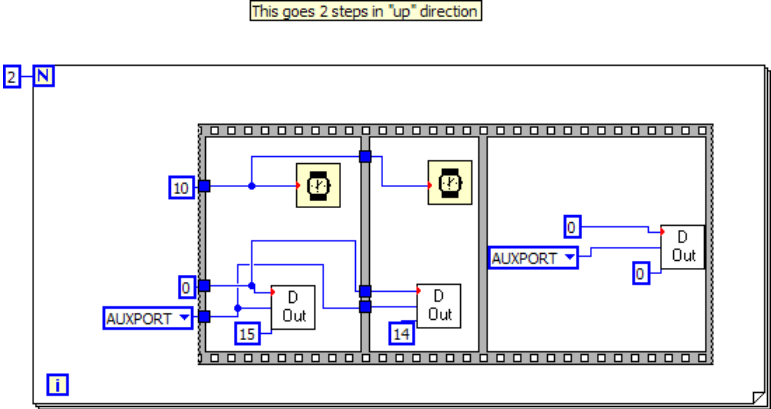
Figure F.8: Subroutine driving the actuator two steps upwards (2stepsback).
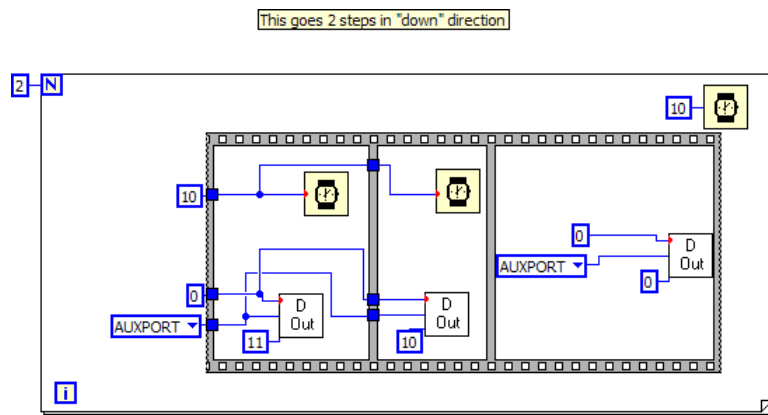
Figure F.9: Subroutine driving the actuator two steps downwards (2stepsdown).
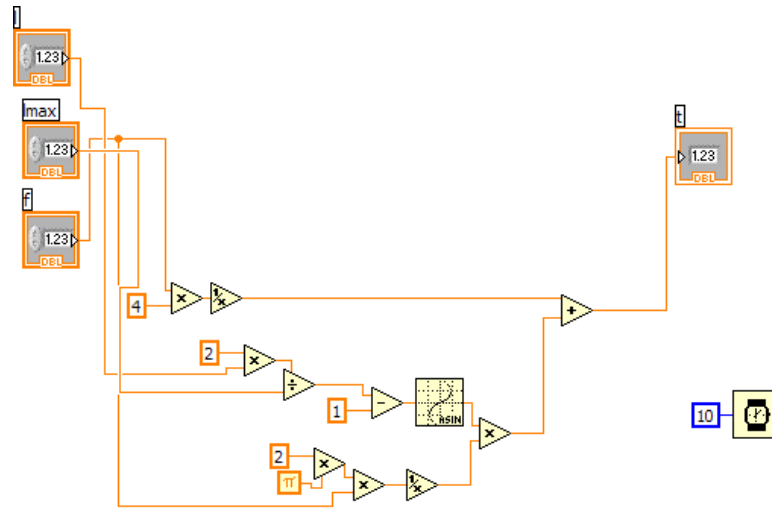
Figure F.10: Subroutine generating a sinus value at a given timepoint for the displacement (calcsinus).
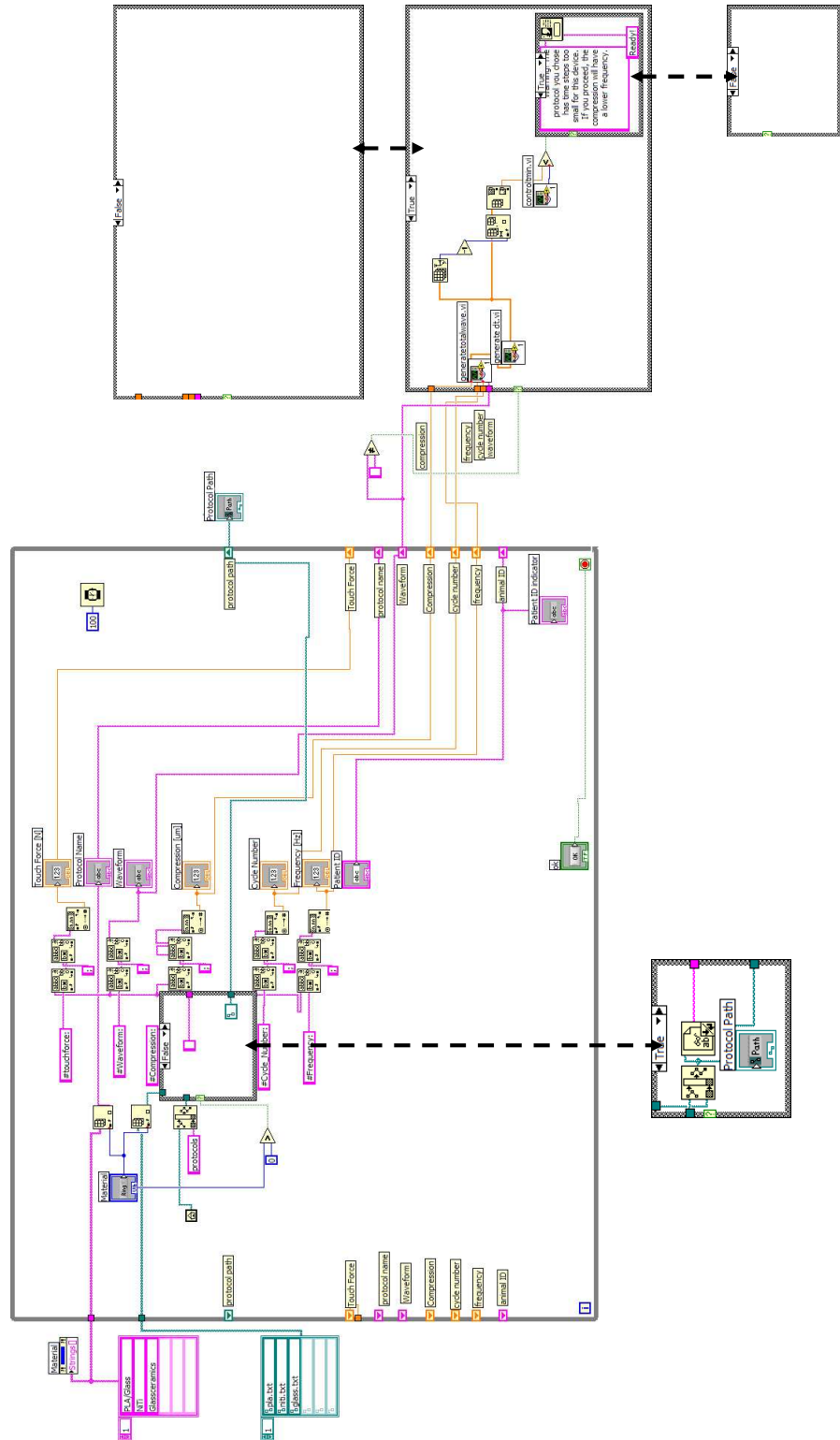
Figure F.11: GUI menu for choosing a protocol and input animal ID (choose_protocol).
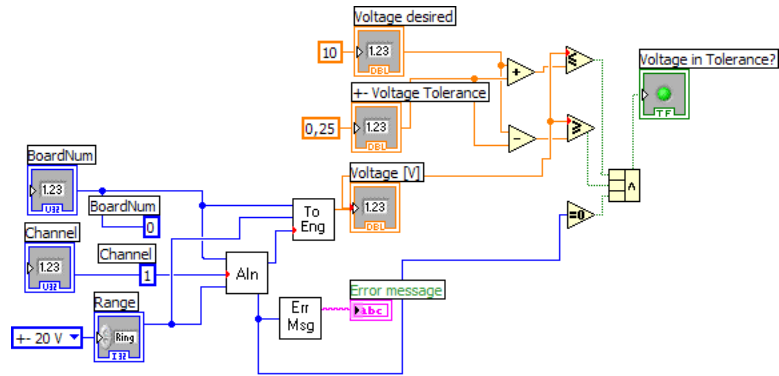
Figure F.12: Subroutine testing if the voltage source of 10 VDC is working (control10V).
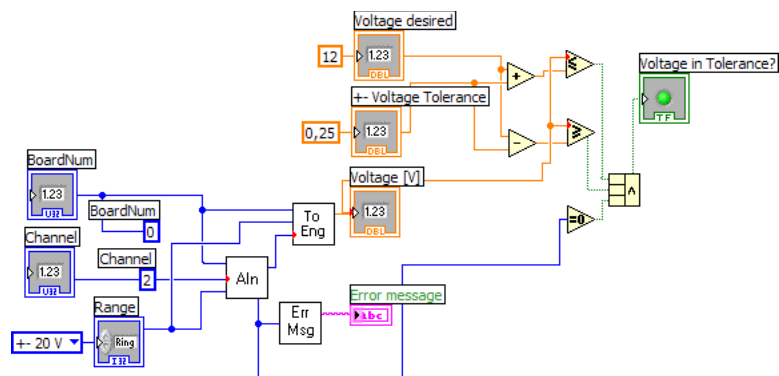
Figure F.13: Subroutine testing if the voltage source of 12 VDC is working (control12V).
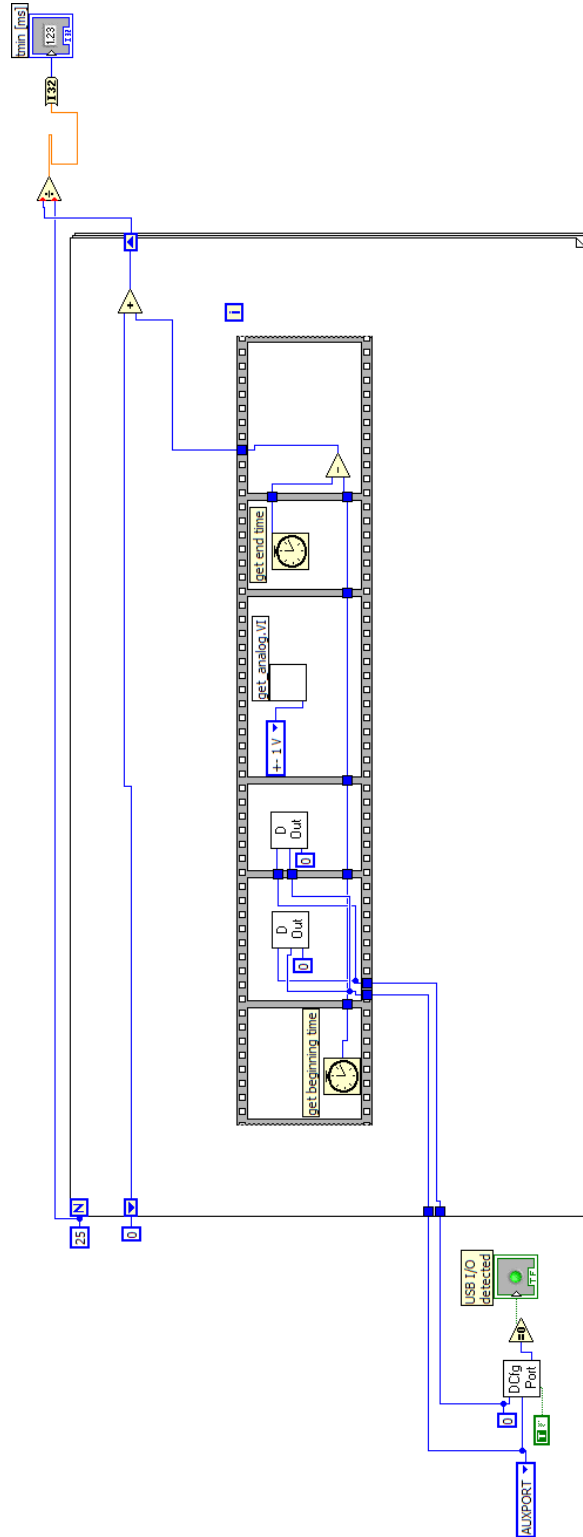
Figure F.14: Subroutine measuring the average time needed to set the digital output twice and read the analogue input once (controltmin).
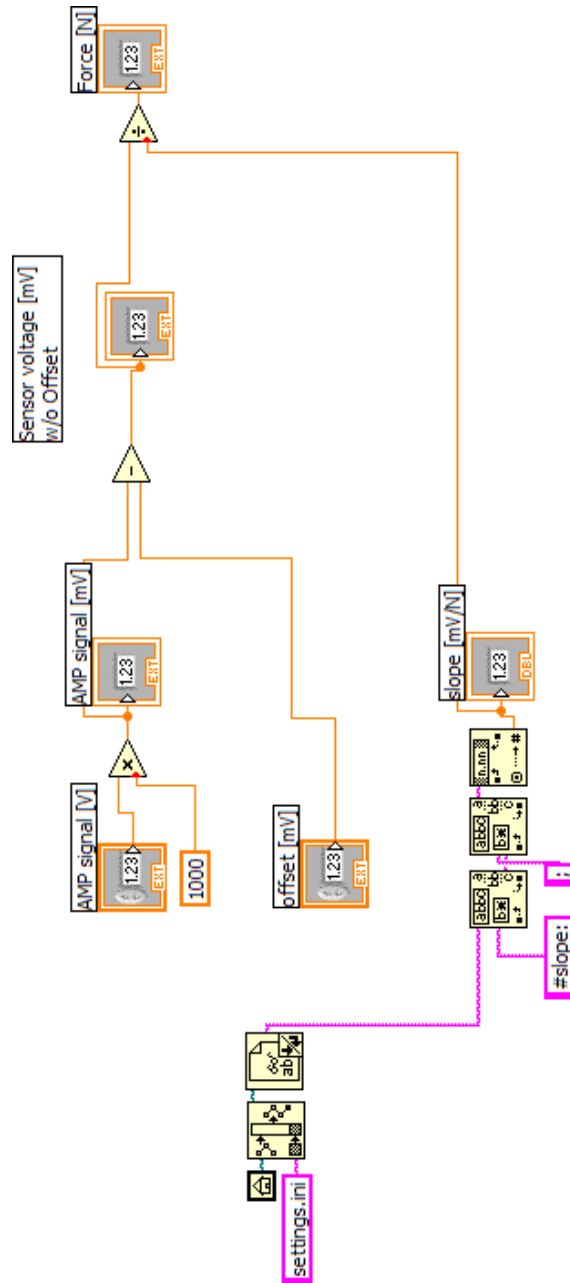
Figure F.15: Subroutine converting the measured voltage to force, taking in account the offset and slope of the calibration (convert_mV_to_N).
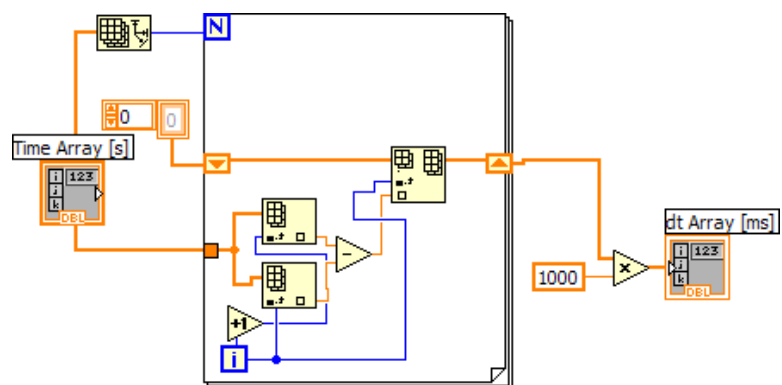
Figure F.16: Subroutine converting a consecutive time array into differential time.(generate dt).
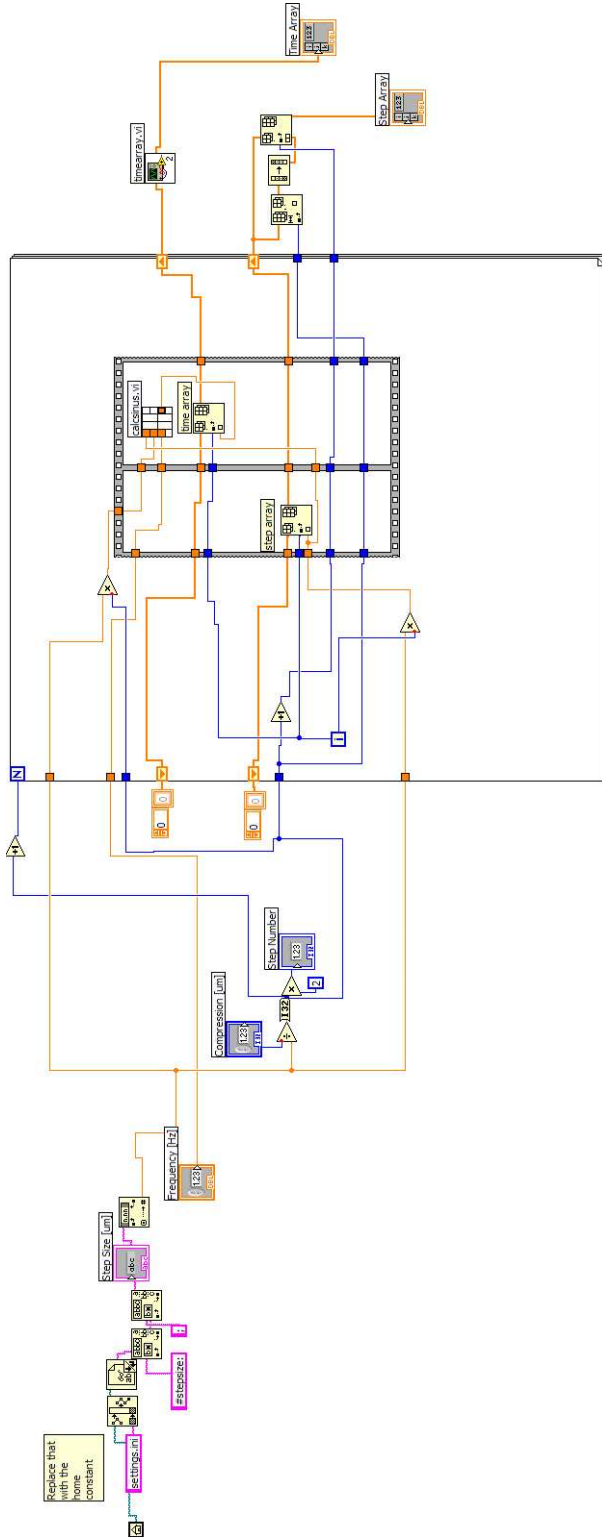
Figure F.17: Subroutine generating a time point for every displacement step for a sinus wave (generatesinus).
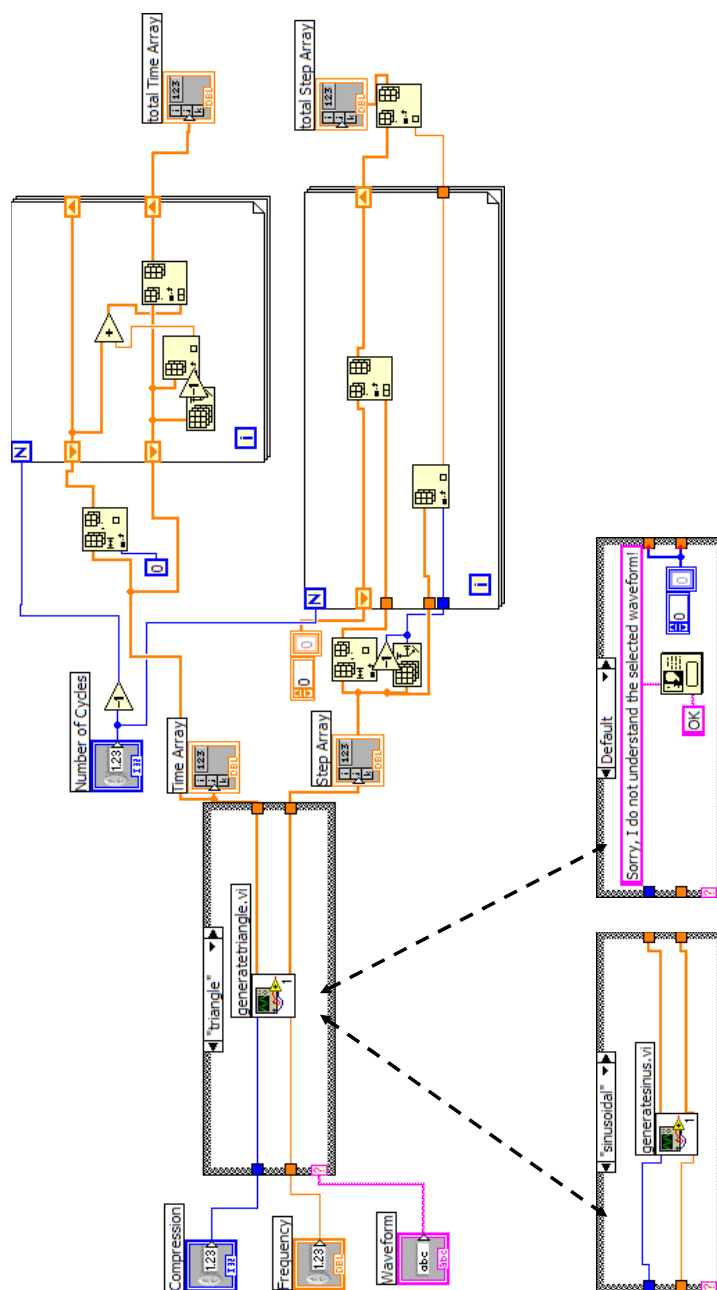
Figure F.18: Subroutine generating the overall waveform for all cycles (generatetotalwave).
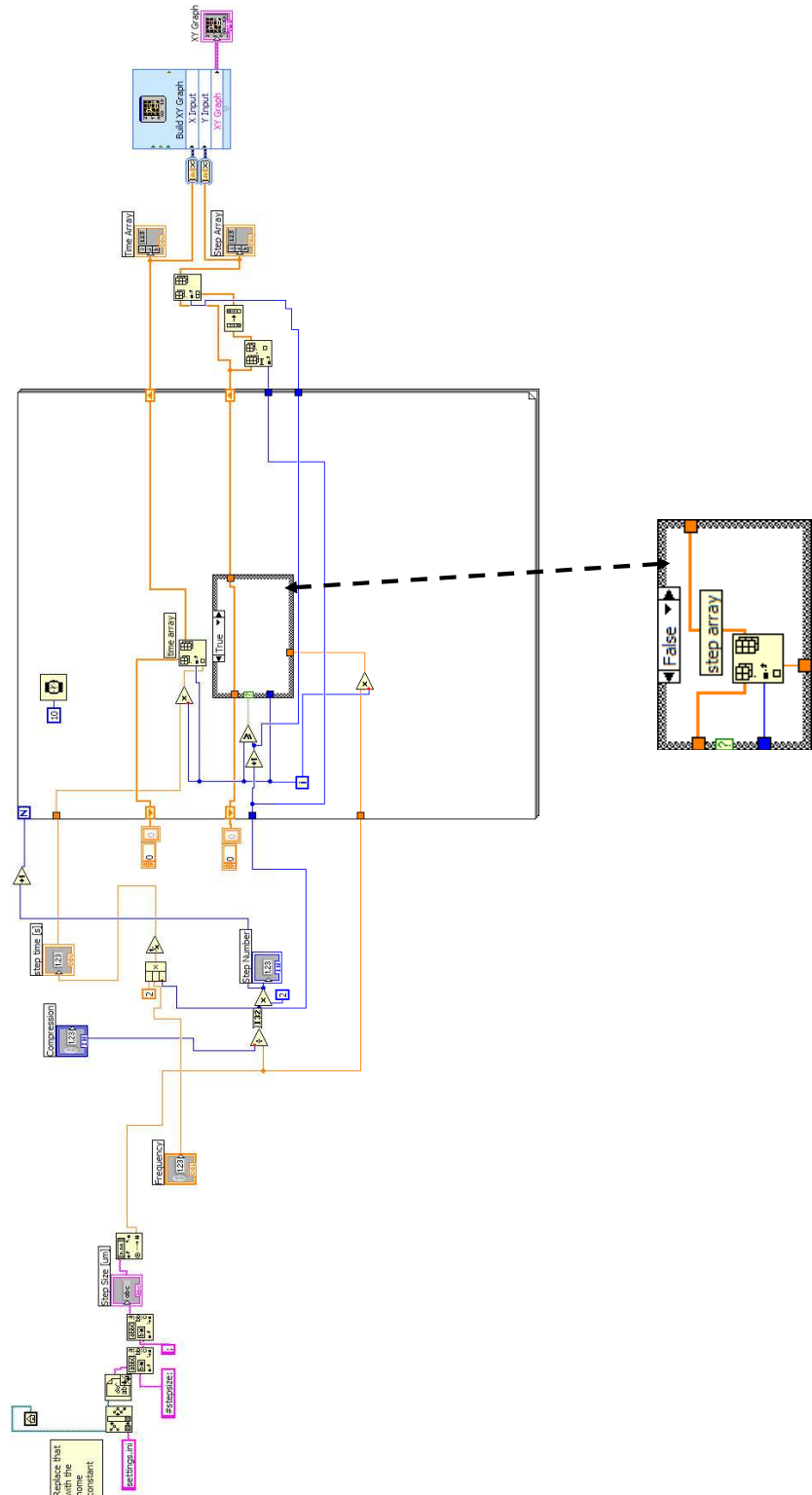
Figure F.19: Subroutine generating a time point for every displacement step for a triangle wave (generatetriangle).
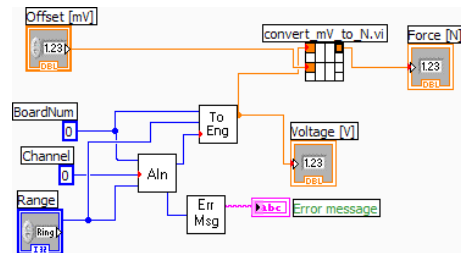
Figure F.20: Subroutine reading the analogue input voltage, converting it to force (get_analog).
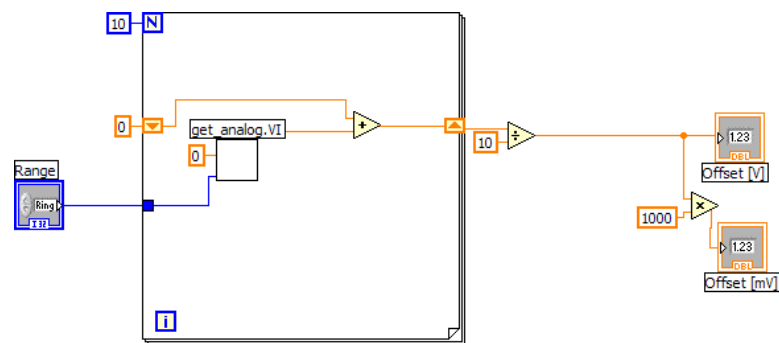
Figure F.21: Subroutine measuring the average momentary force signal (getoffset).
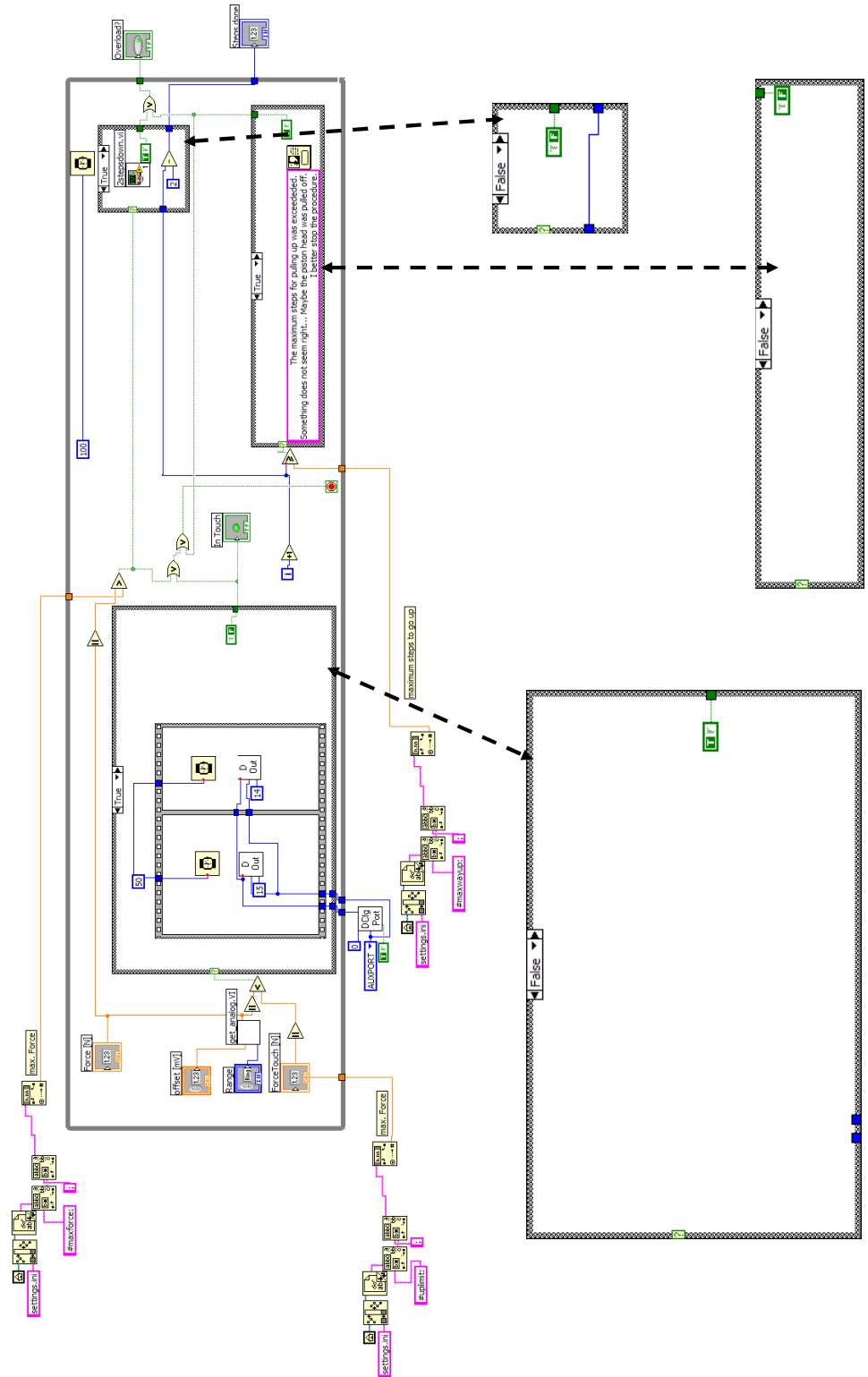
Figure F.22: Subroutine moving piston up, until the piston head hits the upper limit or a certain number of steps have been exceeded (limitsensoric).
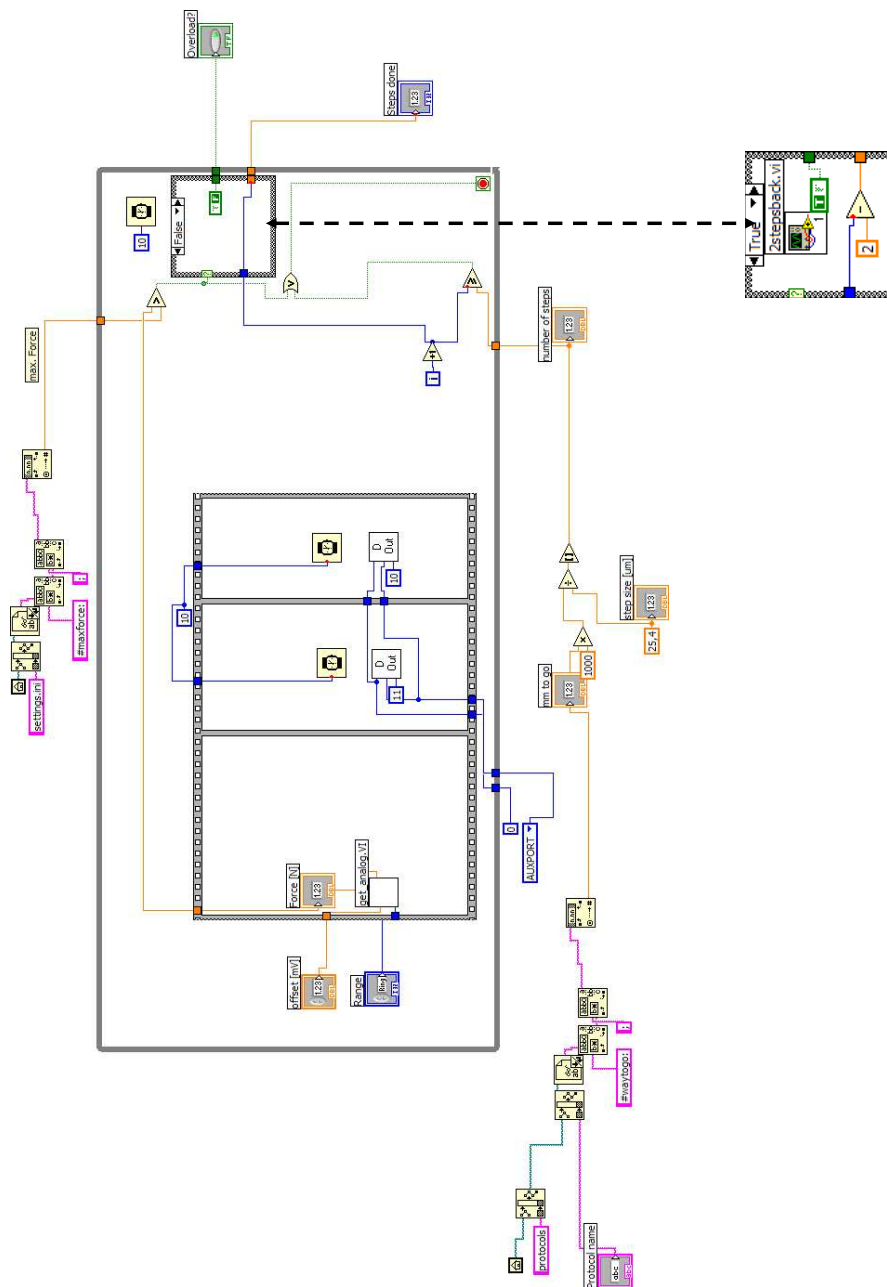
Figure F.23: Subroutine moving the piston downwards for a certain number of steps.(pistontosample).

Figure F.24: Subroutine driving the piston up to its start position (pistonup).
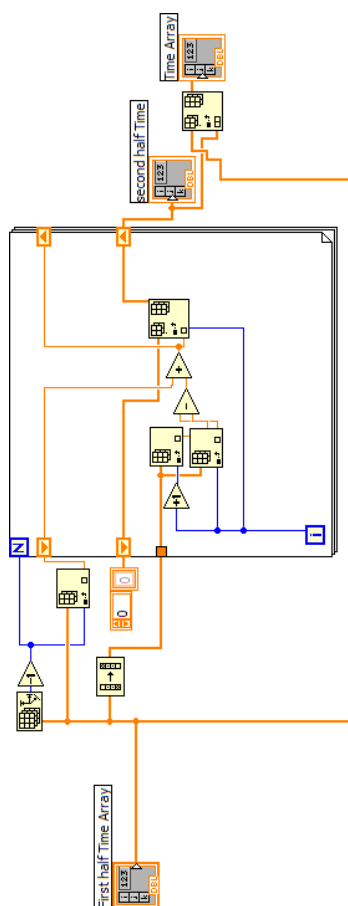
Figure F.25: Subroutine completing a 1D array of half-wave time points to a full-wave time point array (timearray).
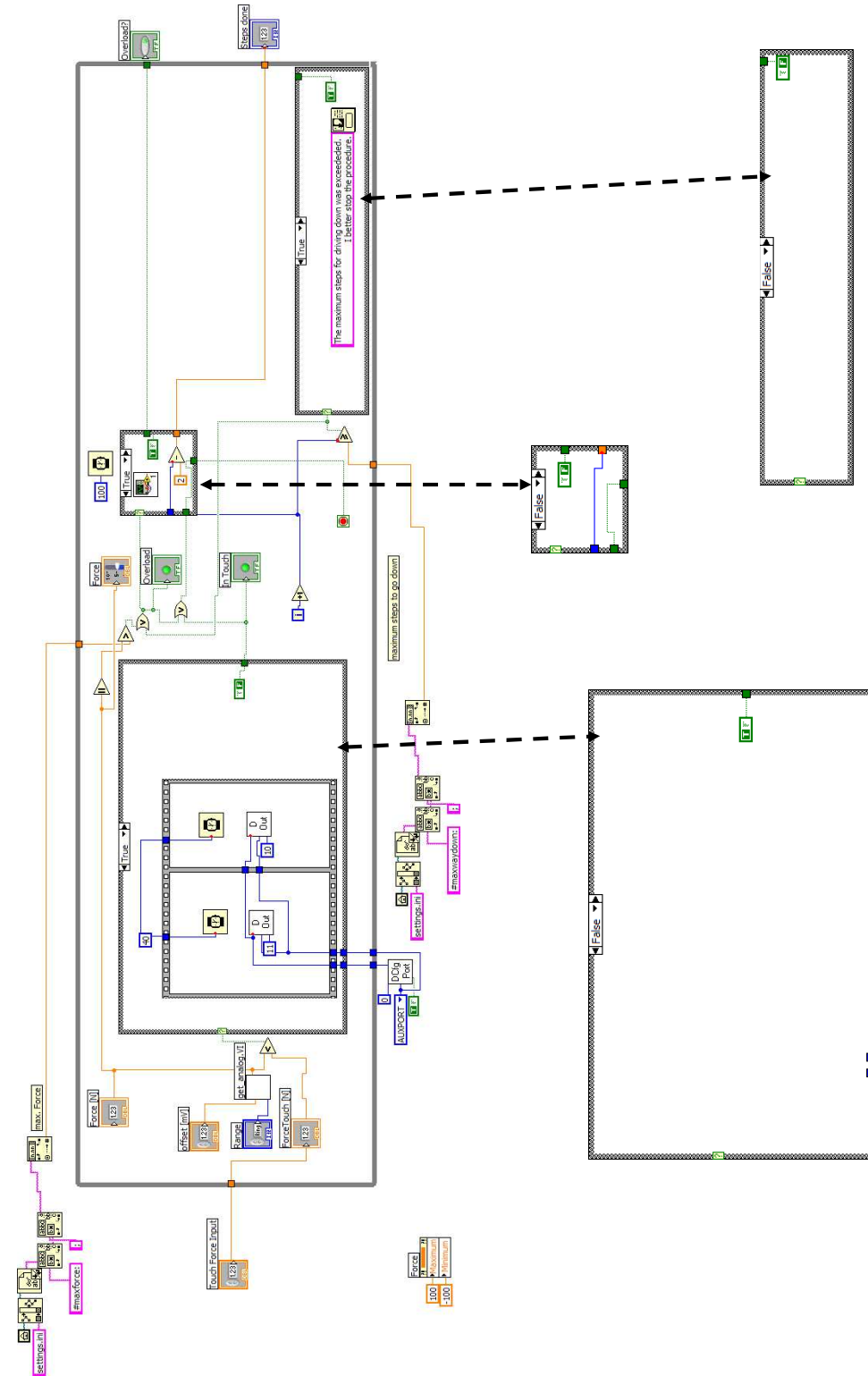
Figure F.26: Subroutine moving the piston downwards, until the sample is touched or a certain number of steps have been exceeded (touchsensoric).
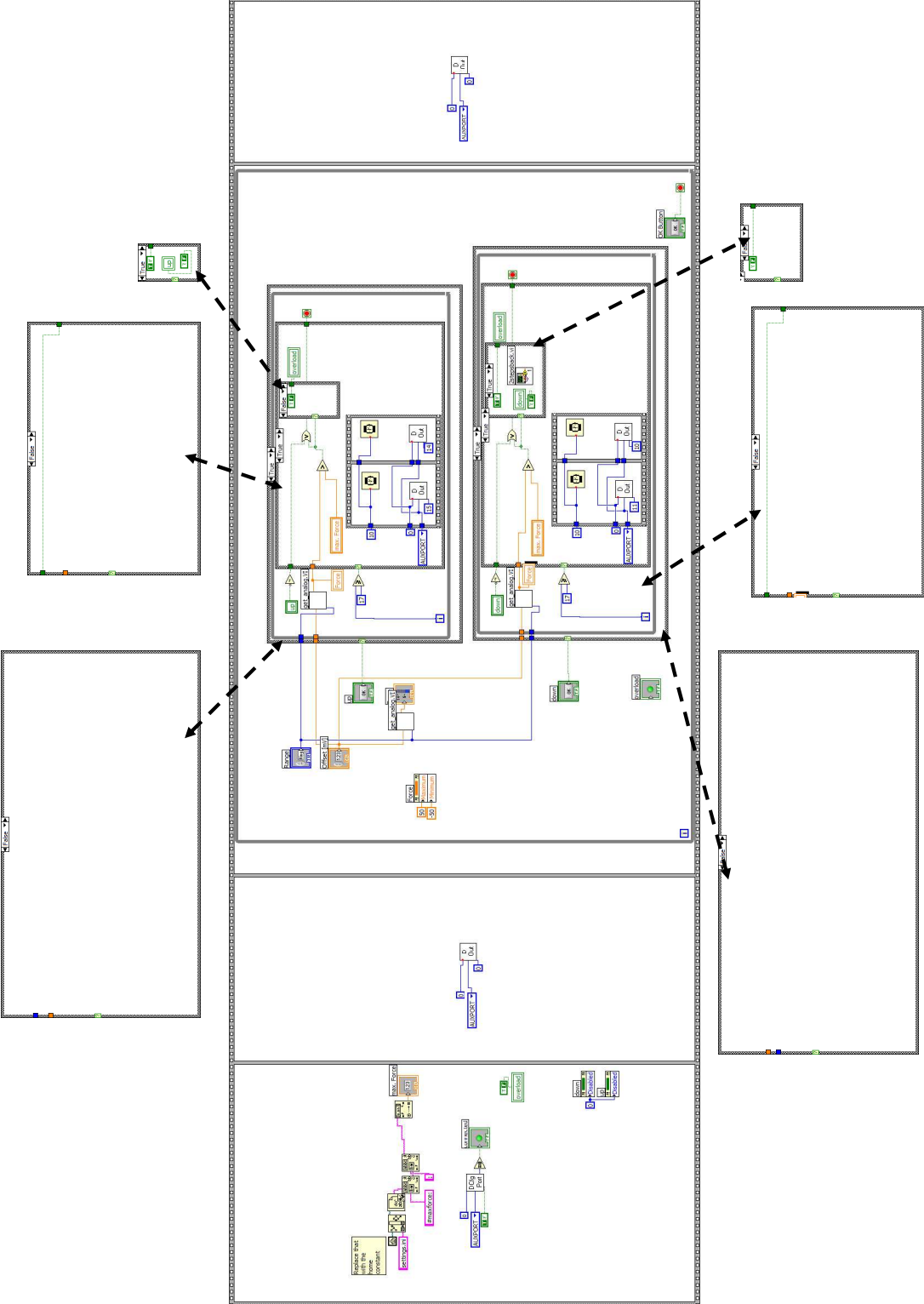
Figure F.27: GUI allowing the user to drive the piston up and down manually (up_down).

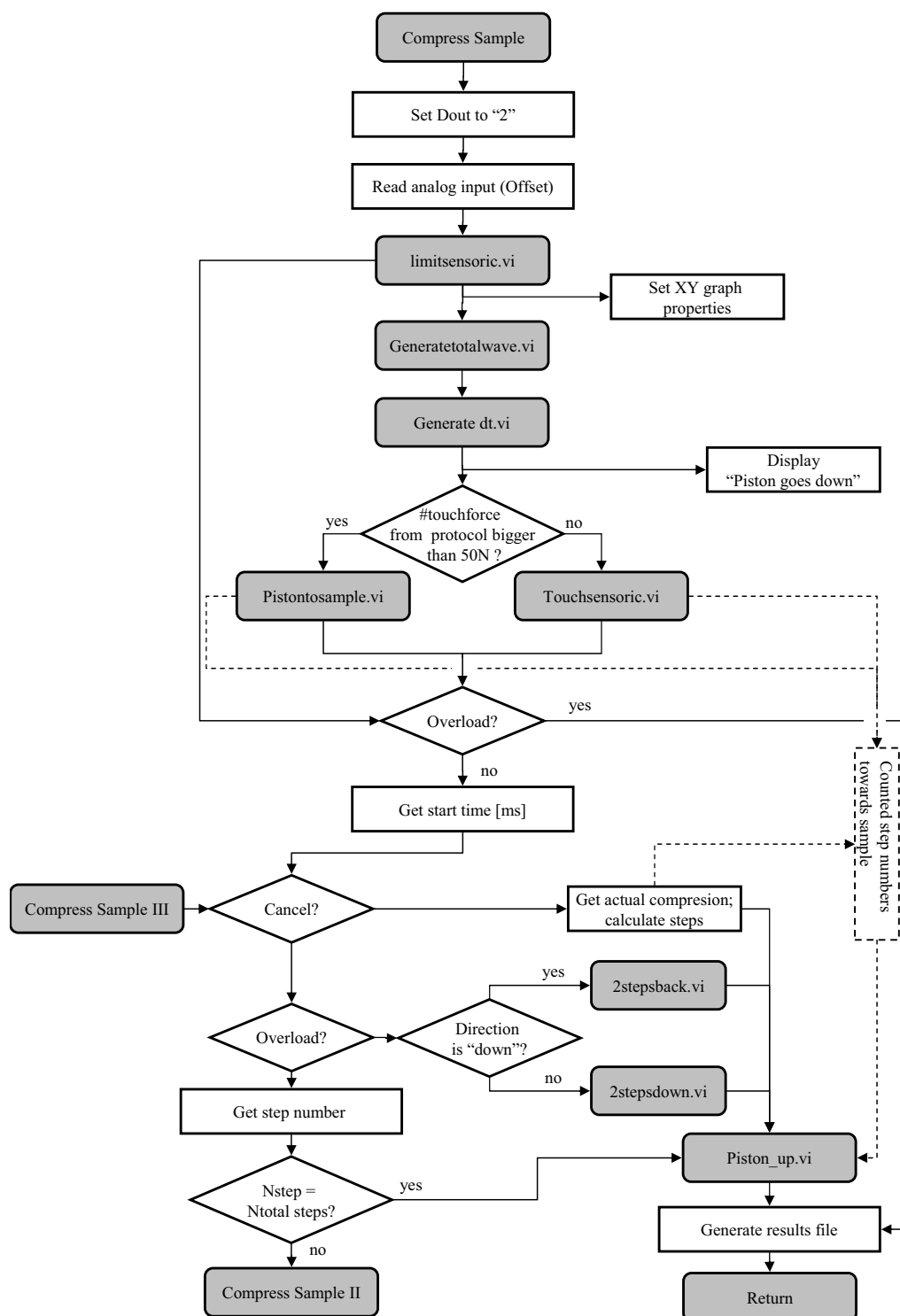# Appendix G

Bone Chamber Control Software Flowcharts
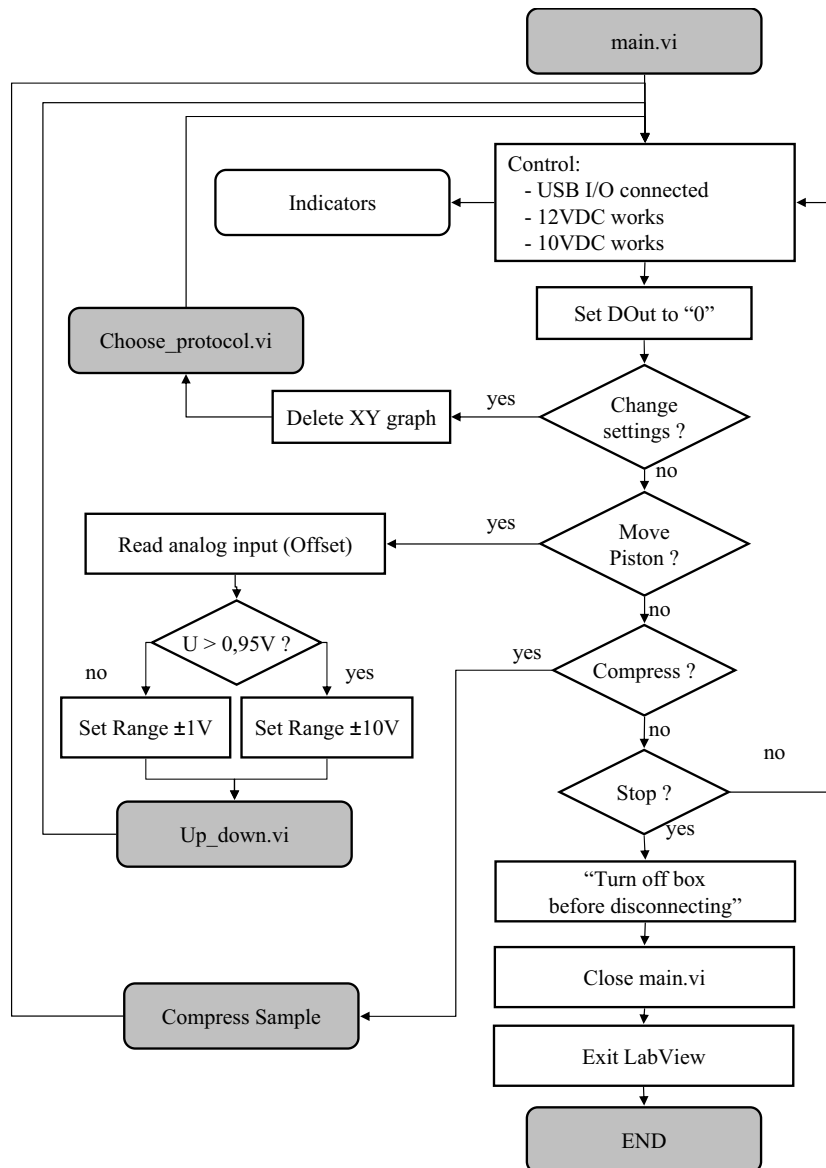
Figure G.1: Flowchart of the compression device control software for the bone chamber experiments (1 of 8).
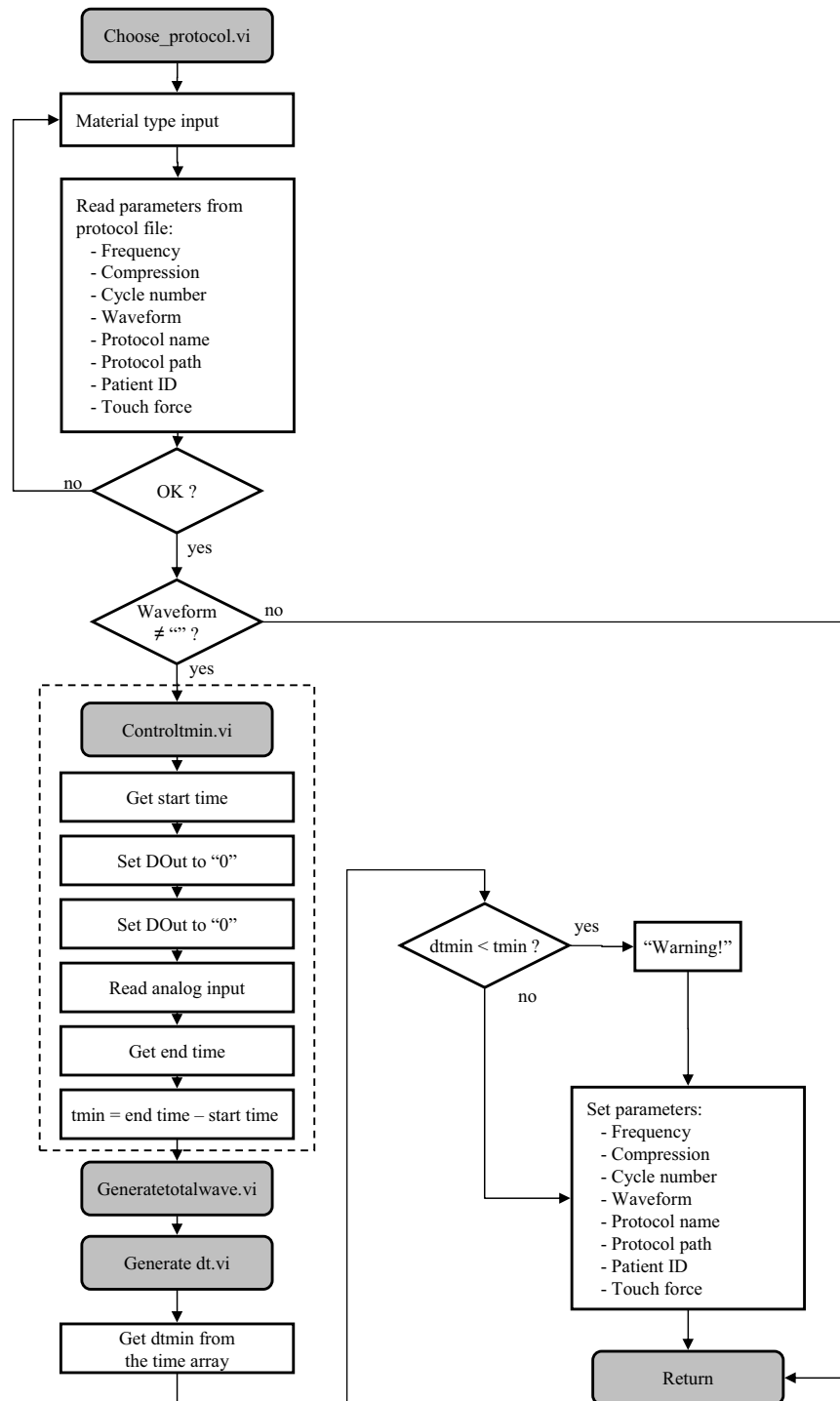
Figure G.2: Flowchart of the compression device control software for the bone chamber experiments (2 of 8).
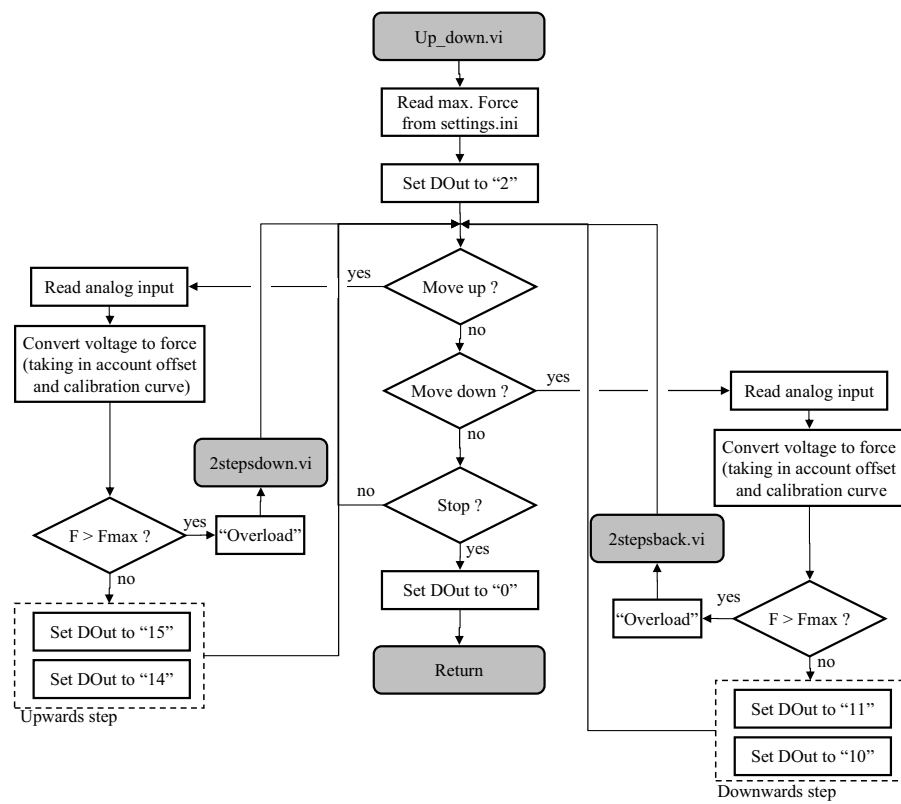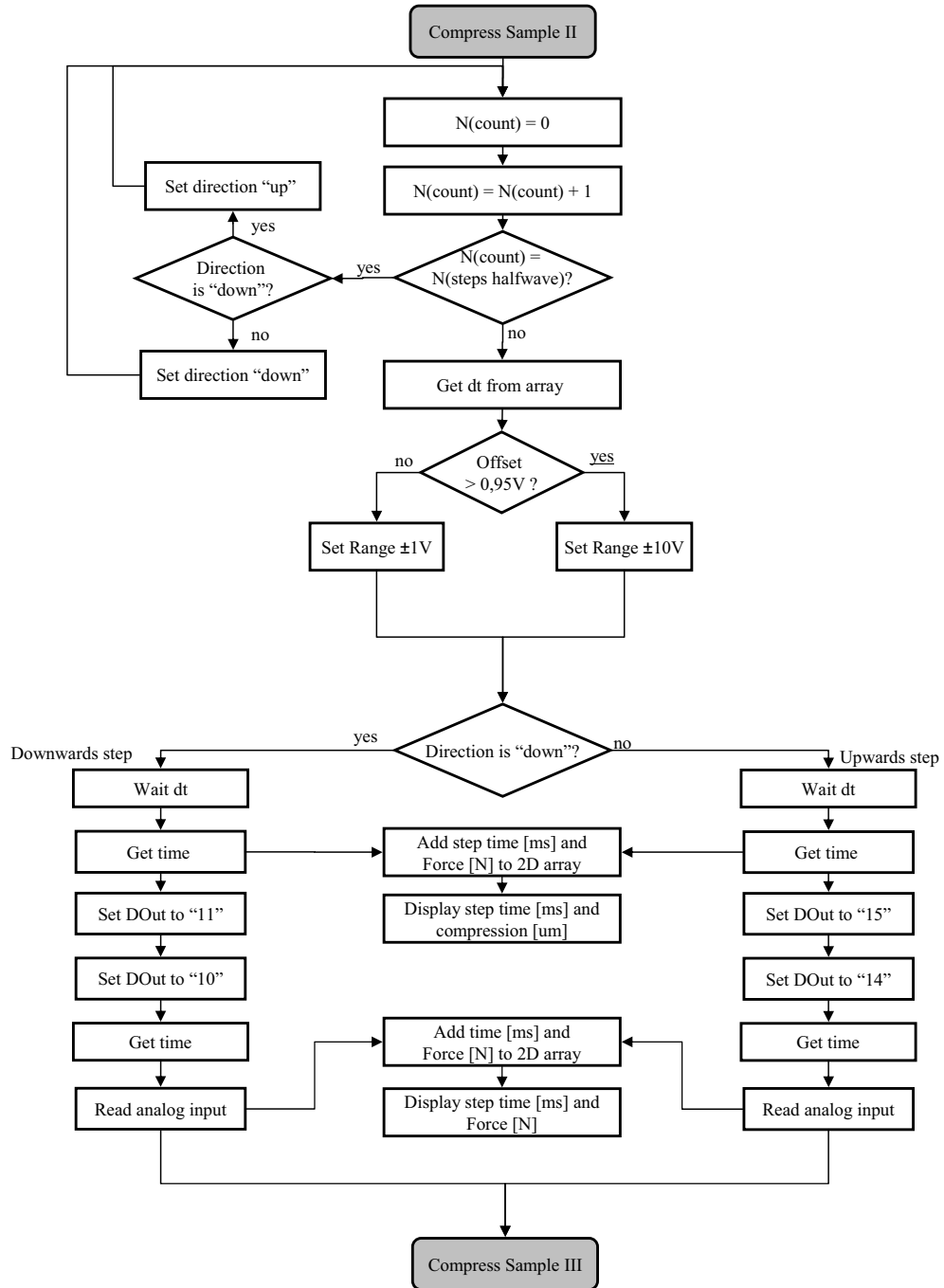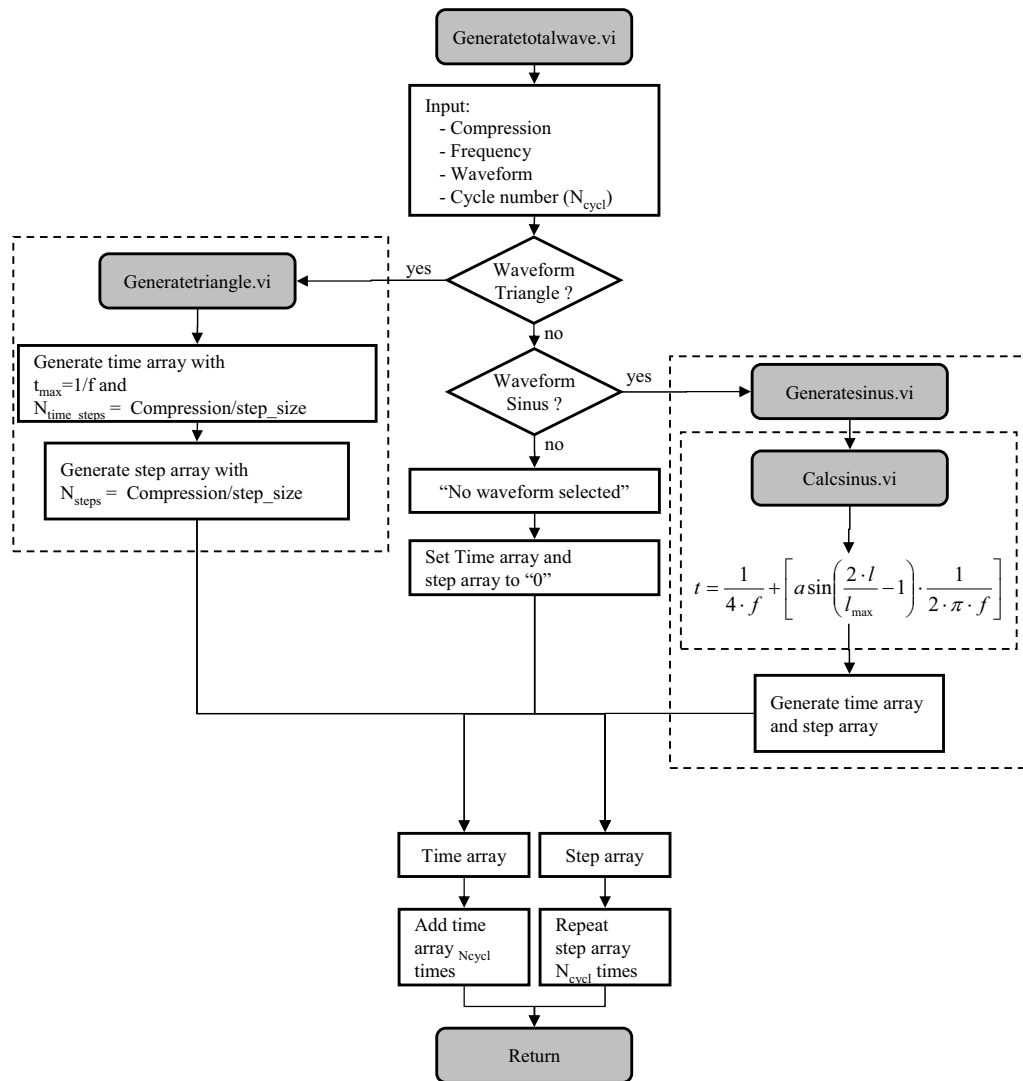
Figure G.3: Flowchart of the compression device control software for the bone chamber experiments (3 of 8).

Figure G.4: Flowchart of the compression device control software for the bone chamber experiments (4 of 8).

Figure G.5: Flowchart of the compression device control software for the bone chamber experiments (5 of 8).

Figure G.6: Flowchart of the compression device control software for the bone chamber experiments (6 of 8).
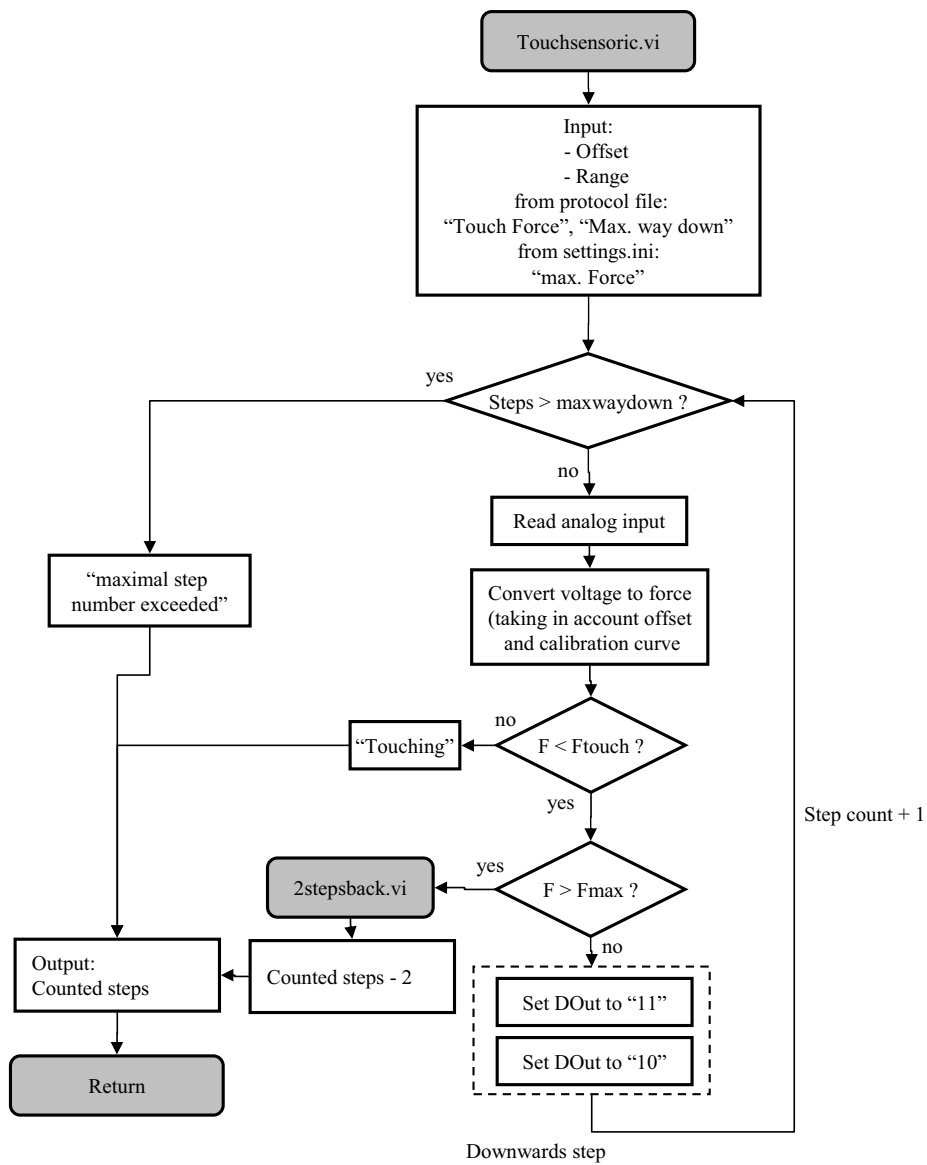
Figure G.7: Flowchart of the compression device control software for the bone chamber experiments (7 of 8).
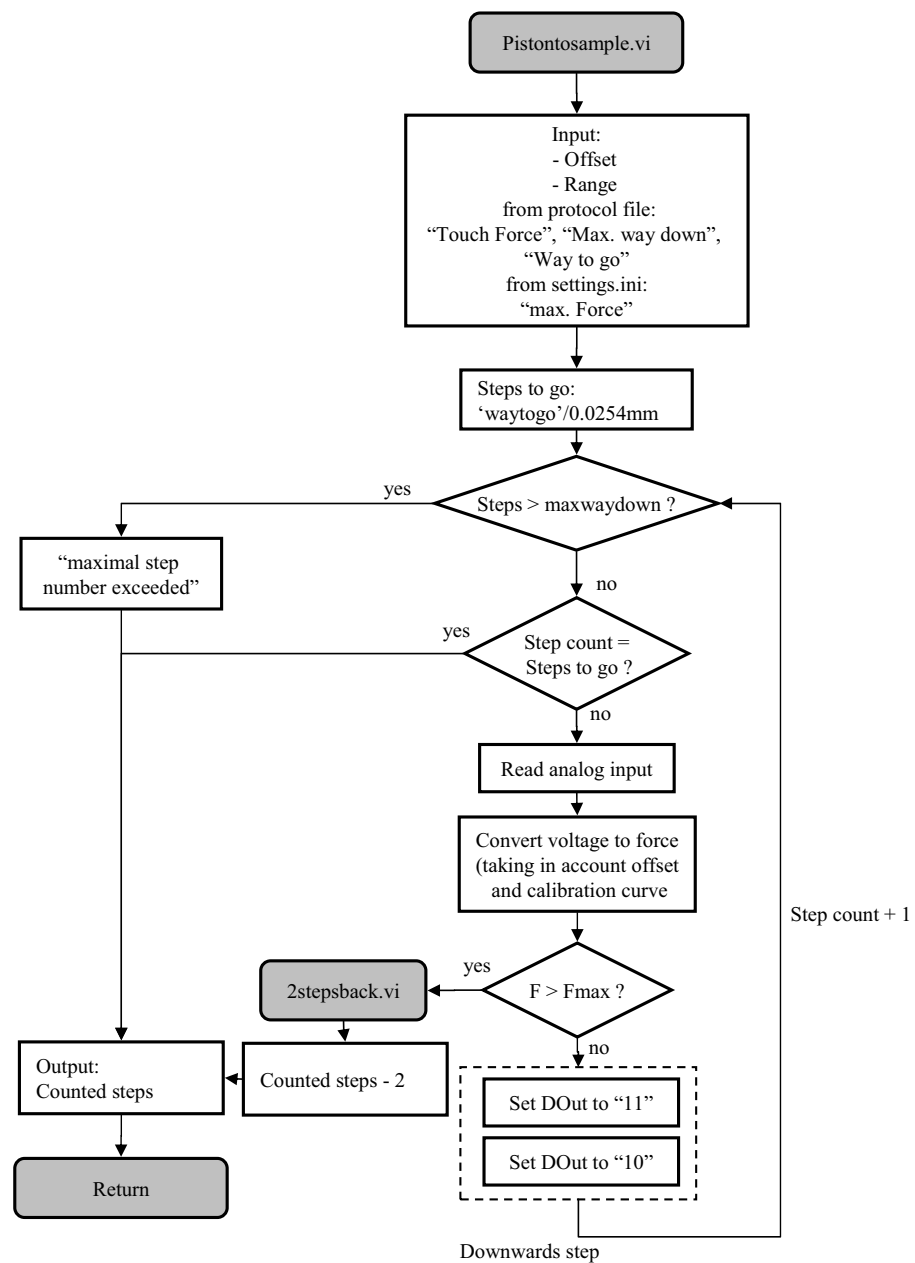
Figure G.8: Flowchart of the compression device control software for the bone chamber experiments (8 of 8).